Involvement of TRPC4 and TRPC5 channels in persistent firing in the hippocampus and in the medial entorhinal cortex

Dissertation

zur Erlangung des akademischen Grades

Doctor rerum naturalium (Dr. rer. nat.)

genehmigt durch die Fakultät für Naturwissenschaften der Otto-von-Guericke-Universität Magdeburg

von M.Sc. Alberto Arboit

geb. am 05.11.1988 in Feltre (ITA)

Gutachter: Prof. Dr. Oliver Stork

Prof. Dr. Philippe Gailly

Eingereicht am: 11.09.2020

Verteidigt am: 21.06.2021

Table of Contents

SUMMARY

Persistent neural activity is a repetitive neural spiking that persists beyond the triggering stimulus and it can last from tens of seconds to even several minutes. This neural activity has been observed *in vivo* during working memory and temporal association tasks and, it has been proposed to support short-term retention of information (up to tens of seconds). Many studies investigated persistent firing (PF) and synaptic and intrinsic cellular mechanisms have been proposed to support it. However, the cellular mechanisms underlying PF are not yet fully understood. Previous studies reported that in brain areas involved in working memory, such as hippocampus and entorhinal cortex, individual neurons showed PF through an intrinsic cellular mechanism supported by transient receptor potential canonical (TRPC) channels. Recent behavioural studies demonstrating the involvement of TRPC channels in working memory, made the hypothesis that TRPC-driven persistent firing supports working memory a very attractive one. However, recent findings, showing that that in TRPC knock out (KO) mice PF is unchanged, put in discussion this hypothesis.

To further assess the involvement of TRPC channels in PF, in my experiments these channels were targeted with different methods aiming to inhibit their activity. Given the expression levels in the medial temporal lobe (MTL), TRPC4 and TRPC5 were chosen as main candidate to support persistent firing. In this dissertation work I focused on two areas of the MTL reported to have a role in temporal association and in working memory tasks: the hippocampal CA1 and the layer II of the medial entorhinal cortex (MEC).

Novel and highly specific TRPC channel blockers (ML204, clemizole hydrochloride, Pico145) were tested for the first time in CA1 pyramidal cells: when TRPC4 and\or TRPC5 were inhibited, also PF was reduced or suppressed. The intracellular application of anti-TRPC4 or anti-TRPC5 antibodies also inhibited PF, confirming the results obtained with the novel blockers. Taken together these results indicate that TRPC4 and TRPC5 channels support PF in CA1 pyramidal neurons. Given the recent controversies raised by studies using KO models, I also tested PF in TRPC4 KO and in TRPC5 conditional KO models. In line with previous studies, I observed PF in TRPC4 KO mice. The TRPC5 conditional KO model was chosen to avoid compensatory mechanisms and up to now this is the first time this model has been used to study persistent firing in the CA1 pyramidal neurons. Quantitative PCRs made on TRPC5 conditional KO mice, showed that the conditional KO happened, however four weeks after infection compensatory mechanisms were already affecting the expression of TRPC3 and TRPC4. Unexpectedly the adenoviral vector used to induce the TRPC5 conditional KO, had unwanted and unspecific side effects affecting the plateau potential during cholinergic stimulation. For this reason, these results were not conclusive. Nevertheless, these results highlighted the crucial importance of planning proper controls when using KO models, often missing even in published studies, and showed that compensatory mechanism can affect also conditional KO models.

In the second project, I focused on the MEC layer II. In this area, immunohistochemical stainings revealed that while TRPC4 were predominantly expressed in clusters of calbindin positive cells, TRPC5 were predominantly expressed out of these TRPC4-calbinind clusters. Given the structural and activation similarities between these two channels, this expression pattern was unexpected but interesting, as a recent model proposed that island (calbindin positive) and ocean (calbindin negative) cells differentially contribute to the memory formation in temporal association, by affecting the processing in CA1. In the MEC layer II, the application of clemizole hydrochloride inhibited PF only when used at higher concentration, but not at lower concentration, when targeting only TRPC5. Although these preliminary data need to be deepened, they suggest that TRPC channels, excluding TRPC5, are involved in the cellular mechanisms supporting working memory.

Taken together, these data indicate that TRPC channels have a central role in supporting persistent in CA1 pyramidal cells and in MEC layer II neurons.

ZUSAMMENFASSUNG

Unter anhaltender neuronaler Aktivität versteht man sich wiederholendes, neuronales Feuern, das über den auslösenden Reiz hinaus und Dutzende von Sekunden bis zu mehreren Minuten andauern kann. Diese neuronale Tätigkeit wurde anhand von *in vivo* während der Vorgänge im Arbeitsgedächtnis und bei zeitlichen Zuordnungen beobachtet. Es wird ebenfalls angenommen, dass sie die kurzfristige Speicherung von Informationen (bis zu mehreren Sekunden) unterstützt. Obwohl viele Studien das anhaltende Feuern untersucht haben – auch wenn bislang angenommen wurde, das synaptische und intrinsische Zellmechanismen es bedingen würden -, fehlt weiterhin das Verständnis der zugrunde liegenden zellulären Mechanismen. In früheren Studien wurde berichtet, dass in Bereichen wie dem Hippocampus und dem entorhinalen Kortex, die mit dem Arbeitsgedächtnis zusammenhängenden, das anhaltende Zünden in einzelnen Neuronen anhand eines spezifischen Zellmechanismus nachweisbar war, der mit den kanonischen Kanälen des transienten Rezeptorpotenzials (engl. transient receptor potential canonical = TRPC) verbunden ist. Neuere Verhaltensstudien, welche die Beteiligung von TRPC-Kanälen am Arbeitsgedächtnis belegen, erbrachten die durchaus ansprechende Hypothese, dass TRPC-gesteuertes anhaltendes Zünden das Arbeitsgedächtnis unterstützt. Jüngste Erkenntnisse, die ein unverändertes anhaltendes Feuern bei TRPC-Knockout-Mäusen zeigen, haben diese Hypothese jedoch zur Diskussion gebracht.

In meinen Experimenten zur weiteren Untersuchung der Beteiligung von TRPC-Kanälen am anhaltenden Feuern wurden diese Kanäle mit verschiedenen Methoden gezielt angegriffen, um ihre Aktivität zu hemmen. In Anbetracht der Ausprägungsebenen im mittleren Schläfenlappen wurden TRPC4 und TRPC5 als Hauptverantwortliche bei der Beteilung am anhaltenden Zünden bestimmt. In dieser Dissertation habe ich mich auf zwei Bereiche des mittleren Schläfenlappen konzentriert, denen eine Rolle bei der zeitlichen Zuordnung und den Aufgaben des Arbeitsgedächtnisses zugeschrieben wird: die CA1-Pyramidenzellen und die Schicht II-Neuronen des medialen entorhinalen Kortex (MEC).

Neuartige und hochspezifische Blocker des TRPC-Kanals (ML204, Clemizol Hydrochlorid, Pico145) wurden erstmalig in der CA1-Pyramidenschicht getestet: Wenn TRPC4 und\oder TRPC5 gehemmt wurden, wurde auch das anhaltende Zünden verringert oder unterdrückt. Die intrazelluläre Verwendung von TRPC4- oder TRPC5- Antikörpern hemmte das anhaltende Feuern ebenfalls und bestätigte damit die mit den neuartigen Blockern erzielten Ergebnisse. Zusammengenommen deuten diese Ergebnisse darauf hin, dass TRPC4- und TRPC5-Kanäle das fortwährende Zünden in CA1-Pyramidenneuronen unterstützen.

Angesichts der jüngsten Kontroversen, die durch Studien mit Knockout-Modellen ausgelöst wurden, habe ich das anhaltende Zünden auch in TRPC4- und zum ersten Mal in einem bedingten TRPC5-Knockout-Modell getestet. In Übereinstimmung mit früheren Studien beobachtete ich das fortwährende Zünden bei TRPC4-Knockout-Mäusen; dennoch deuten meine Daten darauf hin, dass Kompensationsmechanismen den Mangel an TRPC4 ausgleichen könnten. Das konditionale TRPC5-Knockout-Modell wurde gewählt, um Kompensationsmechanismen zu vermeiden. Bisher wurde dieses Modell erstmalig zur Untersuchung des fortwährenden Zündens in den CA1-Pyramidenneuronen verwendet. Anhand der qPCR-Methode, die an TRPC5 konditionierten Knockout-Mäusen durchgeführt wurde, zeigte sich, dass der konditionierte Knockout auftrat, jedoch vier Wochen nach der Infektion bereits Kompensationsmechanismen vorhanden waren, die die Expression von TRPC3 und TRPC4 beeinflussten. Überraschenderweise hatte der adenovirale Vektor, der zur Induktion des TRPC5-Knockouts verwendet wurde, unerwünschte und unspezifische Nebenwirkungen, die das Membranpotential der getesteten Zellen stark depolarisierten. Aufgrund dessen waren die Ergebnisse nicht schlüssig. Trotz allem haben sie die entscheidende Bedeutung geeigneter Kontrollen bei der Verwendung transgener Modelle deutlich gemacht, die selbst in veröffentlichten Studien oft fehlen. Sie haben gezeigt, dass Kompensationsmechanismen auch in konditionalen Knockout-Modellen vorhanden sind.

Im zweiten Projekt konzentrierte ich mich auf die Schicht II-Neuronen des medialen

entorhinalen Kortex‘. In diesem Bereich zeigten immunhistochemische Färbungen, dass TRPC4 vorwiegend *in* Gruppen von Calbindin-positiven Zellen, während TRPC5 vorwiegend *aus* diesen TRPC4-Calbindin-Gruppen in Erscheinung getreten ist. Angesichts der strukturellen und aktivierungsbedingten Ähnlichkeiten zwischen den beiden Kanälen war dieses Muster unerwartet, jedoch interessant, denn: Ein neueres Modell wirft die Theorie auf, dass Insel- (Calbindin-positiv) und Ozeanzellen (Calbindin-negativ) unterschiedlich zur Gedächtnisbildung bei der zeitlichen Zuordnung beitragen, indem sie die Verarbeitung in CA1-Pyramidenzellen beeinflussen. In den Schicht II-Neuronen des medialen entorhinalen Kortex hemmte die Anwendung von Clemizol Hydrochlorid das andauernde Zünden nur dann, wenn es in höherer Konzentration verwendet wurde, jedoch nicht in niedrigerer Konzentration, wenn sie nur auf TRPC5 abzielte. Obwohl diese vorläufigen Daten vertieft werden müssen, suggerieren sie, dass die TRPC-Kanäle an den zellulären Mechanismen, die das Arbeitsgedächtnis unterstützen, beteiligt sind.

Zusammengenommen deuten diese Daten darauf hin, dass TRPC-Kanäle bei der Unterstützung des anhaltenden Zündens in CA1-Pyramidenzellen und in MEC-Schicht-II-Neuronen eine Rolle spielen.

1 INTRODUCTION

1.1 Working memory and medial temporal lobe

Working memory is a crucial ability we use in daily life and its decline, due to aging or due to neurodegenerative diseases, impact quality of life [1]. Working memory is defined as the capacity of keep in mind and manipulate an information for short periods of time while performing a cognitive task [2–4]. We are using working memory when, after reading a phone number, we keep it in mind before dialling it on the phone. Working memory is also a crucial component of other everyday tasks like: performing calculations, comprehending sentences, keeping in mind a series of movements or performing multiple tasks simultaneously [3].

The medial temporal lobe (MTL) includes several anatomically related structures such as the hippocampal formation and the entorhinal, perirhinal and parahippocampal cortices [5]. Traditionally the MTL is known to be crucial for the formation and retrieval of long-term memory and this idea was suggested by early studies on patients having medial temporal lobe damages [6–13]. However, in the last decades new experimental evidence led to revisit this traditional idea, indicating that MTL regions are also involved in working memory by actively maintaining novel information and integrating complex information [4,14–21].

One of the mechanisms proposed to support working memory is persistent neuronal firing [22–26]. Persistent neural firing (PF) is the ability of a neuron to maintain a sustained firing after a stimulus is terminated and it has been proposed to support short-term retention of information for up to tens of seconds. Persistent neural activity has been reported in several brain areas related to memory functions, including the MTL that, comprehend hippocampus and entorhinal cortex [23,25,26]. Although multiple mechanisms have been proposed, the cellular and molecular mechanisms supporting persistent firing still remain largely unclear [23,25].

In the medial temporal lobe, the involvement of the hippocampus in working memory functions has been reported in human [27–29] and animal studies [30–37]. The hippocampus has been reported to be crucial in working memory tasks requiring integration of complex information, such as temporal associations [34,38], spatial or contextual associations [39,40], or multiple associations [41]. In particular, the hippocampal CA1 region has been shown to be important for temporal associations [31,42].

In addition, the entorhinal cortex has also been proposed to support working memory [20,21,43], besides its role in spatial representation and navigation [44]. Experimental evidence collected in both human [45–47] and animal studies [48–50] suggest a role of the entorhinal cortex in supporting working memory functions. Single-unit recording studies in rodents and primates, have shown the presence of persistent neuronal firing in the entorhinal cortex during the maintenance period of delayed matching tasks, in rats during an odor guided delayed non match to sample (DNMS) task [49] and in monkeys during a delayed matching-to-sample (DMS) task using complex visual stimuli [48]. In a human study where a DMS task was coupled with fMRI, it has been reported that, while CA1 and subiculum were more active during the encoding phase, the activity of entorhinal, perirhinal and parahippocampal cortices was higher during the maintenance phase [45].

The integrity of the network between the hippocampus has been shown to be essential to perform task involving temporal association. Lesion in the entorhinal cortex has been reported to impair the performances in trace eyeblink and fear conditioning, both requiring temporal association learning [51,52]. The direct pathway from the layer III of the entorhinal cortex to CA1 has been shown to be essential for temporal association memory: the selective block of the layer III output induces severe deficits in delayed matching to sample tasks and trace fear conditioning [53,54].

In summary, growing evidence indicates that the medial temporal lobe, besides its traditional role in long term memory, is also involved in working memory functions. In the next sections I will give an overview of the anatomy of the medial temporal lobe, focusing on the hippocampus and on the entorhinal cortex, the regions of interest in this dissertation.

1.2 The medial temporal lobe: anatomical structure and connectivity of hippocampus and entorhinal cortex

The medial temporal lobe (MTL) is one of the most studied brain areas and it comprehend the hippocampal formation and the parahippocampal formation. These structures are believed to be involved in memory formation and spatial cognition. The hippocampal formation (HF) comprehends three different subregions: the dentate gyrus (DG), the hippocampus proper (cornu ammonis area: CA3, CA2 and CA1) and the subiculum [55]. The para hippocampal region is adjacent to the subiculum and it comprehends: the pre- and parasubiculum, the entorhinal cortex (EC) and the perirhinal cortex [55]. As the work of this thesis focused on the hippocampus and on the entorhinal cortex, I will focus mainly on these two areas of the MTL.

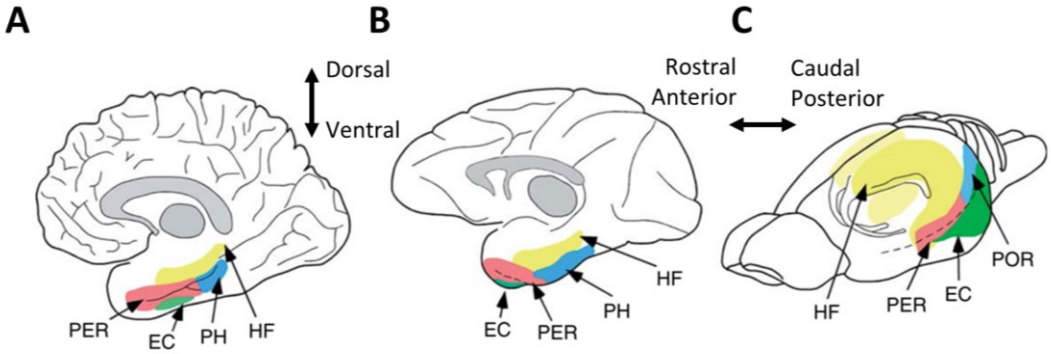

Figure 1 - A comparative view of the medial temporal lobe across species.
The image shows the MTL in a human brain (A), a monkey brain (B) and in a rodent brain (C). The structures included the MTL are the hippocampal formation (HF), the parahippocampal area (PH), the entorhinal cortex (EC), the perirhinal cortex (PER) and postrhinal cortex (POR) (Fig. 1 in Burwell and Agster (2008); modified).

The hippocampal formation is located in the medial portion of the temporal lobe, its structure and function appear to be highly similar and comparable not only in different mammalian species, but also in reptiles and birds [56,57]. In rodents the hippocampal formation is a C-shaped structure that extends in each hemisphere in the dorsal–ventral axis and in the rostral–caudal axis. In primates the hippocampal formation is smaller, located in the ventral region of the brain and it extends in the anterior–posterior axis (Fig. 1). Despite these anatomical differences, the rodent and primate hippocampi are equivalent structures and the functions related to memory and spatial navigation appear to be similar [58,59].

In general, the cortex forming the hippocampal formation appears to have three layers [56,60]. In the hippocampal formation the first layer is the deeper and it includes interneurons

and a mix of afferent and efferent fibers. In the dentate gyrus this layer is called hilus, while in the cornu ammonis (CA) area it is called stratum oriens (Fig. 2). Superficial to the first layer there is the cell layer, formed by principal cells and interneurons. While in the DG this layer is called granule layer and it is formed by densely packed cells, in the CA region and in the subiculum the cell layer is called pyramidal cell layer [61]. Lastly the third layer, called molecular layer, is the most superficial and closer to the hippocampal fissure [60]. In the DG and in the subiculum this layer is named stratum moleculare. In the CA3 area the molecular layer is divided in 3 sublayers: the stratum lucidum, the stratum radiatum and the stratum lacunosum-moleculare. In the CA1 and CA2 regions, the subdivision of the molecular layer is like in the CA3, but the stratum lucidum is missing. In the hippocampus the work of this thesis focused on the CA1 pyramidal layer. In the proper hippocampus, the CA1 layer extends from the border with CA2 to the border with the subiculum and it is formed by pyramidal neurons and interneurons.

The entorhinal cortex (EC) is part of the parahippocampal region and it is separated by the hippocampal formation by the pre- and parasubiculum (Fig. 2B) [55]. The EC is located in the temporal lobe in both rodents and primates, but there are some differences between the species (Fig. 1). In rodents, the entorhinal cortex is located in the caudal end of the temporal lobe and, based on its projections to the dentate gyrus, it can be subdivided in two areas: the medial entorhinal cortex (MEC) which is closer to the pre- and parasubiculum and the lateral entorhinal cortex (LEC) which is adjacent to the neocortex [62]. In primates, the EC is located in the rostral part of the MTL and the projections to the dentate gyrus do not provide such a clear distribution to functionally subdivide EC [63]. The EC has six cortical layers and the main populations of neurons are located in the layers II, III, V and VI (Fig. 2C); pyramidal cells are distributed in all these layers, but stellate cells can only be found in the layer II [63,64]. The layer I has only a low number of interneurons, and the layer IV, also known as lamina dissecans, also contains very low numbers of neurons [64]. The pyramidal and the stellate cells are the two main excitatory neurons present in the layer II of the entorhinal cortex and their properties and morphology have been extensively described in many studies [65–68].

In the layer II of the EC it has been reported the presence of clusters of calbindin positive pyramidal cells forming the so called “island” structures, these calbindin clusters are surrounded by calbindin negative stellate cells forming the “ocean” structure [54,69,70]. However, in recent two recent studies it was reported that clusters of calbindin positive neurons (island structures) are located only in the posterior part of the MEC [64,71].

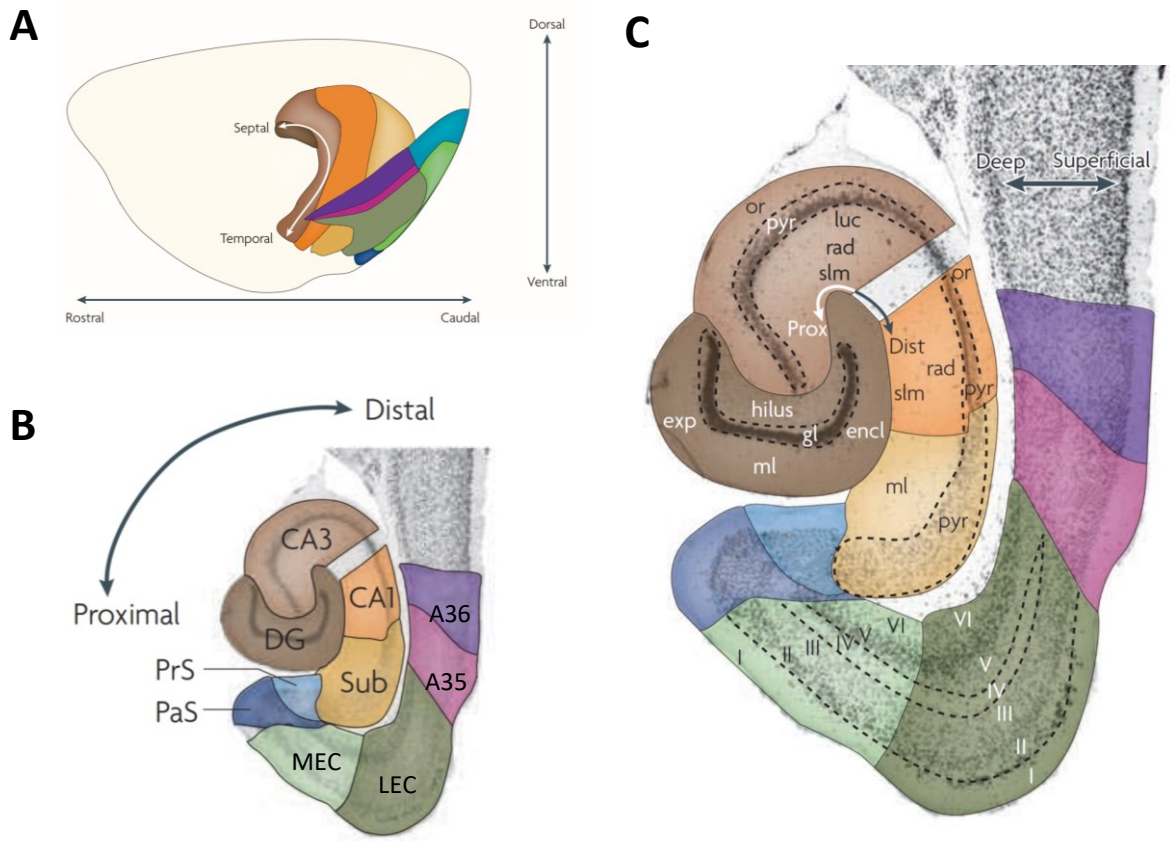

Figure 2 - The hippocampal formation and the parahippocampal region in the rat brain.

(A) Lateral view of the rat brain showing the location of the hippocampal formation and of the parahippocampal region. The hippocampal formation is formed by the dentate gyrus (DG; dark brown), CA3 (light brown), CA2 (not indicated), CA1 (orange) and the subiculum (Sub; yellow). The parahippocampal region is formed by the presubiculum (PrS; light blue) and parasubiculum (PaS; dark blue). The entorhinal cortex is dived in a lateral (LEC; dark green) and a medial (MEC; light green). Finally, the perirhinal cortex (PER) divided in Brodmann areas A35 (pink) and A36 (purple). (B) A Nissl-stained horizontal slice of rat brain showing the hippocampal and parahippocampal formations. The colours code is the same defined in A. (C) An enlarged figure of B in which the cortical layers are marked. The Roman numerals indicate cortical layers. The abbreviations indicate: CA, cornu ammonis; Dist, distal; encl, enclosed blade of the DG; exp, exposed blade of the DG; gl, granule cell layer; luc, stratum lucidum; ml, molecular layer; or, stratum oriens; prox, proximal; pyr, pyramidal cell layer; rad, stratum radiatum; slm, stratum lacunosum-moleculare (Figure. 1 in van Strien et al. (2009) used with the permission of the publisher (Springer Nature) and modified).

A detailed analysis of the connectivity network in the MTL is beyond the scope of this dissertation, however I will give an overview of the circuitry between the hippocampus and the entorhinal cortex (Fig. 3).

In the MTL circuitry, the hippocampus and the entorhinal cortex have a central role in memory encoding and consolidation [72]. The hippocampus has two main unidirectional circuits: an external one that receives highly processed information from the entorhinal cortex and an internal one, also called trisynaptic loop. In general, in the external circuit the EC layer II provides the main input to the DG via the performant path. In addition to this path, the lateral EC layer II project directly and unidirectionally to the CA3 area. In the internal circuit

the DG project to the CA3 via mossy fibers, and the CA3 project to the CA1 via Schaffer collaterals. In addition, while the CA3 area has excitatory recurrent projections, the CA1 neurons are lacking them [73–75]. The CA1 and the subiculum, in addition to the input from CA3, also receive direct projections from the EC layer III via the temporoammonic pathway (EC-CA1). Both the Schaffer collateral and temporoammonic projections to CA1 are unidirectional. The output from the hippocampal formation arises from the CA1 and the subiculum: the CA1 primarily projects to the subiculum but also projects to EC layer V, and finally the subiculum sends projections primarily to layers IV and V of the entorhinal cortex [76]. As we saw, the entorhinal cortex is the major input and also output of the hippocampal formation. The EC form a nodal point between the hippocampal formation and several cortical areas acting as an interface [55,58,60,64]. The lateral EC receives strong inputs mainly from the perirhinal cortex while the medial EC receives mainly input from the postrhinal/parahippocampal cortex that also projects to the lateral EC [77].

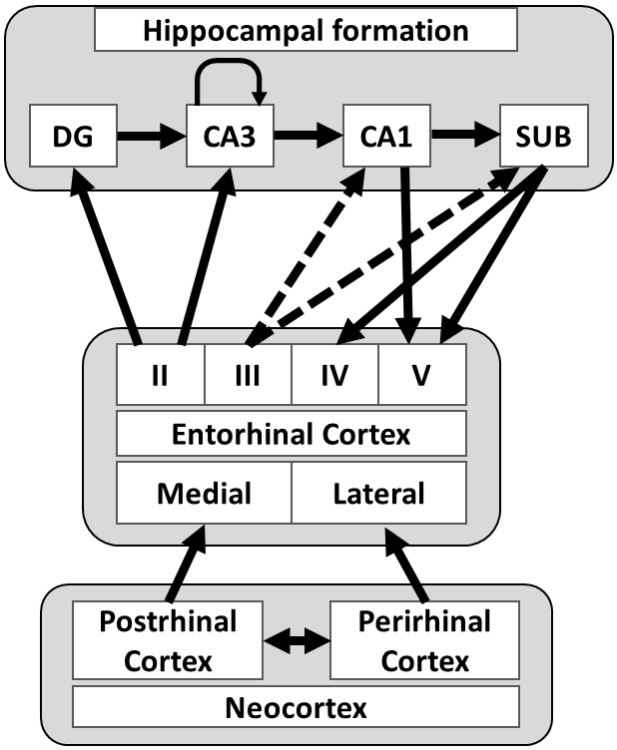

Figure 3 - A schematic view of the medial temporal lobe circuitry.

In this scheme, neocortical projections from the postrhinal and perirhinal cortex aim at the entorhinal cortex, which in turn provide the main source of inputs to the hippocampal formation formed by dentate gyrus (DG), CA3, CA1 and subiculum (SUB). The entorhinal layer II project to the DG and CA3, while the CA3 projects to the CA1 and subiculum (dashed arrows). The trisynaptic pathway describe a unidirectional route connecting all subregions of the hippocampal formation sequentially: the DG project to CA3 via mossy fibers, the CA3 Schaffer collaterals projects to CA1, and finally CA1 projects to the subiculum. CA1 and SUB provide the outputs from the hippocampal formation mainly targeting the deep layers of the entorhinal cortex. The Roman numerals indicate cortical layers (Modified and adapted from van Strien et al. (2009) (Fig. 3) and Clark et al. (2013) (Fig. 2)).

1.3 Temporal association is coordinated by the entorhinal-hippocampal network

In the previous section we saw that the hippocampus and the entorhinal cortex are strongly connected with several pathways. In some recent studies from Tonegawa's group it has been reported besides the well-known inputs to the hippocampal formation (the trisynaptic pathway (ECII-DG-CA3-CA2) and the monosynaptic pathway (ECIII-CA1)), a new circuit between the layer EC layer II and the hippocampus is crucial to regulate learning of temporal associations [54,78]. I will now describe a model proposed by Takashi Kitamura (2017) including this new pathway and focusing on the role of the hippocampus and entorhinal cortex in the formation of temporal association [78].

Based on the expression of calbindin or wolframin (Wfs1) it has been reported that pyramidal and stellate cells are distribute in a specific way in the EC layer II. While pyramidal cells form clusters of calbindin and Wfs1 positive cells forming the so called "islands", the stellate cells are negative to these two markers and they surround these "island" clusters forming the so called "ocean" cells (Fig. 4A-B) [70,79]. The ocean cells projects to the dentate gyrus to form the trisynaptic pathway. The island cells were found to directly project to GABAergic interneurons of the stratum lacunosum (SL) of the CA1 region [79]. The other major input to CA1 originates from ECIII cells that have axons innervating the stratum moleculare (SM), immediately adjacent to the SL (monosynaptic pathway). The position of the GABAergic interneurons located in the SL, is strategic as it allows the island cells innervating these interneurons to control and gate the EC layer III input to the stratum moleculare through feed-forward inhibition (Fig. 4B) [78].

In this model proposed by Kitamura (2017), the cells in the EC layer III support the association between two temporally discontinuous stimuli by firing persistently during this period. In this view, persistent firing in the layer III could be the cellular mechanism supporting working memory and temporal association tasks and then the CA1 cells integrate the inputs from the EC layer III (Fig. 4C). These input to the hippocampus will be regulated by the island clusters located in layer II, projecting to GABAergic interneurons in the stratum lacunosum and forming a feedforward inhibition loop. In this model, while the EC layer III inputs into the CA1 region of the hippocampus are crucial for the formation of temporal association memory, the inputs from island cells in the EC layer II are crucial for the regulation of this temporal association, inhibiting or not the inputs from EC layer III. In this model, the hippocampal CA1 will combine the inputs from the entorhinal cortex and encode

the representation of sequences of successive moments during a trace period between two events and it would be characterized by the sequence of spiking that is characteristic of time cells. Even if the time cells activity differs from persistent neuronal firing, the cellular mechanisms supporting both kind of firing might not be different. In fact a modeling study from our group indicates that both, persistent firing and time cells activity, can be supported by the same intracellular mechanism [80]. In this modelling study it was shown that persistent firing mediated by CAN current could mimic and develop into time cell-like activity when lateral inhibition was added to the network model.

As we can see, the hippocampal CA1 and the entorhinal cortex play an important role in temporal association tasks, in line with other studies presented in the previous section also indicating that these two areas of the MTL are crucial for working memory tasks requiring temporal association.

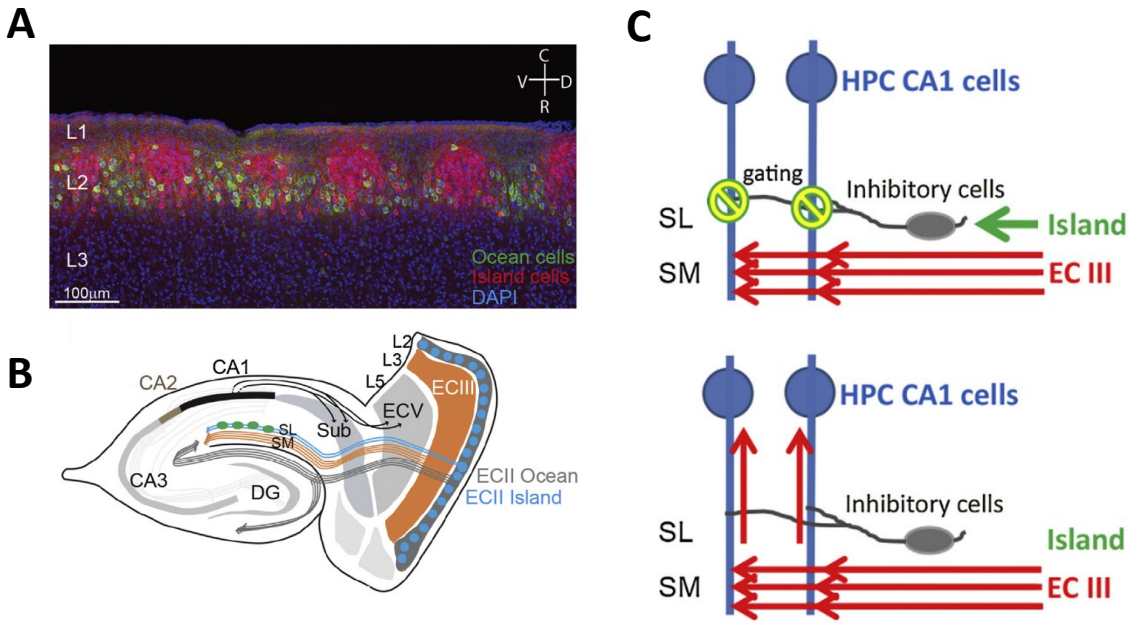

Figure 4 – Island cells and regulation of temporal association.

(A) Sagittal section of medial entorhinal cortex, the immunohistochemical staining of the layer II (L2) shows island cells (wfs1 positive, red) and ocean cells (reelin positive, green). DAPI: nuclei staining (blue). D; dorsal, V; ventral, R; rostral, C; caudal. (B) A new scheme of the entorhinal-hippocampal circuit. Island cells (blue) directly project to stratum lacunosum (SL) of CA1 region to synapse with the GABAergic interneurons (green) in SL (SL-INs), while ECIII cells (orange) project to stratum molecular (SM) of CA1 region to synapse with CA1 pyramidal cells. Ocean cells (grey) project to dentate gyrus, CA3, and CA2. Sub; subiculum. (C) A scheme of the regulation of temporal association by island cells. On top, ECIII cells (red) provide sensory information for temporal association to the hippocampal (HPC) CA1 pyramidal cells (blue). If island cells (green) are active, they will consequently gate (or inhibit) the ECIII input into HPC CA1 via inhibitory cells (grey). As a result, CA1 cells will not receive the ECIII input and then animal will not form temporal association memory. On the bottom, if island cells are silent, there will not be gating activity, meaning that the hippocampal CA1 pyramidal cells will receive the sensory information from the ECIII input and so the animal will successfully form memory. SL; stratum lacunosum, SM; stratum moleculare (Figure. 2-3 in Kitamura (2017) used with the permission of the publisher (Elsevier) and modified).

1.4 The cholinergic system and working memory

Acetylcholine (Ach) is a fast acting neurotransmitter in the peripheral nervous system, however in the central nervous system it acts mainly as modulator regulating neuronal excitability, altering presynaptic release of neurotransmitters and also coordinating the firing of groups of neurons [81]. Extensive evidence from behavioral experiments but also from *in vivo* and *in vitro* electrophysiological recordings, strongly supports the idea that cholinergic innervation influences cortical processing and critically affects the performance of learning and memory tasks [4,81–84]. Experimental evidence shows that acetylcholine has a role in many normal physiological cognitive functions, such as attention to sensory stimuli, coding of location and movement, learning and memory [85,86]. In particular working memory tasks such as those measuring temporal associations, depend on cholinergic innervation [87,88], which is also known to facilitate persistent neural firing.

In the medial temporal lobe, the hippocampus and the entorhinal cortex are both modulated by acetylcholine and the majority of the cholinergic projections targeting these areas originate in the basal forebrain complex (medial septum) [89–92]. To study the role of the cholinergic system in working memory, localized infusions of cholinergic antagonists (e.g. scopolamine) or selective lesions of the cholinergic innervation to the MTL have been used in *in vivo* experiments. Localized infusions of scopolamine in the perirhinal cortex impaired rats and monkeys while performing object recognition tasks [93,94]. The application of scopolamine in the hippocampus [95] or in the medial septum [96] has been reported to impair spatial encoding. Disruption of the hippocampal neural activity and an impairment of the cognitive functions were observed also when scopolamine was locally infused in the medial septum [97]. Not only localized infusion but also systemic application of scopolamine has been reported to impair working memory [98].

Besides scopolamine infusions, selective immuno-toxic lesions have been also used to study the cholinergic system. Localized injections of the toxin saporin conjugated with antibodies has been used to induce selective death of cholinergic neurons. In rats the selective lesion of cholinergic medial septum-diagonal band neurons induced marked deficits in learning memory tasked having a temporal gap [37,99]. Interestingly in one of these studies, the deficit induced by the lesion, was completely reverted by systemic administration of carbachol, a cholinergic agonist [99]. Selective lesion of the cholinergic neurons innervating the entorhinal cortex in rats cause impairments in delayed-match to sample tasks, this impairment was observed only when the stimuli was novel and not familiar [100]. Also a

selective lesion of the cholinergic input to the prefrontal cortex can cause working memory impairments in monkeys [101].

Taking into account all this evidence from experiments in humans, primate and rodents, it has been proposed that the cholinergic system plays an important role in higher cognition and in memory as its modulation and impairment heavily affect performance in behavioral tasks [4,82,84,102,103].

Along with the effects observed *in vivo* experiments, the cholinergic system modulation has been shown to modulate the activity of single neurons in several ways. The application of cholinergic agonists can induce depolarization [104], can lead to a reductions in spike frequency accommodation [105], can enhance long term potentiation [106], can lead to presynaptic inhibition of glutamatergic and GABAergic synaptic transmission [107,108]. In addition, *in vitro* studies from different brain regions reported that the presence of a cholinergic agonist is necessary to induce intrinsic persistent firing triggered by a depolarizing stimulus [50,109–113].

In this section we saw that the cholinergic system plays an important role supporting cognitive functions and the application of cholinergic antagonists or lesions reduced the performance during behavioral tasks. Moreover other experimental evidence and computational models indicate that also the level of acetylcholine plays and important role in modulating cognitive functions [83,114,115]. The level of acetylcholine changes with different mnemonic stages, during encoding of a novel stimuli are high while during retrieval and memory consolidation are low [107,114,116]. In the cortex and in the hippocampal formation an increase of the acetylcholine levels has been reported during active waking and high arousal related to the presentation of a novel or fear stimuli, while during quiet waking (immobility, eating, grooming) the acetylcholine levels were lower [117,118]. In addition, in the hippocampus the acetylcholine concentration increases also when animals are exposed to a novel spatial environment [119–121].

In summary, the cholinergic innervation of the MTL via the septum is required to successfully perform working memory tasks. Changes in the cholinergic tone has been proposed to modulate the network circuits dynamics and the intrinsic cellular properties that may support and regulate cognitive functions, including working memory [114,116].

1.5 Persistent neural firing and working memory

Persistent neural firing is one possible mechanism contributing to the maintenance of information during working memory tasks and it has been observed in several brain areas associated with memory functions [22–26]. In both human and animal experiments, persistent neuronal firing has been reported during the delay-maintenance periods of working memory tasks where the subject had to hold an information for a short period of time, suggesting that this sustained firing activity could be a neuronal mechanism supporting short-term retention of information during working memory tasks [122]. Furthermore, *in vitro* studies showed that cells from different brain regions, including the hippocampus and the entorhinal cortex, show persistent neural activity.

Using various techniques, from electrophysiology to fMRI, persistent neural activity has been shown in rodents, primates, humans, in both *in vivo* and *in vitro* experiments. In the next section I will go through experimental evidence first of *in vivo* persistent neural activity and afterwards I will talk about mechanisms proposed to support persistent firing and I will give an overview of *in vitro* evidence.

1.5.1 *In vivo* evidence of persistent firing

The earliest evidence of persistent neural firing recorded during the maintenance periods of working memory tasks, was reported in primates. In these studies, various types of delayed match to sample or delayed response tasks were used and, while performing these tasks, neurons located in the in the prefrontal cortex (PFC) [123–125] or in the temporal lobe were recorded [126,127].

Fuster and colleagues (1971) tested a delayed-response task in monkey while recording from PFC neurons [123]. In this task during the cue-period two identical objects were presented at the same time to the animal, but only one was “baited” with a reward. The reward was visible to the animal during the cue-period and was afterward hidden during the delay period. After the delay period the animal was trained to choose the baited object in order to retrieve the reward. In this study the delay period lasted from 15 to 60 seconds and, when the delay-periods were shorter than 30 seconds, all the animals performed the task correctly choosing the baited object. While performing the task, the activity of the prefrontal cortex was recorded and during the delay period an increased spiking activity was observed. In addition, during the transition from cue to delay period, it was when the greatest number of PFC neurons were firing at higher levels compared to the inter-trial baseline.

In a study from Funahashi and colleagues (1989) an oculomotor delayed response task

was used to study visuospatial working memory in the prefrontal cortex [125]. In this task a brief stimulus was presented to the subject and, after a delay period (1-6 seconds), the eye movement of the subject was tracked to see if the location of the stimulus was remembered. During the delay period the firing of principal sulcus neurons appeared to be spatially tuned and they showed persistent neuronal firing when the stimulus was presented in the preferred location.

Persistent activity during the delay periods of working memory tasks was also reported in the hippocampal formation of both primates [128,129] and rodents [130,131]. Hampson and Deadwyler (2003) reported that some neurons in the rat subiculum fired throughout the delay period (1-30 seconds) of a DNMS task with no interruptions. In this study they identified five kind of subicular neurons firing preferentially at different point during the task, but mostly of the neurons increased their firing frequency during the sample presentation and during in the early portion of the delay-period [130].

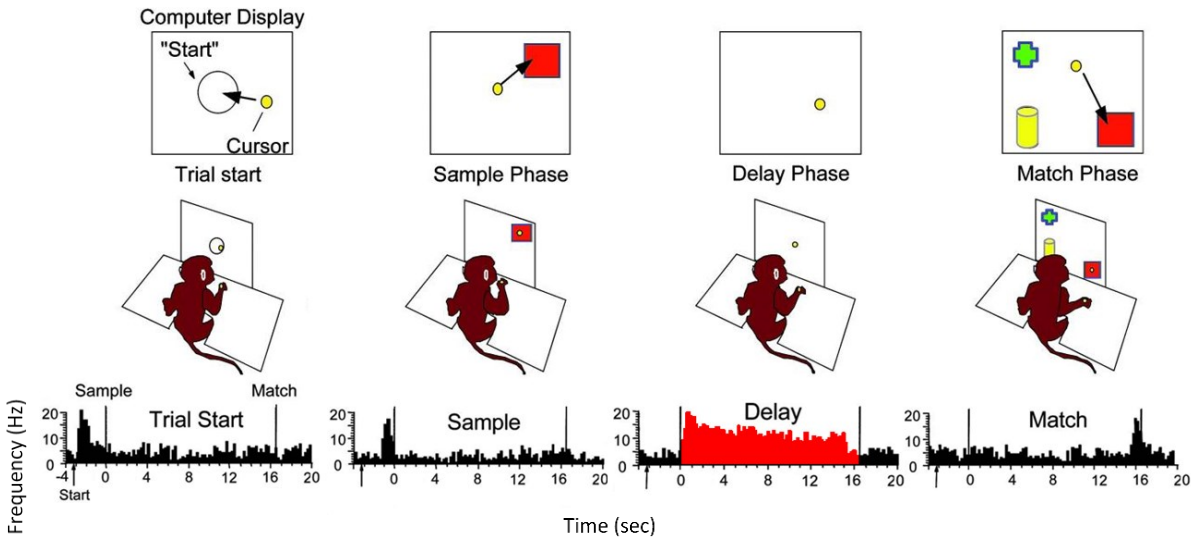

Figure 5 - Sustained action potential firing during delayed period of a DMS task.

In this experiment monkeys were trained to perform a multi-object visual DMS task by moving a cursor on a computer display projected in front of the animal. The neural activity of CA1 was recorded during the experiment (bottom). Trials were initiated by the monkey moving the cursor into the start target centred on the screen. During the sample phase an image was presented on the monitor and the placement of the cursor into the sample image. During this delay phase, when the sample image had to be retained, the hippocampal neurons showed an elevated firing frequency (indicated in red in figure). After the delay phase the monkey had to recognise the sample image during the matching phase (Fig. 1 in Hampson et al. (2004); modified).

In primates, electrophysiological recordings from CA1 showed persistent activity in this area during the delay phase of a delayed match to sample (DMS) memory task [128]. In this experiment after its presentation, a stimulus had to be retained during the delay-phase in order to eventually be recognized afterwards, during the matching-phase. During the delay period of the task, in which the sample had to be retained, the neural activity recorded from

the CA1 hippocampus showed an increased firing activity (Fig. 5). The presence or not of persistent firing bridging the delay period correlated with the money performance [128]. In addition, some other studies reported that the presence or not of persistent firing during the delay-period depended on the correct task performance and, in case of error trials, persistent activity was reduced or even absent [125,132,133]. The disruption of persistent activity during the delay phase has been also reported to impaired and reduced performance in the tested tasks [125,134].

In addition to animal studies, also human fMRI studies reported elevated neural activity during temporal bridging tasks in the prefrontal cortex, hippocampal and parahippocampal structures [14,16,135–138].

In a study from Axmacher et al. (2007) a serial Sternberg paradigm was used to test working memory and data were acquired using intracranial EEG and fMRI [138]. In the task used in the EEG experiments the subject had to memorize one, two or four pictures of unknown female and male faces during the encoding phase and then the subjects had to maintain the faces during a delay period of 3 seconds. After this delay period pictures were presented to the subjects and they had to decide if they matched the one presented during the encoding phase. The task used in the fMRI experiments had the same structure but the period used were all slightly extend so that the BOLD response could be modelled more accurately. In this case the delay period was extended to 6-10 seconds. They observed an increase of neural activity and BOLD response within the medial temporal lobe during the stimulus maintenance phase, in addition they reported that this activity also varied depending on the working memory load. An increase of activity during the delay phase was observed also in a study from Nauer et al. (2015) in which the participants were scanned (fMRI) while performing a delayed match to sample task with novel scene stimuli [16]. During the delay phase (10 seconds) there was an activation of the parahippocampal and perirhinal cortices and of hippocampal subfields (CA1, CA3 and DG). The magnitude of the activation of these areas also predicted how strongly the stimuli were encoded and influenced the subjective memory strength.

In a recent study in humans, persistent neural activity was recorded from single neurons in the medial frontal cortex and the medial temporal lobe while the subjects performed a Sternberg task [139]. In this task used to test working memory, the subjects had to memorize 1-3 images (encoding phase) and after a delay period lasting 2.5-2.8 seconds (maintenance phase), the subjects were asked to judge whether the presented test stimulus was identical to the one presented during the encoding phase. In this study the persistent activity

observed in the hippocampal and amygdala neurons was stimulus specific and the cells remained active during the memory maintenance only if the preferred stimulus was presented. In the cells recorded in the medial frontal cortex, the activity was modulated by memory load but was not stimulus specific.

In summary, persistent neural firing has been observed while performing temporal bridging tasks in rodents, primates and humans. This activity was lasting from hundreds of milliseconds to tens of seconds and it was observed during the delay period of the tasks when an information had to be held in memory. Interestingly the presence of persistent firing corresponded to the correct performance of the task. Altogether this evidence suggests that persistent neuronal firing could be the neuronal mechanism supporting short term retention of information during working memory tasks, making possible to maintain relevant information, bridge temporal gaps and make associations.

However, the theory that persistent neural firing support temporal association by bridging the delay period of working memory tasks is still often challenged [22,24]. In some studies, persistent firing was not consistently observed in rodent hippocampus. While Hampson and Deadwyler (2003) reported that some neurons in the subiculum of rats fired during all the maintenance period of a DNMS task, other studies in rabbit [140] and rat [141] could not find this kind of persistent activity but, they reported cells that fired only briefly and sparse during the delay period. Interestingly in the hippocampus during a temporal association task and while recording from a large number of neurons, single CA1 cells has been reported to fire in sequence during the delay period, as if they were encoding the trace in this way [142]. These neurons named “time cells” fire in a temporally organized manner and has been recorded during the delay period of various tasks offering an alternative theory on how the hippocampus can encode temporal association [142–145]. Even if the “time cells” activity differs from persistent neuronal firing, the cellular mechanisms supporting the firing of “time cells” might not be different from the one supporting persistent firing. In fact, a modeling study from our group suggests that both, persistent firing and “time cells” activity, could be supported by the same intracellular mechanism [80].

1.5.2 Potential mechanisms supporting persistent firing

The function and the mechanism supporting persistent activity *in vivo* are not completely understood, however, *in vitro* experimental evidence and computer simulations support the hypothesis that both, a synaptic network and an intrinsic mechanisms, co-operate in generating persistent firing [23,146,147]. The role of TRPC channels in supporting persistent firing in CA1 pyramidal cells and in EC layer II neurons is the main topic of this dissertation however, before focusing on that, I will give an overview of the different mechanisms supporting persistent firing and I will give an overview of the brain areas in which persistent firing has been reported *in vitro* experiments.

Persistent firing based on circuit connectivity

One of the mechanisms proposed to mediate persistent firing is based on synaptic networks between neurons. The central idea of the synaptic network mechanism is that persistent firing is a reverberating activity based on feedback excitation. The hypothesis is that recurrent excitatory loops within a neural network can sustain a persistent activity in the absence of external inputs when the excitatory loops are sufficiently strengthened, for example during memory encoding [146]. This idea was used with success in several computational models of spatial navigation and memory [148–152].

In addition to the computational models, there are also several experimental evidence supporting this theory. In *in vitro* slice preparation, it has been shown that AMPA and NMDA synaptic conductances support a sustained depolarization state during spontaneous up and down slow oscillations in the neocortex [153,154]. Intact synaptic transmission has been reported to be required to observe stimulus induced persistent firing in CA3 cells in cultured hippocampal slices [155]. The NMDA receptors has been shown to contribute to persistent activity in semilunar granule cells located in the dentate gyrus [156]. Besides *in vitro* evidence and computational models, the AMPA and NMDA receptors has been shown to support persistent activity also in primates *in vivo*. In these experiments performed in awake monkey, the AMPA or NMDA receptor blockade reduced persistent activity in the dorsolateral prefrontal cortex and also impaired working memory performance [157].

Persistent firing based on intrinsic mechanism

The central idea of the intrinsic mechanism is that synaptic connectivity is not essential to mediate persistent firing. In fact persistent firing has been observed in presence of synaptic blockers in the entorhinal cortex, post subiculum, perirhinal cortex and hippocampus [50,110,111,158–162]. All this experimental evidence indicates that persistent firing can be

sustained by intrinsic cellular mechanisms and synaptic connectivity is not required.

In previous studies, several ion currents have been shown to support persistent firing: persistent sodium current, L-type calcium, h-current, ether-a-go-go related gene (ERG) current and CAN current [26,112,159,163–168]. In CA1 pyramidal cells the persistent sodium current has been shown to support persistent firing during cholinergic receptors activation [159]. The persistent sodium current, activated by the stimulation of glutamatergic receptors, has been reported to induce membrane depolarization in the nucleus accumbens in medium spiny neurons [164]. The glutamatergic dependent plateau potential (depolarization) observed in this study usually underlies persistent firing. The L-Type calcium current and the persistent sodium current, activated by the application of serotonin, were reported to support persistent firing in trigeminal motoneurons [163]. In a recent study, ERG current was shown to support persistent activity in neocortical pyramidal cells after the application of a cholinergic agonist [112]. Also the h-current, a cationic current activated by membrane hyperpolarization, has been shown to support persistent firing in prefrontal cortex neurons in rodent slice preparation [165]. Another study in prefrontal cortex reported that the loss or the pharmacological blockage of h-current interfered with persistent firing generation [169]. In addition, in parvalbumin interneurons in the dentate gyrus, h-current dependent persistent firing has been observed [166].

Finally, several experimental evidence suggests that a calcium dependent cationic non-selective (CAN) current plays an important role in the mechanisms mediating persistent activity [50,111,170–172]. In addition, an increasing number of studies are suggesting that TRPC channels are supporting CAN current dependent persistent firing [111,173,174]. These channels will be described extensively in detail in a dedicated section of the introduction.

Co-operation of network and intrinsic mechanisms

As we saw, in the literature there is experimental evidence supporting both network and intrinsic mechanism and, as suggested in some studies, the two mechanism are likely to co-operate in supporting persistent activity in many brain areas in *in vivo* condition [23,80]. Besides all the experimental evidence showing that both network and intrinsic mechanisms can support persistent firing [50,158,166,175,176], there are also other reasons suggesting that a hybrid mechanism, in which the two mechanisms are cooperating, could support persistent firing. One of the main reasons is that pure reverberatory networks tend to be dynamically unstable and are also sensitive to small perturbations [146,147]. On the other hand, the intrinsic cellular mechanism is more robust, but it might not be suited alone to reproduce some of the more complex features of persistent activity reported in some brain areas. In these

areas, different neurons often show different temporal profiles of PF, spanning from stable to ramping, with one or more increases or decreases in activity [23]. A hybrid mechanism using both network and intrinsic mechanism could provide robustness but also has the flexibility necessary to orchestrate the firing of many neurons [147].

1.5.3 Properties of intrinsic persistent firing in different brain areas

In vitro studies reported the presence of intrinsic persistent firing in many brain areas essential for learning and memory, such as the prefrontal cortex, the hippocampal formation, the entorhinal cortex and the amygdala (Fig. 6) [23,25,26]. In the hippocampus persistent firing has been reported in CA1 [110,159,177], in CA3 [160], in the dentate gyrus [156,166] and in the post subiculum [109]. In the entorhinal cortex, neurons in the layer II, III and V showed persistent activity [50,66,111,113,158,161,170,176,178]. Besides the medial temporal lobe, also other brain areas can show persistent activity like the amygdala [175], the prefrontal cortex [165,169,179] and other cortical areas [112,162,180].

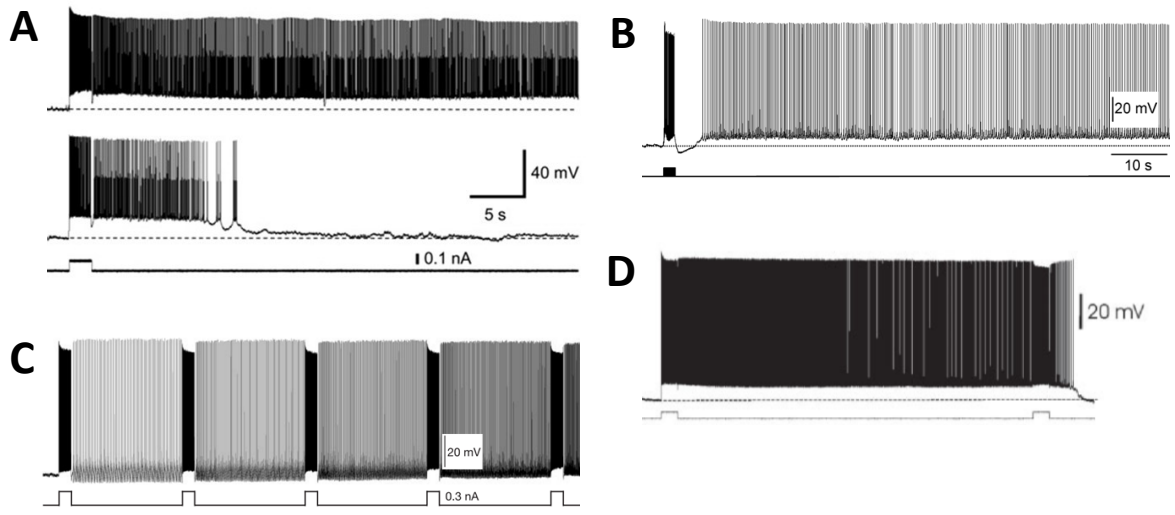

Figure 6 - Examples of *in vitro* persistent different in different brain areas.

(A) Hippocampus, CA1. The figure shows two traces of long lasting (top) and self-terminating (bottom) persistent firing evoked during cholinergic stimulation by a 2 second current pulse (0.1 nA) (Modified from Knauer et al 2013, Fig. 2). (B) EC layer II. The figure shows persistent firing evoked by synaptic stimulation (Modified from Yoshida et al 2008, Fig. 1). (C) EC layer V. The figure shows graded persistent firing evoked by a 4 second current pulse (0.3 nA) during cholinergic stimulation. The consequent application of several stimuli increases the firing frequency of persistent firing (Modified from Egorov et al 2002, Fig. 2A). (D) EC layer III. The figure shows persistent firing evoked by a 4 second current pulse (0.2 nA) during cholinergic stimulation. The application of a second stimulus, identical to the first, terminated persistent firing (Modified from Tahvildari et al 2007, Fig. 2A).

All these *in vitro* studies were performed in brain slice preparations from rats or mice and persistent activity was induced in different ways: by using synaptic stimulation or by

using current injections, with or without the application of exogenous modulators. One of the most common ways to evoke persistent firing is to apply a current pulse to depolarize the membrane over its firing threshold while bath applying a neuromodulator; typically the neuromodulators are muscarinic or glutamatergic agonists such as carbachol or DHPG [50,110,175,177,178,180,181,111–113,160–162,169,170]. In these studies, persistent firing was induced by injecting square current pulses, with different lengths (0.2 to 4 seconds) and intensities (50 to 300pA), applied from under the neurons firing thresholds while bath applying neuromodulators. During control condition, the depolarizing current injection did not induce persistent firing in most of the cases, indicating that the presence of a neuromodulator is required. The activation of muscarinic or glutamatergic receptors attenuates the hyperpolarizing afterpotential that normally follows the stimulus and induces an afterdepolarization potential (plateau potential) that can trigger persistent firing if it brings a neuron over its firing threshold. On the other hand, a study reported that in the EC layer III, persistent firing can be induced by a depolarizing current step in absence of neuromodulators [158]. However in this study the application of a glutamatergic agonist greatly enhanced the strength of persistent firing [158]. In addition, a study in the prefrontal cortex showed that persistent firing can be evoked even by a series of hyperpolarizing current pulses without bath applying any neuromodulator [165].

Another way to induce persistent firing is by synaptic stimulation [50,158,166,175,176]. In this studies, local synaptic activation, with different stimulating protocols (2 to 4 seconds, 10 to 50 Hz), evoked persistent firing. Normally synaptic stimulation requires the presence of a neuromodulator (cholinergic or glutamatergic agonist) to induce persistent firing, however one study reported that, in EC layer III neurons, synaptic stimulation could trigger persistent firing in absence of any agonist (Fig. 6B) [158].

Besides differences in the way persistent firing has been triggered, some other differences in the properties of this neural activity have been reported. Neurons in the medial EC layer V have been reported to respond to repeated applications of a brief stimulus with a graded change in persistent firing frequency (Fig. 6C) [50,161,182]. In these studies, the firing frequency of persistent firing could be up-regulated, by short depolarizing steps, or down-regulated by short hyperpolarizing steps. However in the EC layer III repeated depolarizing steps have been reported to down-regulate the firing frequency (Fig. 6D) [170,178]. Besides in the entorhinal cortex, graded persistent firing has been observed in other brain areas, such as the prefrontal cortex [165], the perirhinal cortex [162] and the amygdala [175]. In addition also in several neural systems, like the oculomotor system, the

somatosensory system and the head direction system, graded persistent firing has been observed [23]. To the best of my knowledge there are no reports of graded persistent firing in the hippocampus. Graded persistent firing has been proposed to potentially allow neurons to store several bits of information at different level of frequency, maintain in this way memory for stimuli that are varying along time [161].

Some differences in the length and in the firing behaviour of persistent firing have been also reported. In literature, persistent firing has been categorized depending on the length of the firing after the end of the stimulus [23,110,160,176,182–184]. Persistent firing is categorized as long-lasting when, after the end of the stimulus, the firing continues for more than 30 seconds (Fig. 7A). When persistent firing terminates within 30 seconds from the end of the stimulus, it is categorized as self-terminating (Fig. 7B). In the MTL and in other brain areas stable and long-lasting persistent firing has been reported in the majority of the cases. In the entorhinal cortex long lasting PF has been observed in layer III in the lateral EC [176], and in the layer II [184] and in the layer V [50,182] of the medial EC. Long lasting persistent firing has been reported in the post subiculum [109] and in the hippocampus in CA1 [110] and in CA3 [160] pyramidal cells. However self-terminating PF has been reported in the hippocampus [110,160] and in the MEC in the layer II [184] and layer V [182].

In the CA area of the hippocampus, besides long-lasting and self-terminating persistent firing, depolarization block (DB) responses have been reported while using the same stimulation and modulators used to induce PF (Fig. 7C) [110,160,171,177]. When showing depolarization block a cell, at any point in time after or during the stimulation, does not fire action potentials even if the membrane potential gets more depolarized than the action potential firing threshold. Up to now depolarization block has been reported in the hippocampus but it has never been reported in the entorhinal cortex. Depolarization block has been observed during cholinergic stimulation and given its similarities to ictal depolarizations observed during cholinergic induced seizures, it has been proposed that DB could play a role in hippocampal epileptogenesis [171,185]. However, it has also been proposed to be a neuroprotective mechanism preventing the neuronal network from the spread of hyper excitability [186,187].

In summary, *in vitro* experiments reported the presence of persistent firing in several brain areas. These previous studies also showed that persistent firing can have different properties and can be evoked in different ways, however the presence of a neuromodulator seems in most of the cases to be crucial to induce persistent firing. In the next section I will

give a short overview of the cholinergic and glutamatergic receptors involved in the induction of CAN-dependent (TRPC) persistent firing, main topic of this dissertation.

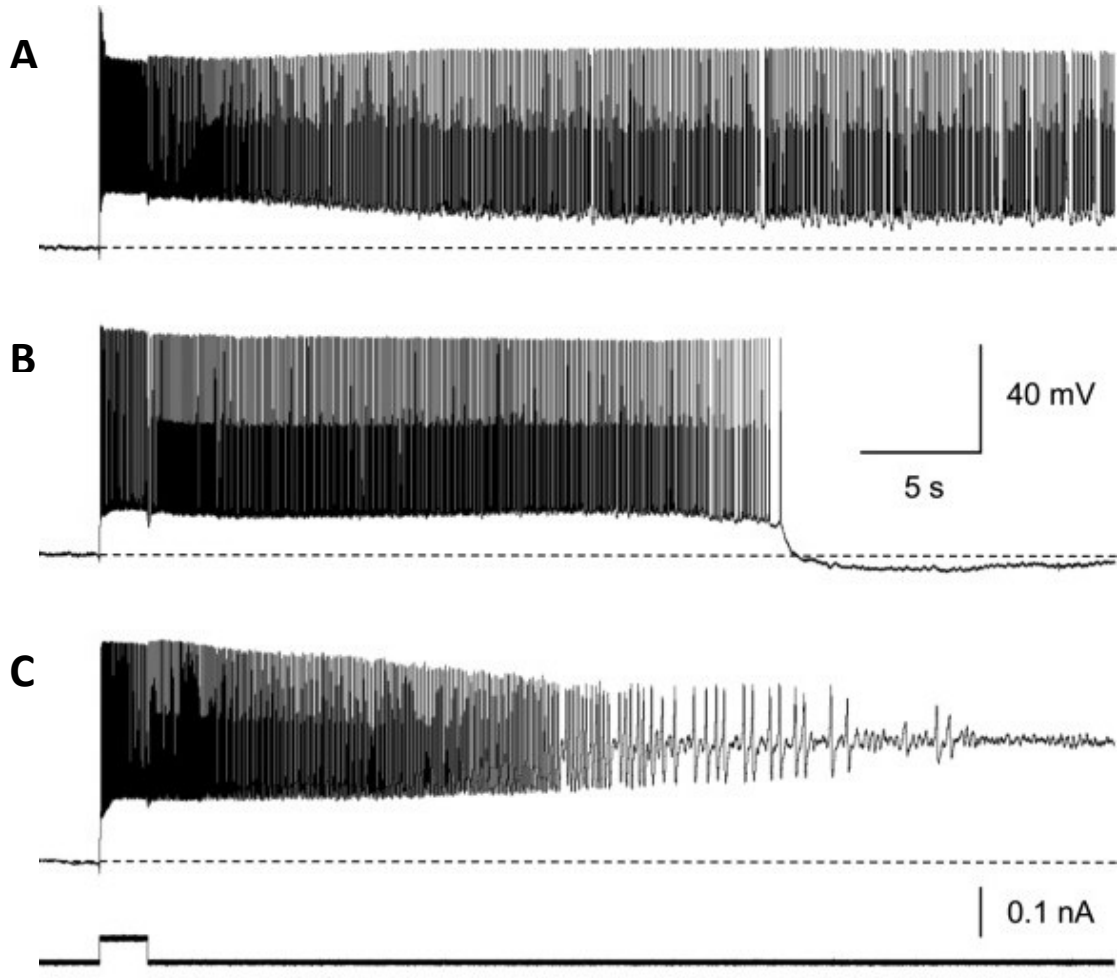

Figure 7 - Persistent firing and depolarization block in rat CA1 pyramidal cells.

(A) Long-lasting persistent firing evoked during carbachol application by a depolarizing current pulse (2 seconds, 0.1 nA) (C, bottom). (B) Self-terminating persistent firing induced using the same condition described in (B). (C) The same stimulus used in A and B was applied to this neuron during carbachol application and, after showing persistent activity, the neuron switch to depolarization block. Neurons can also show depolarization block response already during or shortly after the application of the stimuli (Fig. 2, modified from Knauer et al. (2013)).

1.5.4 Roles of cholinergic and glutamatergic systems in CAN dependent persistent firing

As we saw in the previous section, in brain slice preparation one of the most common way to induce intrinsic persistent firing is to apply a depolarizing current pulse in combination with the application of a neuromodulator activating G-protein coupled receptors. While the muscarinic receptors agonists (e.g. carbachol) used to induce PF mainly activate the heterotrimeric proteins $G_{q/11}$, coupled with M_1, M_3, M_5, and $G_{i/o}$, coupled with M_2, M_4, the glutamatergic agonists activate $G_{q/11}$, coupled with $mGluR_1$ $mGluR_5$, and $G_{i/o}$, coupled with the rest of mGluRs [188].

The application of muscarinic and glutamatergic agonists has been shown to facilitate the induction of persistent firing [23,25,26] by inducing a depolarization of the membrane potential that increase the intrinsic excitability of the neurons [104,189–193]. The activation of cholinergic receptors seems to be crucial to induce persistent firing in many brain areas as the application of cholinergic antagonist (e.g. pirenzepine or atropine) completely blocked carbachol induced PF, indicating also that the activation of M_1 muscarinic receptors is essential [50,113,180,194]. In addition to the muscarinic receptors stimulation, also the activation of group I metabotropic glutamate receptors ($mGluR_1$ and $mGluR_5$) [50,158,180] with glutamatergic agonist (e.g. DHPG) has been proven to support persistent firing. In fact, the application of MPEP, a selective $mGluR_5$ antagonist, blocked glutamatergic induced persistent firing [180]. Interestingly the activation of muscarinic or glutamatergic receptors has been shown to induce persistent activity in neurons in the anterior cingulate cortex, the same group of neurons that showed PF during carbachol application responded in the same way DHPG and vice versa [180].

In summary, multiple studies reported that the activation of muscarinic and/or glutamatergic receptors can facilitate the induction of persistent neuronal firing. Although there is a large consensus about the involvement of these G-protein coupled receptors in supporting PF, up to now we still lack a comprehensive understanding of which ion channels mediate the depolarization plateau potential and persistent firing.

1.6 Persistent firing supported by TRPC channels

In the previous sections we saw that persistent firing is present in many brain areas related to learning and memory, and we saw growing experimental evidence suggesting the involvement of CAN current in supporting intrinsic persistent firing via TRPC channels [26,111,173,174]. In this section I will describe the TRPC channel family, their distribution in the brain and I will give an overview of the experimental evidence suggesting that TRPC channels support persistent firing.

1.6.1 TRPC channel family and structure

TRPCs are the mammalian homologues of drosophila TRP channels and are members of the TRP super-family of cation channels. In general, all the members of the TRP super-family have six transmembrane sequence and are permeable to cations. The TRP channels has been classified in six sub groups based on their primary structure: TRPC, TRPM, TRPP, TRPV, TRPA and TRPV (Fig. 8) [195–197].

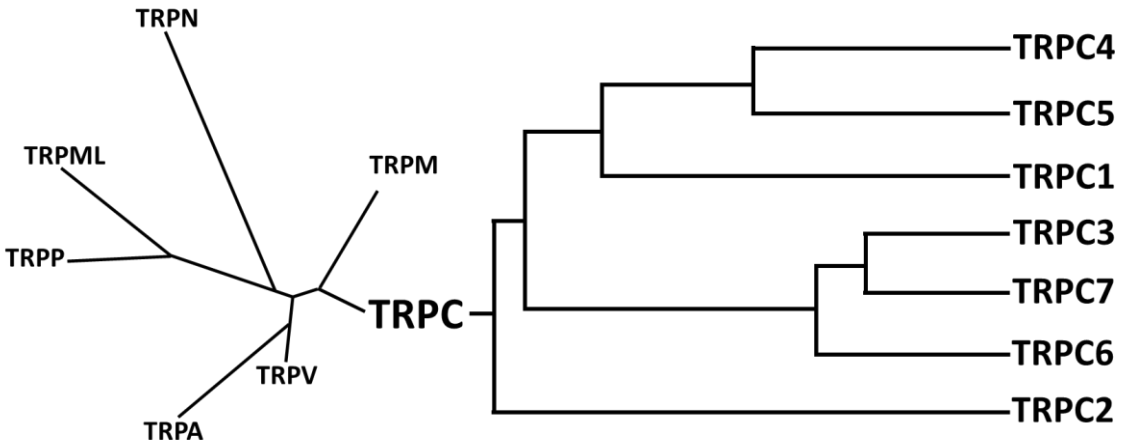

Figure 8 - Phylogenetic tree of the TRP superfamily.
The scheme represents the phylogenetic subdivision of the TRP super family (left) and the subdivision of the TRPC family (right) (Fig. 3 from Venkatachalam et al. 2007, modified and adapted.)

The TRPC subfamily includes seven members (TRPC1 to TRPC7), all of them share a common structure of six transmembrane domains, they are tetrameric and permeable to Na^+, K^+ and Ca^{2+}. These ion channels can be homomultimeric and there is experimental evidence indicating that TRPC1, TRPC4 and TRPC5 or TRPC3, TRPC6 and TRPC7, respectively, can interact and form heteromultimeric channels (Fig. 9) [198–201]. In mammals all the seven TRPCs forms have been identified, except in humans where TRPC2 is a pseudogene and only

six TRPCs forms can be found [202,203]. Based on the amino acid similarities the TRPC family can be divided in 4 subgroups: TRPC1, TRPC2, TRPC4/5 and TRPC3/6/7 [195]. The genetical subdivision also reflect the different activation of these channels: while the activation of TRPC2, TRPC3, TRPC6 and TRPC7 is mediated directly by diacylglycerol (DAG), the activation of TRPC1, TRPC4 and TRPC5 is polymodal [26,174]. The complex and variegated activation mechanisms of TRPC will be discussed in detail in a separated section.

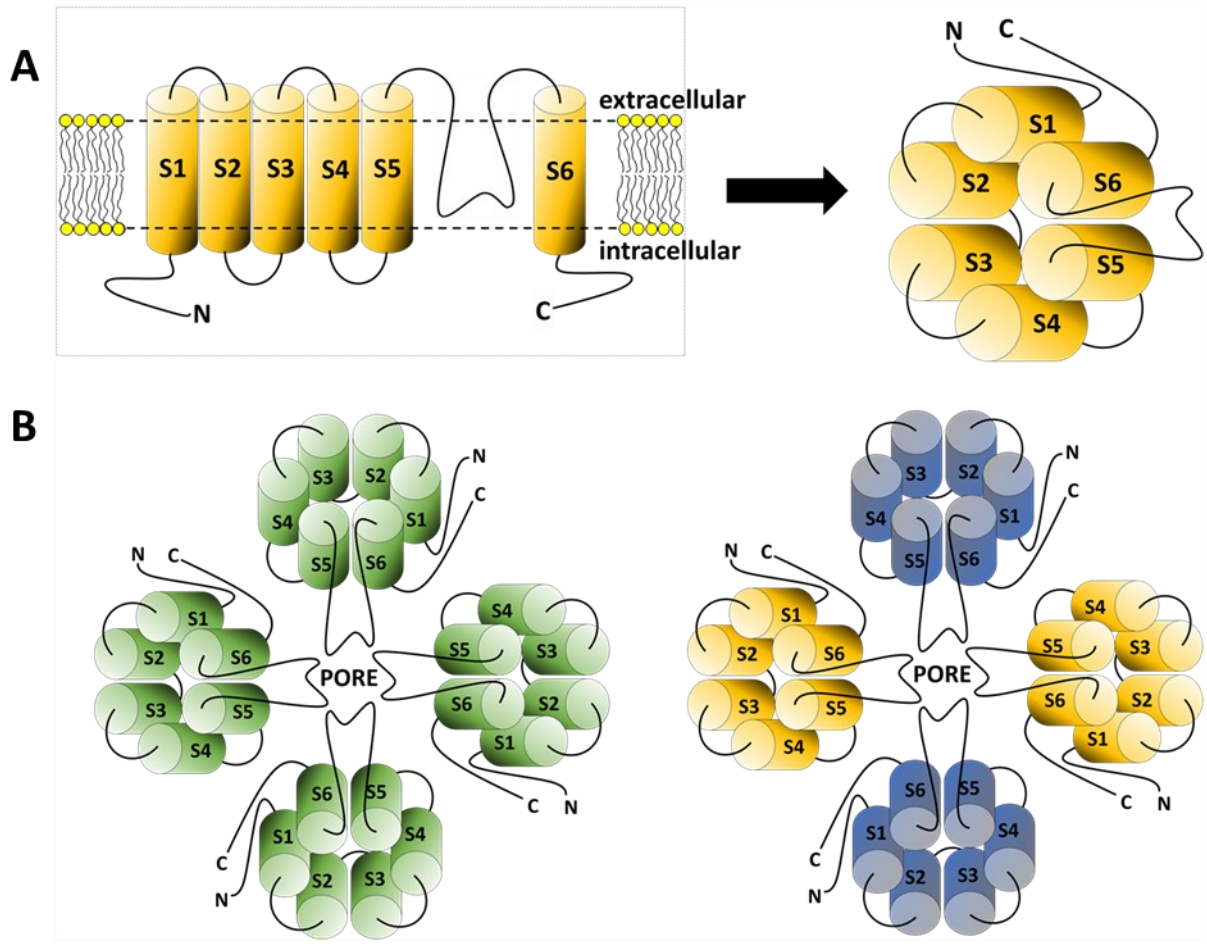

Figure 9 - Structure of TRPC channels.

(A) TRPC channel subunit has six transmembrane domains (S1-S6), and the pore region is between the fifth (S5) and the sixth (S6) transmembrane domain. The dashed line (left) represent the cellular membrane. The N-terminus and the C-terminus lies both in the intracellular side of the membrane. On the right there is the proposed structure of TRPC channels. (B) Structure of a TRPC tetramer. The channels can be homo-tetramers (left) or hetero-tetramers (right).

1.6.2 TRPC channels distribution in the brain

All the TRPC channels are highly expressed in several brain regions of rodents [204]. In a study from Fowler and colleagues (2007) it was reported that TRPC4 and TRPC5 are the predominant forms expressed in the brain [205]. In this study it was also shown that the expression levels of TRPC subunits are similar between rats and mice (Fig. 10A) [205]. In rat hippocampus, TRPC1, TRPC3, TRPC4 and TRPC5 are expressed in the pyramidal neurons in the CA1, CA2, CA3 and in the granule cells in the dentate gyrus (Fig. 10B). TRPC6 are also expressed in the hippocampal formation but their presence seems to be limited only to the molecular layer of the dentate gyrus and to the interneurons [198,206,207]. In mice, TRPC1, TRPC4 and TRPC5 are highly expressed through the hippocampus and also in the amygdala [208,209]. In particular in the CA1 pyramidal cells of the hippocampus, the TRPC1, TRPC4 and TRPC5 mRNA is highly expressed [185,205,210]. TRPC3 are also expressed in the hippocampus, but mainly in the CA1 and CA3 layers and at lower levels when compared to TRPC4 and TRPC5 channels [211]. In the entorhinal cortex TRPC1 and TRPC5 channels show a strong expression in all layers [205,209]. In other brain areas TRPC4 and TRPC5 expression is particularly strong in the corticolimbic system, while in the prefrontal cortex TRPC5 is mainly located in layers II–III and V–VI [205].

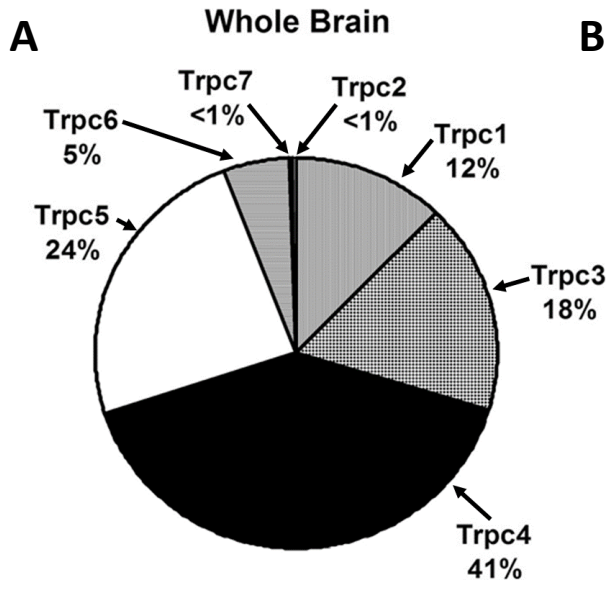

B

	TRPC4	TRPC5
Amygdala	++	+
Caudate putamen	0	0
Cerebellum		
Molecular layer	0	+
Purkinje cell layer	++	++
Granule cell layer	++	++
Corpus collosum	0	0
Entorhinal cortex	++	+++
Habenula	++	+++
Hippocampus		
CA1	+++	+++
CA2	+++	+++
CA3	++	+++
Hilus	+	+++
Dentate gyrus	++	++
Hypothalamus		
Dorsal	0	+
Ventral	++	++
Paraventricular	+	+++
Islands of Caleja	0	+++
Lateral septum	+++	0
Medial Septum	+	0

	TRPC4	TRPC5
Motor cortex		
Layer 1	0	0
Layer 2/3	++	++
Layer 5/6	++	++
Nucleus accumbens		
Core	0	+
Shell	0	++
Orbitofrontal cortex	++	+++
Piriform cortex	++	+++
Prefrontal cortex		
Layer 1	0	0
Layer 2/3	++	+++
Layer 5/6	++	+++
Somatosensory cortex		
Layer 1	0	0
Layer 2/3	++	++
Layer 5/6	++	++
Subiculum	+++	++
Substantia nigra	+	0
Tenia tecta	+++	++
Thalamus	0	++
Rank 0<+<++<+++		

Figure 10 - Expression of TRPC channels in rat brain.

(A) The pie chart shows the relative expression of the seven TRPC subunits determined using real-time PCR. (B) The table represent the results of a qualitative analysis of TRPC4 and TRPC5 mRNA expression in rat brain. The expression level is referred as: (0) no expression, (+) little expression, (++) moderate expression, (+++) high expression (Fig. 2 and Table 2 in Fowler et al. (2007); modified).

1.6.3 TRPC activation and modulation

Several studies, showing pharmacological, molecular and functional evidence, strongly suggest a strong contribution of CAN current in supporting persistent firing [23,50,66,170,171,181]. This kind of persistent firing, supported by CAN current, is thought to be driven mainly by TRPC channels and in general, the activation of these channels is mediated by G-protein coupled receptors [111,174,180,194,212,213]. The activation of phospholipase C (PLC), mediated by the G-coupled receptors, targets PIP_2 and it leads to production of diacylglycerol (DAG) and of inositol 1,2-cyclic phosphodiester that will be hydrolysed to inositol 1,4,5-trisphosphate (IP_3) [214]. Therefore, the two end products of PLC are DAG and IP_3. The TRPC family can be divided in two sub-groups based on the activation mechanisms, one including TRPC1, TRPC4, TRPC5 and the other one including TRPC2, TRPC3, TRPC6 and TRPC7. While the latter group has DAG as specific activator, the activation of the TRPC1/4/5 group can be polymodal and can be mediated by G-protein coupled receptors, vesicular translocation to the membrane or the rise of intracellular Ca^{2+} concentration [174,204]. The activation of the G-coupled receptors can start an intracellular cascade leading to the activation of TRPC channels and inducing a sustained membrane depolarization (plateau potential). If this sustained depolarization reaches the firing threshold of the neuron, it can trigger persistent firing.

We saw that the activation of TRPC channels (CAN current) requires the activation of metabotropic receptors coupled to G-protein pathways [195,215]. However, besides the activation mediated by G-proteins coupled receptors, other intracellular mechanisms have been reported to be involved in the TRPC channels activation (Fig. 11).

The activation and modulation of TRPC channels are complex and not yet fully understood, even if a growing number of studies are unveiling step by step the various cascades and mechanisms regulating these channels activation. An in-depth discussion of these mechanisms is beyond the scope of the introduction to this dissertation; however, I will give a short overview pointing out the pathways known so far and focusing on TRPC4 and TRPC5, the two TRPC forms mostly expressed in the brain.

$G_{q/11}$-PLC cascade

Among the TRPC family, TRPC4 and TRPC5 channels are activated by $G_{q/11}$ stimulation [216,217], and TRPC1/4 heteromers channels can also be activated by $G_{q/11}$ stimulation [218]. The level of phosphatidylinositol 4,5-bisphosphate (PIP_2) has been reported

to affect TRPC1, TRPC4 and TRPC5 and a reduction of the membrane PIP_2 can activate the channels [219,220].

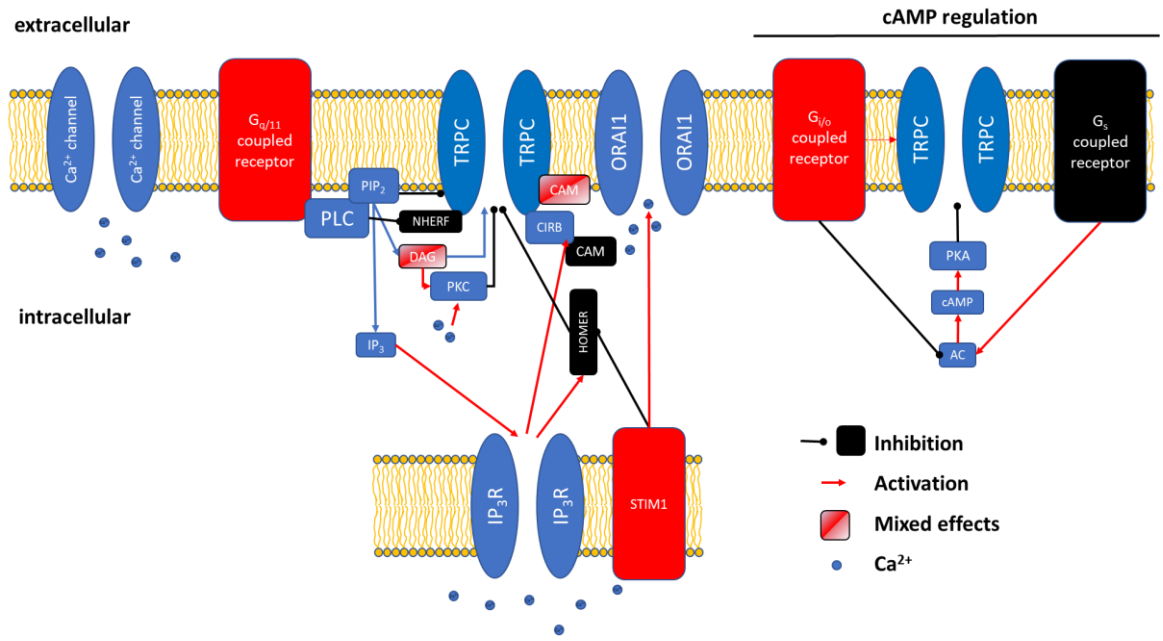

Figure 11 - TRPC channels modulation mediated by intracellular cascade triggered by G-protein coupled receptors.

The intracellular cascade is complex and involve multiple membrane and cytoplasmatic factors: Ca^{2+} from extracellular and intracellular sources that will interact with calmodulin (CAM) which bind to the CIRB and calmodulin binding domains of the TRPC; phosphorylation mechanisms by PKC and PKA; physical coupling with cytoskeletal proteins (Homer, NHERF) that convey physical modifications of other proteins such as IP_3R, STIM1 or PLC; direct interaction with metabolites such as PIP_2 or DAG and binding of other proteins such as IP_3R (Fig. 3 in Reboreda et al. (2007)).

IP_3R and Ca^{2+} regulation

The intracellular concentration of calcium plays a very important role in the TRPC channels modulation and inositol 1,4,5-trisphosphate (IP_3), one of the products of PLC hydrolysis of PIP_2, increases the intracellular concentration of calcium ($[Ca^{2+}]_i$) by releasing it from the intracellular stores and also through calcium influx from voltage gated calcium channels. The regulation of TRPC channels mediated by IP_3 receptors (IP_3R) and by the $[Ca^{2+}]_i$ is extremely complex as TRPC channels have at least one calmodulin/ IP_3R binding domain (CIRB) [221–223] and so IP_3R can directly bind to TRPC channels [224,225]. It has been reported that as the $[Ca^{2+}]_i$ increases, the calmodulin is removed from the CIRB and the IP_3R can bind to CIRB to activate the channel [226]. However, another mechanism of activation involving Homer, a scaffolding protein, has been described. Homer can interact both with TRPC and IP_3R forming a TRPC-Homer-IP_3R complex that normally keeps the channels closed. The dissociation of this complex following IP_3R activation is necessary to

allow STIM1 to get access and open the channel [227]. This may suggest that IP_3R activation leads to TRPC channel opening regardless of activation mechanisms involved. However the activation of IP_3R and the increase of intracellular calcium concentration generally activate the TRPC channels, nevertheless, TRPC4, TRPC5 and the heteromer TRPC1/5 can also be activated by PLC-β or PLC-γ without IP_3R involvement [198,217,228]. In addition to the IP_3 receptors binding domain, TRPC channels have a calmodulin (CAM) binding domain [229] that can modulate the TRPC channels differently depending on the TRPC subunits forming the channel. For example, through CAM binding to TRPC channels an intracellular rise of calcium could potentiate channels containing TRPC5 subunits [229] or suppress channels containing TRPC1 subunits [230]. In summary, the modulation and the activation of TRPC channels mediated by IP_3 and the $[Ca^{2+}]_i$ is complex and variegated, having different effects depending also on the TRPC subunits that are forming the channels.

DAG regulation

The other product of PIP_2 hydrolysis, mediated by PLC, is diacyl glycerol (DAG). DAG can directly activate TRPC2/3/6/7 [228,231,232] but it can also activate PKC. Despite classic studies indicating that PKC phosphorylation of TRPC3/4/5 inhibits these channels [228,233], some recent studies show the opposite [234]. In this study from Storch and colleagues (2016) it was reported that DAG can activate TRPC4 and TRPC5 if it is in concomitance with a decrease of PIP_2.

$G_{i/o}$, G_s and cAMP regulation

$G_{i/o}$ and G_s regulate the activity of adenylate cyclase by inhibiting and activating it, respectively. This leads to changes in cyclic adenosine monophosphate (cAMP) levels and the modulation of protein kinase A (PKA) activity. In HEK293 cells, TRPC4 has been reported to be activated by G_i, G_o and M_2 receptors which activate Gi/G_o [218,235]. On the other hand, this mechanism of activation does not affect TRPC5 or TRPC6 [218,235]. It is interesting to mention that, when TRPC4 is forming heteromer channels with TRPC1, G_i does not longer activates this channel but $G_{q/11,}$ coupled with M_1 or M_3 receptors, does [218]. G_s activation has been shown to inhibit TRPC4 and TRPC5, but not TRPC6. This inhibitory effect is mediated by PKA activated by cAMP and it can be triggered by β2 adrenergic receptors in the presence of GTPγS (a general G-protein activator) [236]. But it was also reported that, depending on the conditions, TRPC5 can be activated or inhibited by G_s activation [237]. β2 adrenergic receptors stimulation, without the presence of GTPγS, can actually activate TRPC5 by release of calcium from the intracellular stores mediated by cAMP [237].

In summary: while Gs and high levels of cAMP seem to impair working memory and suppress TRPC channels, Gi/o and inhibition of cAMP seem to improve working memory and enhance TRPC activation.

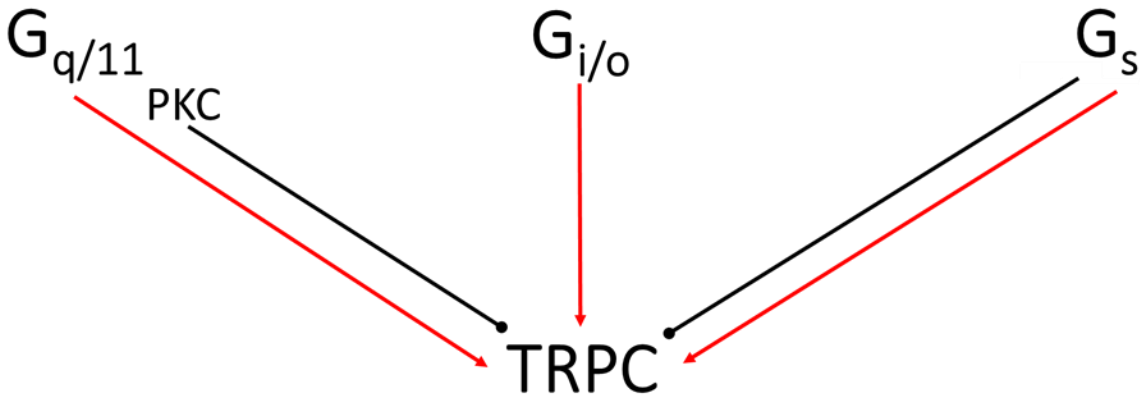

Figure 12 - Effects of G-protein coupled receptors on TRPC channel activation.

The red arrows indicate positive effects and black lines with circle ends indicate negative effects. The $G_{q/11}$ cascade (left) is necessary for TRPC activation, but through PKC it can also inhibit TRPC. $G_{i/o}$ (middle) activation reduces cAMP and activated TRPC. G_S inhibits TRPC channels (right), however in some conditions it can activate TRPC5 (Fig. 4 from Reboreda et al. (2018); modified).

As we can see, the signaling pathway activating and modulating TRPC channels are complex and depending on many factors like: which subunits form the channels, the concentration of the agonist used, which receptors and G-proteins are activated (Fig. 12). However, despite their complex modulation, several studies suggest that the activation of TRPC channels via G-protein coupled receptors supports persistent neuronal firing.

1.7 Involvement of TRPC channels in persistent firing

Cholinergic receptor activation has been reported to be crucial for working memory performance and for persistent firing [4,238,239]. In the hippocampus and other cortical areas, *in vitro* evidence showed that the stimulation of muscarinic receptors can activate a *calcium-activated non selective cationic* (CAN) current [191,240,241] while suppressing potassium currents [242–244]. When the CAN current is activated by muscarinic receptors stimulation, a brief period of spiking activity can lead to a further activation of the CAN current by increasing the extracellular calcium influx, subsequentially leading to membrane depolarization (plateau potential) and, if the depolarization is strong enough, to persistent firing [171,181,193,241,245]. Growing experimental evidence suggests that CAN current mediate persistent firing and several studies indicate TRPC channels as main candidates to support CAN current [111,173,174]. Persistent firing mediated by TRPC channels (CAN current) has been shown in the hippocampus, in the entorhinal cortex and in many brain areas including amygdala, perirhinal cortex, cingulate cortex, prefrontal cortex, auditory cortex and neocortex [50,66,109,111,162,170,171,181].

In the following sections I will present evidence indicating that TRPC channels support persistent neuronal firing and I will also present some critics to this hypothesis.

1.7.1 Pharmacological evidence

Pharmacological TRPC blockers have been used to test the role of these channels in supporting persistent neuronal firing and plateau potential. In several brain area general TRPC blockers, such as flufenamic acid (FFA), SKF96365 and 2-APB, have been shown to suppress both PF and plateau potential in the hippocampus [110,160], postsubiculum [109], entorhinal cortex [50,111,170], prefrontal cortex [194,205,246], perirhinal cortex [162], amygdala [175] and cingulate cortex [180]. I will now present some of these pharmacological evidence focusing first on studies indicating that TRPC channels can support plateau potential and then I will focus on studies focusing on the role of TRPC in supporting persistent firing.

In a study from Fowler and colleagues (2007) in the PFC, patch clamp recordings were performed in the layer V pyramidal neurons and a delayed after-depolarization was induced during glutamatergic stimulation by a brief burst of action potentials. The consequent application of FFA or SKF96365 on top of DHPG, significantly reduced the delayed after-depolarization induced by the stimulus [205]. Interestingly in this study they investigated the expression levels of TRPC channels using real time PCR and showed that TRPC4 and TRPC5

were the two mostly expressed channels in the whole brain. In this study from Fowler and colleagues (2007), in situ hybridization showed that these two channels are highly expressed in the PFC layers and in the CA1 hippocampus and in the EC [205]. Taken together, these results indicate that TRPC channels support the after stimulus depolarization observed during glutamatergic stimulation.

Besides glutamatergic stimulation also muscarinic stimulation has been shown to induce an after stimulus depolarization in the PFC layer V neurons [246]. In this study the ionic mechanism underlying the slow and fast depolarization induced by muscarinic activation were studied using patch clamp recording in slice preparation. It was shown that the slow after depolarization induced by the application of carbachol was suppressed after the application of FFA. This suggested that an inward and non-selective cation current, like CAN current supported by TRPC channels, was mediating it [246].

The application of general TRPC blockers has been reported to affect not only the plateau potential, but also persistent firing. In a study from Egorov and colleagues (2002), sharp electrode recordings were performed in the layer V of the entorhinal cortex and they reported that the application of FFA completely suppressed persistent firing [50]. In this study PF was induced by local synaptic stimulation or by the application of a depolarizing pulse in presence of carbachol and synaptic blockers. These results indicate that in this neurons PF can be mediated both by network and intrinsic mechanisms. The application of atropine or pirenzepine, both muscarinic antagonists, suppressed PF indicating that this neural activity was muscarinic dependent. In this study it was also reported that mEC layer V neurons could show graded persistent firing [50]. Another study on the EC layer V focused on how the plateau potential and persistent firing are generated [111]. In this study it was shown that muscarinic receptors-evoked persistent firing required: phospholipase C activation, decrease of PIP_2 levels and an optimal intracellular calcium concentration. TRPC general blockers, FFA, SKF-96365 and 2-APB, were tested and all of them suppressed persistent firing induced during carbachol application indicating that TRPC channels were mediating persistent firing in these neurons [111].

Persistent firing supported by TRPC channels has been reported not only in the layer V but also in the layer III of entorhinal cortex. Tahvildari and colleagues (2008) reported that in the lateral EC layer III, pyramidal neurons showed cholinergic-dependent persistent firing and the bath application of FFA suppressed both persistent firing and the post stimulus plateau potential [170]. In addition, PF was abolished by calcium removal from the extracellular solution, suggesting again that CAN current, activated in response to the calcium

influx during the application of the depolarizing stimulus, was supporting it [170]. Persistent firing sensitive to FFA has been reported also in other cortical areas such as the perirhinal cortex [162] and the cingulate cortex [180].

Finally, also in the hippocampus persistent firing sensitive to flufenamic acid, general TRPC blocker, has been reported. In a previous study from our lab, muscarinic dependent and intrinsic persistent firing was observed in rat hippocampus in CA1 pyramidal cells [110]. In this study, persistent firing was induced by a depolarizing current step applied from under the firing threshold of the neurons during carbachol application. The application of flufenamic acid suppressed persistent firing suggesting a role of TRPC channels (CAN current) in supporting this mechanism (Fig. 13). In addition, in these experiments persistent firing was triggered in presence of synaptic blockers, indicating that intrinsic mechanisms were supporting it.

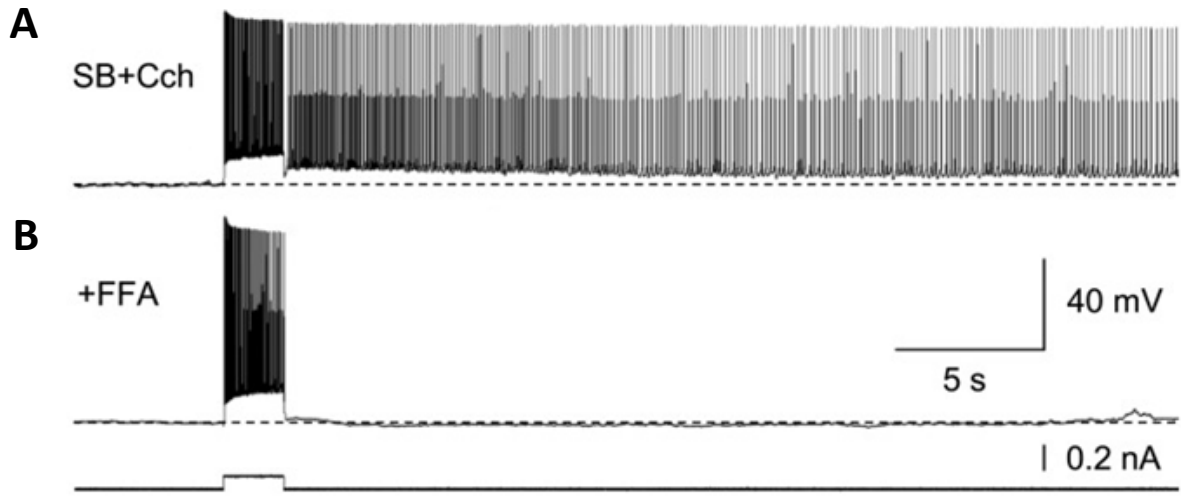

Figure 13 – Flufenamic acid suppression of persistent firing in rat CA1 pyramidal neuron.
(A) Persistent firing induced by a current pulse (2 sec, 0.2 nA) during carbachol (Cch) application and in presence of synaptic blockers (SB). (B) In the same neuron recorded in (A), persistent firing was blocked after the application of flufenamic acid (FFA) (Fig. 5 from Knauer et al. (2013); modified).

In another study of our lab, patch clamp recordings in CA3 pyramidal neurons reported the presence of intrinsic and muscarinic-dependent persistent firing sensitive to FFA. During the application of carbachol, PF was observed in presence of synaptic blockers and the application of atropine suppressed it. The application of flufenamic acid blocked persistent firing suggesting that CAN current was supporting it [160]. In a very recent paper from our lab, ML204, a novel TRPC selective blocker, was tested to assess the role of TRPC channels in supporting cholinergic-dependent depolarization block in rat CA1 pyramidal neurons [177]. Cells were categorized as showing depolarization block when at any point in time after, or

during the stimulation, the membrane potential was more depolarized than the cells action potential threshold but nonetheless, they did not fire action potentials. In this experiment depolarization block was induced by a depolarizing current pulse during cholinergic stimulation. The application of ML204 successfully decreased the intensity and the strength of the strong depolarization triggered by the stimulus and leading to depolarization block. This indicated that TRPC channels are supporting the mechanism generating depolarization block. However, in this study ML204 was not directly used to assess the role of TRPC channels in supporting persistent firing [177].

Many studies using general TRPC channels blockers, such as SKF-93635, 2-APB and flufenamic acid, are supporting the hypothesis that these channels are mediating persistent activity, however some critics raised because these classical blockers are not selective and can also affect other ion channels, some of which have been proven to support persistent firing. Among the affected channels there are L- and T-type calcium channels [172,194,247], voltage-gated sodium channels [248,249], chloride channels [250], cardial potassium currents [251], and some subtypes of TRPM, TRPV and TRPA channels [252]. In addition, these general blockers do not show selectivity for specific TRPC channel subfamilies. Therefore, in my thesis I tested more recently identified and more specific antagonists such as ML204 [253], clemizole hydrochloride [254] and Pico145 [255].

1.7.2 Intracellular application of anti-TRPC antibodies

Before the advent of more selective TRPC antagonists, some groups successfully used antibodies to target TRPC channels [189,211,256,257]. In these studies, anti-TRPC antibodies were reported to inhibit the activity of TRPC channels activated by glutamatergic or neurotrophic stimulation. In one of the aforementioned studies, El-Hassar and colleagues (2011) applied intracellularly antibodies to study the role of TRPC channels in supporting a glutamatergic dependent depolarization in CA1 pyramidal cell [189]. The application of antibodies targeting TRPC1/4/5 channels reduced the amplitude of a depolarization observed after DHPG puff application. Interestingly, the application of FFA and SKF-96365 gave the same result. In this study the depolarization mediated by CAN current was induced by glutamatergic activation via $G_{q/11,}$ indicating that the ion mechanism supporting the depolarization was very similar to the one involved in persistent firing, induced by glutamatergic and also cholinergic activation.

Experimental evidence shows that the intracellular application of anti-TRPC

antibodies can inhibit these channels, however, until now anti-TRPC antibodies were never used to test the involvement of these channels in cholinergic-dependent persistent firing.

1.7.3 Molecular and genetic evidence

To overcome the lack of specific inhibitors for TRPC channels, some groups used molecular and genetic approaches to study functions and properties of these channels [111,113,173,185,194,258,259]. In these studies, it was investigated the role of TRPC in supporting CAN current, plateau potential and persistent firing. I will first present studies that tested the role of TRPC channels in supporting CAN current and cholinergic-dependent plateau potential [173,194].

A study from Yan and colleagues (2009) reported that TRPC channels mediate a calcium-activated afterdepolarization (ADP) induced by muscarinic activation, in addition it was also reported that this mechanism involves G$\alpha_{q\text{-}11}$ coupled receptors and PLCβ [194]. In this study performed in HEK-293 cells, the co-expression of TRPC5 and α1G calcium channels were sufficient to observe a muscarinic dependent inward current. While the over expression of TRPC5 or TRPC6 seemed to facilitate the slow ADP, the application of FFA, or the expression of a pore dead TRPC5 subunit, inhibited it. All these experiments indicate that TRPC channels are underlying CAN current and mediating the cholinergic-dependent slow after-depolarization [194]. Also in cultured CA1 pyramidal neurons TRPC5 channels have been shown to underly CAN current and the cholinergic-dependent plateau potential [173]. In this study it was reported that muscarinic stimulation significantly enhances the levels of TRPC5 on the membrane surface, but it did not increase the levels of TRPC1 and TRPC4.

Besides testing the involvement of TRPC channels in supporting CAN current and plateau potential, genetic approaches have also been used to study the role of TRPC in supporting persistent firing. Zhang and colleagues (2011) extensively studied the function of TRPC channels in the layer V of the entorhinal cortex. Besides using the classical TRPC channels blockers, such as FFA, 2-APB, SKF96365, they also used the peptide EQVTTRL that selectively disrupts interactions between TRPC4/5 subunits and PDZ (PSD-95/Discs-large/ZO-1). TRPC4/5 channels have a PDZ binding domain in their C-terminal region that mediate the association with PDZ, a cytoskeletal protein belonging to the NHERF family [260]. A disruption of the TRPC-NHERF interactions has been reported to reduce the channels activation [260,261]. In the study from Zhang and colleagues, the intracellular application of the peptide EQVTTRL reduced the activity of TRPC channels and strongly suppressed persistent firing, suggesting that TRPC channels support persistent activity [111].

Several studies also used TRPC knock out (KO) mice to assess the role of these channels in supporting the plateau potential and persistent firing [113,185,258,259]. Phelan and colleagues reported that the plateau potential is suppressed in TRPC1/4 double KO, TRPC1 KO [185] and TRPC7 KO mice [258]. In the study focusing on TRPC1 and TRPC4 [185], the plateau potential was induced in septal neurons by a current pulse while bath applying an mGluR agonist. In the TRPC1/4 double KO animals the plateau potential (depolarization) was completely abolished while in the TRPC1 KO animals it was abolished in 74% of the neurons, indicating that TRPC4 and TRPC1/4 heteromer play a crucial role in this mechanism.

Despite all this evidence supporting the role of TRPC channels underlying persistent firing, some of the recent studies using TRPC KO mice challenge this view. While plateau potential was suppressed in TRPC1/4, TRPC4 and TRPC7 KO mice in septal, CA1 and CA3 neurons [185,258], Dasari and colleagues (2013) reported that plateau potential was not altered in the medial prefrontal cortex of TRPC1, TRPC5, TRPC6 and TRPC5/6 double KO mice [259]. Egorov and colleagues (2019) have shown that persistent firing in TRPC1/4/5 triple KO and TRPC1-7 hepta-KO was intact in the EC layer V [113]. Besides these studies using KO models, also a recent study using pharmacological tools suggested that, in prefrontal cortex, cholinergically induced persistent firing is supported by the hERG potassium channels and not by TRPC channels [112]. Nevertheless, recent behavioral studies reported that TRPC 1/4/5 triple KO mice [262] and TRPC1 KO mice [263] are impaired in working memory tasks, which is very much in line with the idea that TRPC dependent persistent firing supports working memory.

As we can see, experimental evidence collected with general TRPC inhibitors and anti-TRPC channels suggests that TRPC channels, by mediating CAN current, support intrinsic persistent firing in many brain areas. However, these results are challenged by the fact that the general blockers have been proven to be not specific, affecting also other ion channels. In addition, recent studies using TRPC KO yield mixed and controversial results: while some studies suggest a role of these channels in supporting persisting firing, other state the opposite. Therefore, further investigation is needed to assess the involvement of TRPC channels in intrinsic persistent firing.

2 METHODS

2.1 Animals and housing

Twelve to fourteen-week-old male mice were used for all the experiments. The animals were maintained in standard condition with a 12:12 hours light-dark cycle. Food and water were provided ad libitum. For the *in vitro* electrophysiology experiments the following strains were used: 129S6/SvEvTac provided by Taconic, TRPC5 flx/flx provided by Dr. Lutz Birnbaumer (NIEHS), TRPC4 KO provided by Dr. Marc Freichel (Heidelberg University) [264] and C57BL/6 provided by Charles River or by the local animal facility.

129S6/SvEvTac were the wild type mice used in all the experiments testing drugs, antibodies and also used as control for the experiments using TRPC5 flx/flx. These genetically modified animals were in fact developed from 129S6/SvEvTac mice. C57BL/6 mice were used for the *in vitro* electrophysiology experiments performed in the medial entorhinal cortex. The immunohistochemistry experiments were all performed on C57BL/6 animals.

All experimental protocols were approved by the local ethic committee (Der Tierschutzbeauftragte, Ruhr-Universität Bochum and Deutsches Zentrum für Neurodegenerative Erkrankungen) and by the Ethical Committee on Animal Health and Care of Saxony-Anhalt state, Germany (license number: 42502-2-1388).

2.2 Chemicals and drugs

All drugs were purchased from Sigma Aldrich and Carl Roth (unless stated otherwise). Carbachol was purchased from Alfa Aesar, clemizole hydrochloride and ML204 were purchased from Tocris, Pico145 was obtained from Dr. Robin Bon (University of Leeds). Carbachol is very frequently used in our lab and its stock solution (water based) is known to last unspoiled for months at +4°C. Clemizole hydrochloride, ML204 and Pico 145 were diluted in DMSO and, to prevent degrading, they were all stocked at -20°C and de-frozen right before use. The drug dissolved in DMSO were diluted in nACSF 1000 times or more.

2.3 Antibodies

2.3.1 Antibodies used in the immunohistochemical stainings

Several antibodies were tested for TRPC4, TRPC5 and calbindin to establish the immunohistochemical (IHC) staining protocols (Table 1). The primary antibodies where chosen based on the epitope they could target and then tested. When possible, antibodies used in previous publications were used. The minimum working concentrations of the primary antibodies were chosen based on the results of the stainings or based on previous publications. The secondary antibodies were chosen accordingly to the primary antibodies and their specificity was confirmed by minimal level of background signal in the control experiments.

Primary Antibody	Clone type	Source	Manufacturer	Dilution
Anti-TRPC4 (extracellular)	polyclonal	Rabbit	Alomone Labs	1:500
Anti-TRPC5	monoclonal	Mouse	NeuroMab/NIH	1:1000
Anti-Calbindin D-28k	polyclonal	Rabbit	Swant	1:1000
Anti-Calbindin D-28k	monoclonal	Mouse	Swant	1:1000

Secondary Antibody	Target	Source	Manufacturer	Dilution
HRP Conjugate	Mouse	Sheep	Jackson Labs	1:1000
HRP Conjugate	Rabbit	Goat	Jackson Labs	1:1000

Table 1 - List of antibodies used in this thesis for the immunohistochemical stainings.

Different anti-TRPC4 and anti-TRPC5 antibodies have been tested, but only two showed results comparable to previous publication when used at low concentration. The anti-TRPC antibodies chosen for the IHC stainings were the anti-TRPC4 (extracellular) antibodies from Almone Labs (Israel) and the anti-TRPC5 antibodies from Neuromab (USA). The anti-TRPC4 antibodies (Alomone) are directed against an epitope located in the second extracellular loop of the channels (Epitope: 458-469). The anti-TRPC5 antibodies (Neuromab) are directed against an epitope located close to the intracellular C-terminus (Epitope: 827-845). To test the presence of calbindin in the medial entorhinal cortex, antibodies from Swant Inc. (Switzerland) were used. Anti-calbindin antibodies have been extensively used in previous studies, like in the study from Naumann et al., (2016) [71]. In my IHC stainings I used anti-calbindin D-28k from mouse or rabbit depending on the primary antibodies used to target the TRPC channels. The secondary antibodies were conjugated with horseradish peroxidase and were obtained from Jackson ImmunoResearch Lab. Sheep anti-

mouse and goat anti-rabbit antibodies were used in my experiments as secondary antibodies. In my IHC stainings, the detection was made possible by horseradish peroxidase on the secondary antibodies reacting with a fluorescent dye (Cy3/Cy5 TSA plus fluorescence kit).

All antibodies were ordered in the lyophilized powder form and were stored at -20°C upon arrival. After reconstitution antibodies were aliquoted and stored at -70°C. After de-freezing, aliquots were kept up to two weeks at +4°C. After this time, they were discarded.

2.3.2 Antibodies used in patch clamp experiments

The antibodies used in the patch clamp experiments were the anti-TRPC4 from Neuromab (USA) and the anti-TRPC5 from Almone Labs (Israel). Both antibodies targeted an epitope in the intracellular part of the channels. The anti-TRPC4 antibodies targeted the C-terminal tail of the channel (Epitope: 930-947) while the anti-TRPC5 antibodies targeted the C-terminal tail of the channel (Epitope: 959-973). The storing conditions of the antibodies used in the patch clamp experiments were the same described in the IHC stainings, the only difference was that, after de-freezing, the aliquots were stored at +4°C and used up to 5 days. After this time, they were discarded. Inactivation of the antibodies was achieved by incubating the antibodies at 90°C for 10 min.

2.4 Immunohistochemical stainings

Mice were euthanized via intraperitoneal injection of narcobarbital overdose before being transcardially perfused with ice cold isotonic NaCl solution containing Na-heparin (25000 IE). Afterwards the animals were perfused with 4% paraformaldehyde (PFA) in phosphate buffered solution (PBS, pH 7.4) until the liver became brighter and the body stiff. After extraction, the brains were additionally post fixed in a 4% PFA-solution overnight and transferred to 30% sucrose in PBS (sucrose-solution) for 24 hours for cryoprotection. At the end of the 24 hours the brains normally sank, meaning that the cryoprotection step succeeded. The cryoprotected brains were finally snap frozen with dry ice. Brains were stored at -80°C until use. Coronal 60 µm thick section were cut with a Leica CM3050 cryostat using Sakura Tissue-Tek OCT compound and collected as free-floating sections in antifreeze-solution (50% glycerol + 50% sucrose-solution). The brain sections were stored in -20°C until staining.

For staining, sliced tissue sections were rinsed (3 times in PBS), quenched by 0.2% H_2O_2 in PBS for 30 minutes at room temperature (RT). Slices were again rinsed before blocking by incubation in 0.3% Triton-X in PBS (PBST) and 3% bovine serum albumin (BSA) for 30 min. Afterwards primary antibodies (AB) were applied in the same blocking solution overnight at RT. Primary antibodies against mouse were additionally incubated with a mouse anti-mouse blocking agent (Vector Labs) in PBS for 30 min after the first blocking step. After rinsing, secondary AB were applied in blocking solution and incubated for 60 min at RT, followed by another rinsing step. Peroxidase-conjugated antibodies were used against the corresponding origin animal of the first AB: goat anti-rabbit (Jackson, 1:1000) or sheep anti-mouse (Jackson, 1:1000). A signal amplification kit (TSA plus cyanide 4 or cyanide 5, PerkinElmer) was applied. Sections were therefore incubated in the dark for 7 min, rinsed 3 times with 0.3% Tween 20 in Tris buffered solution (TBST) and then DAPI stained for 20 min. After rinsing with TBST, slices were mounted on glass object slides with glycerol and sealed. All mounted sections were stored at 4°C until image acquisition.

In case of double stainings, the protocol used for the first staining was then repeated for the second staining using a different primary antibody. In this extended protocol used for double stainings the main procedures were not changed, but the staining with DAPI was performed only once at the end of the labelling (for more details about protocol and solutions please refer to the supplementary material section).

Analysis for stainings in the medial entorhinal cortex layer II

Images were acquired using a fluorescence microscope (Keyence BZ-9000) and data analysis was performed with Matlab. Images were taken at different magnification (x2, x4, x10, x20) and for higher magnifications (x10, x20) multi-plane (z-stack) images (1-2 µm focal distance per image) were taken if needed. For intensity measurements, only raw or equally processed images were used.

In each image three region of interest (ROI) were manually selected: “island”, “ocean” and “layer II of MEC”. The “island ROI” was placed inside a calbindin positive clusters (island). The “ocean ROI” was placed above or below the calbindin cluster. Both the “island” and “ocean” ROI were circular and had a standard size, smaller than the average island cluster in mouse. The third region of interest, “layer II of MEC” ROI was manually selected using a polygonal ROI. The borders of the layer II were identified by using the island clusters borders following the approach used also in a previous study from Naumann et al. (2015) [71]. This procedure was repeated in case multiple calbindin islands were present in the same brain section.

The brightness (pixel intensity) was used to measure the expression level. Although absolute quantitative detection was not intended, depending on signal intensity, with this method it was possible to compare the expression levels in the same sections. First the intensity of the “layer II of MEC” was measured to obtain the average intensity of the whole layer II. Then, the average intensity values of calbindin and TRPC4 or TRPC5 were measured in the manually selected “island” and “ocean” ROIs. Afterwards the intensities of “island” and “ocean” ROIs were normalized using the average intensity of the “layer II ROI”. This analysis was performed by Jens Schweihoff under my supervision.

2.5 In vitro patch clamp recording

2.5.1 Solutions used for the recording in the hippocampal CA1

Current clamp experiments

In the current clamp experiments, three kind of solutions were used: normal artificial cerebrospinal fluid (nACSF), a choline chloride based cutting solution and a potassium gluconate based intracellular fluid (ICF). The nACSF contained (in mM) 126 NaCl, 1.2 NaH_2PO_4, 26 $NaHCO_3$, 1.5 $MgCl_2$, 1.6 $CaCl_2$, 3 KCl and 10 glucose (~305mOsm). The pH was adjusted by saturation with 95% O_2 - 5% CO_2. The choline chloride based cutting solution contained (in mM): 110 choline Cl, 7 $MgCl_2$ ($6H_2O$), 0.5 $CaCl_2$, 2.5 KCl, 25 glucose, 1.2 NaH_2PO_4, 25 $NaHCO_3$, 3 pyruvic acid, 11.5 ascorbic acid, 100 D-Mannitol (~415mOsm). I used this cutting solution because an ACSF containing choline chloride has been reported to be particularly suitable for the preparation of brain slices in aged animals (*brainslicesmethods.com*). The pH was adjusted by saturation with 95% O_2 - 5% CO_2. After preparation nACSF and cutting solution were stored up to 5 days at 4°C. In both nACSF and cutting solution the pH was adjusted by saturation with 95% O_2 - 5% CO_2. The intracellular solution contained (in mM): 120 K-gluconate, 10 HEPES, 0.2 EGTA, 20 KCl, 2 $MgCl_2$, 7 PhCreat di(tris), 4 Na_2ATP, 0.3 Tris-GTP (~290mOsm). The pH was adjusted at 7.3 with KOH. For labeling purposes, biocytin was added into the intracellular solution at 0.1% concentration.

During the experimental procedures both cutting and recording solutions were constantly bubbled with carbogen (95% O_2 - 5% CO_2) to oxygenate the slices and to maintain the pH stable. After recording the slices were stored at 4°C in a PBS solution with PFA 4% to preserve them before performing a biocytin staining. The 4% PFA PBS solution was either prepared in our lab and contained (in mM): 19 NaH_2PO_4 and 81 NaH_2PO_4 or it was bought from Carl Roth (Roti®- Histofix 4 %). In some cases, the slices, after the fixation with PFA, were preserved in a cryoprotective solution at -20°C before the staining. The sucrose based cryoprotective solution contained 50% glycerol and 50% of PBS 0.1M with 30% sucrose. The cryoprotective preservation did not alter the morphological properties of the neurons.

Voltage Clamp

In the voltage clamp experiments the intracellular solution and the recording solution were slightly different from the one used in the current clamp experiments. The intracellular solution contained (in mM): 130 Cs^+ methanesulphonate, 5 CsCl, 5 NaCl, 2 $MgCl_2$, 10

HEPES, 0.5 EGTA, 2 ATP, 0.4 GTP (the pH was adjusted to 7.2 with KOH). For labeling purposes, biocytin was added into the intracellular solution at 0.1% concentration. The nACSF had the same composition of the one used in the current clamp experiments but mixed with 500 nM TTX and 5 mM Cesium. The cutting solution and the preservation of the slices did not differ from the one used in the current clamp experiments.

2.5.2 Solutions used for the recording in the entorhinal cortex

In the current clamp experiments performed in the medial entorhinal cortex I used three kind of solutions: normal artificial cerebrospinal fluid (nACSF), a sucrose based cutting solution and a potassium gluconate based intracellular fluid (ICF).

The nACSF contained (in mM): 124 NaCl, 1.25 NaH_2PO_4, 1.8 MgO_4S, 3 KCl, 10 glucose, 26 $NaHCO_3$, 1.6 $CaCl_2$. The cutting solution contained (in mM): 87 NaCl, 25 $NaHCO_3$, 10 glucose, 75 sucrose, 2.5 KCl, 1.25 NaH_2PO_4, 0.5 $CaCl_2$, 7 $MgCl_2$, 3 pyruvic acid, 1 ascorbic acid. In both nACSF and cutting solution the pH was adjusted by saturation with 95% O_2 - 5% CO_2. After preparation nACSF and cutting solution were stored up to 5 days at 4°C. The intracellular solution used in these experiments was the same one used in the current clamp experiments in the hippocampus. In the MEC experiments performed at DZNE and testing 3 μM clemizole hydrochloride, the solutions used were like the solutions used for the current clamp experiments performed in hippocampus. The only change was the addition of kynurenic acid (2 mM) and picrotoxin (0.1 mM) in the nACSF. These synaptic blockers were always freshly mixed in ACSF the same day of the experiments. The storage solutions and the preservation of the slices did not differ from the one used in the current clamp experiments performed in the hippocampus.

2.5.3 Preparation of brain slices

Mice were deeply anesthetized with isoflurane and cervical dislocation was performed. The brain was quickly removed from the skull and immersed in oxygenated ice-cold cutting solution. After one minute the cerebellum and the rostral part of the brain were removed. For the preparation of hippocampal slices, the brain was glued with cyanoacrylate to the bottom of the slicing chamber with the rostral part in contact with the glue. For the preparation of MEC slices, the ventral part of the brain was glued to the bottom of the slicing chamber. About six coronal brain slices per hemisphere (350 μm thick) were obtained with a vibrating-blade microtome (Leica VT1000S, Leica Biosystems, Wetzlar, Germany). Brain slices were then individually transferred to a holding chamber filled with normal ACSF (nACSF). In this

holding chamber, the slices were incubated at 37°C for 35 min in nACSF and additionally for at least 30 min at room temperature before recording. The pH of the cutting solution and nACSF were adjusted by a constant saturation with carbogen (95% O_2 - 5% CO_2).

Due to differences in the ethical committee decision, the sacrificing procedure of the experiments performed at the RUB University was slightly different. This refers to all the MEC experiments excluding the one testing 3 μM clemizole hydrochloride. In these experiments the mice were deeply anesthetized with an intraperitoneal injection of ketamine/xylazine (120 mg/Kg ketamine and 16 mg/Kg xylazine). After extinction of the reflexes, the animals were intracardially perfused with ice-cold cutting solution and then the brain was quickly removed from the skull. The following procedures did not differ from the one previously described.

2.5.4 Recording procedures

Brain slices were transferred from the holding chamber to a submerged recording chamber fixed on an anti-vibration table. In the recording camber the slices were continuously super fused with nACSF, kept at 35°C ± 1.0. In the first part of the project, the solution was warmed only by an in line-heater (Warner Instruments) placed right before the chamber. With this heating system to obtain the desired recording temperature, the solution had to be pre-heated to 45-50°C. Unfortunately high temperatures has been reported to compromise the stability and effectivity of ML204 [177,253]. For this reason, we designed a new custom recording chamber. With this new chamber it was possible to drastically reduce the temperature of the in-line heater to maximum 33-35°C and still achieve the desired recording temperature (Fig. 14). This change made possible to test ML204 at my standard recording temperature (35°C). The influx of nACSF to the recording chamber was provided by gravity and the efflux of the nACSF was provided by a peristaltic pump (Minipuls 3, Gilson). The brain slices were placed in the recording chamber, fixed with a custom-made anchor, and visualized with an upright microscope (Zeiss Axioskop 2FS plus, Carl Zeiss Microscopy) equipped with a 4x objective lens, a 40x water-immersion objective lens and a monochrome camera (WAT-902H Ultimate). The desired region on the brain slice was targeted using the 4x objective lens and then the pyramidal layer was identified with the 40x lens. Patch pipettes (3-8 MΩ) obtained from borosilicate glass capillaries (Science Products), were pulled on a P-87 horizontal puller (Sutter instrument). Pipettes were filled with intracellular solution filtered using a 0.2 μm cellulose acetate syringe filter.

The whole-cell patch configuration was achieved by forming tight seals (>1 GΩ) on the soma and rupturing the membrane with light negative pressure. Liquid junction potential was not corrected. The access resistance was compensated several times during the recordings, and it was done using a negative current pulse injection (50 pA, 100 ms). Electrical signals were amplified with a Multiclamp 700B amplifier (Axon Instruments), low pass filtered at 10 kHz and sampled at 20 kHz and recorded using WinWCP software (John Dempster, University of Strathclyde). After recording, the slices were stored at 4 °C in a PBS solution with 4% PFA.

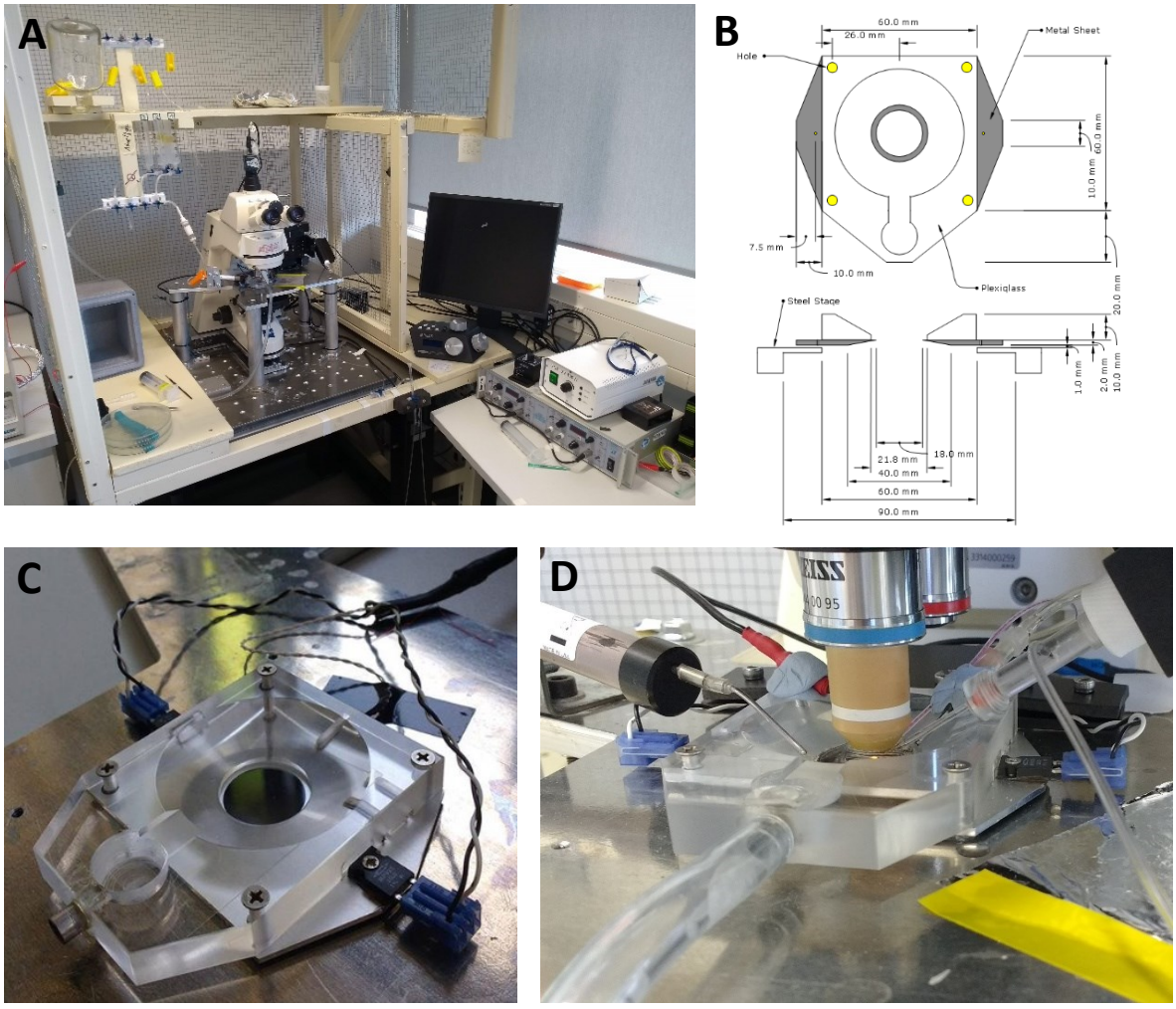

Figure 14 - *In vitro* electrophysiology setup.

(A) A picture of my patch clamp set up. (B) A detailed project of the custom-made recording chamber with the new heating plate under the recording chamber (grey). (C-D) Picture of the recording chamber out of the patch clamp set up (C) and a picture of the same chamber during an experiment with a 40x lens immersed in the recording bath.

2.5.5 Biocytin staining

In my projects two different biocytin staining protocols were used to assess the anatomical position and morphology of the recorded neurons. In the experiments performed in Bochum the biocytin labeling of neurons was made using an avidin–biotinylated horseradish peroxidase complex (ABC) and visualized using DAB (3,3'-Diaminobenzidine) as a chromogen, which forms a black reaction product (for more details please refer to the supplementary material section). In this staining, the black reaction product prevented the visualization of GFP fluorescent protein in the recorded cells infected with an AAV vector (Fig. 15A). Therefore, I tried with success another biocytin staining protocols using streptavidin covalently attached to a fluorescent label (Fig. 15B). Beside permitting to visualize GFP, this new staining was also more reliable compared to the previous one base on horseradish peroxidase.

In the new staining protocol, the brain slices containing the recorded cells (biocytin filled) were stored at +4°C in a PBS solution with PFA 4% for maximum 3-4 weeks, afterwards the staining was performed or the slices were preserved in a cryoprotective solution at -20°C before the staining. The sucrose based cryoprotective solution contained 50% glycerol and 50% of PBS 0.1 M with 30% sucrose. The cryoprotective preservation did not alter the morphological properties or the staining of the neurons. The first step of the staining was to rinse the slices in a tris-buffered saline solution containing 0.5% Triton-X-100 (TBS-Tx) 5x15 minutes. Afterwards the slices were incubated overnight at RT with the streptavidin conjugated to a fluorescent tag (1:300; Streptavidin, Alexa Fluor 647 conjugate, Thermo Fisher Scientific). The day after the slices were rinsed again in TBS-Tx three times for 15 minutes and mounted on microscope slides with Mowiol and cover slips. The mounted slices were then stored at +4°C in the dark. The TBS-Tx contained (in mM): 153 NaCl, 50 Trizma Base and 0.5% Triton X-100. The pH was adjusted to 8.0 using HCl. After preparation, the solution was stored at +4°C up to 1 week.

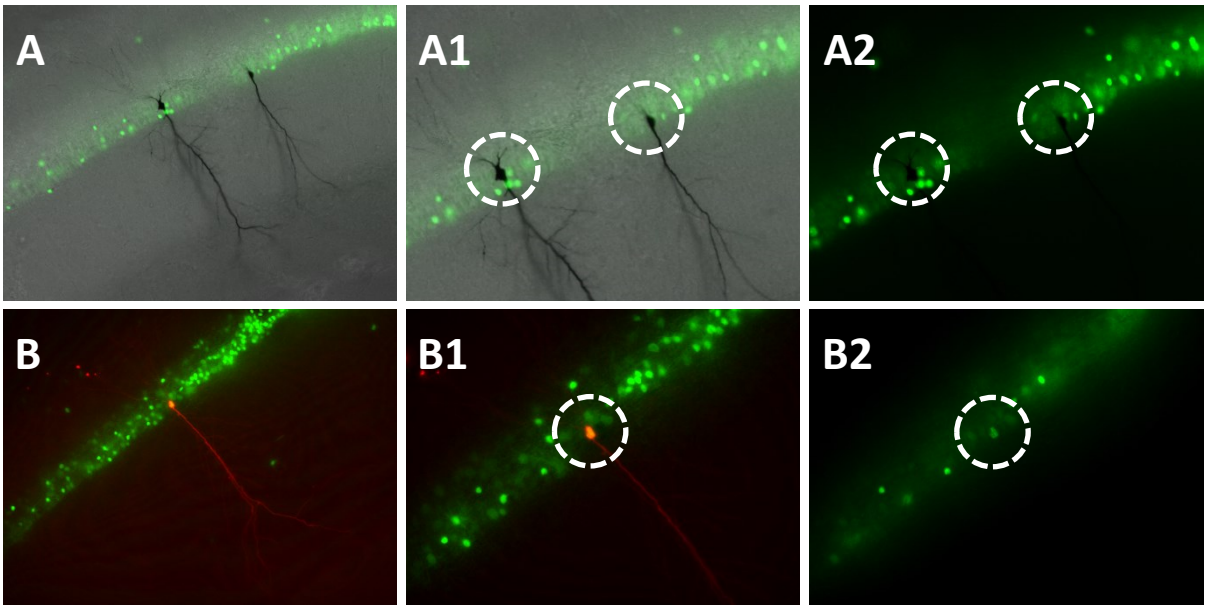

Figure 15 - Examples of different biocytin stainings.

(A) Picture of two pyramidal cells (in black) stained using DAB as chromogen. The neurons were recorded in the CA1 region infected with an adenoviral vector (AAV-Cre-GFP). In this image the pictures obtained from the bright field and fluorescence channels were overlaid. (A1) Higher magnification of the picture showed in (A). (A2) Same picture showed in (A1) but showing only the image from the fluorescence channel. The dashed circles highlight two cells in which, due to the chromogen, it was not possible to detect GFP fluorescence. (B) Picture of a pyramidal cell (in red) stained using a fluorescent marker. The neuron was recorded in the CA1 pyramidal layer infected with an adenoviral vector (AAV-Cre-GFP). In this image the pictures obtained from two different fluorescence channels were overlaid. (A1) Higher magnification of the picture showed in (A). The dashed circle highlights the recorded GFP positive cell. (A2) Same picture showed in (A1) but showing only the image from the GFP fluorescence channel. In the middle of the dashed circle the recorded GFP positive cell is visible.

2.6 Viral infection

The adeno-associated viruses used in the experiments were purchased first from UPenn and then from Addgene. Even if the supplier name changed, the virus producer and the virus were the same. The viruses were shipped in dry ice and upon arrival it was stored at -70°C. To prevent degradation of the viruses due to freeze-thaw cycles, they were aliquoted in mono-dose Eppendorf tubes defrosted moments before the bilateral stereotaxic injection. In the patch clamp experiments two viruses were tested: AAV5.CMV.GFP-Cre.SV40 and AAV5.CMV.eGFP.SV40.

The AAV-Cre-GFP virus (AAV5.CMV.GFP-Cre.SV40) fluorescently marked with GFP the infected cells and led to the expression of Cre recombinase. In these infected cells, Cre recombinase induced the excision of the target sequence between the two loxP sites leading to the TRPC5 conditional knock out in the TRPC5 flx/flx animals (Cre-lox system). In these animals the two loxP sites are flanking the exon 5 of the TRPC5 gene. After infection, the Cre recombinase expression lead to the loss of the exon 5 preventing the formation of a functional channel.

The AAV-GFP virus (AAV5.CMV.eGFP.SV40) was meant to serve as control in my experiments, as it marked the infected cells with GFP, but it did not induce the expression of Cre recombinase. However, the GFP expression was not strong enough to be detected by the microscope and the camera available in the patch clamp set up. For this reason, I used as controls for the patch clamp experiments GFP negative cells, recorded from animals infected with AAV-Cre-GFP virus, and WT cells, recorded from non-infected wild type animals.

2.6.1 Stereotaxic viral injections

The AAV injections were performed in 8-9 week-old mice. The mice were anesthetized with a with a cocktail of ketamine (65 mg/kg), xylazine (20 mg/kg) and acepromazine (3 mg/kg) injected intraperitoneally and positioned in a stereotaxic frame. The virus was administered bilaterally targeting the dorsal and ventral hippocampal CA1 areas in each hemisphere. The coordinates for the two injections targeting the dorsal hippocampus were: -2.1 AP, ± 1.25 ML and -1.2 DV. The coordinates for the two injections targeting the ventral hippocampus were: -2.7 AP, ± 2.2 ML and -1.4 DV. In every injection site, 0.65 µL of virus was injected at a rate of 0.3 µL/minute by using a Hamilton syringe. Following the virus delivery, the syringe was left in place for 6 minutes before being slowly withdrawn from the injection site. After surgery, the animals were housed in single cages and the patch clamp experiments were performed two or four weeks after the viral infection.

2.7 Genotyping

As in the work of this dissertation genetically modified animals were used, the genotype of the different strains was checked to be sure that the used mice had the right genotype. In my experiments genotyping was performed for the TRPC5 flx/flx mice, the TRPC4 KO animals and for the WT as a control. The genotyping experiments were performed in Bochum with the help of Prof. Lars I. Leichert (Institute of Biochemistry and Pathobiochemistry, Microbial Biochemistry, Ruhr-Universität Bochum) and in Magdeburg by the Leibniz-Institute for Neurobiology (LIN), having a genotyping service.

TRPC5 flx/flx mice genotyping

Tail samples were collected with a scissor and were stored at 4°C for a short storing period or at -20°C for a longer storing period. Afterwards the samples went under lysis to prepare the DNA sample for the PRC. The primer pairs for the wild type alleles and for the flx/flx mutant allele were the same (5'- GGCGCAGAAAGAGTTTATGGGGA' and 5'- GGATGTTGGCTCTGTGAAACAATGACTC) and the length of the products was ~450 bp for the wild type and ~550 bp for the flx/flx animals. When interpreting into these data it was important to remember that the gene expressing TRPC5 channels is situated on the X chromosome, so male mice have only one allele and so they can only be homozygous, wild type or flox/flox. Therefore, heterozygous can only be observed in female mice. The first step of the PCR reaction was at 94°C for 3 minutes, then followed 40 cycles of 30 sec at 94°C, 45 sec at 58°C and 1 min at 72°C. Then a final 7 min step at 72°C. To check the results was used a QIAxcel Advanced System (Qiagen) with the QIAxcel DNA Screening Kit.

TRPC4 KO mice genotyping

For the TRPC4 KO animals the procedure to check their genotype was the same one described above besides that the primer pairs used for the KO animals were: 5´-ACAGTGCTCTGAACCCACGG - 3´and 5´- GCCTGCTCTTTACTGAAGGCTCT- 3´. The length of the products was 290 bp for the wild type and 364 bp for the TRPC4 KO animals.

2.8 Quantitative PCR

Quantitative PCR (qPCR) was used to examine TRPC5 flx/flx animals injected with AAV-GFP (n = 5) or AAV-Cre-GFP (n = 5). Four weeks after infection the animals were anesthetized and perfused with PBS and 4% PFA prepared under RNAse-free conditions. Afterwards the brains were quickly removed and post fixated in 4% RNAse-free PFA 24 hours at 4°C. The perfusion and extracting procedure were exactly like the one previously described, the main difference was in the additional steps made to avoid RNA contamination. In all the procedures RNAse free solutions were used and to achieve that the distilled water used to prepare the PBS and the PFA was treated with dimethyldicarbonate (DMDC, Sigma). The DMDC water was prepared by adding 0.01% DMDC to distilled water. To prevent undesired contamination all the glass ware used to prepare the solutions used during the perfusion was baked for at least 3 hours at 180°C in an oven. After the post fixation in 4% PFA the brains were snap-frozen in cooled methylbutane. The collected brains were then cut in coronal slices (20 µm thick) using a cryostat and mounted on 0.05 % poly-L-lysine coated RNase-free PEN membrane slides (Carl Zeiss). Afterwards the infected CA1 and CA3 regions were micro dissected using a laser microbeam dissection system (Carl Zeiss) by marking them up using the PALM software under 5x magnification, cutting them out by the laser and capturing them in an adhesive cap capture device.

Sample lysis, removal of genomic DNA and isolation of total RNA were done with the RNeasy FFPE kit (Qiagen) according to manufacturer's instructions. First-strand cDNA was synthetized using the Takara Prime Script reverse transcription kit (Clontech Laboratories), specifically designed for low amounts of RNA, in the presence of 10 mM dNTPs and a mix of 2.5 µM Oligo dT and 20 µM random hexamer first strand primers at 42°C for 30 min followed by enzyme inactivation step at 94°C for 5 min.

A multiplex real-time PCR was performed with a 1:5 dilution of cDNA using the ABI Prism Step One real-time PCR apparatus (Life Technologies) and TaqMan reagents with predesigned assays for the target genes (assay IDs: TRPC1: Mm00441975_m1, TRPC3: Mm00444690_m1, TRPC4: Mm00444280_m1, TRPC5: Mm00437183_m1, TRPC6: Mm01176083_m1, TRPC7: Mm00442606_m1) and for the housekeeping gene glycerinaldehyd-3-phosphat-dehydrogenase (GAPDH; endogenous control; Life Technologies) that was labeled with another fluorescent dye, allowing for quantitative evaluation.

All samples were run in triplicates with 50 cycles of 30 sec at 95°C and 60 sec at 60°C, preceded by an initial denaturation step at 95°C for 5 min.

Relative mRNA expression levels were determined using the ddCT method. The mean cycle threshold (CT) of each triplicate assay was first normalized to the overall content of cDNA using GAPDH as an internal control (dCT; $dCT_{\text{target gene}} = CT_{\text{target gene}} - CT_{\text{GAPDH}}$) and then to the control group with $ddCT = dCT_{\text{sample}} - \text{mean } dCT_{\text{control group}}$.

Applying the formula $RQ\% = 2^{-ddCT} \times 100$ allowed for a relative quantification (RQ) of a specific target gene by calculating the percentage of its expression of the control group.

The quantitative PCR is not a technique normally performed in our group, for this reason these experiments were performed in Prof. Dr. Oliver Storks lab under the supervision of Dr. Anne Albrecht (Department of Genetics & Molecular Neurobiology, Institute of Biology, Otto-von-Guericke University Magdeburg).

2.9 Data analysis and statistical analysis

Data analysis was performed using GNU Octave (4.4.1, John W. Eaton, David Bateman, Søren Hauberg, Rik Wehbring), MATLAB R2014b/R2017b (MathWorks), and Prism (7.0, GraphPad Software).

After the rupture of the membrane in nACSF and in absence of current injection, cells showing spontaneous firing, or resting membrane potential more depolarized than -55 mV, were discarded and not included in the analysis, as this could indicate a cellular disequilibrium proper of injured and unhealthy cells. Persistent firing was quantified using the firing frequency and membrane potential depolarization.

Membrane potential properties

The membrane potential measure after the end of the stimulus (MP1) was calculated as the difference between the average of membrane potential during a 3 seconds period after the end of the stimulus, and the average of the baseline potential which was measured in a 3 seconds period directly before the stimulus onset. The 3 seconds period of MP1 started from the minimum membrane potential measured 0.2 seconds after the end of the stimulus.

The second membrane potential measure after the end of the stimulus (MP2) was calculated as done for MP1, but in this case the 3 seconds period of MP2 started 27 seconds after the minimum membrane potential measured 0.2 seconds after the end of the stimulus.

The membrane potential depolarization during the stimulus was measured as the difference between the average membrane potential during the 2 seconds stimulus and the average of the baseline potential which was measured in a 3 seconds period directly before the stimulus onset. Action potentials and fast after hyperpolarization potentials were not removed from the membrane potential analysis.

The input resistance was calculated by measuring the voltage peak in response to negative current pulse (1 s, -50pA) applied from -65 mV. The input resistance was calculated according to Ohm's law:

$$\text{Input Resistance} = (V_{BL} - V_{Peak}) / (I_{BL} - I_{Peak})$$

V and I were the membrane potential and the current values, respectively. V_{BL} refers to the average of the membrane potential during an interval of 0.5 seconds before the application of the negative pulse. I_{BL} represent the current used to hold the membrane at -65mV. V_{Peak} refers

to the minimum membrane potential value recorded during the pulse application. I_{Peak} is the value of the current at the peak point.

The sag ratio was calculated by measuring the voltage responses to a negative current pulse lasting 1 second. The intensity of this negative stimulus was chosen to achieve the sag peak as close as possible to -90 mV. This was made to be sure to have a good visualization of the sag by facilitating the activation of the current supporting it. The protocol was always applied from -65 mV. The sag ratio was calculated by using the following formula:

$$\text{Sag Ratio} = (MP_{Peak} - MPss) / (MP_{Peak} - MP_{BL})$$

MP_{Peak} represents the minimum voltage value recorded during the current injection. The steady state potential (MPss) was measured as an average of the membrane potential during the last 0.2 seconds of the current injection. The baseline membrane potential (MP_{BL}) was measured as an average of the membrane potential for 0.2 seconds right before the current injection.

Spike latency

The cells were kept at -65 mV and positive current pulses lasting 1 second (1s, 50pA) were consecutively applied increasing at every sweep the current intensity of 50 pA. The spike latency was calculated using the first sweep that could induce an action potential. The latency interval was measured from the beginning of the stimulus to the peak of the first spike.

Firing frequency of persistent firing

Persistent firing was induced using a 100 pA stimulus lasting 2 seconds holding the membrane potential right below the firing threshold of the cell. By always bringing the membrane potential just below the firing threshold, persistent firing could be analyzed and compared among different conditions. Persistent firing was measured during a 3 seconds period after the termination of the stimulation. The frequency of persistent firing was measured as the division of the number of spikes during these 3 seconds period by 3. The 3 seconds interval used to calculate the firing frequency after the end of the stimulus is the same also used to measure MP1. None of the recorded cell included in the analysis showed any spontaneous activity for at least 5 seconds before the application of the stimulation.

Statistical analysis

All statistical analyses were conducted with Prism (GraphPad Software). Shapiro–Wilk test was used to inspect the normality, F-test or Brown-Forsythe test were used to inspect the homogeneity of the variance, depending on the statistical requirements. Comparisons were made with parametric tests (unpaired, paired t-tests, ANOVA one way) or with non-parametric tests (Wilcoxon test, Mann-Whitney U test, Kruskal Wallis test). For multiple comparisons, Tukey's and Dunn's post-hoc tests were performed depending on the requirements. Significance level $\alpha < 0.05$ (* $p < 0.05$, ** $p < 0.01$, *** $p < 0.001$) was used. Unless stated otherwise, data were expressed as mean ± SEM (standard error mean).

3 RESULTS – Persistent firing in hippocampal CA1 pyramidal cells

3.1 TRPC4 and TRPC5 channels expression in mouse hippocampus

The TRPC channels are widely expressed in the brain [204] and, as reported in previous studies, among the seven TRPC channel subtypes (TRPC1-7), TRPC4 and TRPC5 are the most widely expressed in rodent hippocampus [205,209]. In situ hybridizations, provided by the Allen brain mouse atlas, also suggests that TRPC4 and TRPC5 are the subtypes mainly expressed in the hippocampus (http://portal.brain-map.org/). However, data on sub region specific expression of TRPC4 and TRPC5 within mouse hippocampus is still rather scarce. Therefore, immunohistochemical (IHC) stainings for TRPC4 and TRPC5 were performed in mouse brain before testing persistent firing in CA1 pyramidal neurons. The main goal was to assess the presence of TRPC4 and TRPC5 in CA1 mouse hippocampus. In the IHC stainings performed in the hippocampus, several primary antibodies were tested for both TRPC4 and TRPC5 and the results were compared to already published data when possible, or to the expected expression estimated from the mRNA expression levels provided by the Allen brain mouse atlas (http://portal.brain-map.org/). The primary antibodies were chosen according to their specificity in labelling the hippocampal region and to their effective concentration. The secondary antibodies were chosen accordingly to the primary antibodies and their specificity was confirmed by low level of background signal in the control experiments.

3.1.1 TRPC4 expression

Among the three TRPC4 antibodies tested, only the anti-TRPC4 (extracellular) from Alomone Labs gave the most comparable result to the already published data [208]. The immunohistochemical stainings targeting the TRPC4 revealed that these channels appear to be uniformly expressed among all the hippocampal sub regions (CA1, CA2 and CA3) (Fig. 16). This pattern of expression was shown in brain slices from three different animals. For more details about protocols and antibodies please refer to the methods section.

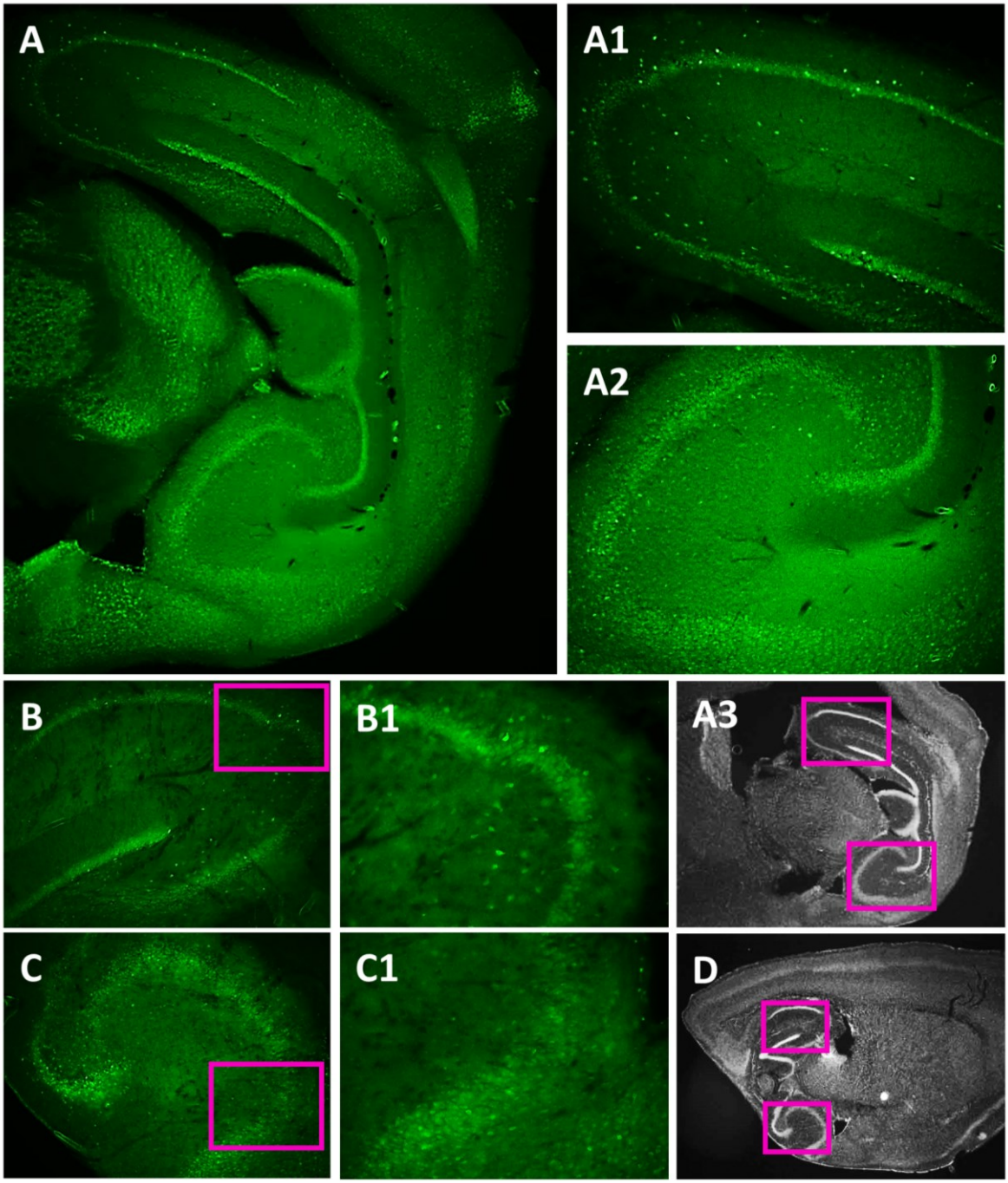

Figure 16 - TRPC4 expression in mouse hippocampus.

(A) TRPC4 expression in a sagittal slice of the hippocampus. (A1-2) Higher magnification images of dorsal and ventral hippocampus showed in (A). (A3) Low magnification image indicating the locations of the images in (A1) and (A2). (B) TRPC4 expression in dorsal hippocampus. (B1) Higher magnification image of (B). (C) TRPC4 expression in ventral hippocampus. (C1) Higher magnification image of (C). (D) Low magnification image indicating the locations of the images showed in in (B) and (C).

3.1.2 TRPC5 expression

The TRPC5 IHC stainings unveiled a different expression pattern among the ventral and dorsal hippocampus. In the ventral hippocampus, the TRPC5 expression appeared to be uniform among CA1, CA2 and CA3 (Fig. 17). In the dorsal hippocampus, TRPC5 seemed to have a different expression pattern (Fig. 17B): while CA2 and CA3 showed a uniform expression of TRPC5, the CA1 area appeared to have a different distribution of TRPC5. In the distal part of dorsal CA1, the cells seemed to express more TRPC5 compared to the proximal neurons. However, TRPC5 were expressed in all dorsal CA1 (Fig. 17B1). This pattern of expression was shown in brain slices from three different animals. For more details about protocols and antibodies please refer to the methods section.

In conclusion, the IHC stainings confirmed that both TRPC4 and TRPC5 were expressed in all subregions of hippocampus, including CA1, the area of interest of this project.

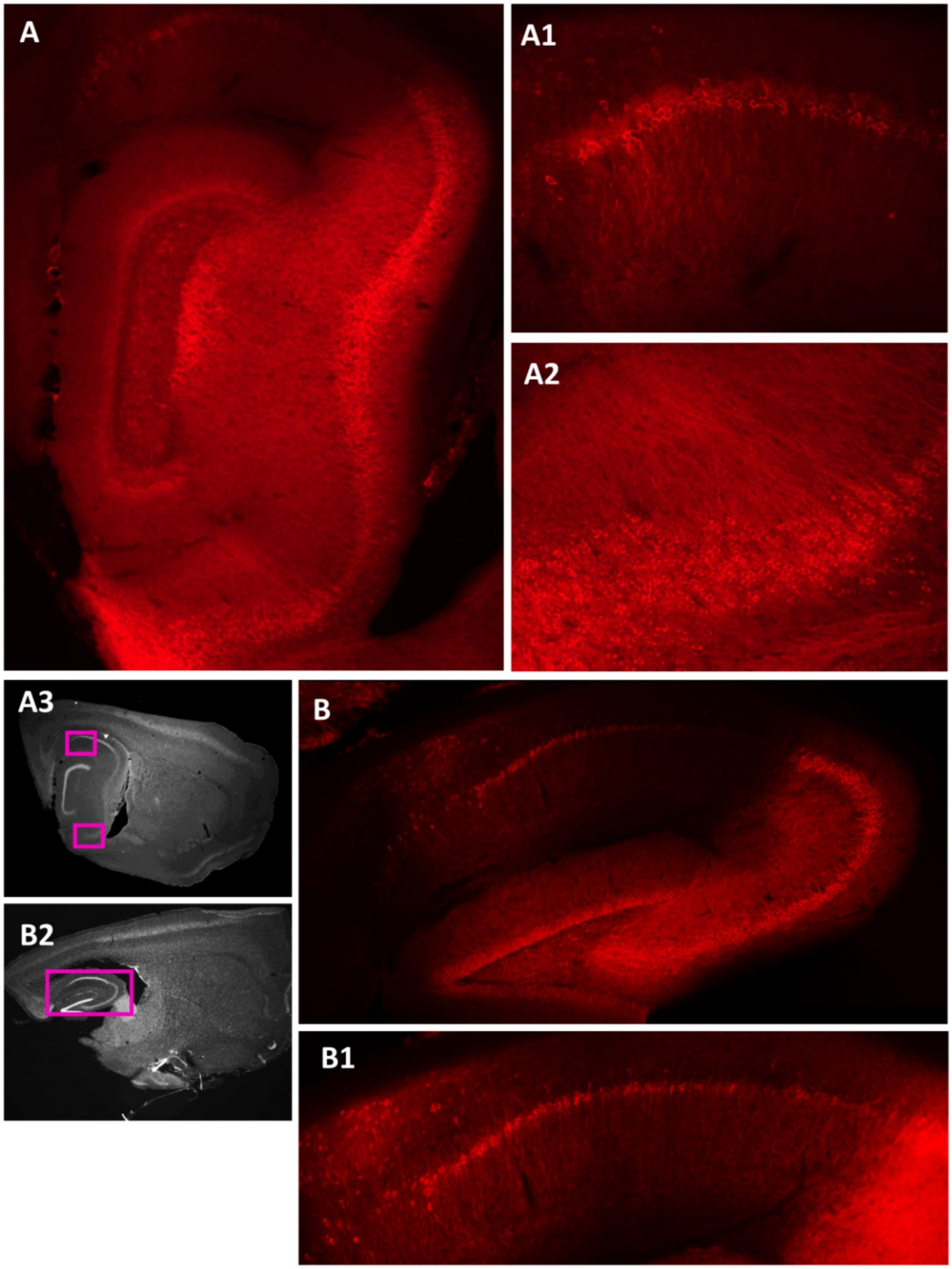

Figure 17 - TRPC5 expression in mouse hippocampus.

(A) TRPC5 expression in a sagittal slice of the hippocampus. (A1-2) Higher magnification images of dorsal and ventral hippocampus showed in (A). (A3) Low magnification image indicating the locations of the images showed in (A1) and (A2). (B) TRPC5 expression in dorsal hippocampus in a sagittal slice. (B1) Higher magnification image showing the expression pattern in CA1. (B2) Low magnification image indicating the location of the image in (B).

3.2 Cholinergic-dependent persistent firing of CA1 pyramidal neurons in the mouse hippocampus

Persistent firing has been reported in many brain areas related to working memory [22–26] and in previous studies of our lab it has also been observed in the in rat hippocampus in CA1 [110] and CA3 [160]. In my experiments, to trigger persistent firing in CA1 pyramidal neurons, I used protocols and methods similar to the ones used in our previous studies [110,160]. In these studies, persistent firing was induced by a depolarizing current pulse applied from under the firing threshold of the neuron during the application of a cholinergic agonist. Since the previous studies from our lab used rats instead of mice, I first tested if persistent firing was present in CA1 pyramidal neurons.

3.2.1 Cholinergic-dependent persistent firing

In my patch clamp experiments, the cells from a brain slice preparation were first recorded in normal artificial cerebrospinal fluid (nACSF) and then 10 μM carbachol (CCh) was bath applied. Carbachol is a non-selective cholinergic agonist that, in previous studies of our lab, has been shown necessary to induce persistent firing in the hippocampus [110,160]. After the application of carbachol, the membrane potential was slowly depolarized until its firing threshold by using a constant current injection. At this point, a square current pulse of 100 pA lasting for 2 seconds was applied to induce persistent firing (Fig. 18E). By always bringing the membrane potential just below the firing threshold, persistent firing could be analysed and compared among different conditions. All the recordings were performed at a temperature of 35°C ± 1.0.

In control condition, while the neurons were perfused with nACSF, none of the tested cells continued firing action potentials after the end of the stimulation (Fig. 18A, n = 35), confirming that, in CA1 neurons, the induction of persistent firing requires the activation of cholinergic receptors. After the application of carbachol, a cholinergic agonist, 80% of the cells showed persistent firing (Fig. 18B-E, n = 28). The remaining 20% of cells did not show persistent firing (n = 7).

Persistent firing was divided into three categories depending on how long the firing lasted and, on the membrane depolarization strength (Fig. 18F). These categories were: long lasting persistent firing (Fig. 18B), self-terminating persistent firing (Fig. 18C) and depolarization block (Fig. 18D). The majority of the recorded neurons showed self-terminating persistent firing (51%, 18/35 cells), in these neurons persistent firing lasted for

less than 30 seconds after the termination of the stimulus. The cells showing long lasting persistent firing were the 23% (8/35 cells), in these neurons the firing lasted more than 30 seconds after the end of the stimulus (Fig. 18B). A small number of neurons (6%, 2/35 cells), showed depolarization block during and/or after the end of the stimulus (Fig. 18D). During depolarization block, the membrane potential was so depolarized that normal action potentials could no longer occur. Normally these cells recovered by themselves, getting again less depolarized and starting to fire normal action potentials again (Fig. 18D).

During carbachol application, the average firing frequency of persistent firing of the all recorded neurons was 6.76 Hz ± 0.78 and was significantly higher compared to control condition (Fig. 18G, Wilcoxon, *** $p < 0.001$, $n = 35$). The firing frequency was measured during a 3 seconds interval after the end of the stimulus (Fig. 18B). When the firing frequency was measured only in neurons responding with persistent firing, the firing frequency was 8.44 Hz ± 0.66 ($n = 28$).

3.2.2 Membrane depolarization during persistent firing

To better quantify persistent firing, the membrane potential depolarization after the end of the stimulus was analysed in addition to the firing frequency. Two intervals were chosen to investigate the effects of cholinergic stimulation on the membrane potential. The first was a 3 seconds interval after the end of the stimulus, the second was a 3 seconds interval 27 seconds after the end of the stimulation (Fig. 18B). The first interval (MP1) was chosen to have a measure of how strong the cholinergic-dependent depolarization was after the stimulus and to have an overview of how pharmacological or genetical manipulation could affect the initial part of the cholinergic-dependent depolarization underlying persistent firing (plateau potential). The second interval (MP2) was chosen to measure if the depolarization induced by the cholinergic stimulation was long lasting or decreasing with time.

In control condition (nACSF), the membrane potential got first hyperpolarized after the end of the stimulus and then, after several seconds, it slowly depolarized back to baseline membrane potential (Fig. 18A, red horizonal bar). This behaviour is well represented by the average values of both MP1 and MP2. After the end of the stimulus, the average MP1 value shows a hyperpolarization of the membrane potential (Fig. 18H) and afterwards, as showed by the average MP2 value, the membrane potential went back to values close to the one it had before the stimulation (Fig. 18I).

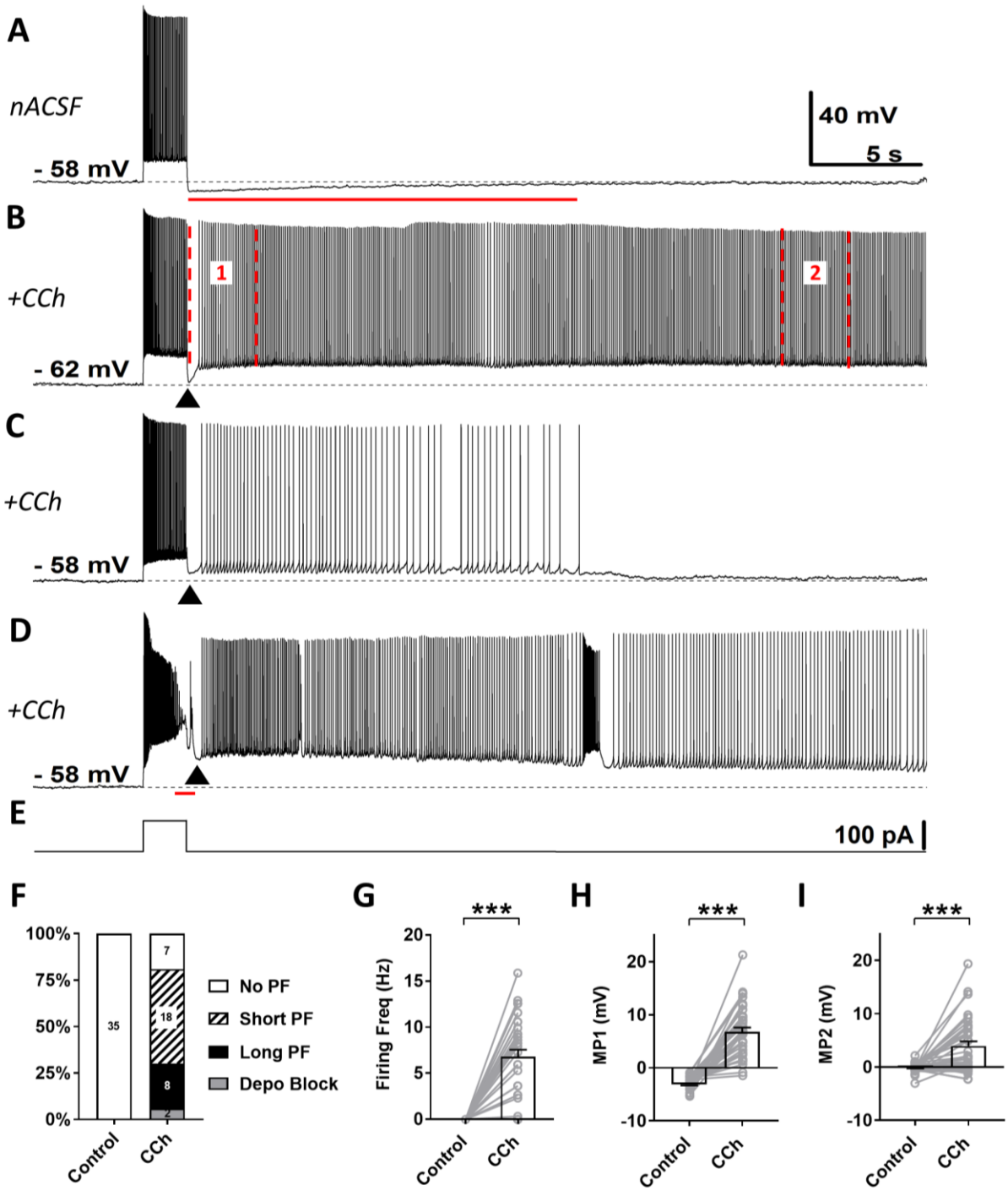

Figure 18 – Cholinergic-dependent persistent firing in CA1 pyramidal neuron.

(A-D) The traces show the membrane potential of different cells in response to the stimulus (2 seconds, 100 pA) showed in (E). The dotted line represents the baseline membrane potential, whose value is indicated in every trace before the stimulus application and expressed in millivolts (mV). For (A-E) the horizontal scale bar represents 5 seconds and the vertical scale bar represent the voltage, 40 mV. For (E) the vertical scale bar represents the current: 100 picoampere (pA). For (B-D) the black triangles highlight the short hyperpolarization of the membrane potential right after the end of the stimulus observed during cholinergic stimulation. (A) The trace shows a cell recorded in control condition (nACSF). The cell fired action potential only during the application of the stimulus (E). After the end of the stimulus the cell stopped firing action potentials and the membrane hyperpolarized for several seconds before going back to baseline. The red bar under the trace highlights the hyperpolarization previously mentioned. (B) Example of long lasting persistent in presence of 10 µM carbachol (CCh). In this trace the 3 seconds interval used to measure the firing frequency and MP1 is delimited with dashed lines and marked with "1". The 3 seconds interval 27 seconds after the end of the stimulus used to measure MP2 is marked with "2". (C) Example of self-terminating persistent in presence of CCh (10 µM). (D) Example of a cell exhibiting depolarization block in presence of CCh (10 µM). The red bar under the

trace highlights the depolarization block. (F) Percentages of cells that showed persistent firing in control condition (nACSF) and during the application of carbachol. The numbers on the graph represent the sample size. (G) Post-stimulus firing frequency (Wilcoxon test, *** $p < 0.001$, $n = 35$). (H) Post-stimulus depolarization (MP1) measured in an interval 3 seconds after the end of the stimulus (paired t-test, *** $p < 0.001$, $n = 35$). (I) Post-stimulus depolarization (MP2) measured in an interval 27 seconds after the end of the stimulus (Wilcoxon test, *** $p < 0.001$, $n = 35$). All the recorded cells, shown in (F), were included in (G, H, I).

After the application of 10 μM carbachol, most of the cells responded to the stimulus with a short hyperpolarization (Fig. 18B-D, black triangles) followed by a strong depolarization that supported persistent firing. The MP1 and MP2 average values, measured during carbachol application, were significantly higher. MP1 was 6.77 ± 0.88 mV (Fig. 18H, paired t-test, *** $p < 0.001$, $n = 35$) and MP2 was 3.95 ± 0.86 mV (Fig. 18I, Wilcoxon test, *** $p < 0.001$, $n = 35$). When the plateau potential was measured only in neurons responding with persistent firing, MP1 was 8.38 Hz ± 0.73 ($n = 28$) and MP2 was 5.05 ± 0.97 ($n = 28$).

In summary, these results indicated that the majority of CA1 pyramidal cells in mice can show persistent firing during cholinergic receptor activation. The stimulation of muscarinic acetylcholine receptors triggers a multitude of intracellular signalling cascades leading also to the facilitation of a calcium-activated nonspecific cationic (CAN) current that has been suggested to be mediated by TRPC channels [174]. CAN current and TRPC channels has been reported to support cholinergic-dependent plateau potential and persistent firing [50,111,170–174]. However, none of the previous studies focused on mice CA1 neurons or used novel and selective TRPC blockers. In the following sections I will investigate the involvement of TRPC channels in persistent firing in CA1 pyramidal neurons.

3.3 Effects of TRPC antagonists on persistent firing

After showing that during cholinergic stimulation persistent firing could be induced in mice CA1 pyramidal neurons, I started to test if TRPC channels were supporting persistent firing. In the literature TRPC4 and TRPC5 channels have been reported to be highly expressed in the CA1 hippocampal pyramidal cells [205,210] and, my IHC stainings results confirmed their presence in mice CA1 hippocampus. For these reasons TRPC4 and TRPC5 channels were chosen as main candidates to underlie persistent firing in mouse CA1 pyramidal neurons.

Several *in vitro* studies showed that CAN current, supported by TRPC channels [111,173,174], underlie persistent firing [50,111,170–172]. However, even if the majority of studies point in this direction, some studies do not agree with the idea of TRPC channels supporting persistent firing [112,113,259]. Hence to give a conclusive answer, the question was tackled combining different approaches to target these ion channels by using pharmacological tools, antibodies, and genetically modified mice.

The precise gating mechanisms of TRPC channels are still not completely understood [26,174] and, for this reason, selective pharmacological agents modulating TRPC channels are lacking. Some of the classic TRPC channels inhibitors used in the last decades have been shown to have limited selectivity. Some of these commonly used inhibitors, such as SKF-93635, 2-APB and FFA, are non-specific, and beside affecting TRPC channels they can affect other ion channels [172,249,250]. In addition, the TRPC inhibitors mentioned above, do not show selectivity for specific TRPC channels sub families.

Recently, novel agonist and antagonists with higher selectivity for TRPC channels have been found. ML204, clemizole hydrochloride (CLE) and Pico145 are the novel TRPC antagonists I used to selectively target these channels in this project. ML204 and CLE can target the TRPC channels at micromolar concentration and show also selectivity for different TRPC subfamilies [253,254]. Pico145 is the most recently discovered antagonist for TRPC channels. It is so far the most selective available and it can affect the TRPC channels at nanomolar concentration [255,265]. Our lab obtained this compound only at the end of my project, but some preliminary results were obtained while testing this compound in the experiments on TRPC5 conditional KO mice.

3.3.1 Targeting TRPC4 channels with ML204

To test the involvement of TRPC4 in supporting persistent firing I used ML204. This TRPC antagonist was chosen as it has a higher selectivity for TRPC4 over TRPC3 over TRPC5 and over TRPC6 (in descending order), however it has been reported to be heat sensitive [177,253,266]. The concentration of ML204 used in these experiments was 10 μM. At this concentration, the drug is mainly selective for TRPC4 channels, but it may also partially affect TRPC5. In isolated cells and at room temperature, 10 μM ML204 was reported to block ca 50% of TRPC5 [253]. I opted to use this concentration for one main reason, the recording temperature I used. While in the studies from Miller and colleagues all experiments were performed at room temperature [253,266], I always kept my brain slice at 35°C ± 1. In our hands ML204 is very sensitive to temperature and its stability seems to be compromised by high temperatures. In unpublished and published observation from our lab, when ML204 was used with a bath temperature of 35°C neither 10 μM or 20 μM had an effect on persistent firing in rat CA1 pyramidal cells [177]. This probably happened because to achieve the temperature of 35°C in the recording chamber, nACSF needed to be pre-heated to 45-50°C by an in-line heater. This could have affected the stability of the compound and explain why ML204 was not effective in our previous experiments at 35°C, even when it was used at 20 μM. To overcome this obstacle, and to perform recordings with a bath temperature of 35°C, a new heated chamber was developed. In this way to achieve a bath temperature of 35°C the in-line heater could be set only to 33-35°C (for more details please refer to the methods section).

In summary, I tried to overcome the heat sensitivity of ML204 by not overheating my solutions to reach the desired recording temperature, and by using a slightly higher concentration of ML204 to compensate in this way a possible loss of the drug potency mediated by the heat.

ML204 suppresses cholinergic-dependent persistent firing

In these experiments, the recordings were done first in nACSF and then 10 μM carbachol was bath applied. Persistent firing was induced as previously described: the cells were depolarized until their firing threshold and then, a short 100 pA square stimulus lasting for 2 seconds was applied to induce persistent activity. If persistent firing was observed during the application of carbachol, 10 μM ML204 was subsequently applied (Fig. 19). The firing frequency of the cells showing persistent firing was strongly reduced 15 minutes after the bath application of 10 μM ML204 (Fig. 19B). In 4 out of 6 cells persistent firing was completely blocked and in the 2 remaining cells it was strongly reduced (Fig. 19E). The

reduction of the firing frequency observed was significant (Fig. 19F, Wilcoxon test, * $p < 0.05$, $n = 6$). In the two cells still showing persistent firing, clemizole hydrochloride was applied on top of ML204 and completely suppressed persistent firing, these results will be presented in detail in another section.

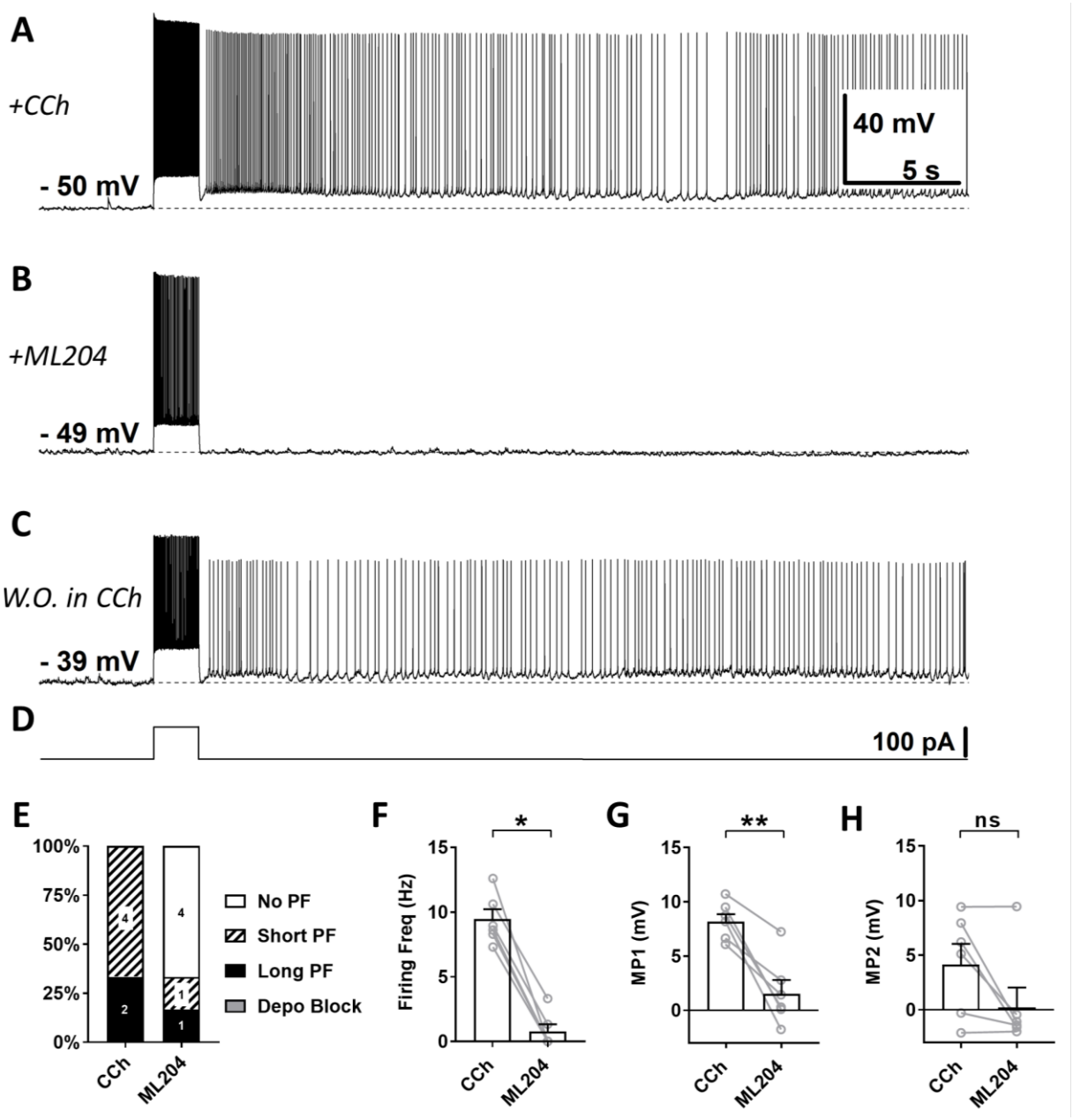

Figure 19 - The effect of ML04 on persistent firing.

(A) Example of persistent firing in CCh (10 µM). (B) Suppressed persistent firing in ML204 (10 µM) in the same cell shown in (A). (C) Persistent firing was recovered after washing out (W.O.) in CCh. The cell is the same cell shown in (A, B). (D) Current injection used in (A, B, C) (100 pA, 2 s). (E) Percentages of cells that showed persistent firing in CCh and during the application of ML204. The numbers on the graph represent the sample size. (F) Post-stimulus firing frequency (Wilcoxon test, * $p < 0.05$, $n = 6$). (G) Post-stimulus depolarization (MP1, paired t-test, ** $p < 0.01$, $n = 6$). (H) Post-stimulus depolarization (MP2, Wilcoxon test, ns, $p = 0.156$, $n = 6$).

The blocking effect of ML204 has been reported to be reversible [253] and to test if this was possible in my slice preparation I washed out ML204 and bath applied again CCh. In my experiments it was possible to wash out ML204 in 2 cells and in both of them PF partially recovered from the block mediated by ML204, indicating that the inhibitory effect mediated by the drug is reversible (Fig. 19C).

The application of 10 μM ML204 had a strong impact also on the cholinergic-dependent depolarization induced by the stimulus. In 4 out of 6 cells the application of ML204 strongly reduced the cholinergic-dependent depolarization (MP1), and in the remaining 2 cells the depolarization was reduced but still present; the reduction observed was significant (Fig. 19G, paired t-test, ** $p < 0.01$, $n = 6$). The membrane potential depolarization measured in the second interval (MP2) was in average reduced, however as most of the cells showed self-terminating persistent firing during CCh application, the observed reduction was not significant (Fig. 19H, Wilcoxon test, ns, $p = 0.156$, $n = 6$).

In summary, persistent firing was significantly reduced by the application of ML204. These results suggest an involvement of TRPC4 channels in the mechanism underlying persistent firing.

ML204 control experiments

As ML204 is a relatively new drug, I decided to perform some pilot control experiments to see if, without cholinergic stimulation, ML204 could have any effect on the membrane potential without cholinergic stimulation. In these experiments the cells were first recorded in nACSF and afterwards 10 μM ML204 was applied on top (Fig. 20).

As expected, without the application of the cholinergic agonist, the stimulation protocol did not induce persistent firing in control condition (nACSF), also 15 minutes after the application of ML204 there were no effects on the tested neurons (Fig. 20D-E, $n = 2$). The membrane depolarization values after the end of the stimulus (MP1 and MP2) were also both not affected by the application of ML204 (Fig. 20F-G, $n = 2$).

The sample size of this pilot experiments is small, however these data suggest that the effect of ML204 previously observed was exerted on channels that were activated by the cholinergic stimulation.

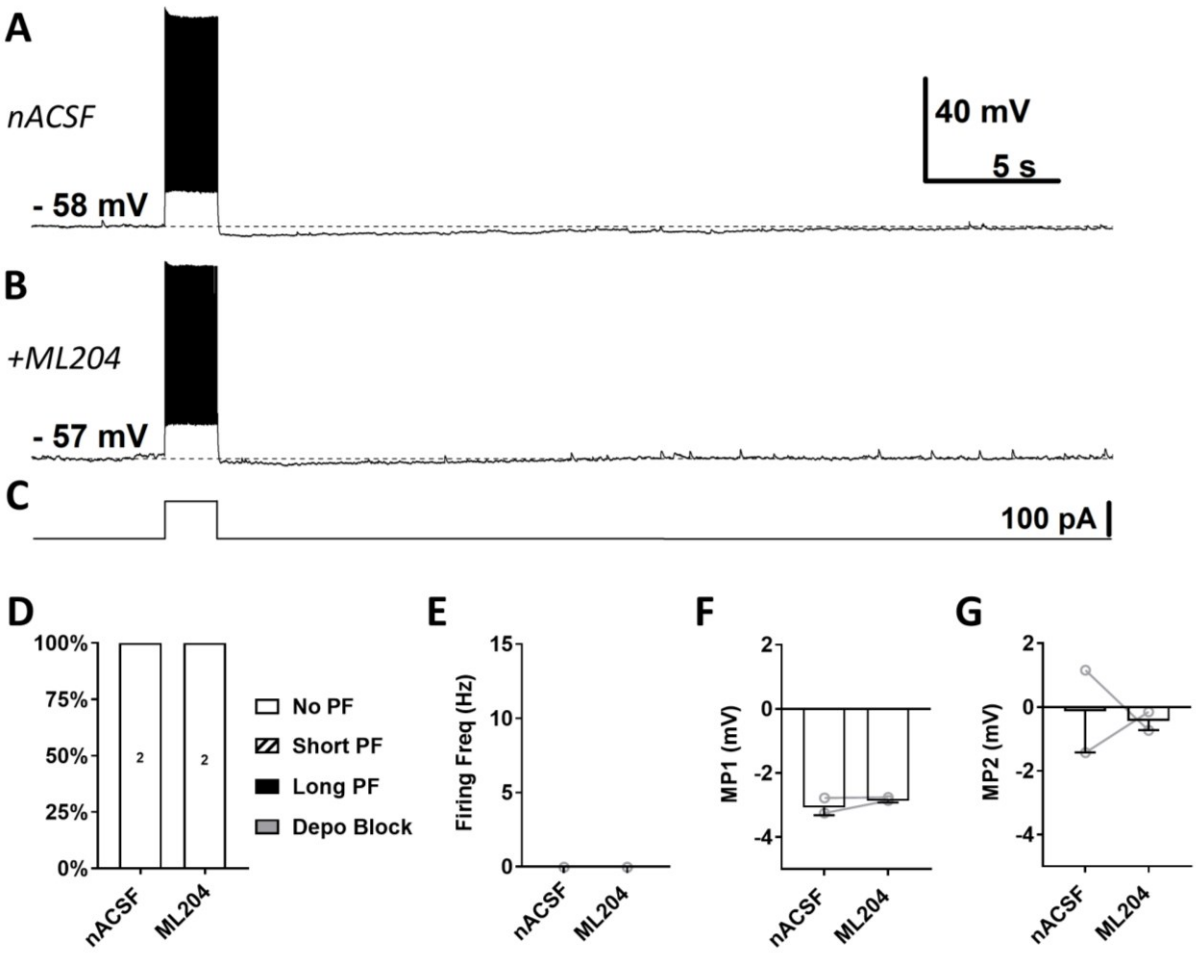

Figure 20 - Control experiments with ML204.

(A) Example of a cell recorded in control condition (nACSF). (B) The trace shows the same cell showed in (A) during the application of ML204 (10 μM). (C) Current injection used in (A, B) (100 pA, 2 s). (D) Percentages of cells that showed persistent firing in nACSF and during the application of ML204. The numbers on the graph represent the sample size. (E) Post-stimulus firing frequency (n = 2). (F) Post-stimulus depolarization (MP1, n = 2). (G) Post-stimulus depolarization (MP2, n = 2).

3.3.2 Targeting TRPC5 channels with 3 μM clemizole hydrochloride

To test the involvement of TRPC5 channels in supporting persistent firing I used clemizole hydrochloride (CLE). This novel blocker, besides being selective for the TRPC channels family, it can also selectively target TRPC subfamilies depending on its concentration [254]. When used at low concentration, CLE has a higher selectivity for TRPC5 over TRPC4, and when used at high concentration it can affect both TRPC4 and TRPC5 channels. The half-maximal inhibitory concentration (IC_{50}) for TRPC5 is 1.1 μM and it is 6.4 μM for TRPC4 [254]. As mentioned in the introduction, TRPC subunits can form homomeric or heteromeric channels however clemizole hydrochloride can block efficiently both TRPC5 homomers and TRPC1-TRPC5 heteromers, acting directly on the TRPC5 subunit [254].

In these experiments I used the same approach already used when testing ML204. Patch clamp recordings were first done in nACSF, then persistent firing was induced during the application of 10 μM carbachol. When persistent firing was observed, clemizole hydrochloride was subsequently co-applied with CCh. The stimulation protocol was the same previously used: a current injection of 100 pA was applied for 2 seconds while holding the cells under its firing threshold. In my project clemizole hydrochloride was used at two concentrations: 3 μM and 20 μM. I chose the lower concentration to target TRPC5 channels and the higher to target at the same time both TRPC4 and TRPC5 channels. I will first present the results using a lower concentration of CLE and, in a separated section, I will present the results obtained using a higher concentration.

Clemizole hydrochloride (3 μM) suppresses cholinergic-dependent persistent firing

The first series of experiments, using a lower concentration of clemizole hydrochloride, aimed to test the role of TRPC5 in supporting persistent firing. After the application of 10 μM carbachol persistent firing was induced in 9 neurons and clemizole hydrochloride (3 μM) was consequently bath applied on top (Fig. 21).

After 15 minutes from the bath application of CLE, in 6 out of 9 cells persistent firing was completely suppressed (Fig. 21B), in 1 cell persistent firing was strongly reduced and, in the remaining 2 cells, persistent firing was not affected (Fig. 21D). The firing frequency of persistent firing was strongly and significantly reduced by the application of 3 μM clemizole hydrochloride (Fig. 21E, Wilcoxon test, * $p < 0.05$, $n = 9$). In the cells still showing persistent firing after the application of CLE, ML204 was applied on top of clemizole hydrochloride aiming to completely suppress persistent firing. These results will be presented in detail a separated section.

The application of clemizole hydrochloride had a strong effect also on the cholinergic-dependent depolarization induced by the stimulus. In all cells but 1, the plateau potential was reduced by the application of CLE. The application of the TRPC5 antagonist significantly reduced the depolarization after the end of the stimulus (MP1) (Fig. 21F, Wilcoxon test, * $p < 0.05$, $n = 9$). The membrane depolarization measured in the second interval (MP2) was in average reduced after the application of CLE, however, as most of the cells showed self-terminating persistent firing during CCh application, the difference between the two conditions was not significant (Fig. 21G, paired t-test, ns, $p = 0.095$, $n = 9$).

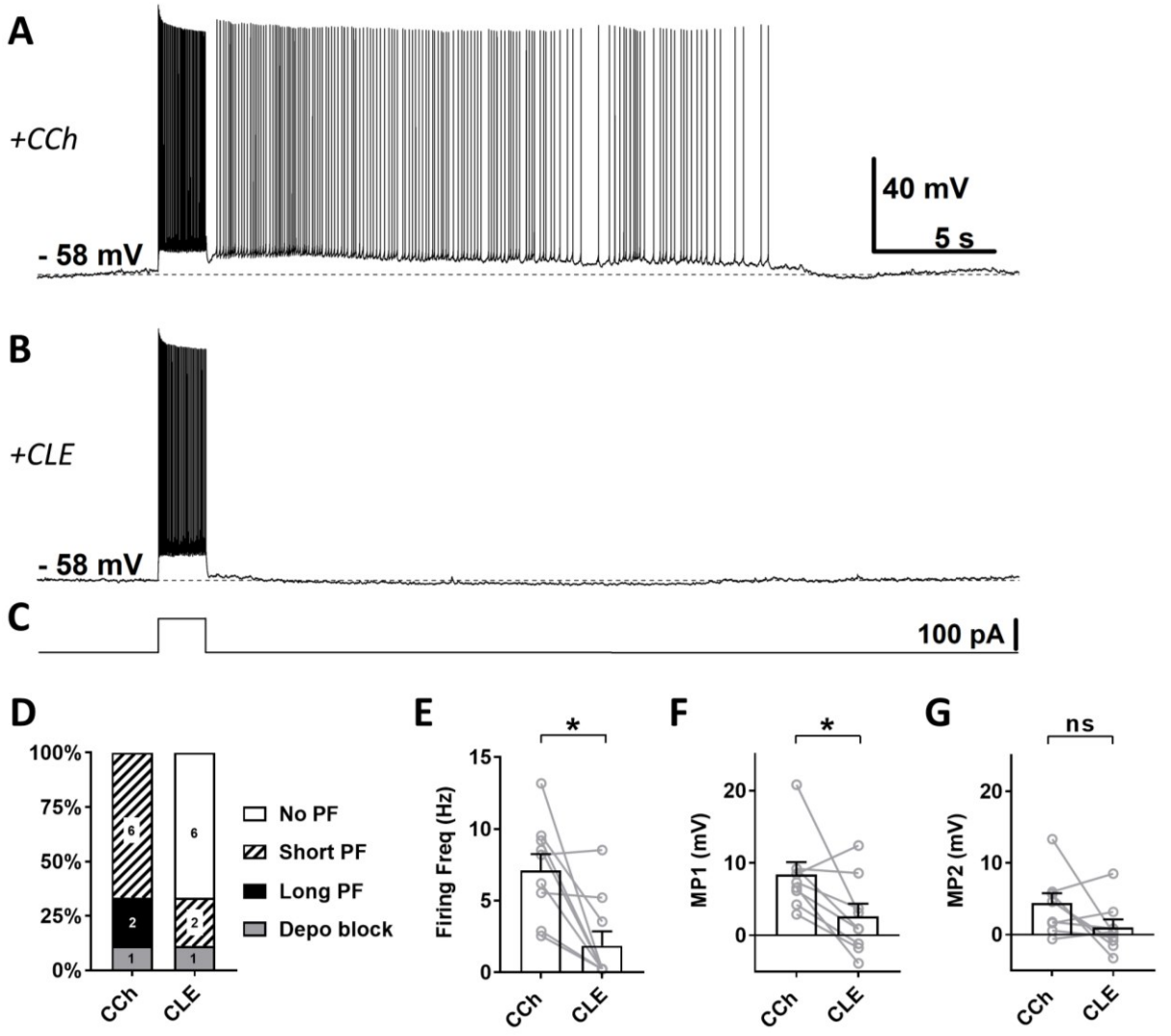

Figure 21 - The effect of clemizole hydrochloride (3 µM) on persistent firing.

(A) Example of persistent firing in CCh (10 µM). (B) Suppressed persistent firing in clemizole (CLE, 3 µM) in the same cell shown in (A). (C) Current injection used in (A, B) (100 pA, 2 s). (D) Percentages of cells that showed persistent firing in CCh and during the application of CLE. The numbers on the graph represent the sample size. (E) Post-stimulus firing frequency (Wilcoxon test, * $p < 0.05$, $n = 9$). (F) Post-stimulus depolarization (MP1, Wilcoxon test, * $p < 0.05$, $n = 9$). (G) Post-stimulus depolarization (MP2, paired t-test, ns, $p = 0.095$, $n = 9$).

In these experiments using clemizole hydrochloride, it was possible to partially wash out the drug in only one cell (Fig. 22). Even if persistent firing did not recover, the cell was again more excitable and able to fire some action potentials even if after several seconds from the end of the stimulus (Fig. 22C). In a study from Richter et al. (2014), a reversible block of CLE has been reported, however in my experiments in the CA1 neurons I never observed a full recovery of persistent firing [254].

In summary, these results using clemizole hydrochloride at low concentration suggest an involvement of TRPC5 channels in the mechanism underlying persistent firing evoked during the stimulation with a cholinergic agonist.

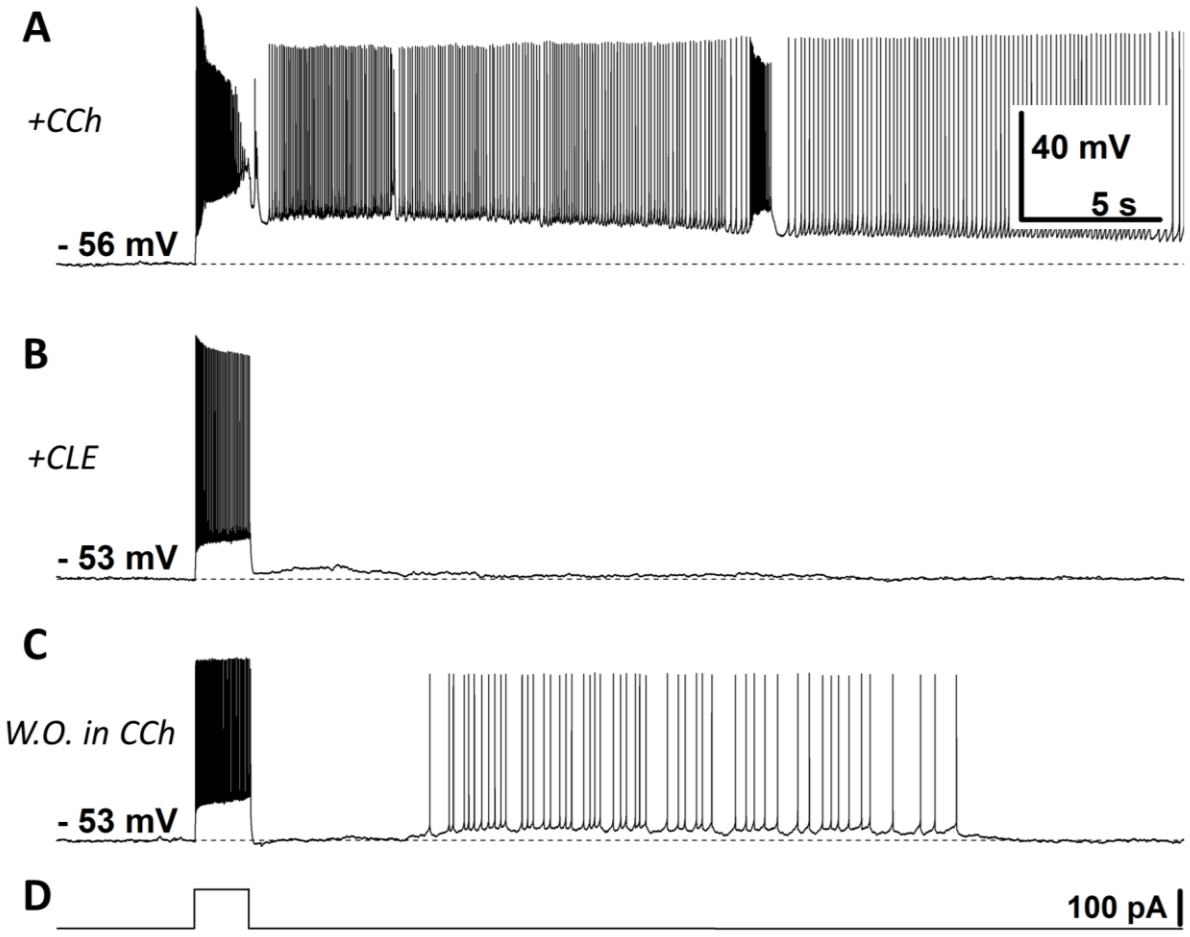

Figure 22 - Attempt of clemizole hydrochloride wash out in carbachol.

(A) Example of persistent firing in CCh (10 µM). The cell showed depolarization block. (B) Suppressed persistent firing in clemizole hydrochloride (CLE, 3 µM) in the same cell shown in (A). (C) Persistent firing was not recovered after washing out (W.O.) in CCh. The cells is the same cell shown in (A, B). (D) Current injection used in (A, B, C) (100 pA, 2 s).

3.3.3 Effect of simultaneous blockade of TRPC4 and TRPC5 channels by using ML204 and clemizole hydrochloride

In the previous sections it was shown that the selective block of TRPC4 or TRPC5 channels significantly suppressed persistent firing. However, in some cells persistent firing was not completely blocked by the application of either ML204 or clemizole hydrochloride (Fig. 23). To test whether this remaining activity was due to remaining TRPC4 or TRPC5 channels, I tested dual application of both ML204 and clemizole hydrochloride in these cells.

In the 2 cells which continued to respond with persistent firing after the application of ML204, persistent activity was completely suppressed when 3 μM clemizole hydrochloride was additionally applied (Fig. 23G, n = 2). In these 2 cells, the post-stimulus depolarization was also suppressed (Fig. 23H-I, n = 2).

In the 3 cells in which persistent firing was not completely suppressed by 3 μM clemizole hydrochloride, 10 μM ML204 was additionally co-applied (Fig. 23A-E). After the application of ML204, in all 3 cells persistent firing was completely blocked, and the post-stimulus depolarization was strongly suppressed (Fig. 23L-O). While performing these experiments, in 1 cell it was also possible to wash out CLE and ML204 and persistent firing fully recovered (Fig. 23D).

Taken together, these data suggest that TRPC4 and TRPC5 support persistent firing in a synergistic manner.

Fig. 23 - The effects of clemizole hydrochloride and ML204 co-application (figure on next page).

(A) Example of persistent firing in CCh (10 μM). (B) Partially suppressed persistent firing in clemizole hydrochloride (CLE, 3 μM) in the same cell shown in (A). (C) Persistent firing was completely suppressed after ML204 (10 μM) application. The cell is the same cell shown in (A, B). (D) Persistent firing was recovered after washing out (W.O.) back in CCh. The cell is the same cell shown in (A, B, C). (E) Current injection used in (A, B, C, D) (100 pA, 2 s). (F) Percentages of cells that still showed persistent firing in ML204 (10 μM) and after the application of CLE (3 μM). The numbers on the graph represent the sample size. (G) Post-stimulus firing frequency of the cells showed in (F) (n = 2). (H) Post-stimulus depolarization (MP1) of the cells showed in (F) (n = 2). (I) Post-stimulus depolarization (MP2) of the cells showed in (F) (n = 2). (L) Percentages of cells that still showed persistent firing in CLE (3 μM) and after the application of ML204 (10 μM). The numbers on the graph represent the sample size. (M) Post-stimulus firing frequency of the cells showed in (L) (n = 3). (N) Post-stimulus depolarization (MP1) of the cells showed in (L) (n = 3). (O) Post-stimulus depolarization (MP2) of the cells showed in (L) (n = 3).

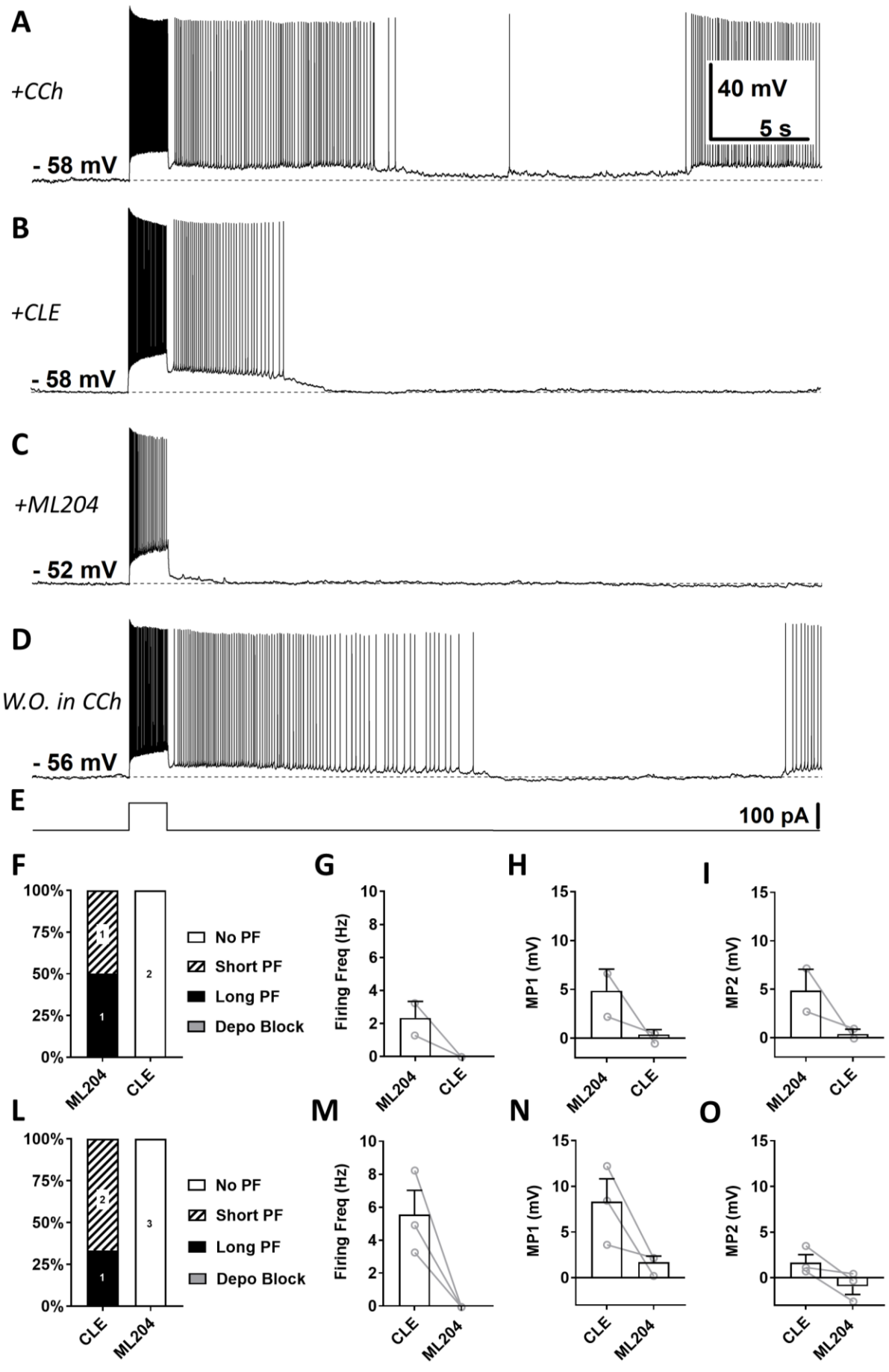

Figure 23 - The effects of clemizole hydrochloride and ML204 co-application (caption on previous page).

3.3.4 Targeting TRPC4 and TRPC5 channels with 20 μM clemizole hydrochloride

In the previous sections, we saw that ML204 and clemizole hydrochloride significantly reduced persistent firing, but we also saw that in some cells persistent firing was completely suppressed only when both drugs were co-applied. For this reason, I tested another way of simultaneously block TRPC4 and TRPC5 by applying clemizole hydrochloride at higher concentration (Fig. 24), in fact, when used at 20 μM, this drug affects both TRPC4 and TRPC5 channels [254]. The experimental approach and the stimulation protocol were the same used in the previous experiments made with CLE at lower concentration.

In 7 out of 7 cells the firing frequency of persistent firing was significantly reduced after the application of 20 μM CLE (Fig. 24E, paired t-test, ** $p < 0.01$, $n = 7$). Interestingly, the application of CLE reduced the firing frequency of persistent firing but also induced depolarization block in 5 out of 7 cells (Fig. 24D). Depolarization block is when a cell gets so depolarized that, even if its membrane potential is more depolarized than its firing threshold, it does not fire any action potential. In the 5 cells which responded with depolarization block, the application of CLE increased the depolarization after the end of the stimulus rather than decreasing it like previously shown by CLE used at lower concentration. In the 2 remaining cells not showing depolarization block, clemizole hydrochloride partially reduced, but did not block, the cholinergic-dependent depolarization.

During CLE application, the increase of the depolarization after the end of the stimulus was not significant (MP1), but it showed a trend of the cells to respond mostly with depolarization block (Fig. 24F, ns, paired t-test, $p = 0.161$, $n = 7$). The depolarization block observed during the application of 20 μM CLE was normally starting during the stimulus and lasting for only few seconds after the end of the current pulse. This can be seen looking at the measure of MP2, the membrane potential measured in an interval 27 seconds after the end of the stimulus, that showed no difference when compared to the carbachol condition (Fig. 24G, ns, paired t-test, $p = 0.097$, $n = 7$).

The depolarization block started very often already during the stimulus application, for this reason in this dataset it was interesting to analyse also what happened to the membrane potential during the stimulation. In fact, in 6 out of 7 cells, the membrane potential during the stimulus application was more depolarized during the application of 20 μM CLE (Fig. 24H, * paired t-test, $p < 0.05$, $n = 7$). This strong depolarization, observed during the stimulation, was not observed during the application of 10 μM ML204 or 3 μM CLE. In both cases there were

no significant changes of the membrane potential values during the stimulation (Fig. 24I, ML204: ns, paired t-test, p = 0.854, n = 6; CLE: ns, Wilcoxon test, p = 0.301, n = 9).

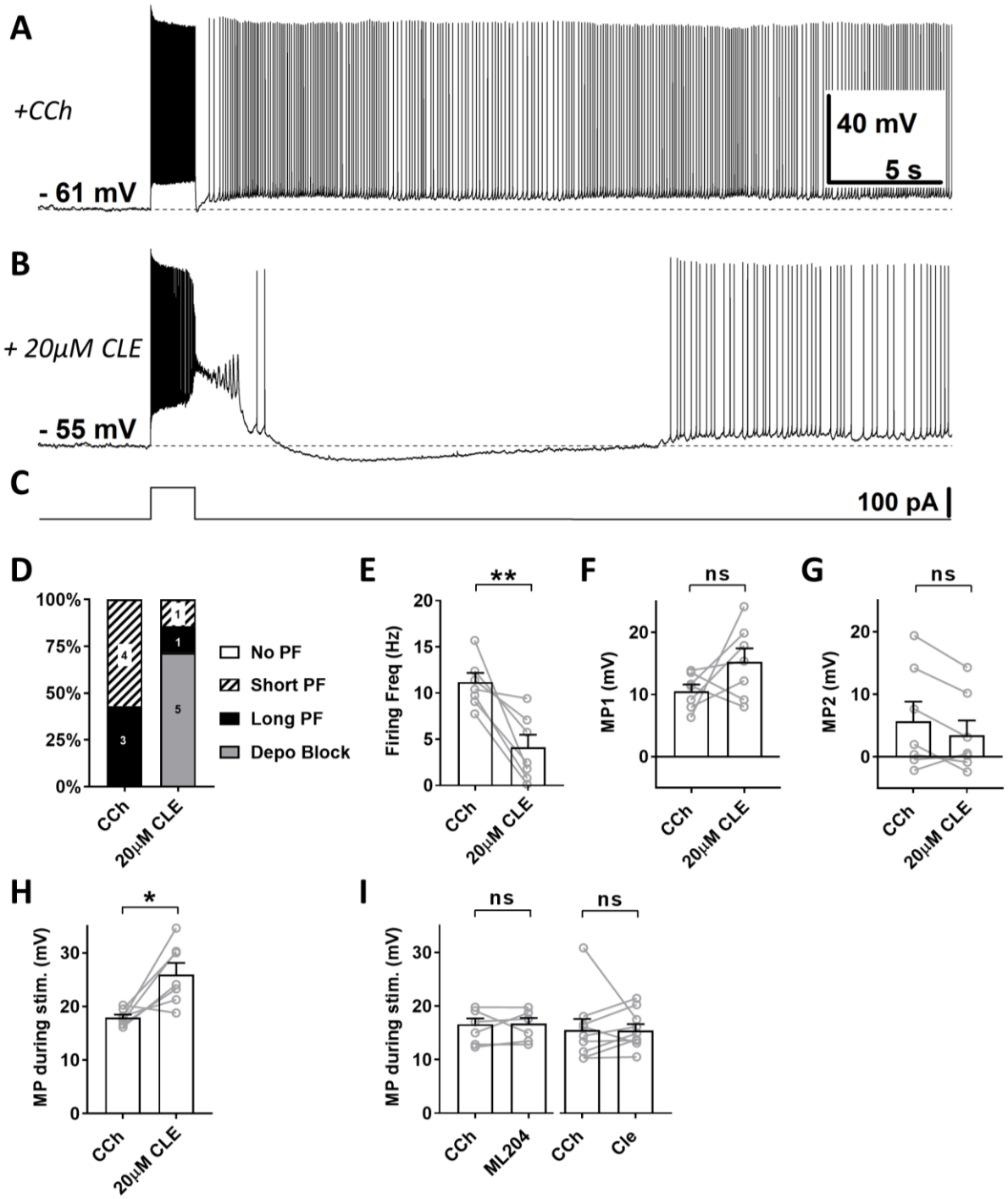

Figure 24 - The effect of clemizole hydrochloride (20 µM) on persistent firing.

(A) Example of persistent firing in CCh (10 µM). (B) Suppressed persistent firing and depolarization block in clemizole (CLE, 20 µM) in the same cell shown in (A). (C) Current injection used in (A, B) (100 pA, 2 s). (D) Percentages of cells that showed persistent firing in CCh and during the application of CLE. The numbers on the graph represent the sample size. (E) Post-stimulus firing frequency (paired t-test, ** $p < 0.01$, n = 7). (F) Post-stimulus depolarization (MP1, paired t-test, ns, p = 0.161, n = 7). (G) Post-stimulus depolarization (MP2, paired t-test, ns, p = 0.097, n = 7). (H) Membrane potential depolarization during the stimulus application (paired t-test, * $p < 0.05$, n = 7). (I) Membrane potential depolarization during the stimulus application in the experiments with ML204 (10 µM) (left, paired t-test, ns, p = 0.854, n = 6) and in the experiments with CLE (3 µM) (right, Wilcoxon test, ns, p = 0.301, n = 9).

These results, given the effect of CLE on the firing frequency, suggest that TRPC channels, including TRPC4 and TRPC5, support persistent firing. However, clemizole hydrochloride (20 μM) induced depolarization block in most of the tested cells indicating that this blocker could have unspecific effects when used at this concentration.

Clemizole hydrochloride control experiments

To test if the depolarization block induced by CLE application was cholinergic-dependent, I performed control experiment in which 20 μM clemizole hydrochloride was applied in absence of carbachol. These experiments were meant to see if CLE, when applied at high concentration, could activate ion channels directly and independently from the cholinergic stimulation.

After recording in control condition (nACSF), 20 μM clemizole hydrochloride was applied and, after bringing the cells at their firing threshold, the same square pulse stimulus used in the previous experiments was applied. (Fig. 25). As expected, none of the tested cells showed persistent firing in control condition and during the application of CLE (Fig. 25D-E). The membrane depolarization after the end of the stimulus (MP1) was not affected by the application of CLE at high concentration and in no cell depolarization block was observed (Fig. 25F, paired t-test, ns, $p = 0.358$, $n = 4$). Also the values of MP2 did not show any significant difference (Fig. 25G, Wilcoxon test, ns, $p = 0.625$, $n = 4$). The membrane potential depolarization during the stimulation, significantly increased in the previous experiments during the co-application of CCh and CLE, was not affected by the application of CLE alone (Fig. 25H, ns, paired t-test, $p = 0.392$, $n = 4$).

These results indicate that the depolarization block effect induced by the application of CLE was cholinergic-dependent.

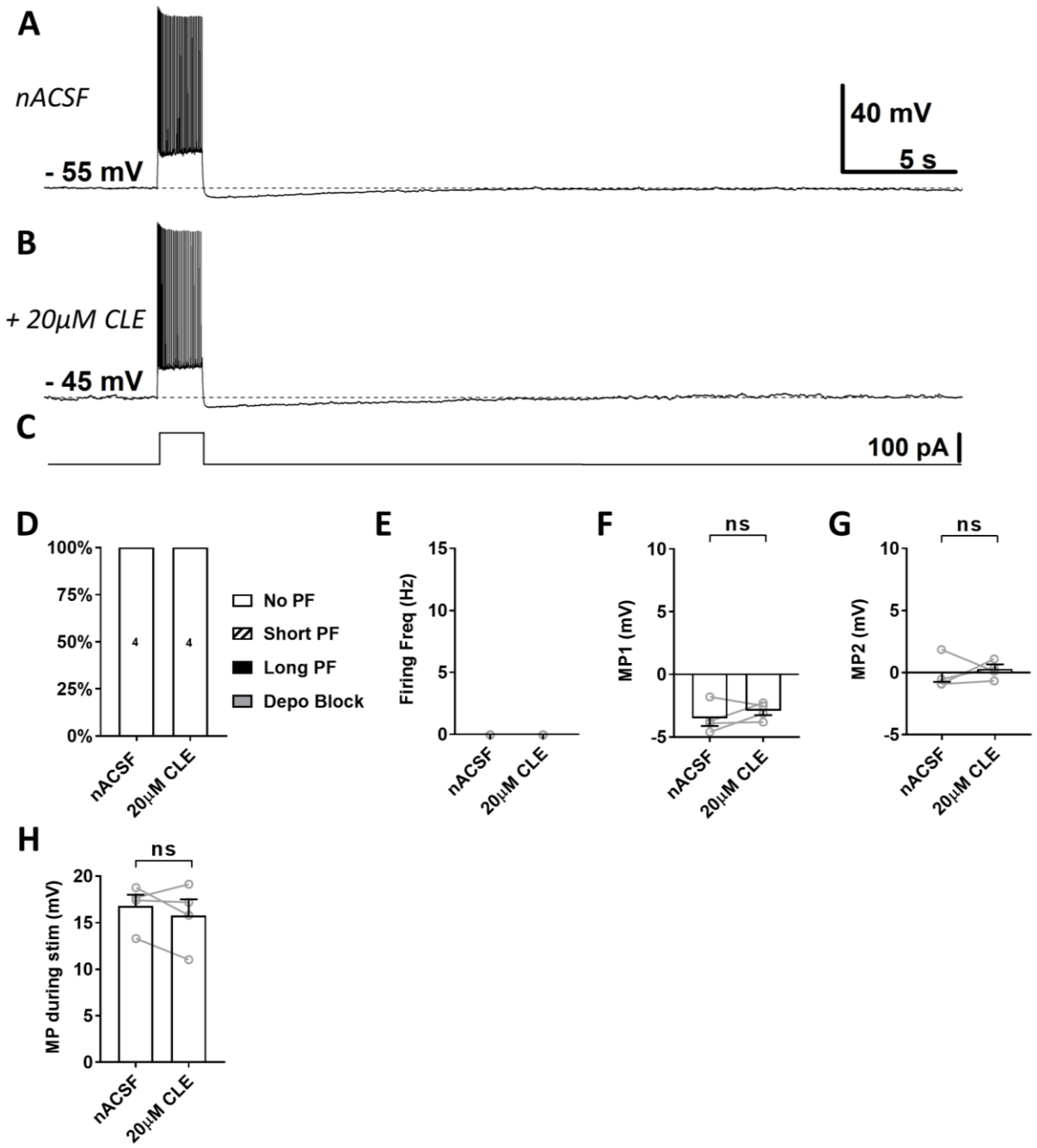

Figure 25 - Control experiments with clemizole hydrochloride (20 µM).

(A) Example of a cell recorded in control condition (nACSF). (B) The application of CLE (20 µM) did not induced persistent firing in the same cells shown in (A). (C) Current injection used in (A, B) (100 pA, 2 s). (D) Percentages of cells that showed persistent firing in nACSF and during the application of CLE. The numbers on the graph represent the sample size. (E) Post-stimulus firing frequency (n = 4). (F) Post-stimulus depolarization (MP1, paired t-test, ns, p = 0.358, n = 4). (G) Post-stimulus depolarization (MP2, Wilcoxon test, ns, p = 0.625, n = 4). (H) Membrane potential depolarization during the stimulus application (Wilcoxon test, paired t-test, ns, p = 0.392, n = 4).

3.3.5 Effect of 20 µM clemizole hydrochloride on CAN current

In the previous experiments using 20 µM clemizole hydrochloride to suppress persistent firing, it was shown that the TRPC blocker led to a reduction of the firing frequency, however it also induced depolarization block in most of the tested cells. The strong increase of the depolarization was never observed when 20 µM CLE was applied without carbachol, meaning that this effect was cholinergic-dependent. When used at higher concentration, clemizole hydrochloride should block both TRPC4 and TRPC5 channels and, as these channels are supposed to support CAN current, it should also reduce this current [174]. However, as 20 µM is a relatively high concentration, CLE could affect TRPC ion channels in other ways, maybe increasing their activity instead of suppressing it and consequently leading to depolarization block. To determine how 20 µM CLE affected CAN current, a series of voltage clamp recordings were performed. In these voltage clamp experiments the recording condition and the protocols were different from all the other current clamp experiments performed in this project. Protocols and solutions were taken and adapted from a study by Magistretti and colleagues (2004) that investigated CAN current in entorhinal cortex layer II neurons [267].

In my experiments, to isolate CAN current as much as possible, several compounds were applied to block ion currents not supporting it. The recording solution (control solution) was nACSF containing 500 nM TTX and 5 mM cesium, to block respectively sodium and potassium conductances. To improve the voltage clamp condition, the ICF contained 0.5 mM EGTA, a calcium chelator, and cesium. The concentration of carbachol used in these voltage clamp experiments (20 µM) was higher compared to the one used in the current clamp (10 µM) to be sure to have the maximum activation of the CAN current (for more details about the solutions please refer to the methods section).

The brain slices were kept in nACSF and, as soon as a seal was established with a neuron, the solution was changed to nACSF containing TTX and cesium, I will refer to this solution as control solution. The recordings started as soon the TTX was effective and preventing the cell to fire action potentials. After the recordings in the control condition were done, 20 µM carbachol was applied on top and the protocol used to induce the activation of the CAN current was applied. After checking the presence of CAN current, 20 µM clemizole hydrochloride was applied on top to test its effect on the calcium activated non-selective cationic (CAN) current.

To evoke CAN current, the membrane potential was held at -70 mV and a 70 mV depolarization step lasting 300 ms was applied (Fig. 26D). This protocol was similar to the

one used in the study by Magistretti and colleagues to evoke CAN current in the EC layer II [267]. Before the application of carbachol, the amplitude of the current evoked was small and lasted few hundred milliseconds (Fig. 26A). After the application of 20 µM carbachol, the stimulation protocol induced a pronounced inward current that lasted 1.5-2 seconds (Fig. 26B). When compared to control, the average amplitude of the evoked current increased significantly (Fig. 26E, paired t-test, * $p < 0.05$, $n = 6$). At this point 20 µM CLE was applied on top of CCh and the cholinergic-dependent current was significantly suppressed by the TRPC antagonist (Fig. 26F, Wilcoxon test, * $p < 0.05$, $n = 6$).

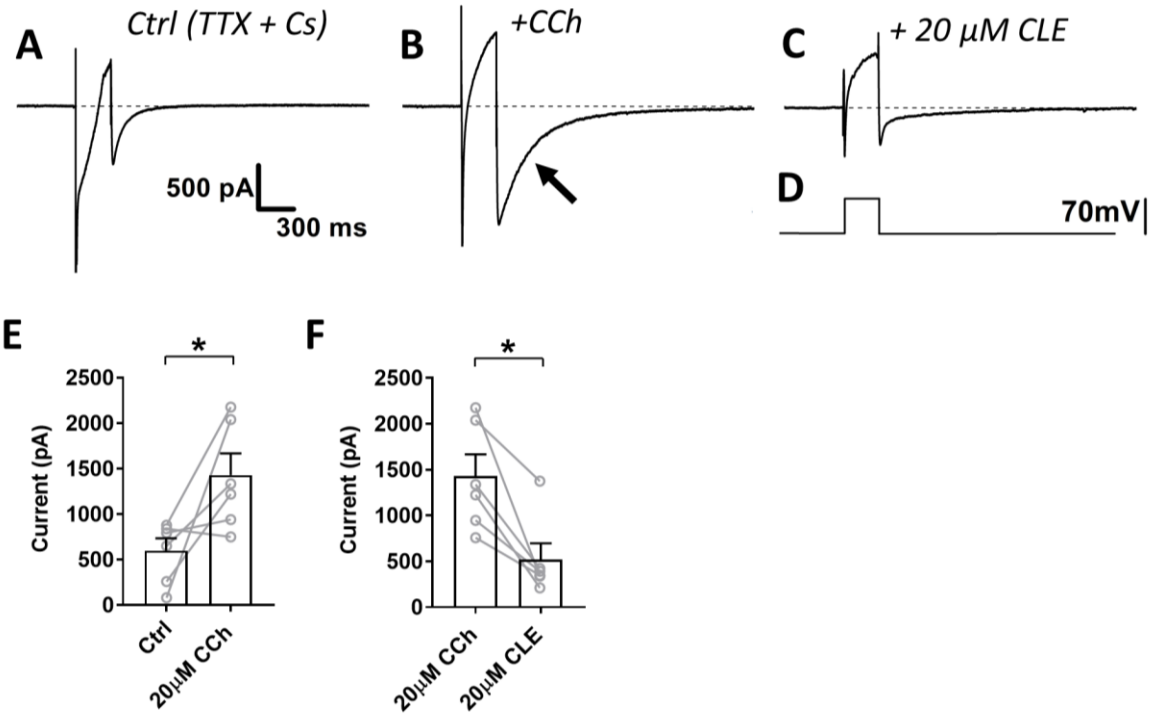

Figure 26 - The effect of clemizole hydrochloride (20 µM) on CAN current.

(A) Example of a cell recorded in control condition (nACSF + TTx (500 nM) + Cs (5 mM)). (B) Example of CAN current (black arrow) evoked during carbachol (20 µM) application in the same cell showed in (A). (C) Clemizole hydrochloride (20 µM) suppressed CAN current in the same cell showed in (A, B). (E) Amplitude of the current measured in control and during carbachol application (paired t-test, * $p < 0.05$, $n = 6$). (F) Amplitude of the current measured during CCh application and after CLE application (Wilcoxon test, * $p < 0.05$, $n = 6$).

In summary: 20 µM clemizole hydrochloride suppressed the CAN current evoked during cholinergic stimulation. These data indicated that this drug had an inhibitory effect on the TRPC channels supporting CAN current. In addition, these results also suggested that the strong depolarization block, observed in the current clamp experiments presented previously, was not induced by a positive modulation of clemizole hydrochloride on TRPC channels.

Taken together these data indicate that the depolarization block effect previously observed was not mediated by CLE activating TRPC channels. This phenomenon was probably mediated by other ion channels affected by a possible unspecific effect of clemizole hydrochloride when used at higher concentration.

3.4 Anti - TRPC antibodies suppress persistent firing

After the experiments using pharmacological blockers, to further assess the involvement of TRPC channels in persistent firing, I used antibodies to selectively target the TRPC4 and TRPC5 channels. In published studies from other labs, anti-TRPC antibodies have been successfully used in patch clamp experiments to selectively reduce the activity of TRPC channels [189,211,256]. Following these previous studies, I applied antibodies in the intracellular solution to selectively target TRPC4 or TRPC5. The aim of these experiments was to assess if the reduction or block of their activity could also affect persistent firing. This approach was chosen to have an additional proof supporting the results obtained in the experiments using novel pharmacological blockers. When antibodies were diluted in the intracellular solution after the rupture of the membrane, they were free to diffuse in the cytosol and to selectively interact with the target channels. When antibodies bind ion channels, depending on the targeted epitope, they can either activate or inhibit the activity of the channels. Based on the previous literature, I chose antibodies targeting epitopes leading to an inhibition of the ion channel activity [189,211,256].

3.4.1 Effect of anti - TRPC4 antibodies on persistent firing

To test if TRPC4 channels support persistent firing, anti-TRPC4 antibodies were diluted in the intracellular solution and, after the rupture of the membrane, they were able to diffuse inside the cytosol targeting the TRPC4 channels. As ML204 is a relatively novel drug I decided to also use this approach to give an extra proof supporting the role of TRPC4 channels underlying persistent firing. The antibodies were first used with a dilution 1:100 and then 1:500. The first dilution used, 1:100, was chosen based on a study made by another lab in which they blocked TRPC channels intracellularly with antibodies [189].

Compared to the experiment using pharmacological blockers the approach with these experiments was slightly different. The recording procedure used was the same but performed with a different time schedule. The cells were kept in nACSF and, as soon as the membrane was ruptured, 10 μM carbachol was applied as fast as possible. The effect of the antibodies was in some cases very fast, therefore it was important to assess the presence of persistent firing during CCh application as soon as possible before the antibodies could exert their effect on the targeted channels. Normally persistent firing was induced 3 minutes after the application of 10 μM carbachol using the same stimulation protocol previously described. At this time point, 3 minutes after the application of CCh, the membrane was ruptured for 5 minutes and the antibodies were diluting in the cytosol. During carbachol application, when

persistent firing was observed, the same stimulating protocol was applied at 15 minutes after the rupture of the membrane to assess the effect of the antibodies on persistent firing. In these experiments no pharmacological blocker was applied on top of 10 µM carbachol.

Application of anti - TRPC4 antibodies 1:100

In these experiments, 3 minutes after the application of carbachol, which was 5 minutes after the rupture of the membrane, persistent firing was induced using the same current injection used in the previous experiments (2 s, 100 pA). This recording in CCh served as control recording (Fig. 27A). Then, 15 min after rupturing the membrane, persistent firing was tested again (Fig. 27B). Out of 7 cells which showed persistent firing in control condition, 15 min after rupturing the membrane persistent firing was completely blocked in 5 cells and the remaining 2 cells exhibited a weaker persistent firing. The firing frequency of persistent firing was significantly suppressed compared to the control recordings (Fig. 27E; Wilcoxon test, * $p < 0.05$, $n = 7$).

The post stimulus depolarization induced during carbachol application, was reduced by the anti-TRPC4 antibodies application. After 15 min from the rupture of the membrane all 7 neurons showed a reduction of the post stimulus depolarization (MP1) (Fig. 27F; Wilcoxon test, * $p < 0.05$, $n = 7$). The values of MP2 were also in average reduced but the difference was no significant (Fig. 27G, unpaired t-test, ns, $p = 0.136$, $n = 7$).

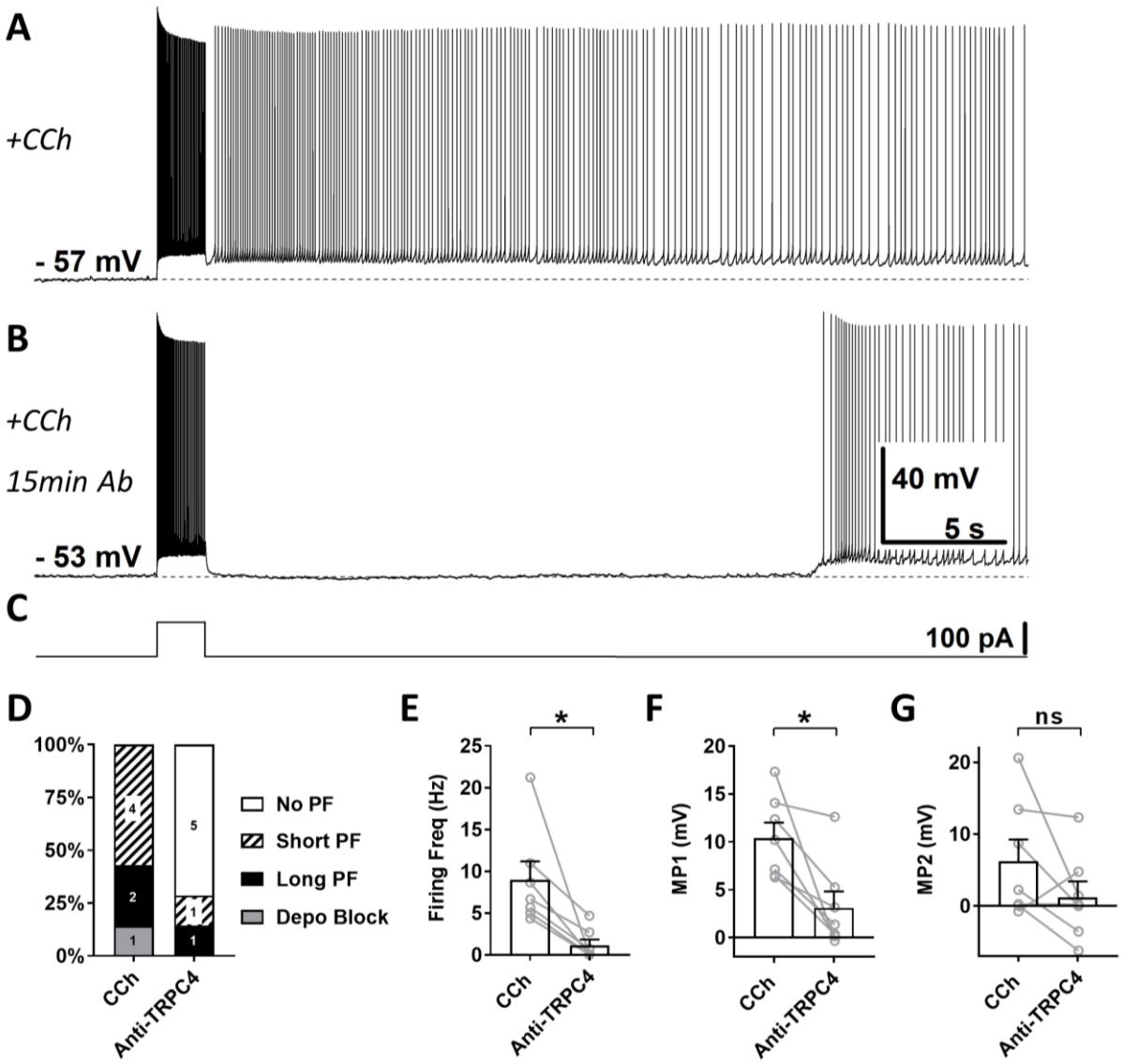

Figure 27 - The effect of intracellular application of anti-TRPC4 antibody (1:100) on persistent firing.

(A) Example of persistent firing recorded 5 min after the rupture of the membrane in CCh (10 μM). (B) Suppressed persistent firing recorded 15 min after the rupture of the membrane in the same cell shown in (A). (C) Current injection used in (A, B) (100 pA, 2 s). (D) Percentages of cells that showed persistent firing in control (5 min) and 15 min after the rupture of the membrane. The numbers on the graph represent the sample size. (E) Post-stimulus firing frequency (Wilcoxon test, * $p < 0.05$, $n = 7$). (F) Post-stimulus depolarization (MP1, Wilcoxon test, * $p < 0.05$, $n = 7$). (G) Post-stimulus depolarization (MP2, unpaired t-test, ns, $p = 0.136$, $n = 7$).

Application of anti - TRPC4 antibodies 1:500

After testing the 1:100 dilution I decided to dilute the antibodies 1:500 in the intracellular solution (Fig. 28). This was made to test if the antibodies could be still effective at lower concentration. The protocols and the experimental procedures were the same previously used while testing the antibodies at higher concentration.

During the application of 10 μM carbachol, persistent firing was induced in 5 cells. After 15 minutes from the rupture of the membrane, persistent firing was strongly reduced in 3 cells, completely blocked in 1 cell and in 1 cell it was not affected. The firing frequency of persistent firing was significantly suppressed compared to the control recordings (Fig. 28E; paired t-test, * $p < 0.05$, $n = 5$). The post stimulus depolarization induced during carbachol application (MP1), was not reduced by the application of anti-TRPC4 antibodies at lower concentration (Fig. 28F; paired t-test, ns, $p = 0.355$, $n = 5$). After 15 min from the rupture of the membrane, the post stimulus depolarization was reduced in 3 cells, not affected in 1 cell, and increased in 1 cell that showed depolarization block at this point. However, after 15 minutes from the application of the anti-TRPC4 antibodies the depolarization values observed in MP2 were significantly reduced (Fig. 28G, paired t-test, * $p < 0.05$, $n = 5$).

In summary, the results of the experiments using anti-TRPC4 antibodies (1:100 and 1:500) indicate that TRPC4 are involved in the mechanism supporting persistent firing in CA1 pyramidal neurons.

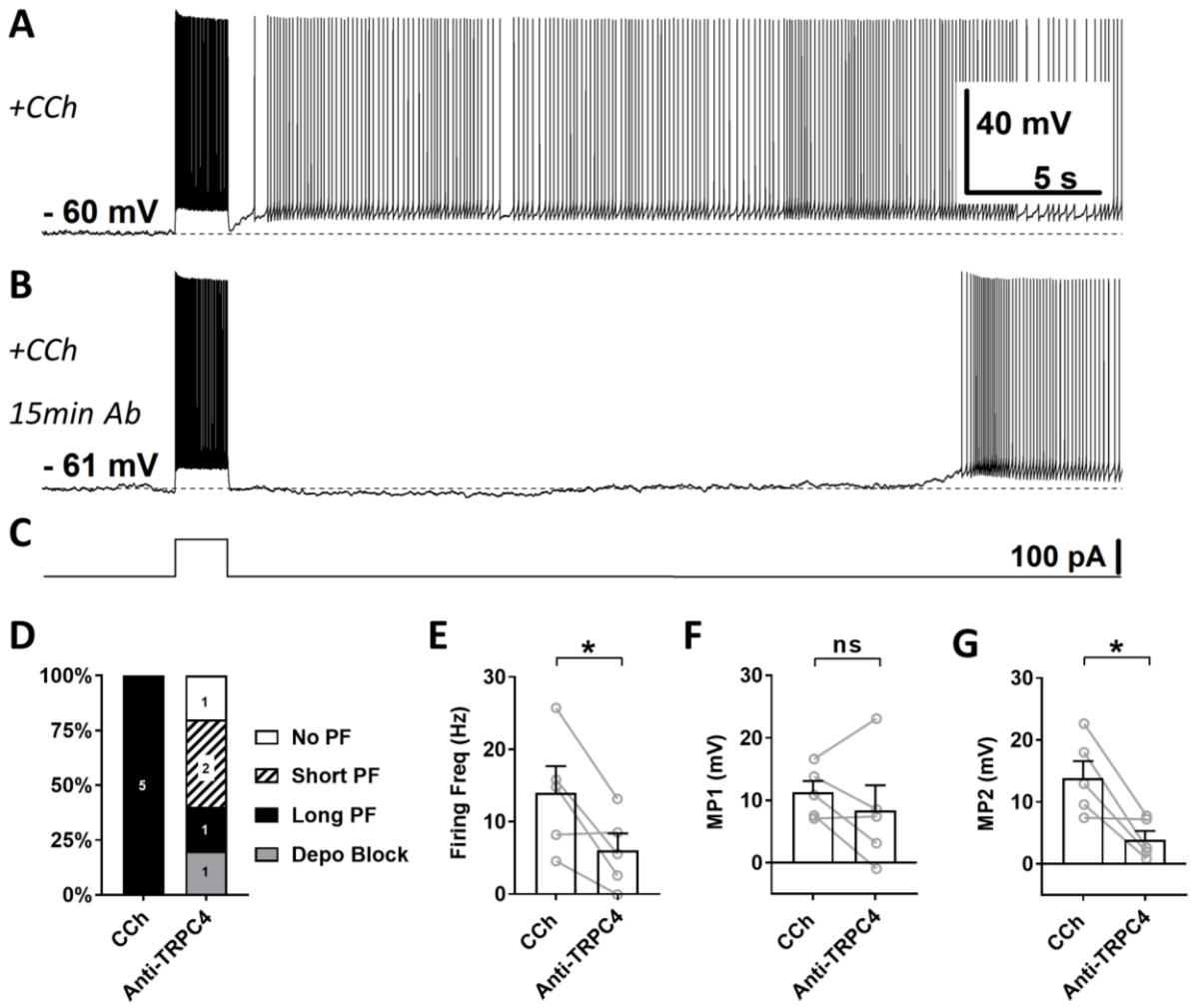

Figure 28 - The effect of intracellular application of anti-TRPC4 antibody (1:500) on persistent firing.

(A) Example of persistent firing recorded 5 min after the rupture of the membrane in CCh (10 μM). (B) Suppressed persistent firing recorded 15 min after the rupture of the membrane in the same cell shown in (A). (C) Current injection used in (A, B) (100 pA, 2 s). (D) Percentages of cells that showed persistent firing in control (5 min) and 15 min after the rupture of the membrane. The numbers on the graph represent the sample size. (E) Post-stimulus firing frequency (paired t-test, * $p < 0.05$, $n = 5$). (F) Post-stimulus depolarization (MP1, paired t-test, ns, $p = 0.355$, $n = 5$). (G) Post-stimulus depolarization (MP2, paired t-test, * $p < 0.05$, $n = 5$).

3.4.2 Effect of anti - TRPC5 antibodies on persistent firing

Anti-TRPC5 antibodies were used to test if TRPC5 channels support persistent firing. The approach used was like the one used to target the TRPC4 channels: the ion channels were targeted intracellularly using antibodies to block them and/or decrease their activity. As clemizole hydrochloride is a novel drug that has never been tested to block persistent firing, I decided to perform also experiments using anti-TRPC5 antibodies to have an extra proof supporting the role of TRPC5 channels underlying persistent firing in CA1 pyramidal cells.

Application of anti - TRPC5 antibodies 1:100

The firing frequency of persistent firing was affected by the application of the anti-TRPC5 antibodies. In these experiments 5 cells showed persistent firing during the application of carbachol (Fig. 29A). After 15 minutes from the rupture of the membrane, in 4 out of 5 cells persistent firing was completely suppressed, and it was not affected in 1 cell. Even if the effect of the antibodies showed a suppressing trend, the observed difference was not significant (Fig. 29E; Wilcoxon test, ns, $p = 0.125$, $n = 5$). The post stimulus membrane depolarization (MP1) was significantly suppressed by the anti-TRPC5 antibodies application (Fig. 29D; paired t-test, * $p < 0.05$, $n = 5$). After 15 minutes from the rupture of the membrane 4 out of 5 cells showed a reduction of the membrane potential depolarization, only in 1 cell it was not reduced. The values of MP2 were also in average suppressed by the application of the anti-TRPC5 antibodies, however the observed difference was not significant (Fig. 29G; paired t-test, ns, $p = 0.068$, $n = 5$).

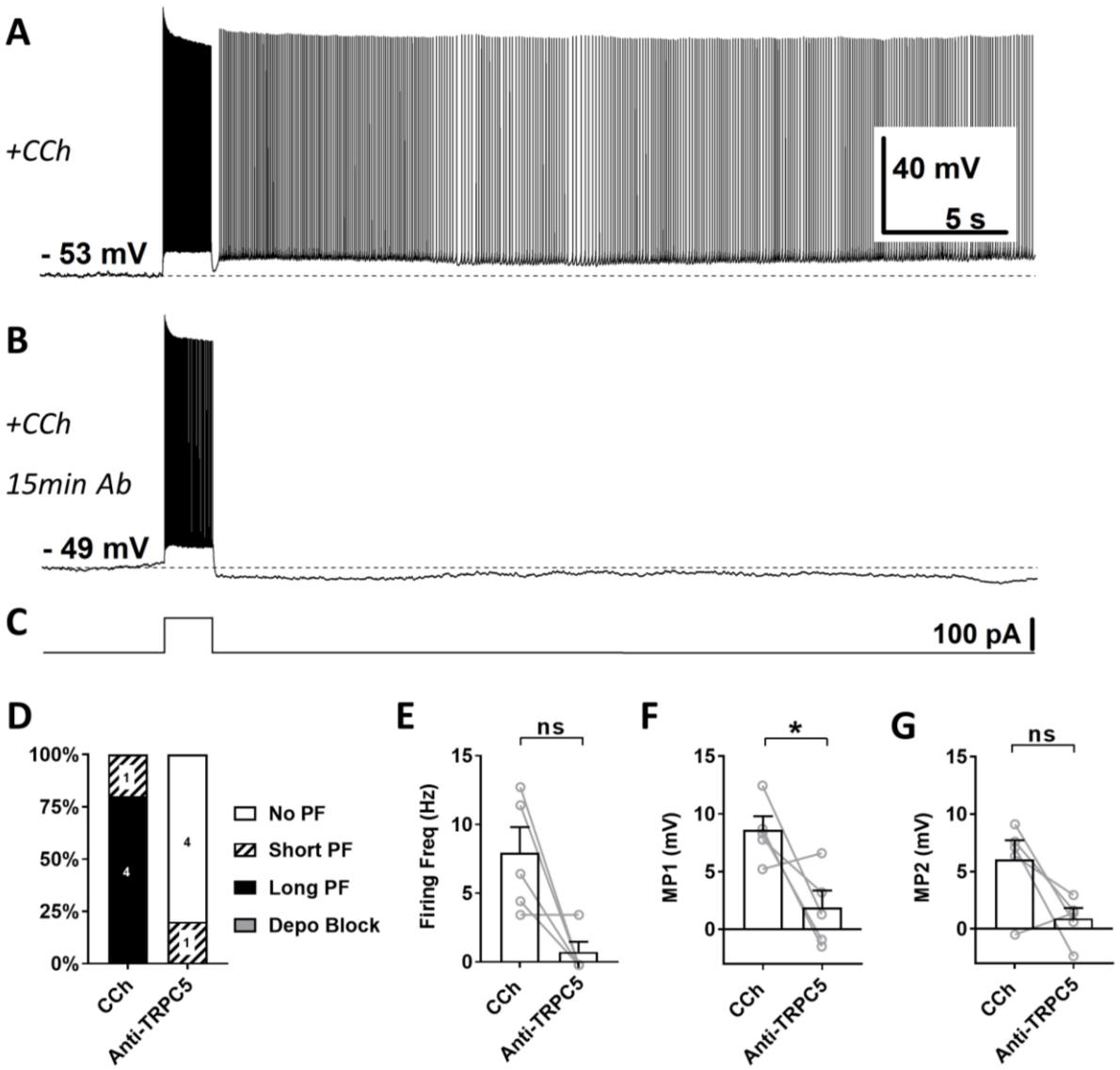

Figure 29 - The effect of intracellular application of anti-TRPC5 antibody (1:100) on persistent firing.

(A) Example of persistent firing recorded 5 min after the rupture of the membrane in CCh (10 μM). (B) Suppressed persistent firing recorded 15 min after the rupture of the membrane in the same cell shown in (A). (C) Current injection used in (A, B) (100 pA, 2 s). (D) Percentages of cells that showed persistent firing in control (5 min) and 15 min after the rupture of the membrane. The numbers on the graph represent the sample size. (E) Post-stimulus firing frequency (Wilcoxon test, ns, $p = 0.125$, $n = 5$). (F) Post-stimulus depolarization (MP1, paired t-test, * $p < 0.05$, $n = 5$). (G) Post-stimulus depolarization (MP2, paired t-test, ns, $p = 0.068$, $n = 5$).

Application of anti - TRPC5 antibodies 1:500

As already done for the TRPC4 antibodies, also for the TRPC5 antibodies in addition to the 1:100 dilution, the 1:500 dilution was tested (Fig. 30). The aim of these experiments was to test if the antibodies could still show a suppressing effect on persistent firing even when used at a lower concentration.

Of the 5 cells showing persistent firing in the control condition, after 15 minutes from the rupture of the membrane, 4 cells showed no persistent firing and 1 showed a reduced firing frequency. Again, even if the effects of the antibodies show a clear effect, the strong suppression of the firing frequency was not significant (Fig. 30E; Wilcoxon test, ns, $p = 0.065$, $n = 5$). The post stimulus membrane depolarization (MP1) was affected by the anti TRPC5 antibodies 1:500 application. After 15 minutes from the rupture of the membrane there was a suppression of the membrane depolarization in all the tested cells (Fig. 30F; paired t-test, * $p < 0.05$, $n = 5$). The values of MP2 were also in average reduced by the application of the antibodies, however the difference was not significant (Fig. 30G; paired t-test, ns, $p = 0.083$, $n = 5$).

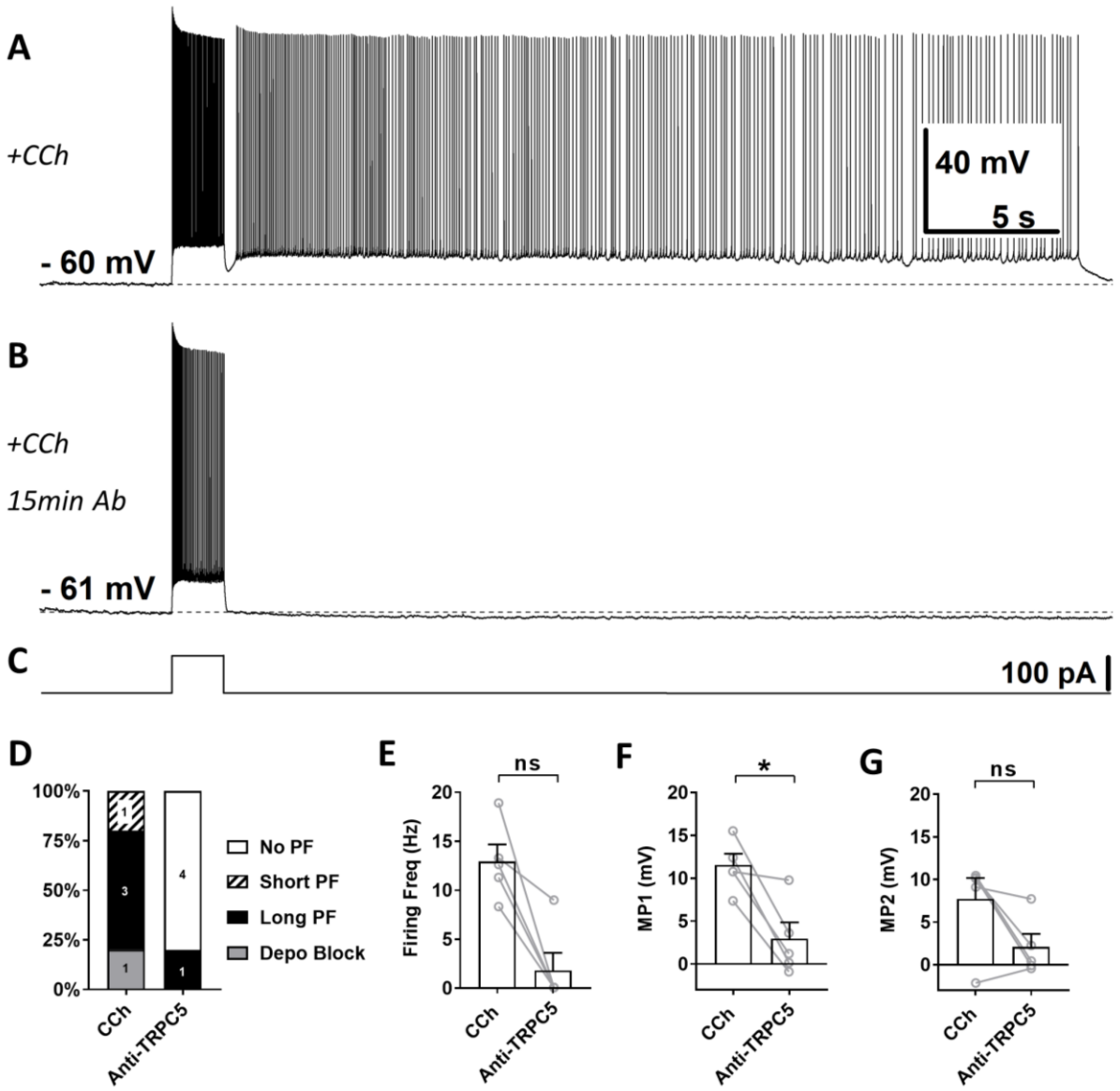

Figure 30 - The effect of intracellular application of anti-TRPC5 antibody (1:500) on persistent firing.

(A) Example of persistent firing recorded 5 min after the rupture of the membrane in CCh (10 μM). (B) Suppressed persistent firing recorded 15 min after the rupture of the membrane in the same cell shown in (A). (C) Current injection used in (A, B) (100 pA, 2 s). (D) Percentages of cells that showed persistent firing in control (5 min) and 15 min after the rupture of the membrane. The numbers on the graph represent the sample size. (E) Post-stimulus firing frequency (Wilcoxon test, ns, $p = 0.065$, $n = 5$). (F) Post-stimulus depolarization (MP1, paired t-test, * $p < 0.05$, $n = 5$). (G) Post-stimulus depolarization (MP2, paired t-test, ns, $p = 0.083$, $n = 5$).

In summary, the results of the experiments using the anti-TRPC5 antibodies (1:100 and 1:500), indicate that TRPC5 are involved in the mechanism supporting persistent firing. However, even if at both concentrations the anti-TRPC5 antibodies strongly suppressed the firing frequency of persistent firing, surprisingly the results were not significant. To check if this was just a sample size problem I grouped and analysed both conditions together (Fig. 31).

As expected, the suppressing effect of the anti-TRPC5 antibodies (1:100-500) on persistent firing was significant (Fig. 31B, Wilcoxon test, ** $p < 0.01$, $n = 10$). The suppressing effect observed on the post-stimulus depolarization was confirmed to be significantly reduced for MP1 (Fig. 31C, paired t-test, *** $p < 0.001$, $n = 10$) and was significantly reduced also for MP2 (Fig. 31D, Wilcoxon test, * $p < 0.05$, $n = 10$).

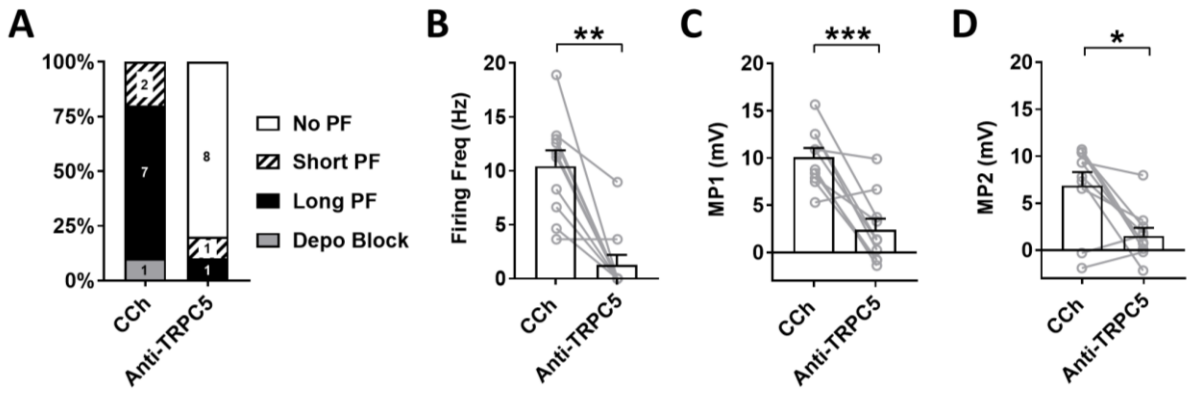

Figure 31 - The effect of intracellular application of anti-TRPC5 antibody (1:100–500) on persistent firing.
(A) Percentages of cells that showed persistent firing in control (5 min) and 15 min after the rupture of the membrane. The numbers on the graph represent the sample size. (B) Post-stimulus firing frequency (Wilcoxon test, ** $p < 0.01$, $n = 10$). (C) Post-stimulus depolarization (MP1, paired t-test, *** $p < 0.001$, $n = 10$). (D) Post-stimulus depolarization (MP2, Wilcoxon test, * $p < 0.05$, $n = 10$).

3.4.3 Intracellular application of inactivated antibodies

Heat inactivated antibodies can often, but not always, be used to assess potential non-specific effect of antibodies [189,268]. Therefore, I tested the effects of heat inactivated anti-TRPC4 and anti-TRPC5 antibodies on persistent firing.

Heat-inactivated anti-TRPC4 antibody (1:100) did not reduce the firing frequency of persistent firing significantly (Fig. 32E; paired t-test, ns, $p = 0.11$, $n = 8$). However, even the post-stimulus depolarization (MP1) was significantly reduced (Fig. 32F; paired t-test, * $p < 0.05$, $n = 8$), the degree of the reduction was smaller compared to the antibody without heat treatment (Heat treated: 53 %, non-heat treated: 70 %). The values of MP2 did not show any significant difference (Fig. 32G, paired t-test, ns, $p = 0.821$, $n = 8$).

These results indicate that either not all the antibodies were inactivated or that the inactivation protocol only partially destroyed the antigen binding site. However, the inactivated TRPC4 antibodies had a smaller suppressing effect on persistent firing suggesting that these antibodies did not have non-specific effects.

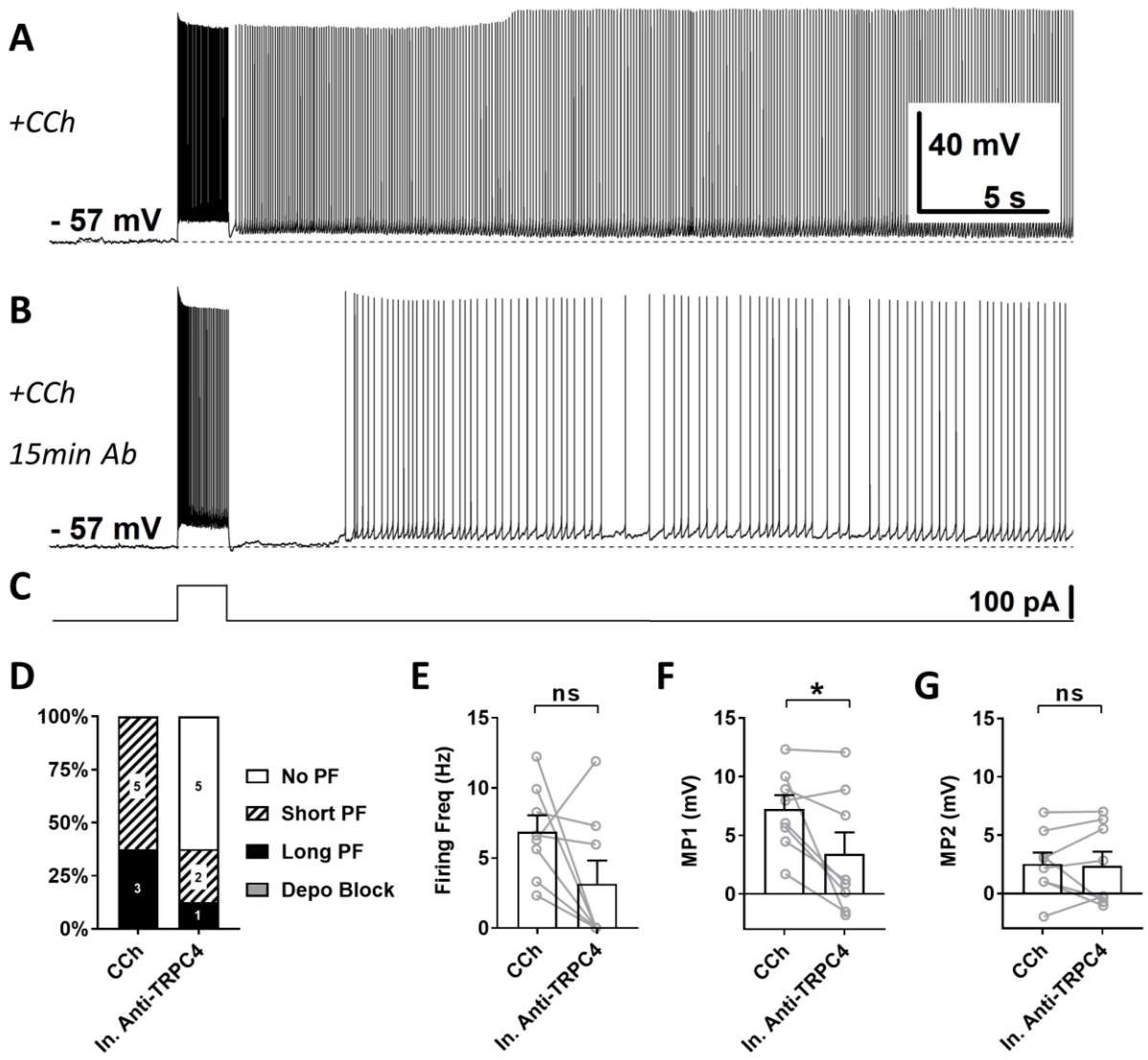

Figure 32 - The effect of intracellular application of heat inactivated anti-TRPC4 antibody (1:100) on persistent firing.

(A) Example of persistent firing recorded 5 min after the rupture of the membrane in CCh (10 μM). (B) Suppressed persistent firing recorded 15 min after the rupture of the membrane in the same cell shown in (A). (C) Current injection used in (A, B) (100 pA, 2 s). (D) Percentages of cells that showed persistent firing in control (5 min) and 15 min after the rupture of the membrane. The numbers on the graph represent the sample size. (E) Post-stimulus firing frequency (paired t-test, ns, $p = 0.11$, $n = 8$). (F) Post-stimulus depolarization (MP1, paired t-test, * $p < 0.05$, $n = 8$). (G) Post-stimulus depolarization (MP2, paired t-test, ns, $p = 0.821$, $n = 8$).

When heat-inactivated anti-TRPC5 antibodies (1:100) were tested, neither the firing frequency nor the post-stimulus depolarization, MP1 and MP2, were reduced significantly (Fig. 33E-G; firing frequency: paired t-test, p = 0.820, n = 4; MP1: paired t-test, p = 0.640, n = 4; Wilcoxon test, ns, p = 0.875, n = 4). These results indicate that the anti-TRPC5 antibodies did not have non-specific effects.

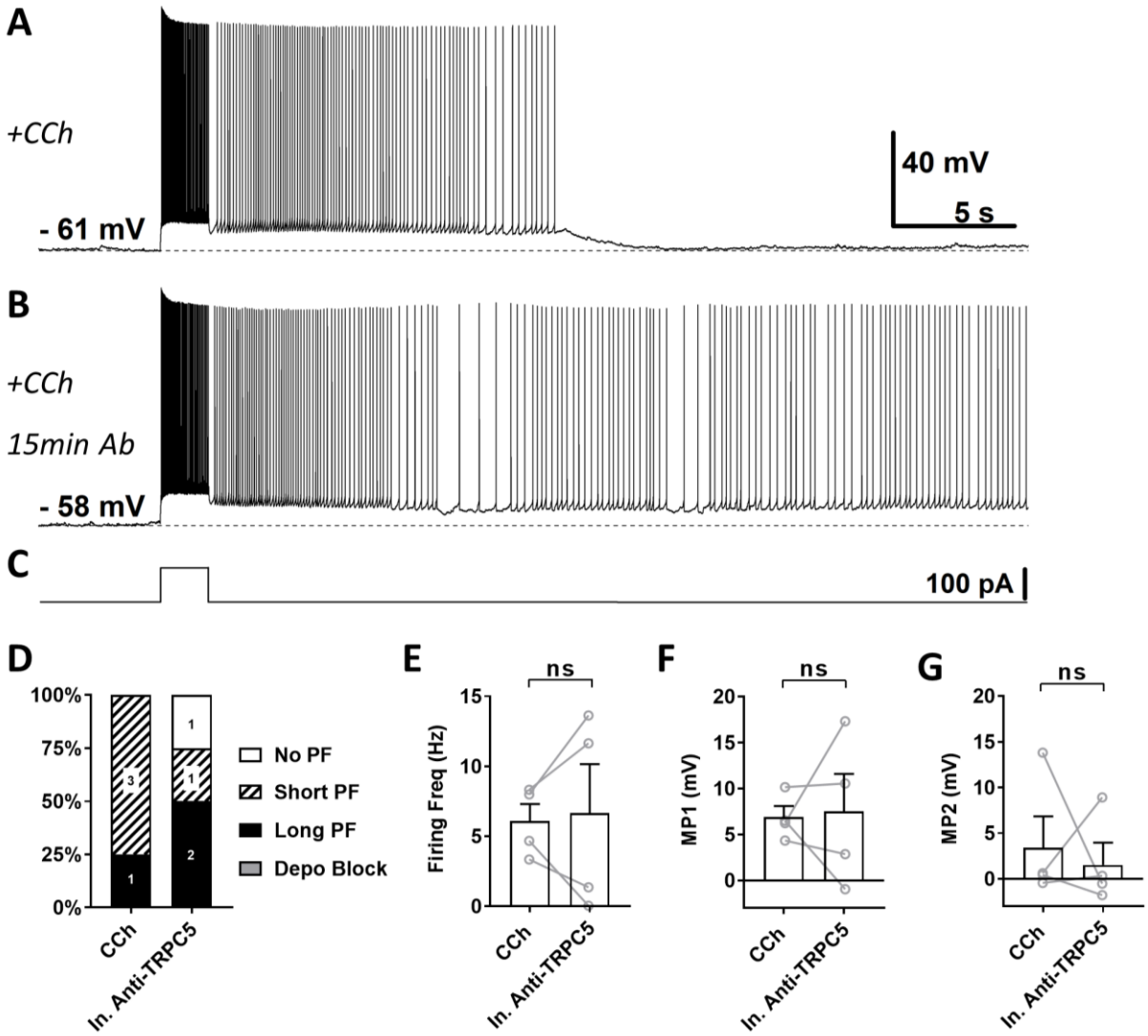

Figure 33 - The effect of intracellular application of heat inactivated anti-TRPC5 antibody (1:100) on persistent firing.

(A) Example of persistent firing recorded 5 min after the rupture of the membrane in CCh (10 µM). (B) Suppressed persistent firing recorded 15 min after the rupture of the membrane in the same cell shown in (A). (C) Current injection used in (A, B) (100 pA, 2 s). (D) Percentages of cells that showed persistent firing in control (5 min) and 15 min after the rupture of the membrane. The numbers on the graph represent the sample size. (E) Post-stimulus firing frequency (paired t-test, ns, p = 0.820, n = 4). (F) Post-stimulus depolarization (MP1, paired t-test, ns, p = 0.640, n = 4). (G) Post-stimulus depolarization (MP2, Wilcoxon test, ns, p = 0.875, n = 4).

3.5 Effects of TRPC channels knockout on persistent firing

Despite a number of studies indicating the involvement of TRPC channels in supporting persistent firing, some studies using TRPC KO did not show a clear link between TRPC channels and persistent firing or the plateau potential supporting it [113,259]. In the studies from Dasari et al. (2013) and Egorov et al. (2019) different TRPC KO models have been tested: single KO, triple KO (TRPC1/4/5 KO) and hepta-KO. In these different KO models, cells from the layer V of medial prefrontal cortex and from the layer V of medial entorhinal cortex were recorded. In all cases the deletion of TRPC subunits did not affect the after-stimulus depolarization and\or persistent firing, indicating that these channels are not supporting them. However, in the study from Dasari et al. (2013) it is considered that compensatory mechanisms, such as expression of alternative subunits and/or families of TRP channels (like TRPM or TRPV channels), could have biased their results leaving open the possible role of TRPC channels supporting cholinergic responses [259]. This hypothesis would be in line with the results of my experiments and also with the results of previous studies, showing that persistent firing was always inhibited when TRPC channels were targeted either with selective blockers or with antibodies.

To further assess the role of TRPC channels in supporting persistent firing, in addition to the approaches used so far, I decided to use TRPC4 KO and TRPC5 conditional KO mice. The TRPC4 KO model was chosen to see if persistent firing was present in the CA1 pyramidal neurons or if it was somehow affected by the lack of TRPC4. The TRPC5 conditional KO model was chosen to assess the involvement of TRPC5 in supporting persistent firing in hippocampal CA1 and to avoid possible compensation by overexpression of other ion channels that can happen in total KO animals [269]. Unfortunately, up to today the conditional KO model is only available for TRPC5.

I will first present the results collected in the TRPC4 KO mice and then I will focus on the results obtained with the TRPC5 conditional KO mice.

3.5.1 Persistent firing in TRPC4 KO mice

After the experiments using pharmacological blockers or antibodies to target TRPC channels, genetically modified mice were also used and the first ones to be tested were the TRPC4 KO mice. The aim of these experiments was to test if persistent firing could be induced with my experimental condition in this knock out model in CA1 pyramidal neurons. The TRPC4 total KO mice were provided by Dr. Marc Freichel (Heidelberg University) [264]. To check the presence of persistent firing in these KO animals, I used the same approach used in the previous experiments: current clamp recordings were made first in nACSF and then 10 μM carbachol was applied. The stimulation protocol, a square pulse of 100 pA lasting 2 seconds, was always applied while holding the membrane potential at the firing threshold of the neuron.

Persistent firing was present in mouse CA1 pyramidal cells and the firing activity did not show any abnormalities when compared to the one observed in experiments performed using wild type animals (Fig. 34). To have a better overview I will now compare the electrophysiological properties of all the cells recorded from TRPC4 KO mice with cells recorded in wild type mice used as control.

In TRPC4 KO mice, during the application of carbachol, persistent firing was induced in 5 out of 6 cells and in these cells the firing frequency was slightly higher compared to wild type cells. However, the difference observed was not significant (Fig. 34E, Mann-Whitney test, ns, $p = 0.167$, $n_{TRPC4\ KO} = 6$, $n_{WT} = 35$). There were also no significant differences between the two groups when comparing the plateau potential after the end of the stimulus (MP1 and MP2) during carbachol application (Fig. 34F-G; MP1, unpaired t-test, ns, $p = 0.892$, $n_{TRPC4\ KO} = 6$, $n_{WT} = 35$; MP2, Mann-Whitney test, ns, $p = 0.627$, $n_{TRPC4\ KO} = 6$, $n_{WT} = 35$). Besides the membrane potential values after the end of the stimulus, in these animals also the membrane potential during the stimulus application was analysed to assess if the lack of TRPC4 could affect it. During the application of CCh, the average membrane potential depolarization during the application of the stimulus was not significantly different between the two groups (Fig. 34H, Mann-Whitney test, ns, $p = 0.505$, $n_{TRPC4\ KO} = 6$, $n_{WT} = 35$).

In control condition (nACSF), the average membrane potential value after the end of the stimulus (MP1) of the TRPC4 KO mice did not show any differences compared to the wild type animals (Fig. 34I, unpaired t-test, ns, $p = 0.398$, $n_{TRPC4\ KO} = 6$, $n_{WT} = 35$). Interestingly in nACSF, membrane potential depolarization during the application of the stimulus significantly differed between the two groups and the TRPC4 KO cells were more depolarized (Fig. 34L, Mann-Whitney test, * $p < 0.05$, $n_{TRPC4\ KO} = 6$, $n_{WT} = 35$).

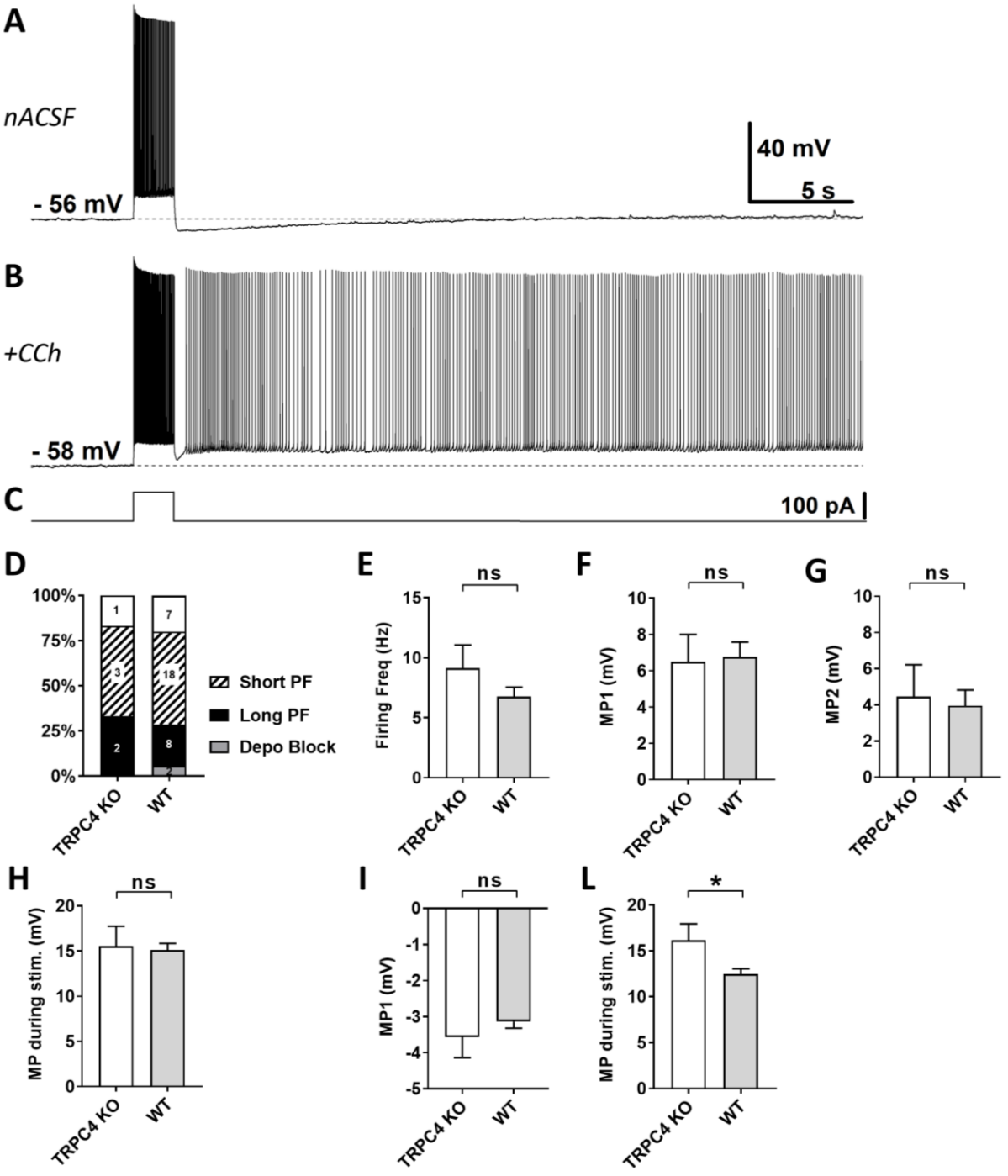

Figure 34 - Persistent firing in TRPC4 KO mice.

(A) Example of a cell recorded in control condition (nACSF). (B) Example of a cell showing persistent firing in CCh (10 µM). (C) Current injection used in (A,B) (100 pA, 2 s). (D) Percentages of type of persistent firing in CCh in TRPC4 KO and in wild type (WT) mice. The numbers on the graph represent the sample size. (E) Post-stimulus firing frequency in CCh (Mann-Whitney test, ns, $p = 0.167$, $n_{TRPC4\ KO} = 6$, $n_{WT} = 35$). (F) Post-stimulus depolarization in CCh (MP1, unpaired t-test, ns, $p = 0.892$, $n_{TRPC4\ KO} = 6$, $n_{WT} = 35$). (G) Post-stimulus depolarization in CCh (MP2, Mann-Whitney test, ns, $p = 0.627$, $n_{TRPC4\ KO} = 6$, $n_{WT} = 35$). (H) Membrane potential depolarization during the stimulus application (Mann-Whitney test, ns, $p = 0.505$, $n_{TRPC4\ KO} = 6$, $n_{WT} = 35$). (I) Post-stimulus depolarization in control condition (MP1, unpaired t-test, ns, $p = 0.398$, $n_{TRPC4\ KO} = 6$, $n_{WT} = 35$). (L) Membrane potential depolarization during the stimulus application in control condition (Mann-Whitney test, * $p < 0.05$, $n_{TRPC4\ KO} = 6$, $n_{WT} = 35$). All the recorded cells, shown in (D), were included in (E-L).

In summary, TRPC4 KO cells showed cholinergic-dependent persistent firing under my experimental conditions and both the firing frequency and the after-stimulus depolarization were not significantly different compared to wild type cells. The only difference between TRPC4 KO and WT animals was observed in the membrane potential during stimulation in control condition (nACSF) where the TRPC4 KO neurons responded in average with a bigger depolarization. This result could be explained by the presence of compensatory mechanisms probably balancing the lack of TRPC4.

Taken together these results indicate that in this TRPC4 KO model, TRPC4 are not necessary to support persistent firing in CA1 pyramidal neurons.

3.5.1.1 Effect of clemizole hydrochloride on persistent firing in TRPC4 KO mice

After testing the presence of persistent firing in CA1 pyramidal neurons of TRPC4 KO mice, 20 μM clemizole hydrochloride (CLE) was applied on cells showing persistent firing to see if other TRPC channels were still supporting the mechanism (Fig. 35).

In these experiments, persistent firing was observed in 4 cells during the application of carbachol and the firing frequency was strongly reduced after 15 minutes after the application of CLE: in 3 cells the firing frequency was strongly reduced and in 1 cell persistent firing was completely suppressed (Fig. 35E, paired t-test, ** $p < 0.01$, $n = 4$). In TRPC4 KO neurons, 20 μM CLE induced depolarization block in 3 out of 4 of the cells (Fig. 35B and Fig. 35D). This effect was also observed in the experiments using wild type animals. The membrane potential depolarization (MP1) increase induced by the application of CLE was not significant, however it showed a trend of the neurons to be more depolarized during 20 μM CLE application after the end of the stimulus (Fig. 35F, paired t-test, ns, $p = 0.401$, $n = 4$). The values of MP2 showed that the application of CLE in average reduced the depolarization, however the difference was no significant (Fig. 35G, paired t-test, ns, $p = 0.148$, $n = 4$). As already observed in the WT animals, the application of CLE on top of carbachol affected the membrane potential during the application of the stimulus and not only after it. The membrane potential during the stimulation was significantly more depolarized during the application of CLE (Fig. 35H, paired t-test, ** $p < 0.01$, $n = 4$).

In summary, the application of 20 μM CLE suppressed persistent firing in TRPC4 KO neurons and induced depolarization block in most of the tested cells exactly like it was previously observed in WT. These data suggest that, in TRPC4 KO animals, the remaining TRPC channels are still involved in the mechanism supporting persistent firing. However, as

this interpretation is challenged by the potential unspecific effect of clemizole hydrochloride (20 µM), more experiments will be necessary to deepen these findings.

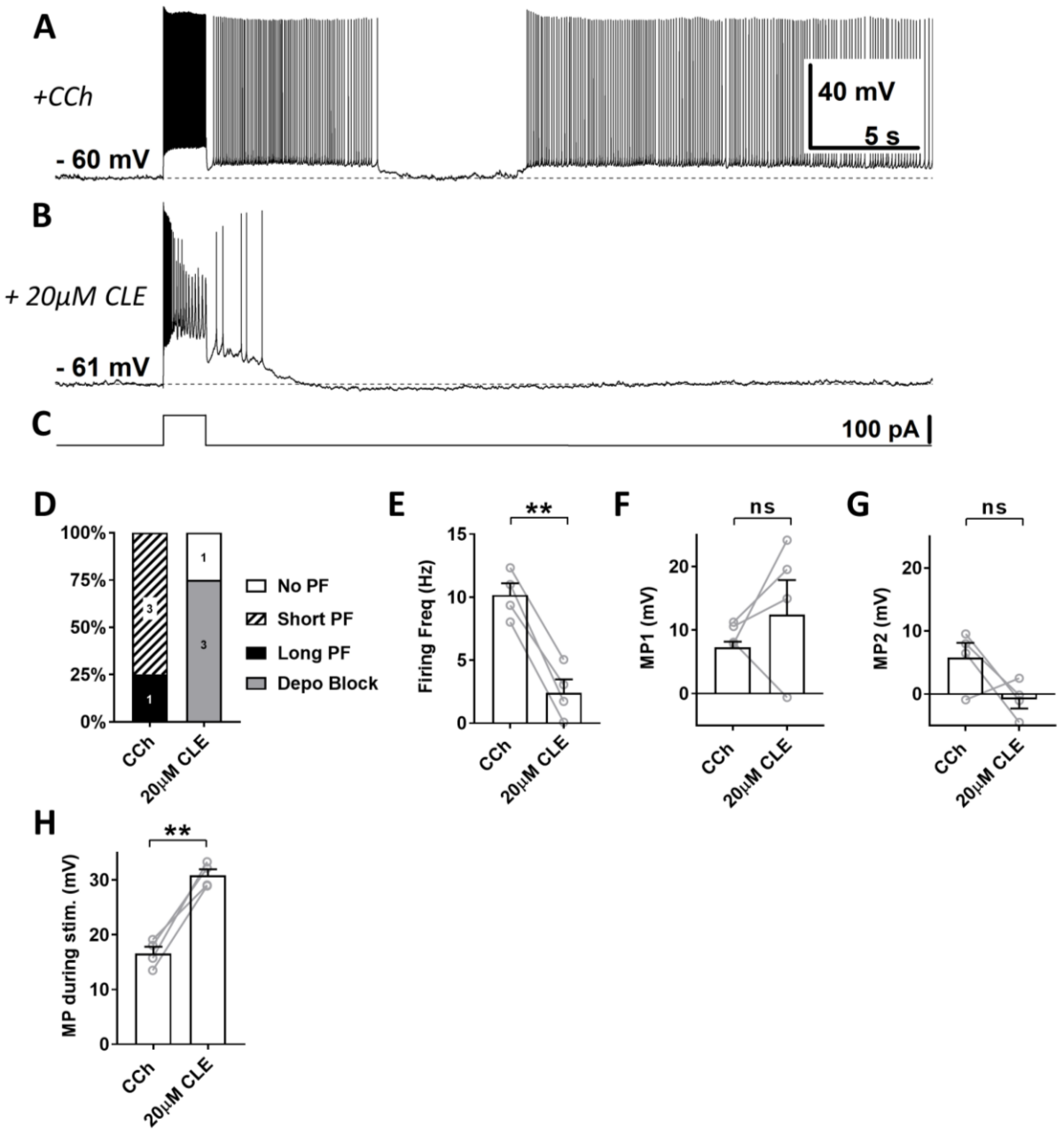

Figure 35 - The effect of clemizole hydrochloride (20 µM) on persistent firing in TRPC4 KO mice.

(A) Example of persistent firing in CCh (10 µM). (B) Suppressed persistent firing and depolarization block in clemizole (CLE, 20 µM) in the same cell shown in (A). (C) Current injection used in (A, B) (100 pA, 2 s). (D) Percentages of cells that showed persistent firing in CCh and during the application of CLE. The numbers on the graph represent the sample size. (E) Post-stimulus firing frequency (paired t-test, ** $p < 0.01$, $n = 4$). (F) Post-stimulus depolarization (MP1, paired t-test, ns, $p = 0.401$, $n = 4$). (G) Post-stimulus depolarization (MP2, paired t-test, ns, $p = 0.148$, $n = 4$). (H) Membrane potential depolarization during the stimulus application (paired t-test, ** $p < 0.01$, $n = 4$).

3.5.2 TRPC5 conditional KO model

After the experiments using TRPC4 KO mice, I tested the presence of persistent firing in TRPC5 conditional KO mice. In the following sections I will present the data collected from these animals. First I will focus on the quantitative PCR results done to confirm the TRPC5 conditional KO, then I will present the results of the patch clamp experiments, showing data collected in infected TRPC5 flx/flx and WT animals, 4 and 2 weeks after infection. The TRPC5 flx/flx mice were provided by Dr. Lutz Birnbaumer (NIEHS).

3.5.2.1 Confirmation of the TRPC5 conditional KO in the hippocampus

The conditional KO model was chosen with the aim of obtaining TRPC5 KO neurons not affected by compensatory mechanisms. Quantitative PCR (qPCR) was used to assess if the TRPC5 conditional knockout was happening and at which level. In addition, qPCR was used to test if the other TRPC subtypes changed their expression level to compensate the lack of TRPC5. These experiments were performed in the laboratories of Prof. Dr. Oliver Storks under the supervision of Dr. Anne Albrecht (Department of Genetics & Molecular Neurobiology, Institute of Biology, Otto-von-Guericke University Magdeburg).

In these experiments, TRPC5 flx/flx mice were infected with two different viruses. One group of animals was infected with an AAV-Cre-GFP virus (Fig. 36A) and the other group was infected with an AAV-GFP virus as control (Fig. 36B). In the group injected with the AAV-Cre-GFP virus, the infected cells expressed both GFP and Cre recombinase. As the TRPC5 flx/flx mice have two loxP sites around part of the sequence coding for TRPC5, the Cre recombinase will excise that part of DNA leading to an incomplete transcription of a structural part of the channel. This will result in the formation of non-functional channels that will be destroyed, leading in this way to a decreased expression of TRPC5 and to the conditional KO. In the control group, injected with the AAV-GFP virus, the infected cells were marked by the GFP expression but, as the Cre recombinase was absent, no genetic modifications were supposed to happen.

The hippocampal CA1 of each hemisphere was infected in five animals per group, after 4 weeks from the infection the brains were processed, and the qPCRs performed. The qPCRs were used to test the whole TRPC family, excluding TRPC2 channels as these channels almost not expressed in rodents brain [205]. By checking the expression levels of the TRPC family, I aimed to detect potential compensation effects mediated by over or under expression of these channels. The qPCRs were used to test the CA1 and CA3 regions in animals injected with AAV-GFP (control) or AAV-GFP-Cre (conditional knock out). The

CA3 area was tested not only to compare it with CA1, but also to have an internal control in every animal. I will first give an overview of the mRNA expression in the control animals and then focus on the TRPC5 conditional KO animals.

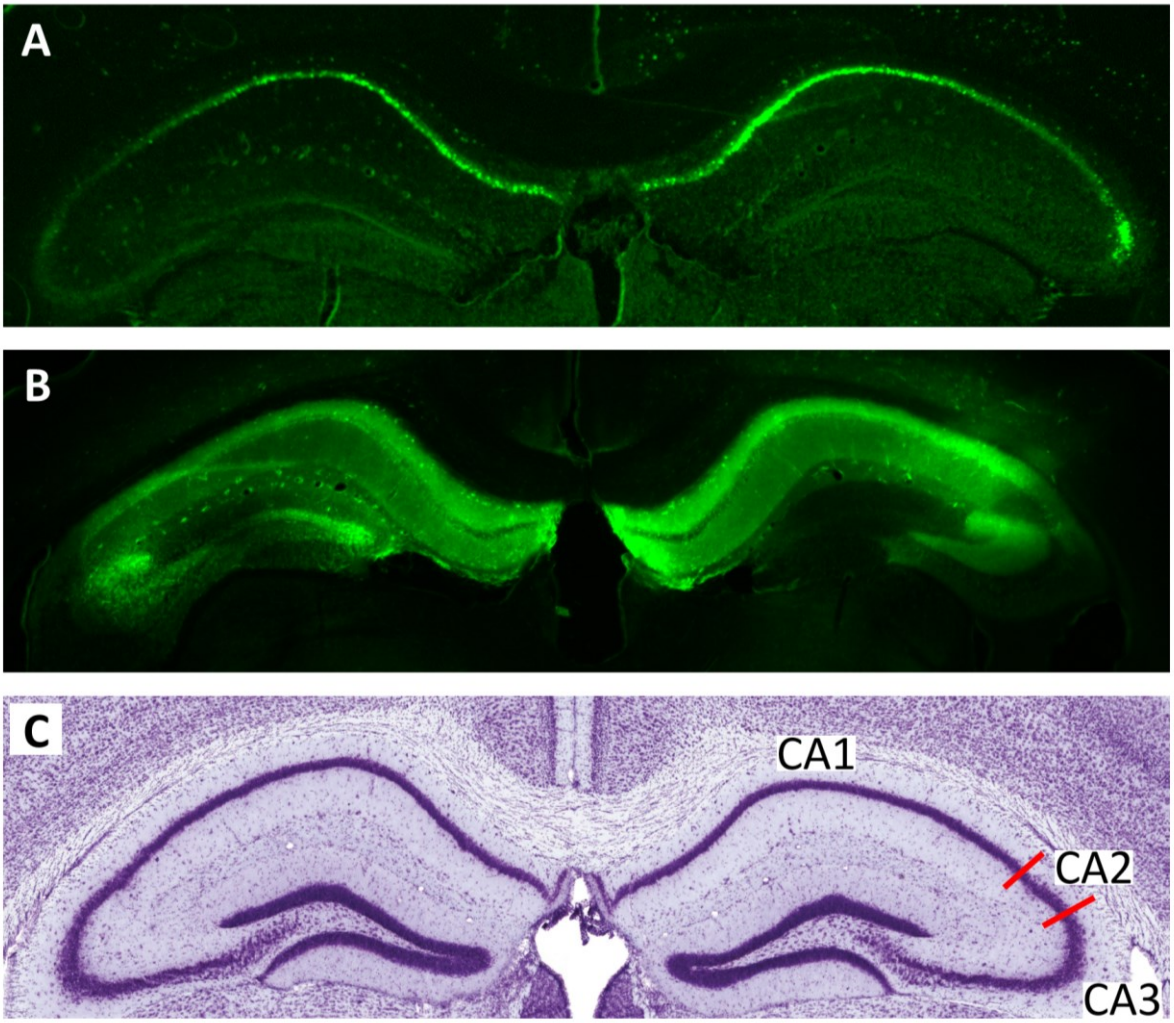

Figure 36 – Expression of GFP in infected TRPC5 flx/flx mice.

(A) GFP expression in a coronal slice of the hippocampus in a mouse infected with AAV-Cre-GFP. (B) GFP expression in a coronal slice of the hippocampus in a mouse infected with AAV-GFP. (C) A Nissl staining image of a coronal hippocampal slice highlighting the position of the CA1, CA2 and CA3 areas. This image was modified from the Allen brain mouse atlas (http://portal.brain-map.org/).

In the control animals (AAV-GFP), based on the dCT values (difference of cycle times, compared to the housekeeping gene), the channels mostly expressed in the CA1 area were: TRPC1, TRPC4, TRPC5 and at lower level TRPC6 (Fig. 37A-left). TRPC3, and especially TRPC7, were almost not expressed in CA1 as their dCT values were high. The dCT values with more negative values indicate a higher channel expression as they needed less cycle to be detected. When the dCT values are high it means that the expression of the tested channels

was low and consequently they needed more cycle to be detected. In the CA3 area the channels mostly expressed were TRPC1, and at lower level TRPC5 and TRPC6 (Fig. 37A-right). TRPC4 and TRPC3 mRNA was present, but at a lower level. The TRPC7 were almost absent in the CA3 area.

As expected, in the CA1 area the infection with the AAV-Cre-GFP virus significantly reduced the TRPC5 expression compared to the control virus (Fig. 37A-left, Mann-Whitney test, ** $p < 0.01$, $n_{AAV\text{-}GFP} = 5$, $n_{AAV\text{-}Cre\text{-}GFP} = 5$). Besides the expected change in the TRPC5 expression, also TRPC3 and TRPC4 were affected. In the CA1 region, while the TRPC3 expression was significantly increased (Fig. 37A-left, unpaired t-test, ** $p < 0.01$, $n_{AAV\text{-}GFP} = 5$, $n_{AAV\text{-}Cre\text{-}GFP} = 5$), the TRPC4 expression was reduced by the conditional knock out and the difference to the control was small but highly significant (Fig. 37A-left, Mann-Whitney test, ** $p < 0.01$, $n_{AAV\text{-}GFP} = 5$, $n_{AAV\text{-}Cre\text{-}GFP} = 5$). The expression of the other tested channels, TRPC1, TRPC6 and TRPC7, did not show any significant change in their mRNA expression (Fig. 37A-left; TRPC1, ns, unpaired t-test, $p = 0.995$; TRPC6, ns, Mann-Whitney test, $p = 0.548$; TRPC7, unpaired t-test, ns, $p = 0.070$; for TRPC1/6/7 the sample size was: $n_{AAV\text{-}GFP} = 5$, $n_{AAV\text{-}Cre\text{-}GFP} = 5$).

In the CA3 area the TRPC5 mRNA was also significantly reduced by the knock out (Fig. 37A-right, unpaired t-test, *** $p < 0.001$, $n_{AAV\text{-}GFP} = 5$, $n_{AAV\text{-}Cre\text{-}GFP} = 5$). The other tested channels showed an expression pattern similar to the one observed in the CA1 region. The TRPC4 expression was reduced also in CA3 and the difference observed was significant (Fig. 37A-right, unpaired t-test, * $p < 0.05$, $n_{AAV\text{-}GFP} = 4$, $n_{AAV\text{-}Cre\text{-}GFP} = 5$). The expression of the other channels, TRPC1, TRPC3, TRPC6 and TRPC7, did not show any significant change compared to control. (Fig. 37A-right; TRPC1, unpaired t-test, ns, $p = 0.320$; TRPC3, unpaired t-test, ns, $p = 0.827$; TRPC6, unpaired t-test, ns, $p = 0.268$; TRPC7, unpaired t-test, ns, $p = 0.071$; for TRPC1/3/6/7 the sample size was: $n_{AAV\text{-}GFP} = 5$, $n_{AAV\text{-}Cre\text{-}GFP} = 5$).

In summary: in the CA1 area of the animals infected with AAV-Cre-GFP, the dCT values showed that while the mRNA levels of TRPC4 and TRPC5 were significantly lower compared to control animals, the expression level of TRPC3 was significantly increased in CA1 in animals injected with AAV-Cre-GFP. Also in the CA3 area of the animals infected with AAV-Cre-GFP, the expression level of TRPC4 and TRPC5 were significantly lower compared to control. The rest of the channels, including TRPC3, showed a similar expression pattern.

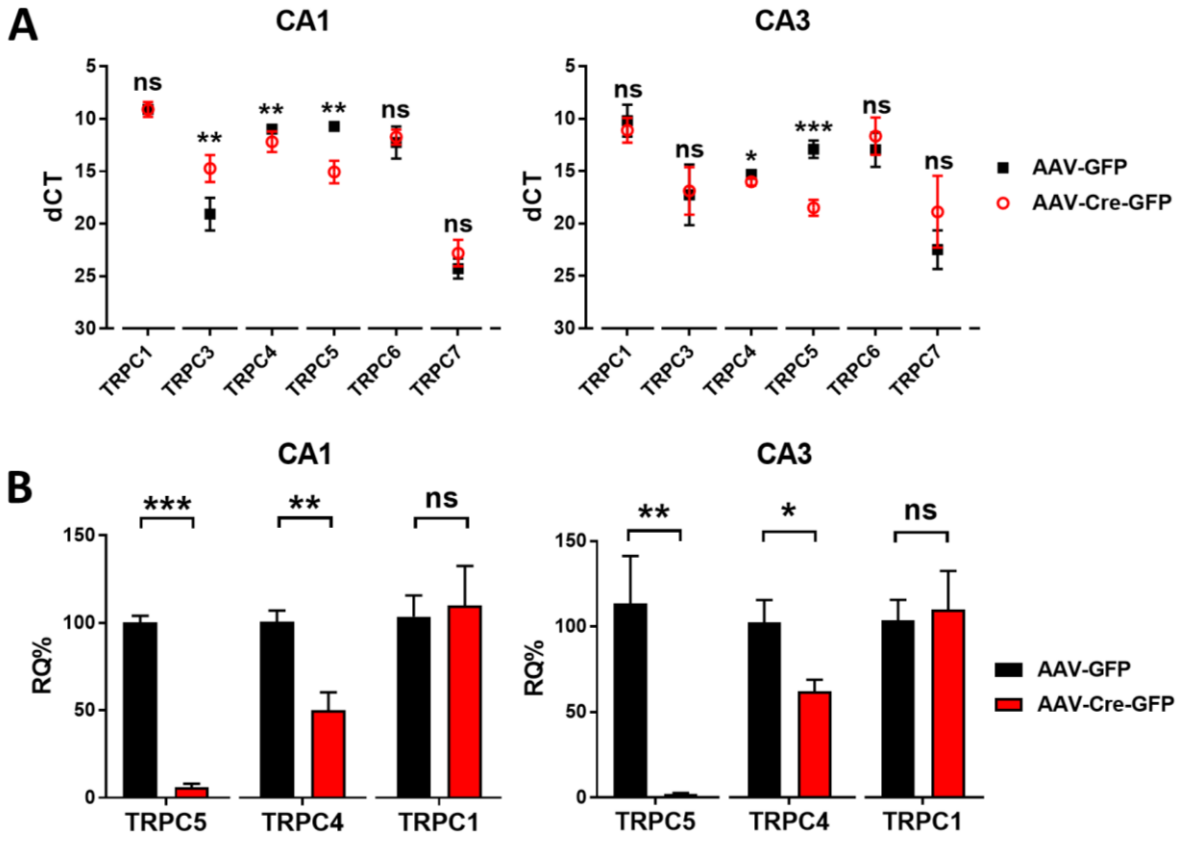

Figure 37 - Results of the qPCR experiments in infected TRPC5 flx/flx mice.

(A) dCT values (difference of cycle times) of the tested TRPC channels in TRPC5 flx/flx mice. In each ion channel the dCT values obtained in mice infected with AAV-Cre-GFP (red circle) were compared with AAV-GFP (control, black square). In CA1 (left): TRPC1 (Unpaired t-test, ns, $p = 0.995$), TRPC3 (Unpaired t-test, ** $p < 0.01$), TRPC4 (Mann-Whitney test, ** $p < 0.01$), TRPC5 (Mann-Whitney test, ** $p < 0.01$), TRPC6 (Mann-Whitney test, ns, $p = 0.548$), TRPC7 (Unpaired t-test, ns, $p = 0.070$). For TRPC1/3/4/5/6/7: $n_{AAV\text{-}GFP} = 5$, $n_{AAV\text{-}Cre\text{-}GFP} = 5$. In CA3 (right): TRPC1 (Unpaired t-test, ns, $p = 0.320$), TRPC3 (Unpaired t-test, $p = 0.827$), TRPC4 (Unpaired t-test, * $p < 0.05$), TRPC5 (Unpaired t-test, *** $p < 0.001$), TRPC6 (Unpaired t-test, ns, $p = 0.268$), TRPC7 (Unpaired t-test, ns, $p = 0.071$). For TRPC1/3/5/6/7: $n_{AAV\text{-}GFP} = 5$, $n_{AAV\text{-}Cre\text{-}GFP} = 5$. For TRPC4: $n_{AAV\text{-}GFP} = 4$, $n_{AAV\text{-}Cre\text{-}GFP}$. The y-axis is inverted in the graph because the dCT values with more negative values indicate a higher channel expression. For some data points the error bar was shorter than the height of the symbol. (B) Relative quantification (RQ%) values of qPCRs showed in (A). The values measured in animals infected with AAV-Cre-GFP (red) were compared with AAV-GFP (control, black). In CA1 (left): TRPC5 (Unpaired t-test, *** $p < 0.001$), TRPC4 (Unpaired t-test, ** $p < 0.01$), TRPC1 (Unpaired t-test, ns, $p = 0.811$). For TRPC1/4/5: $n_{AAV\text{-}GFP} = 5$, $n_{AAV\text{-}Cre\text{-}GFP} = 5$. In CA3 (right): TRPC5 (Mann-Whitney test, ** $p < 0.01$), TRPC4 (Unpaired t-test, * $p < 0.05$), TRPC1 (Unpaired t-test, ns, $p = 0.181$). For TRPC1/5: $n_{AAV\text{-}GFP} = 5$, $n_{AAV\text{-}Cre\text{-}GFP} = 5$. For TRPC4: $n_{AAV\text{-}GFP} = 4$, $n_{AAV\text{-}Cre\text{-}GFP}$.

For TRPC5, TRPC4 and TRPC1, I will also show the relative quantification (RQ%) measure. I chose these channels because they were among the mostly expressed in the CA1 and CA3 and because these three subunits were of particular interests for my project as they can form homomer and heteromer channels. The relative quantification reflects the changes compared to the average of the control group. When the variability is high, it can happen that the total percentage in the control will not be exactly 100%. This was shown by TRPC1 in

CA1 and by TRPC5 and TRPC1 in CA3 (Fig. 37B).

In the CA1 area of animals infected with AAV-Cre-GFP, only the 6% of the TRPC5 mRNA was left, confirming that the knock out mediated by the virus was working very well (Fig. 37B-left, unpaired t-test, *** $p < 0.001$, $n_{AAV\text{-}GFP} = 5$, $n_{AAV\text{-}Cre\text{-}GFP} = 5$). As already pointed out while observing the dCT values, in the CA1 the TRPC4 mRNA showed a reduction. In fact, in the animals infected with AAV-Cre-GFP, only the 50% of the TRPC4 mRNA was still present and, when compared to the control, the difference was significant (Fig. 37B-left, unpaired t-test, ** $p < 0.01$, $n_{AAV\text{-}GFP} = 5$, $n_{AAV\text{-}Cre\text{-}GFP} = 5$). The TRPC1 expression was not affected by the knock out (Fig. 37B-left, unpaired t-test, ns, $p = 0.811$, $n_{AAV\text{-}GFP} = 5$, $n_{AAV\text{-}Cre\text{-}GFP} = 5$).

In the CA3 region of animals infected with AAV-Cre-GFP, the expression pattern was following the one shown in the CA1 area. The TRPC5 mRNA was strongly reduced and only the 2% ca. of the mRNA was left (Fig. 37B-right, Mann-Whitney test, ** $p < 0.01$, $n_{AAV\text{-}GFP} = 5$, $n_{AAV\text{-}Cre\text{-}GFP} = 5$). The TRPC4 mRNA was also reduced an only the 62% of the mRNA was left (Fig. 37B-right, unpaired t-test, * $p < 0.05$, $n_{AAV\text{-}GFP} = 4$, $n_{AAV\text{-}Cre\text{-}GFP} = 5$). The TRPC1 expression was again not affected by the knock out (Fig. 37B-left, unpaired t-test, ns, $p = 0.181$, $n_{AAV\text{-}GFP} = 4$, $n_{AAV\text{-}Cre\text{-}GFP} = 5$).

In summary, the qPCR results confirmed that the TRPC5 conditional KO was happening in the TRPC5 flx/flx mice, in both CA1 and CA3, the AAV-Cre-GFP strongly suppressed the TRPC5 mRNA expression. Interestingly, the AAV-Cre-GFP infection, not only affected TRPC5, but affected also the expression of TRPC3 and TRPC4, increasing and decreasing it, respectively. Taken together these results indicate that the TRPC5 conditional KO was successful, however they also indicate that, 4 weeks after the infection, compensatory mechanisms were already buffering the lack of TRPC5.

3.5.3 Persistent firing in TRPC5 conditional KO cells

After showing with qPCR that the TRPC5 conditional KO happened after the viral infection with AAV-Cre-GFP, I performed *in vitro* patch clamp experiments to test if and how persistent firing could have been affected by lack of the TRPC5 channels. In this series of experiments, the animals were bilaterally injected with AAV-Cre-GFP in the dorsal and in the ventral hippocampus and used four weeks after infection. In these animals two groups of cells were recorded: GFP positive and GFP negative cells.

The GFP positive (GFP+) cells were TRPC5 KO and were recorded to see how the absence of TRPC5 could have affected persistent firing. The GFP negative (GFP-) cells were recorded from animals that have been infected, but as these cells were not GFP, the virus did not infect them. These GFP negative cells were recorded as control to see if their electrophysiological behaviour was similar to the one observed in cells recorded in non-infected wild type animals. In fact, GFP negative cells besides having two flox sites, were genetically like WT cells. For this reason, GFP negative cells were used as control for the GFP positive cells infected with AAV-Cre-GFP. There is also another reason why I used GFP negative cells as control. The viral infection was made aiming to infect the CA1 area, however the infection spread in most of the cases and also the CA3 area was infected. As I did not use synaptic blockers, by using GFP- cells recorded in infected animals, I could exclude potential side effects mediated by CA3 input to CA1, altered by the viral infection.

As additional control group, also GFP positive cells recorded from TRPC5 flx/flx animals infected with AAV-GFP should have been used. This virus was the same adenovirus lacking Cre previously tested in the qPCRs. However, the expression of GFP in the infected cells was not high enough to be detected during my patch clamp experiments using an upright microscope (Zeiss Axioskop 2FS plus, Carl Zeiss Microscopy) equipped with a 40x water-immersion objective lens, and a monochrome camera (WAT-902H Ultimate). The fluorescence was only detectable using fluorescence microscopes, such as a BZ-9000 (Keyence). For this technical reason, after some infructuous experiments using mice infected with AAV-GFP, I used as controls only the GFP negative cells recorded from TRPC5 flx/flx animals infected with AAV-Cre-GFP.

3.5.3.1 Persistent firing in GFP positive and negative cells in TRPC5 flx/flx mice

In this section I will show the properties of the GFP positive and negative cells recorded from TRPC5 flx/flx mice infected with the AAV-Cre-GFP virus. To have a better overview, I will compare together: GFP positive and negative cells and, in addition, cells recorded in wild type animals. The GFP positive cells were TRPC5 conditional KO cells, the GFP negative cells were recorded in infected animals and used as control, as they were not affected by the infection. I will refer to them as GFP+ (flx/flx) and GFP- (flx/flx), respectively. Finally, the wild type (WT) cells were recorded from non-infected wild type animals and were used as additional control. In these comparisons I took in account all the population of recorded neurons, showing and not showing persistent firing. For all the cells the stimulation protocol used was always the same, 100 pA lasting 2 seconds applied from the firing threshold, and the concentration of carbachol was 10 μM.

During cholinergic stimulation, among the 21 GFP positive cells recorded in TRPC5 flx/flx mice, 50% of them responded with a strong depolarization block (Fig. 38B), 45.5% of the cells showed persistent firing with a very depolarized burst firing activity (Fig. 38D) and finally, 4.5% of the cells did not show persistent firing or depolarization block (Fig. 39A). The GFP+ (flx/flx) cells showing a strong depolarization block, either were not able to fire action potentials or they showed only some little spikelets in some part of the recording (Fig. 38B). When the firing frequency was measured only action potentials were counted and for this reason, in the cells showing a strong depolarization block the measured firing frequency was often zero.

In the GFP- (flx/flx) cells, during the application of carbachol, the firing behaviour was comparable to WT neurons. During or after the end of the stimulus, the cells showed a normal firing behaviour and they did not show depolarization block or depolarized bursting activity (Fig. 38F). Of the recorded cells 44% showed long persistent firing, 25% showed short persistent firing and 31% of the cells showed no persistent firing (Fig. 39A).

Figure 38 - Persistent firing in TRPC5 flx/flx mice infected with AAV-Cre-GFP (figure on next page).

(A) The trace shows a GFP+ (flx/flx) cell recorded in control condition (nACSF). (B, top) Example of depolarization block in presence of 10 μM carbachol (CCh) in the same cell recorded in (A). At the end of the trace the cell partially recovered but it only fired spikelets. (B, bottom) Current injection used in (A, B) (100 pA, 2 s). (C) The trace shows a GFP+ (flx/flx) cell recorded in control condition (nACSF). (D, top) Example of bursting persistent firing in presence of 10 μM carbachol (CCh) in the same cell recorded in (C). (D, bottom) Current injection used in (C, D) (100 pA, 2 s). (E) The trace shows a GFP- (flx/flx) cell recorded in control condition (nACSF). (F, top) Example of long-lasting persistent firing in presence of 10 μM carbachol (CCh) in the same cell recorded in (E). (F, bottom) Current injection used in (E, F) (100 pA, 2 s).

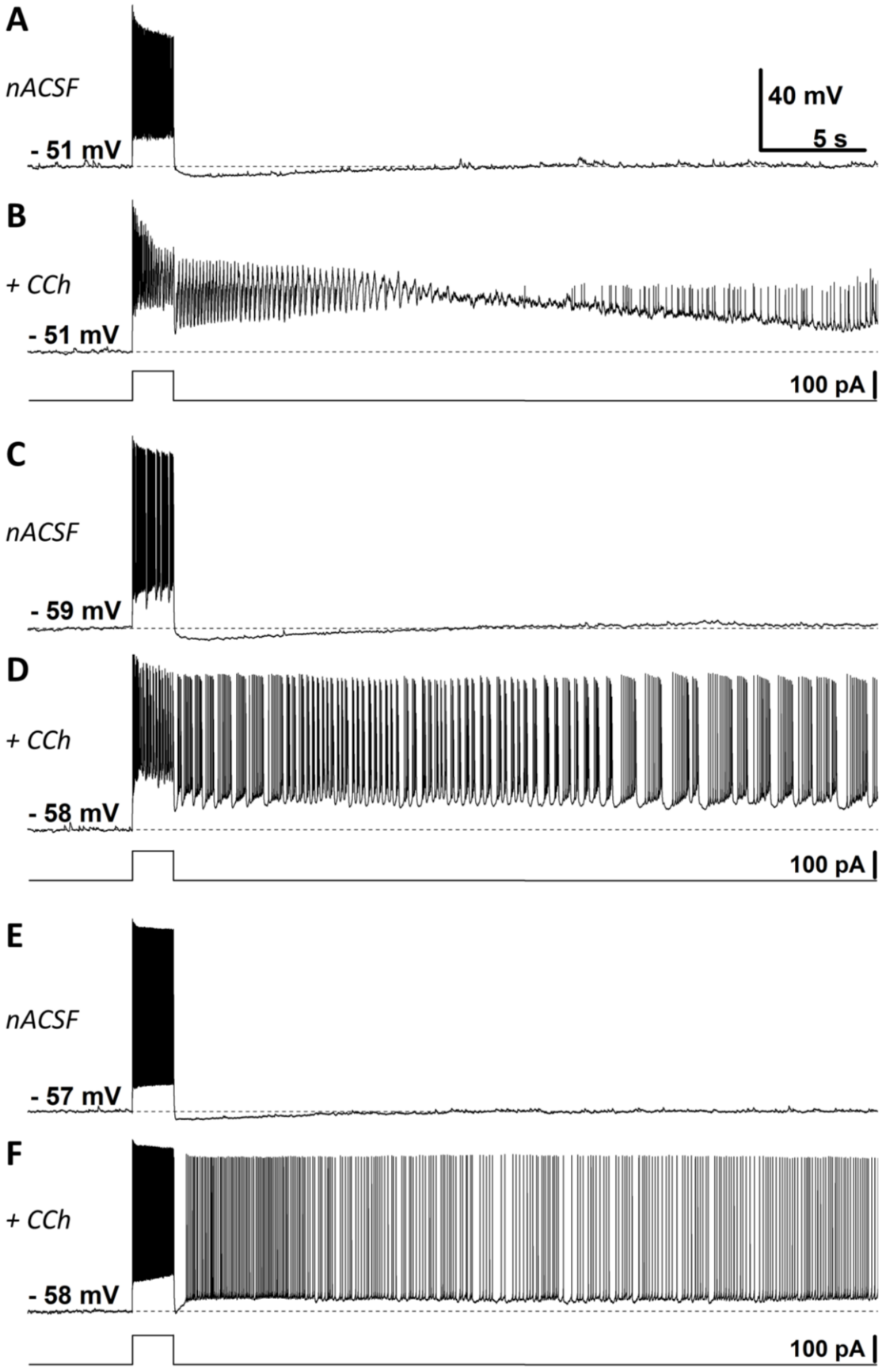

Figure 38 - Persistent firing in TRPC5 flx/flx mice infected with AAV-Cre-GFP (caption on previous page).

The firing frequency of the GFP+ (flx/flx) and GFP- (flx/flx) cells was in average lower compared to WT cells, however there were no significant differences between the groups (Fig 39B, one-way ANOVA, F (2, 70) = 1.338, ns, p = 0.269, n_{WT} = 35, n_{GFP+} = 22, n_{GFP-} = 16).

The membrane potential of the GFP+ (flx/flx) cells during and after the end of the stimulus was strongly influenced by the effect of the viral infection. In the GFP+ (flx/flx) cells, during the application of 10 μM carbachol, the depolarization induced after the end of the stimulus (MP1) was highly increased: as already mentioned, half of the cells showed depolarization block and 45.5% showed a very depolarized bursting persistent firing. In the GFP+ (flx/flx) cells the average membrane potential in the 3 seconds after the end of the stimulus (MP1) was 18.89 mV ± 1.31, which is a much larger depolarization compared to the one observed in the GFP- (flx/flx) cells (4.58 mV ± 1.12) showing a depolarization comparable to the one observed in WT cells (6.77 mV ± 0.81). When looking at the MP1 values there were differences between the groups (Fig. 39C, one-way ANOVA, F (2, 70) = 47.4, ### p < 0.001, n_{WT} = 35, n_{GFP+} = 22, n_{GFP-} = 16). A Tukey's multiple comparisons post hoc test showed that the membrane depolarization (MP1) of the GFP+ (flx/flx) cells was significantly higher compared to both GFP- (flx/flx) (Fig. 39C, *** p < 0.001) and WT cells (Fig. 39C, *** p < 0.001). As expected, the MP1 values of WT and GFP- (flx/flx) cells did not differ (Fig. 39C, ns, p = 0.349). In the GFP positive (flx/flx) cells, the cholinergic-dependent depolarization induced by the stimulation was not only strong, but also long lasting. The average membrane potential value 27 seconds after the end of the stimulus (MP2) was 12.92 mV ± 2.10 in the GFP+ (flx/flx) cells, which is again a much higher depolarization compared to the GFP- (flx/flx) and WT cells (Fig. 39D, Kruskal-Wallis test, H(2) = 13.44, ## p < 0.01, n_{WT} = 35, n_{GFP+} = 22, n_{GFP-} = 16). A Dunn's multiple comparisons post hoc test showed that the membrane depolarization (MP2) of the GFP+ (flx/flx) cells was significantly higher compared to both GFP- (flx/flx) (Fig. 39D, * p < 0.05) and WT cells (Fig. 39D, ** p < 0.01). Like previously observed for MP1, the MP2 values of WT and GFP- (flx/flx) cells, the two groups did not differ (Fig. 39D, ns, p > 0.999). During the application of the stimulus, the GFP positive (flx/flx) cells were already responding differently compared to both GFP negative (flx/flx) and WT cells. In fact, half of the GFP+ (flx/flx) cells showed already depolarization block during the stimulus application. In the GFP+ (flx/flx) cells, the average depolarization during the stimulation was almost double compared to GFP- (flx/flx) and WT cells recorded in the same conditions (Fig. 39E, one-way ANOVA, F (2, 70) = 72.8, ### p < 0.001, n_{WT} = 35, n_{GFP+} = 22, n_{GFP-} = 16). A Tukey's multiple comparisons post hoc test

showed that the membrane depolarization during the stimulus of the GFP+ (flx/flx) cells was significantly higher compared to both GFP- (flx/flx) (Fig. 39E, *** $p < 0.001$) and WT cells (Fig. 39E, *** $p < 0.001$). The values of WT and GFP- (flx/flx) cells did not differ (Fig. 39E, ns, $p = 0.966$).

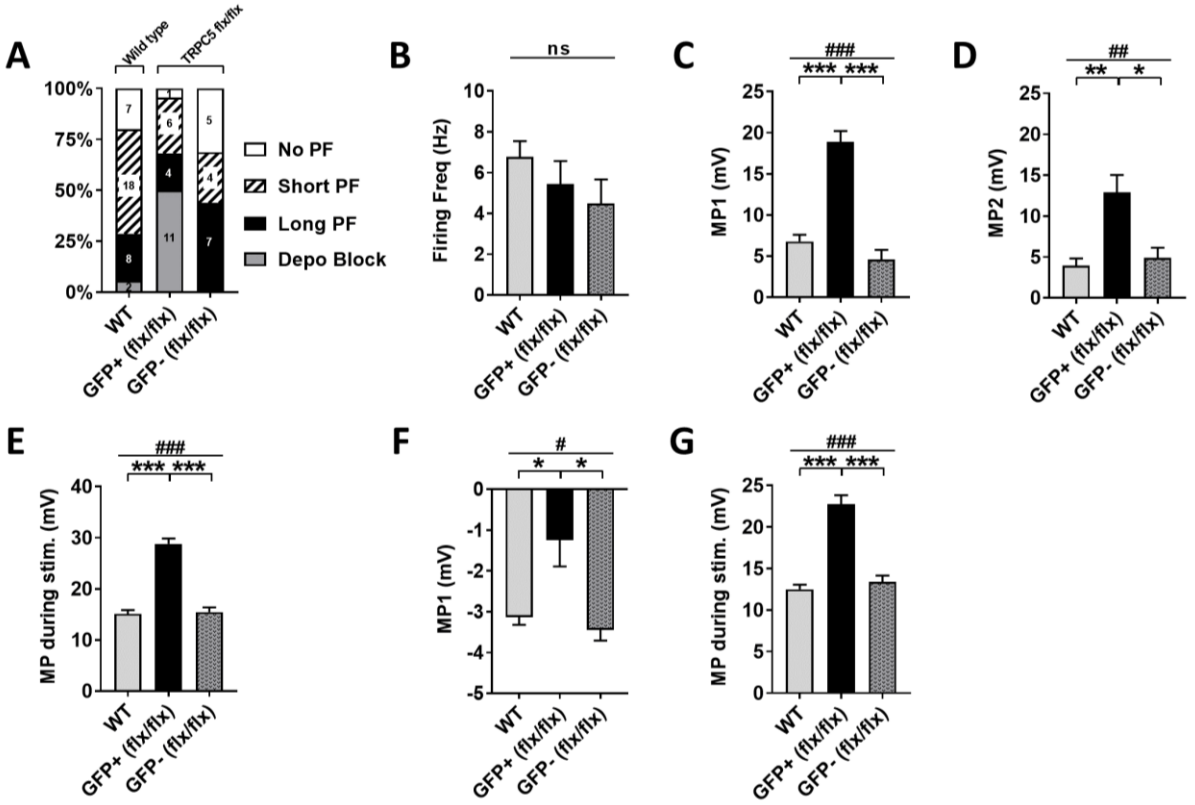

Figure 39 - Properties of GFP positive and negative cells in TRPC5 flx/flx mice infected with AAV-Cre-GFP, 4 weeks after infection.

(A) Percentages of cells that showed persistent firing in carbachol (10 μM) in wild type animals (WT) and in GFP positive and negative cells recorded from TRPC5 flx/flx animals infected with AVV-Cre-GFP. The numbers on the graph represent the sample size. (B) Post-stimulus firing frequency in CCh (one-way ANOVA, ns, $p = 0.269$, $n_{WT} = 35$, $n_{GFP+} = 22$, $n_{GFP-} = 16$). (C) Post-stimulus depolarization in CCh (MP1, one-way ANOVA, ### $p < 0.001$, $n_{WT} = 35$, $n_{GFP+} = 22$, $n_{GFP-} = 16$). Tukey's multiple comparison test: WT vs. GFP+ (flx/flx), *** $p < 0.001$; GFP+ (flx/flx) vs. GFP- (flx/flx), *** $p < 0.001$, WT vs GFP- (flx/flx), ns, $p = 0.349$. (D) Post-stimulus depolarization in CCh (MP2, Kruskal-Wallis test, ## $p < 0.01$, $n_{WT} = 35$, $n_{GFP+} = 22$, $n_{GFP-} = 16$). Dunn's multiple comparison test: WT vs. GFP+ (flx/flx), ** $p < 0.01$; GFP+ (flx/flx) vs. GFP- (flx/flx), * $p < 0.05$, WT vs GFP- (flx/flx), ns, $p > 0.999$. (E) Membrane potential depolarization during the stimulus application (one-way ANOVA, ### $p < 0.001$, $n_{WT} = 35$, $n_{GFP+} = 22$, $n_{GFP-} = 16$). Tukey's multiple comparison test: WT vs. GFP+ (flx/flx), *** $p < 0.001$; GFP+ (flx/flx) vs. GFP- (flx/flx), *** $p < 0.001$, WT vs GFP- (flx/flx), ns, $p = 0.966$. (F) Post-stimulus depolarization in control condition (nACSF) (MP1, Kruskal-Wallis test, # $p < 0.05$, $n_{WT} = 35$, $n_{GFP+} = 22$, $n_{GFP-} = 16$). Dunn's multiple comparison test: WT vs. GFP+ (flx/flx), * $p < 0.05$; GFP+ (flx/flx) vs. GFP- (flx/flx), * $p < 0.05$, WT vs GFP- (flx/flx), ns, $p > 0.999$. (G) Membrane potential depolarization during the stimulus application in control condition (nACSF) (Kruskal-Wallis test, ### $p < 0.001$, $n_{WT} = 35$, $n_{GFP+} = 22$, $n_{GFP-} = 16$). Dunn's multiple comparison test: WT vs. GFP+ (flx/flx), *** $p < 0.001$; GFP+ (flx/flx) vs. GFP- (flx/flx), *** $p < 0.001$, WT vs GFP- (flx/flx), ns, $p = 0.799$). All the recorded cells, shown in (A), were included in (B-G).

Also in control condition (nACSF), the GFP positive (flx/flx) cells showed differences compared to the other two control groups, GFP- (flx/flx) and WT. The membrane potential after the end of the stimulus (MP1) of the GFP+ (flx/flx) cells was in average more depolarized compared to the controls and, a difference between the groups was present (Fig. 39F, Kruskal-Wallis test, $H(2) = 8.83$, # $p < 0.05$, $n_{WT} = 35$, $n_{GFP+} = 22$, $n_{GFP-} = 16$). A Dunn's multiple comparisons post hoc test showed that the membrane depolarization (MP2) of the GFP+ (flx/flx) cells was significantly higher compared to both GFP- (flx/flx) (Fig. 39F, * $p < 0.05$) and WT cells (Fig. 39F, * $p < 0.05$). The membrane depolarization values of WT and GFP- (flx/flx) cells did not differ (Fig. 39F, ns, $p > 0.999$). In control condition, also the membrane potential during the stimulus was influenced by the viral infection. The GFP+ (flx/flx) cells were again very depolarized during the stimulus application and some of them already showed depolarized burst firing very similar to the one observed during the application of carbachol. Neither the GFP negative cells nor the wild type cells showed this behaviour in control condition (nACSF). As a result, the GFP+ (flx/flx) cells had a membrane potential depolarization almost twice as high compared to the GFP- (flx/flx) and WT cells (Fig. 39G, Kruskal-Wallis test, $H(2) = 40.32$, ### $p < 0.001$, $n_{WT} = 35$, $n_{GFP+} = 22$, $n_{GFP-} = 16$). A Dunn's multiple comparisons post hoc test showed that the membrane depolarization (MP2) of the GFP+ (flx/flx) cells was significantly higher compared to both GFP- (flx/flx) (Fig. 39G, *** $p < 0.001$) and WT cells (Fig. 39G, *** $p < 0.001$). The values of WT and GFP- (flx/flx) cells did not differ (Fig. 39G, ns, $p = 0.799$).

In summary, in TRPC5 conditional KO neurons (GFP+ (flx/flx)) persistent firing was still present. During cholinergic stimulation the GFP+ (flx/flx) cells responded unexpectedly to the stimulus with a strong plateau potential that was lasting for a long time, leading to depolarization block or to bursting persistent firing. The differences in the firing properties and membrane potential of the GFP+ (flx/flx) neurons were already visible in control condition (nACSF), however these effects were amplified during cholinergic stimulation. As expected, the GFP negative cells, recorded as internal control in TRPC5 flx/flx mice, did not show differences when compared to wild type cells. In all cases, firing frequency and membrane depolarization were very similar showing no significant differences.

The strong plateau potential observed in GFP positive (flx/flx) cells could have been caused by (1) compensatory mechanisms leading to an overexpression of other channels causing this depolarization block, (2) lack of the TRPC5 mediated calcium influx reducing calcium activated potassium current leading to hyper excitability, (3) side effects related to the viral infection causing this hyper excitability.

3.5.4 Effect of TRPC antagonists on persistent firing in TRPC5 flx/flx mice

After showing that the viral infection was affecting the membrane potential properties and the firing behaviour, a series of experiments were made to understand what could mediate the strong depolarization observed in the GFP positive (flx/flx) cells during and after the end of the stimulus during carbachol application and also in control condition (nACSF) during the stimulus application.

The TRPC5 conditional KO, mediated by the AAV infection, led already after four weeks to changes in the expression level of the TRPC family and potentially changed the expression patterns of other ion channels. The channels belonging to the TRP superfamily, and in particular to the TRPC family, share a very similar structure and activation mechanisms [174,196,270]. Given these similarities, it is possible that ion channels belonging to the TRPC or TRPM family could have compensate the loss of TRPC5. TRPC4 are the closest relatives to TRPC5, they share a very similar structure, have similar gating properties, activation mechanisms [174,195] and they are expressed in the CA1 area. Even if the qPCR results showed a reduction of TRPC4 mRNA after viral infection, it is important to remember that TRPC4, besides homomeric channels, can also form heteromeric channels with TRPC1, whose expression was not altered. In these way, even if the expression level of TRPC4 was reduced, the formation of heteromeric channels could have been used as compensatory mechanism. In addition, even if reduced the expression of TRPC4 was still higher compared to TRPC3, whose expression was increased after infection.

Given the structure homology and possible compensation via heterometric channels, I chose TRPC4 heteromer\homomer as first candidates to support the strong depolarization observed in the GFP positive cells in TRPC5 flx/flx mice.

3.5.4.1 Application of 3 µM carbachol and 10 µM ML204 on GFP positive cells

In the previous experiments in TRPC5 flx/flx mice, we saw that GFP positive neurons showed to be more depolarized already in control condition and that the cholinergic stimulation strongly amplified this effect. To test if the strong depolarization observed in the GFP positive cells during carbachol application could be modulated by the cholinergic agonist concentration, after the application of 10 µM carbachol, 3 µM carbachol was applied to see if the strong depolarization would be affected. After the application of carbachol at lower concentration, ML204 was co-applied to test if the block of TRPC4 channels (homo and heteromeric) could also affect the strong depolarization observed. The experimental conditions were very similar to the one previously used: the cells were first kept in nACSF,

then 10 μM carbachol was applied and afterwards the carbachol concentration was reduced to 3 μM. Finally, when persistent firing or depolarization block were observed, 10 μM ML204 was applied on top of 3 μM carbachol (Fig. 40). The stimulation protocol used was the same previously described. To make it clearer I will first analyse the effects of 3 μM carbachol application compared to 10 μM carbachol and afterwards I will analyse the effects of ML204 application on top of 3 μM carbachol.

Application of 3 μM carbachol

After the application of 10 μM carbachol 6 out of 8 GFP+ (flx/flx) cells responded with a strong depolarization block, one cell showed normal persistent firing and one showed persistent firing with the depolarized bursting previously described (Fig. 40E). Afterwards, 3 μM carbachol was bath applied for 15 minutes leading to a small and non-significant reduction of the average firing frequency of persistent firing (Fig. 40F, ns, Wilcoxon test, $p = 0.625$, $n = 8$).

During the application of lower CCh concentration, the analysis of the membrane potential gave more interesting and descriptive results compared to the measure of the firing frequency, affected by the strong depolarization block. The membrane depolarization after the end of the stimulus (MP1) was reduced by the application of 3 μM CCh, and the observed difference was significant (Fig. 40H, paired t-test, ** $p < 0.01$, $n = 8$). Even if 3 μM CCh had a suppressing effect, the cells were still very depolarized. The average MP1 value during 3 μM application was 17.53 mV ± 2.13 which is incredibly high compared to GFP negative cells or WT cells in which the average MP1 values during the application of higher carbachol were respectively 6.81 mV ± 1.05 and 8.38 mV ± 0.74. The membrane potential depolarization recorded 27 seconds after the end of the stimulus (MP2) was slightly reduced by the application of 3 μM carbachol, but the observed difference was not significant (Fig. 40H, paired t-test, ns, $p = 0.130$, $n = 8$). The membrane potential during the stimulus was not affected by the application of 3 μM carbachol (Fig. 40I, paired t-test, ns, $p = 0.234$, $n = 8$).

Figure 40 - The effect of carbachol (3 μM) and ML204 (10 μM) on persistent firing in GFP positive (flx/flx) cells (figure on next page).

(A) Example of depolarization block in CCh (10 μM). (B) Example of burst persistent firing CCh (3 μM) in the same cell shown in (A). (C) Suppressed persistent firing ML204 (10 μM) in the same cell shown in (A, B). (D) Current injection used in (A, B, C) (100 pA, 2 s). (E) Percentages of cells that showed persistent firing in CCh (10 μM) and CCh (3 μM). The numbers on the graph represent the sample size. (F) Post-stimulus firing frequency (Wilcoxon test, ns, $p = 0.625$, $n = 8$). (F) Post-stimulus depolarization (MP1, paired t-test, ** $p < 0.01$, $n = 8$). (H) Post-stimulus depolarization (MP2, paired t-test, ns, $p = 0.130$, $n = 8$). (I) Membrane potential depolarization during the stimulus application (paired t-test, ns, $p = 0.234$, $n = 8$).

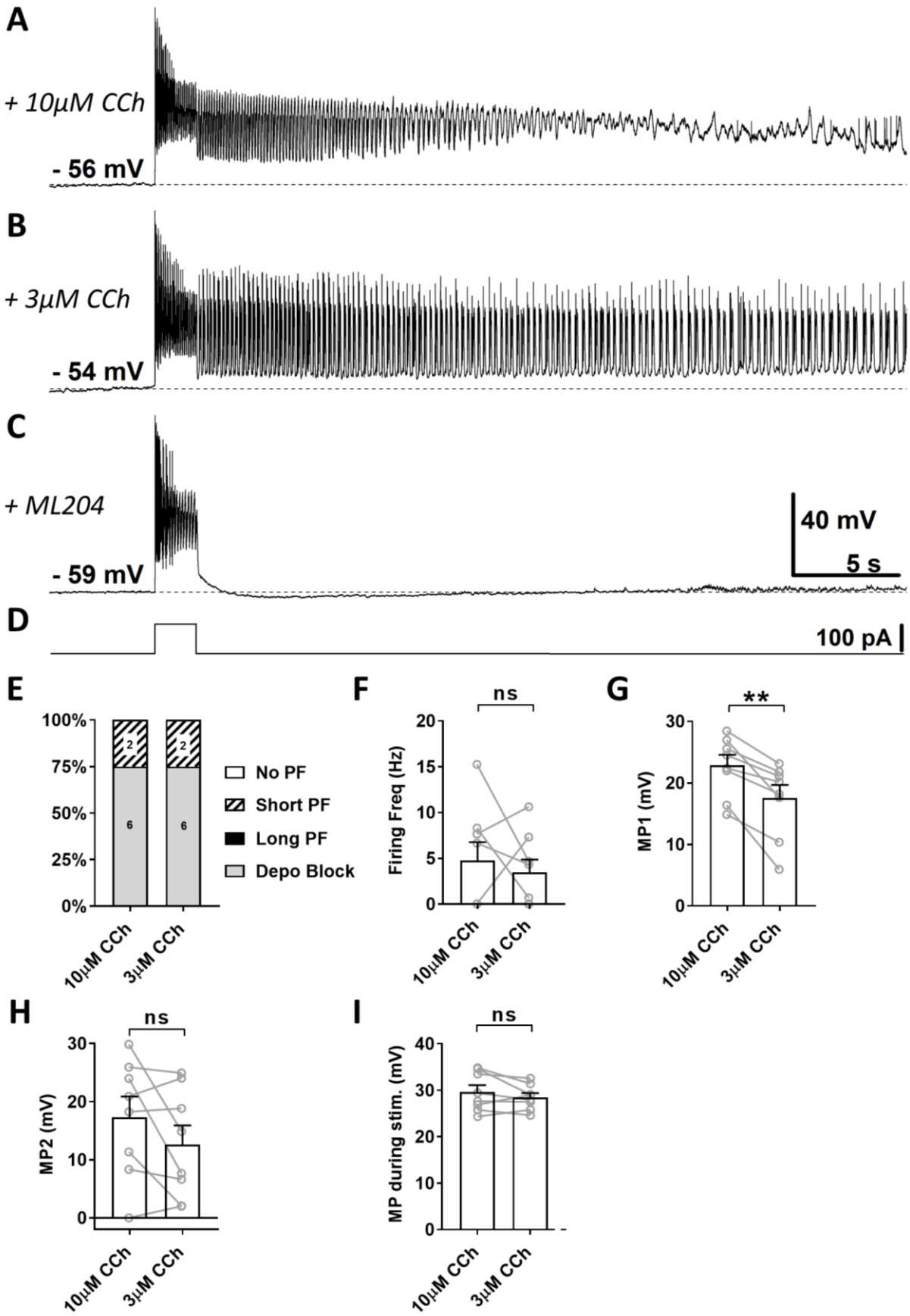

Figure 40 - The effect of carbachol (3 μM) and ML204 (10 μM) on persistent firing in GFP positive (flx/flx) cells (caption on the previous page).

Application of ML204

After testing the effects of 3 µM carbachol, in four cells it was possible to apply 10 µM ML204 on top of it (Fig. 40C). These experiments were made to test if TRPC4, homo and heteromer channels, were supporting the strong membrane depolarization observed in GFP positive (flx/flx). After 15 minutes from the application of ML204, in 3 out of 4 neurons the firing frequency was reduced. 1 out of 4 cells showed a very strong depolarization block in both conditions, as a result the measure firing frequency was zero. Even if the observed difference was not significant it shows a trend of ML204 to reduce the firing frequency (Fig. 41B, ns, paired t test, ns, p = 0.250, n = 4).

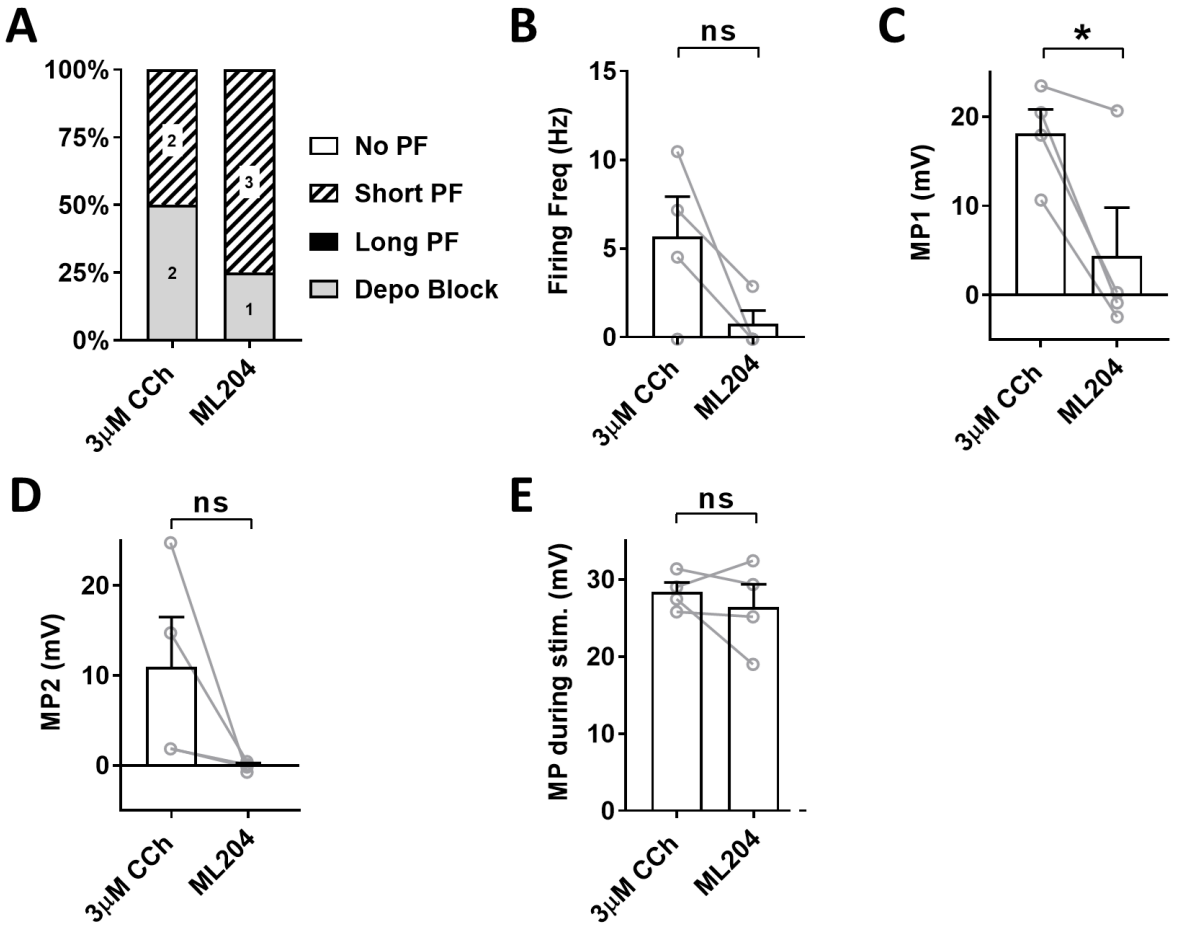

Figure 41 - The effect of ML204 (10 µM) on persistent firing in GFP (flx/flx) positive.

(A) Percentages of cells that showed persistent firing in CCh (3 µM) and ML204 (10 µM). The numbers on the graph represent the sample size. (B) Post-stimulus firing frequency (paired t test, ns, p = 0.250, n = 4). (C) Post-stimulus depolarization (MP1, paired t-test, * p < 0.05, n = 4). (D) Post-stimulus depolarization (MP2, paired t-test, ns, p = 0.150, n = 4). (E) Membrane potential depolarization during the stimulus application (paired t-test, ns, p = 0.489, n = 4).

As it happened in the previous experiment, the measure of MP1 gave a more descriptive measure of the effect of ML204 application as it measured the effect of the drug

on the membrane potential of the tested cells. The application of ML204 significantly reduced the depolarization after the end of the stimulus (MP1) (Fig. 41C, paired t-test, * $p < 0.05$, n = 4). The application of ML204 brought the MP2 values close to baseline values recorded before the stimulation. Nevertheless, the observed reduction was not significant (Fig. 41D, paired t-test, ns, $p = 0.150$, n = 4). The membrane potential during the stimulus was almost not affected by the application of ML204 and the neurons were still very depolarized (Fig. 41E, paired t-test, ns, $p = 0.489$, n = 4).

In summary: reducing the cholinergic stimulation reduced significantly but only partially the plateau potential in GFP positive neurons. The application of ML204 significantly suppressed the strong depolarization observed after the end of the stimulus, however it had no effect on the strong membrane potential depolarization during the stimulus application.

These data suggest that the cholinergic stimulation can modulate the amplitude of the strong depolarization observed in the GFP positive cells. In addition, given the suppressing effect of ML204, these data indicate that TRPC4 could in part support the strong and cholinergic-dependent depolarization in TRPC5 conditional KO cells.

3.5.4.2 Application of 3 µM clemizole hydrochloride on GFP positive cells

To test if TRPC5 channels could still be present in the GFP positive (flx/flx) cells, in some neurons 3 µM clemizole hydrochloride was used to test if the TRPC5 blocker could affect the strong depolarization observed during carbachol application. As the qPCR results showed a drastic reduction of TRPC5 transcription, 3 µM clemizole hydrochloride was expected to have no effect, given that at this lower concentration is targeting TRPC5. In these pilot experiments the procedure was like the one already used in the previous experiments: the cells were kept in nACSF and then 10 µM carbachol was bath applied. If depolarization block or persistent firing were observed, 3 µM CLE was applied on top of carbachol (Fig. 42).

During the application of carbachol the depolarization induced by the stimulus was very strong 2 cells out of 3 showed depolarization block. After 15 minutes of CLE application, in the tested cells the average firing frequency was slightly reduced (Fig. 42E, n = 3). As it happened in the previous experiments on GFP positive neurons, given the presence of depolarization block, the measure of the membrane potential was more representative to describe this data. During the application of carbachol, the cholinergic-dependent membrane potential depolarization after the end of the stimulus (MP1) was in average not affected by the application of CLE (Fig. 42F, n = 3). During the application of carbachol, the MP2 and the

membrane potential during the stimulus were also in average not affected by the application of clemizole hydrochloride at low concentration (Fig. 42G-H, n = 3).

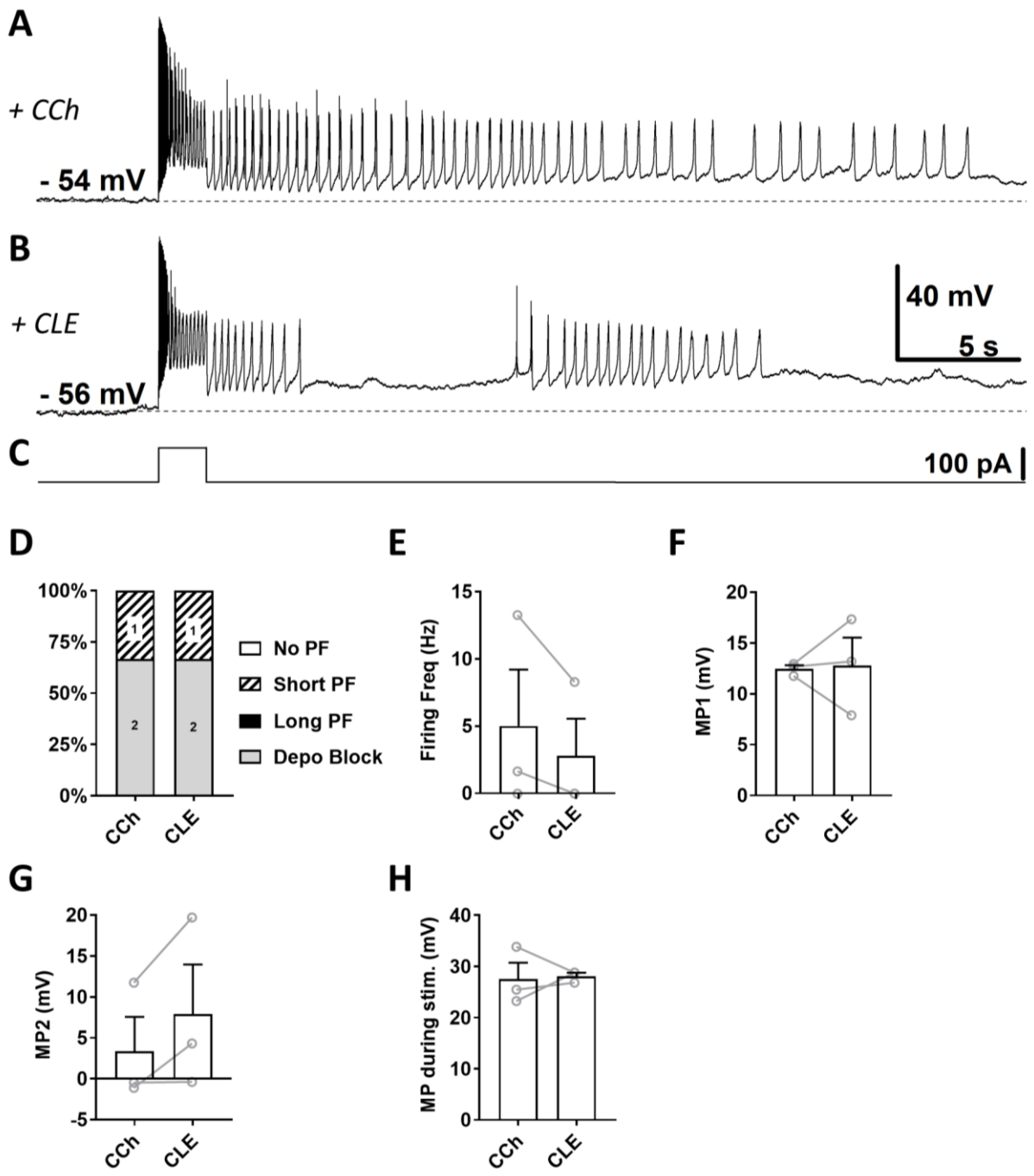

Figure 42 - The effect of clemizole hydrochloride (3 µM) on persistent firing in GFP positive (flx/flx) cells.

(A) Response of a GFP positive (flx/flx) cell in CCh (10 µM). (B) Effect of clemizole hydrochloride (3 µM) in the same cell shown in (A). (C) Current injection used in (A, B) (100 pA, 2 s). (D) Percentages of cells that showed persistent firing in CCh (10 µM) and CCh (3 µM). The numbers on the graph represent the sample size. (E) Post-stimulus firing frequency (n = 3). (F) Post-stimulus depolarization (MP1, n = 3). (G) Post-stimulus depolarization (MP2, n = 3). (H) Membrane potential depolarization during the stimulus application (n = 3).

Although in this pilot experiment the number of tested cells was small, these results seem to indicate that clemizole hydrochloride (3 μM), which selectively block TRPC5, did not affect the strong depolarization observed in the GFP positive cells.

3.5.4.3 Application of Pico145 on GFP positive cells

In these experiments on TRPC5 flx/flx animals, I tested also the most novel and selective TRPC antagonist available: Pico145. Our laboratory obtained this compound from Dr. Robin Bon (University of Leeds). Pico145 is selective at nanomolar concentration for TRPC1, TRPC4 and TRPC5 and it can affect both homo or heteromeric channels [255]. This novel drug was tested on GFP+ (flx/flx) cells using the same protocol used before. As the expression of TRPC5 was drastically reduced and almost completely suppressed in the infected cells, the nanomolar selective blocker was used to assess if the block of TRPC4 channels (homomeric and heteromeric) could affect the strong depolarization block observed in the GFP positive cells. In these experiments after recording the cells in nACSF, 10 μM carbachol was applied and, if persistent firing or a strong depolarization block were observed, 100 nM Pico145 was bath applied (Fig. 43). Given the novelty and the very low working concentration of Pico145, after its application the cells were recorded for longer time compared to the pervious experiments to have a better overview of the drug effect.

Pico145 was tested in 4 GFP+ (flx/flx) cells showing persistent firing or depolarization block during the application of carbachol. After 25 minutes, in 3 cells persistent firing was completely blocked and in 1 cell it was strongly reduced, however the observed reduction was not significant (Fig. 43E, Wilcoxon test, ns, $p = 0.125$, $n = 4$). After a 25 minute from the application of Pico145, the membrane potential after the end of the stimulus (MP1) was strongly reduced in 3 cells and 1 was not affected. The difference was no significant (Fig. 43F, paired t-test, ns, $p = 0.267$, $n = 4$). The MP2 also showed a reduction of the membrane potential depolarization, in all cells Pico145 application led to a reduction, however the difference was not significant (Fig. 43G, paired t-test, ns, $p = 0.100$, $n = 4$). The membrane potential during the stimulation was not affected by Pico145 application (Fig. 43H, paired t-test, ns, $p = 0.842$, $n = 4$).

The results from this pilot experiments using Pico145 were not statistically significant and needs to be deepened, nevertheless the application of this novel TRPC blocker reduced the average firing frequency and MP1 in the tested cells.

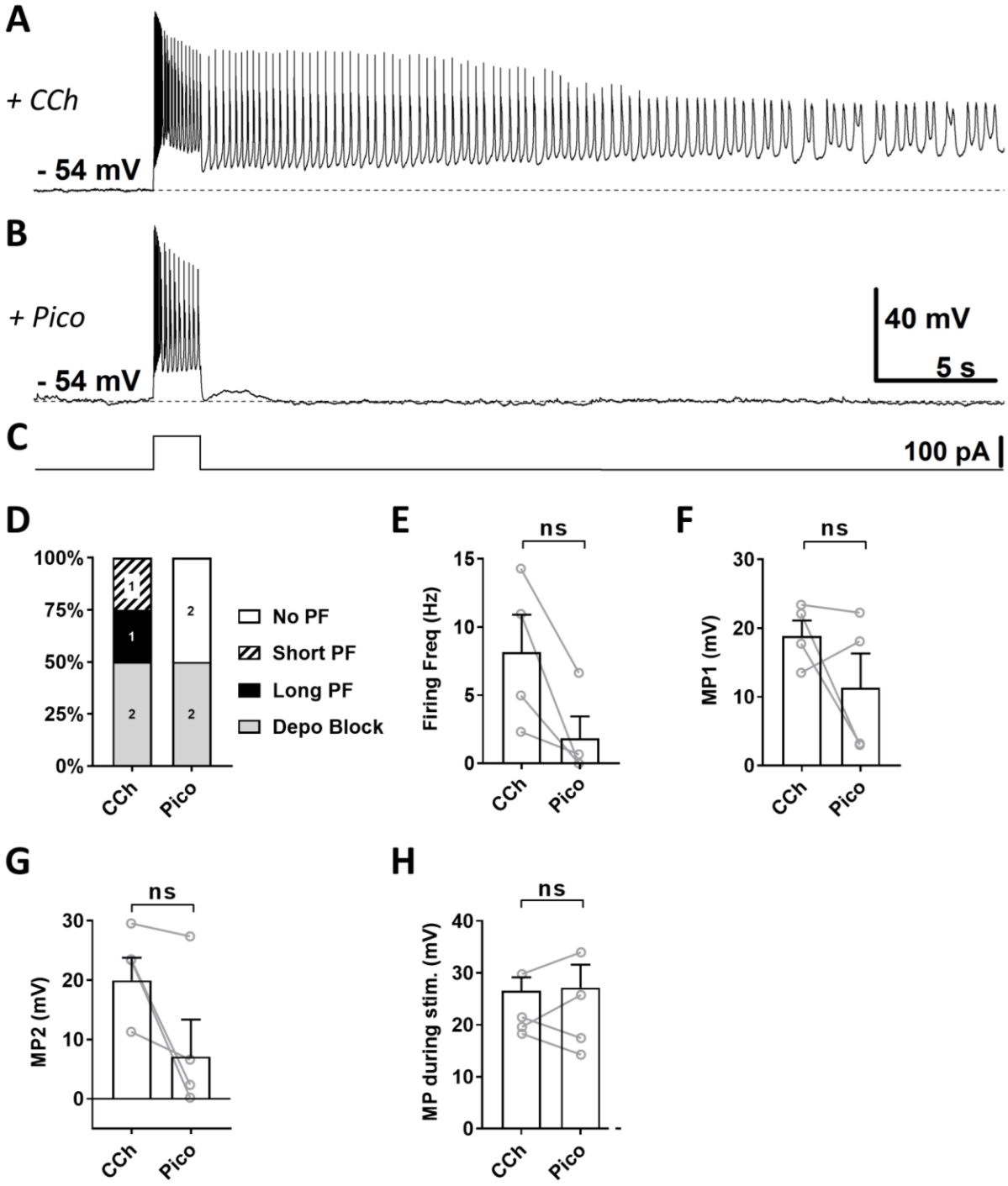

Figure 43 - The effect of Pico145 (100 nM) on persistent firing in GFP positive (flx/flx).

(A) Response of a GFP positive (flx/flx) cell in CCh (10 μM). (B) Suppressing effect of Pico145 (100 nM) in the same cell shown in (A). (C) Current injection used in (A, B) (100 pA, 2 s). (D) Percentages of cells that showed persistent firing in CCh (10 μM) and Pico (100 nM). The numbers on the graph represent the sample size. (E) Post-stimulus firing frequency (Wilcoxon test, ns, $p = 0.125$, $n = 4$). (F) Post-stimulus depolarization (MP1, paired t-test, ns, $p = 0.267$, $n = 4$). (G) Post-stimulus depolarization (MP2, paired t-test, ns, $p = 0.100$, $n = 4$). (H) Membrane potential depolarization during the stimulus application (paired t-test, ns, $p = 0.842$, $n = 4$).

3.5.4.4 Application of Pico145 on GFP negative cells

In a previous section talking about TRPC5 flx/flx infected mice, we saw that GFP negative cells, recorded as control, showed normal persistent firing and depolarization during and after the end of the stimulation. After collecting these data in carbachol, some of these cells were exploited for some preliminary tests using 100 nM Pico145. This novel drug was used to see if its application could affect the firing frequency of persistent firing and the cholinergic depolarization induced by the stimulus (Fig. 44). Even if these results are preliminary and need to be deepen, they will be useful for future experiments using this novel antagonist.

Pico145 was tested in 5 GFP negative (flx/flx) cells showing persistent firing during the application of 10 μM carbachol. After 20 minutes from the application of Pico145, persistent firing was completely blocked in 3 out of 5 cells and reduced in the remaining 2 cells. The average firing frequency was inhibited by Pico145 but not significantly (Fig. 44E, Wilcoxon test, ns, $p = 0.062$, $n = 5$). No significant changes were also observed when looking at the MP1 values, even if the depolarization was reduced in 4 out of 5 cells (Fig. 44F, paired t-test, ns, $p = 0.140$, $n = 5$). The values of MP2 were also in average reduced by Pico145 application, however the difference was not significant (Fig. 44G, paired t-test, ns, $p = 0.052$, $n = 5$). The membrane potential during the stimulation was also not affected by the application of Pico145 (Fig. 44H, paired t-test, ns, $p = 0.786$, $n = 5$).

Like in the previous experiments using Pico145 in GFP+ (flx/flx) cells, the results collected in GFP negative cells were not statistically significant, but they suggest that Pico145 could have inhibitory effects on persistent firing. Also in this case, the drug was acting more slowly compared to the other TRPC antagonist that I previously used. In fact, while Pico145 needed at least 20 minutes before showing any effect, the other TRPC antagonist I previously used had a strong effect already after 15 minutes from their bath application.

The results of these pilot experiments using Pico145 were deepened in a recent study from our lab that confirmed the trend observed in these experiments in TRPC5 flx/flx mice. In this new study, Pico145 was extensively tested in WT mice showing that the selective TRPC4 and TRPC5 blocker significantly inhibited persistent firing, suppressing both firing frequency and membrane depolarization [271].

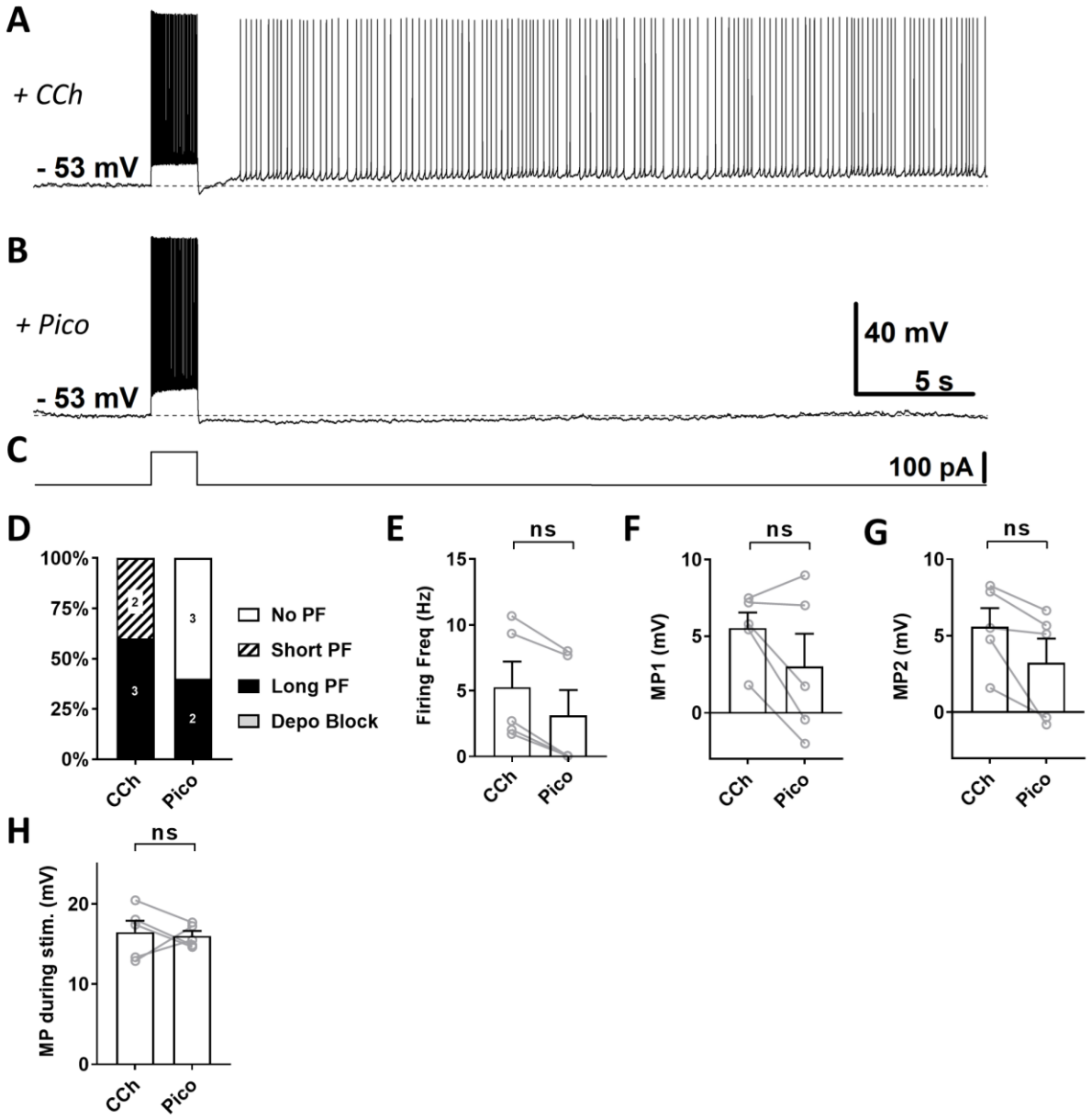

Figure 44 - The effect of Pico145 (100 nM) on persistent firing in GFP negative (flx/flx).

(A) Long-lasting persistent firing in a GFP negative cell in CCh (10 μM). (B) Suppressed persistent firing in Pico145 (100nM) in the same cell shown in (A). (C) Current injection used in (A,B) (100 pA, 2 s). (D) Percentages of cells that showed persistent firing in CCh (10 μM) and Pico (100 nM). The numbers on the graph represent the sample size. (E) Post-stimulus firing frequency (Wilcoxon test, ns, $p = 0.062$, $n = 5$). (F) Post-stimulus depolarization (MP1, paired t-test, ns, $p = 0.140$, $n = 5$). (G) Post-stimulus depolarization (MP2, paired t-test, ns, $p = 0.052$, $n = 5$). (H) Membrane potential depolarization during the stimulus application (paired t-test, ns, $p = 0.786$, $n = 5$).

3.5.5 Effects of AAV infection on wild type mice

So far I presented several experiments made to assess what was underlying the strong membrane depolarization observed in GFP positive cells recorded in TRPC5 flx/flx mice, however it remained unclear what was supporting it. In GFP positive (flx/flx) cells, reducing the cholinergic stimulation slightly inhibited the strong depolarization after the end of the stimulus and the application of TRPC4 blockers only partially affected this depolarization. However, in both cases the neurons still showed depolarization block and the membrane potential during the stimulation was always very depolarized and not affected.

One possible explanation for the strong depolarization observed in GFP+ (flx/flx) cells was that the virus had unspecific effects on the infected cells, possibly mediated by Cre recombinase or GFP overexpression. In the literature, many studies have reported toxicity effects related to Cre and it was also reported that these effects depend on the expression levels of Cre [272–276]. In addition to potential side effects related to Cre, also GFP, the widely used cell marker, in certain condition can lead to cell toxicity [277–280]. These toxicity reports have been rare and, in most cases, cells having GFP or Cre seem to tolerate the genetic modification well without showing recognizable physiological effects.

To test if the viral infection had side effects not related to the TRPC5 conditional KO, I injected wild type mice with the same AAV-Cre-GFP used in the TRPC5 flx/flx mice. In this way, all the effects observed in GFP positive cells recorded in WT animals would have been related to unspecific effects mediated by virus, and not to the TRPC5 conditional KO.

3.5.5.1 Persistent firing in GFP positive cells in wild type mice

Besides the mice strain, in these control experiments the conditions were the same used with the infected TRPC5 flx\flx animals: wild type animals were injected with the AAV-Cre-GFP virus previously used and the patch clamp experiments were performed after 4 weeks. During the recordings, the cells were kept in nACSF and then 10 μM carbachol was bath applied. As control in these experiments I used cells I recorded from the same strain of wild type animals, but non-infected. Solutions and stimulating protocol were the same previously used. To have a better overview of the effect of the infection, I will compare GFP positive cells from WT mice (GFP+ (WT)), cells from non-infected WT mice (WT) and GFP positive cells from TRPC5 flx/flx mice (GFP+ (flx/flx)).

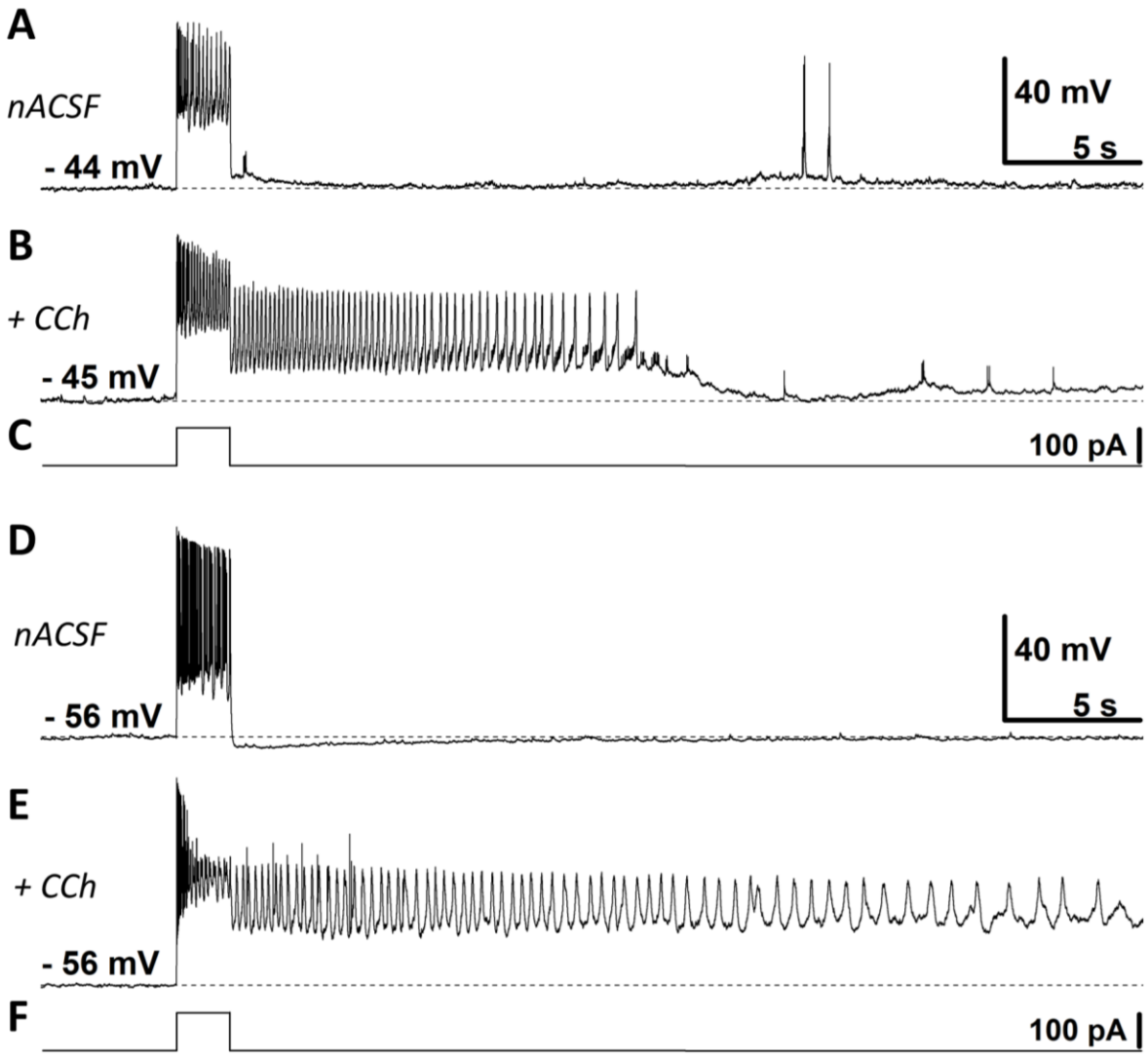

Figure 45 - Persistent firing in wild type mice infected with AAV-Cre-GFP, 4 weeks after infection.

(A) The trace shows a GFP positive (WT) cell recorded in control condition (nACSF). (B) Example of depolarization block mixed with burst firing and spikelets in presence of 10 µM carbachol (CCh) in the same cell recorded in (A). (C) Current injection used in (A, B,) (100 pA, 2 s). (D) The trace shows a GFP positive cell recorded in control condition (nACSF). (E) Example of depolarization block and spikelets in presence of 10 µM carbachol (CCh) in the same cell recorded in (D). (F) Current injection used in (D, E) (100 pA, 2 s).

During the application of carbachol all the recorded GFP positive cells in WT showed a strong depolarization block during and\or after the application of the stimulation. In almost all the cases the cells were not able to fire normal action potential but only small spikelets (Fig. 45B and 45E). The firing behaviour observed in the GFP+ cells recorded in WT animals was very similar to the one observed in the GFP+ cells recorded in the TRPC5 flx/flx animals showing a strong depolarization block. As previously mentioned, the GFP+ (WT) cells were no able to fire normal action potential and the firing frequency of these cells was exactly zero (Fig. 46B, Kruskal-Wallis test, $H(2) = 14.91$, ### $p < 0.001$, $n_{WT} = 35$, $n_{GFP+\ (WT)} = 9$, $n_{GFP+\ (flx/flx)} = 22$). A Dunn's multiple comparisons post hoc test showed that the firing frequency of

the GFP+ (WT) cells was significantly lower compared to both WT (Fig. 46B, *** $p < 0.001$) and GFP+ (flx/flx) cells (Fig. 46B, * $p < 0.05$). The firing frequency of WT and GFP+ (flx/flx) cells did not differ (Fig. 46B, ns, $p = 0.749$).

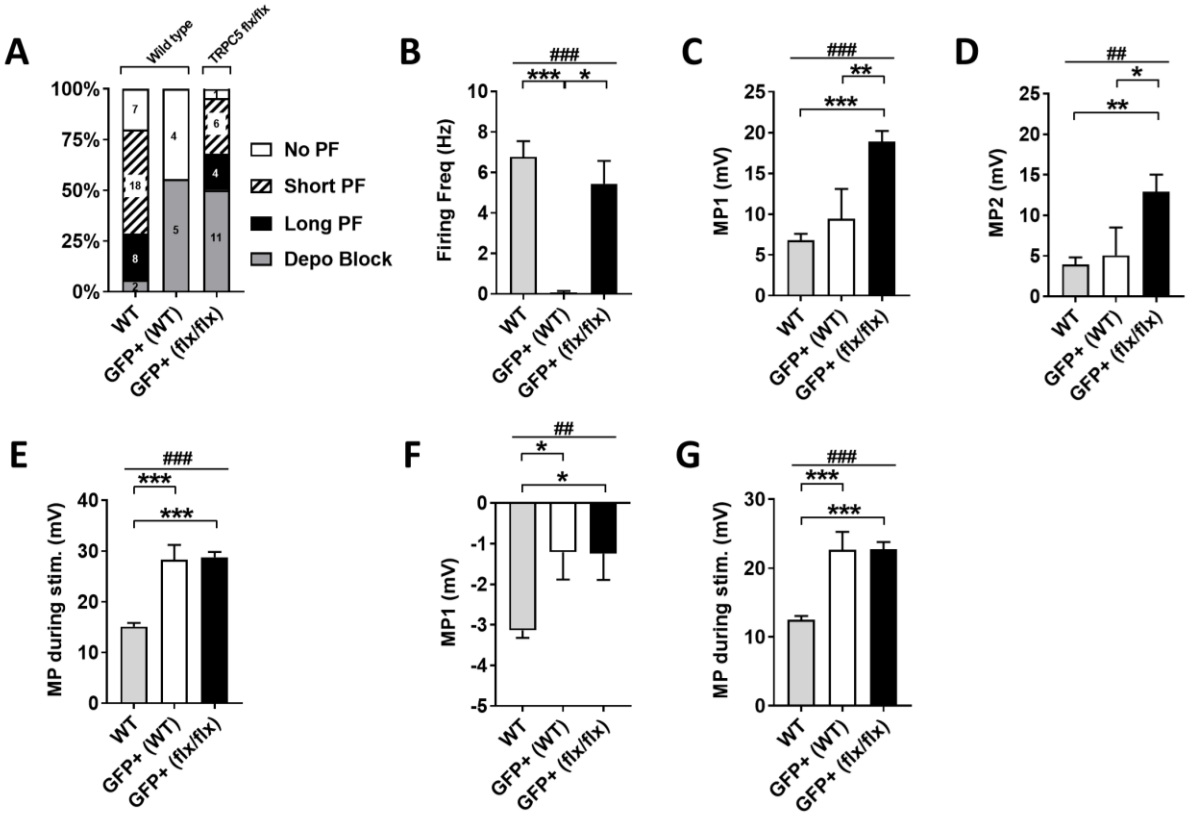

Fig. 46 - Properties of GFP positive cells in wild type mice infected with AVV-Cre-GFP, 4 weeks after infection.

(A) Percentages of cells that showed persistent firing in carbachol (10 μM) in wild type animals (WT) and in GFP positive cells recorded from wild type (WT) and TRPC5 flx/flx mice infected with AVV-Cre-GFP. The numbers on the graph represent the sample size. (B) Post-stimulus firing frequency in CCh (Kruskal-Wallis test, ### $p < 0.001$, $n_{WT} = 35$, $n_{GFP+ (WT)} = 9$, $n_{GFP+ (flx/flx)} = 22$). Dunn's multiple comparison test: WT vs. GFP+ (WT), *** $p < 0.001$; GFP+ (WT) vs GFP+ (flx/flx), * $p < 0.05$, WT vs GFP+ (flx/flx), ns, $p = 0.749$. (C) Post-stimulus depolarization in CCh (MP1, Kruskal-Wallis test, ### $p < 0.001$, $n_{WT} = 35$, $n_{GFP+ (WT)} = 9$, $n_{GFP+ (flx/flx)} = 22$). Dunn's multiple comparison test: WT vs. GFP+ (WT), ns, $p > 0.999$; GFP+ (WT) vs GFP+ (flx/flx), ** $p < 0.01$, WT vs GFP+ (flx/flx), *** $p < 0.001$. (D) Post-stimulus depolarization in CCh (MP2, Kruskal-Wallis test, ## $p < 0.01$, $n_{WT} = 35$, $n_{GFP+ (WT)} = 9$, $n_{GFP+ (flx/flx)} = 22$). Dunn's multiple comparison test: WT vs. GFP+ (WT), ns, $p > 0.999$; GFP+ (WT) vs GFP+ (flx/flx), * $p < 0.05$, WT vs GFP+ (flx/flx), ** $p < 0.01$. (E) Membrane potential depolarization during the stimulus application (Kruskal-Wallis test, ### $p < 0.001$, $n_{WT} = 35$, $n_{GFP+ (WT)} = 9$, $n_{GFP+ (flx/flx)} = 22$). Dunn's multiple comparison test: WT vs. GFP+ (WT), *** $p < 0.001$; GFP+ (WT) vs GFP+ (flx/flx), ns, $p > 0.999$, WT vs GFP+ (flx/flx), *** $p < 0.001$. (F) Post-stimulus depolarization in control condition (nACSF) (MP1, Kruskal-Wallis test, ## $p < 0.01$, $n_{WT} = 35$, $n_{GFP+ (WT)} = 9$, $n_{GFP+ (flx/flx)} = 22$). Dunn's multiple comparison test: WT vs. GFP+ (WT), * $p < 0.05$; GFP+ (WT) vs GFP+ (flx/flx), ns, $p > 0.999$, WT vs GFP+ (flx/flx), * $p < 0.05$. (G) Membrane potential depolarization during the stimulus application in control condition (nACSF) (Kruskal-Wallis test, ### $p < 0.001$, $n_{WT} = 35$, $n_{GFP+ (WT)} = 9$, $n_{GFP+ (flx/flx)} = 22$). Dunn's multiple comparison test: WT vs. GFP+ (WT), *** $p < 0.001$; GFP+ (WT) vs GFP+ (flx/flx), ns, $p > 0.999$, WT vs GFP+ (flx/flx), *** $p < 0.001$. All the recorded cells, shown in (A), were included in (B-G).

The membrane potential of the GFP+ (WT) cells during and after the stimulus was strongly influenced by the effects of the viral infection. In infected WT mice, 5 out of 9 GFP+

cells showed a very strong depolarization block during and after the end of the stimulus. The 4 out of 9 cells not showing PF or depolarization block after the end of the stimulus, were nevertheless very depolarized during the stimulus application, showing depolarization block. When comparing the average values of MP1, differences between the groups were detected (Fig. 46C, Kruskal-Wallis test, H(2) = 27.73, ### $p < 0.001$, $n_{WT} = 35$, $n_{GFP+ (WT)} = 9$, $n_{GFP+ (flx/flx)} = 22$). A Dunn's multiple comparisons post hoc test showed that the MP1 of the GFP+ (WT) cells was not significantly different compared to WT (Fig. 46C, ns, $p > 0.999$) and it was significantly smaller than GFP+ (flx/flx) cells (Fig. 46C, ** $p < 0.01$). This result can be explained by the fact that, even if 5 out of 9 GFP+ (WT) cells showed a strong depolarization block during the application of carbachol, 4 out of 9 did not respond with persistent firing or depolarization block after the end of the stimulus. The same pattern was observed also for the MP2 values (Fig. 46D, Kruskal-Wallis test, H(2) = 12.57, ## $p < 0.01$, $n_{WT} = 35$, $n_{GFP+ (WT)} = 9$, $n_{GFP+ (flx/flx)} = 22$). A Dunn's multiple comparisons post hoc test showed that the MP1 of the GFP+ (WT) cells was not significantly different compared to WT (Fig. 46D, ns, $p > 0.999$) and it was significantly smaller than GFP+ (flx/flx) cells (Fig. 46D, * $p < 0.05$). As it happened in the GFP+ cells in TRPC5 flx/flx animals, also in the GFP+ cells recorded in WT animals most of the cells showed depolarization block or a very depolarized firing already during the stimulus application. During cholinergic stimulation, the average depolarization of the GFP+ (WT) cells measured during the stimulus application was almost twice as big compared to the control group (WT) and very similar compared to GFP+ (flx/flx) (Fig. 46E, Kruskal-Wallis test, H(2) = 40.54, ### $p < 0.001$, $n_{WT} = 35$, $n_{GFP+ (WT)} = 9$, $n_{GFP+ (flx/flx)} = 22$). A Dunn's multiple comparisons post hoc test showed that the average membrane potential during the stimulus of the GFP+ (WT) cells was significantly higher compared to WT (Fig. 46E, *** $p < 0.001$) and it did not differ from the GFP+ (flx/flx) cells (Fig. 46E, ns, $p > 0.999$). As previously showed, the GFP+ (flx/flx) cells were more depolarized compared to WT (Fig. 46E, *** $p < 0.001$).

In nACSF, before applying CCh, the membrane potential of the GFP+ (WT) cells was already responding differently compared to the control group (WT), but similarly to the GFP+ recorded in TRPC5 flx/flx. The average membrane potential after the end of the stimulus (MP1) of the GFP+ (WT) cells was more depolarized compared to the control group, the same behaviour was shown also by the GFP+ (flx/flx) cells (Fig. 46F, MP1, Kruskal-Wallis test, H(2) = 10.81, ## $p < 0.01$, $n_{WT} = 35$, $n_{GFP+ (WT)} = 9$, $n_{GFP+ (flx/flx)} = 22$). A Dunn's multiple comparisons post hoc test showed that the membrane potential after the end of the stimulus (MP1) of the GFP+ (WT) cells was significantly more depolarized compared to WT (Fig.

46F, * $p < 0.05$) and it did not differ from the GFP+ (flx/flx) cells (Fig. 46F, ns, $p > 0.999$). In nACSF, the average membrane potential during the stimulus of the GFP+ (WT) cells was very depolarized and some neurons already showed depolarization block at this stage. The control group cells (WT) never showed this behaviour. The GFP+ (WT) cells, similarly to GFP+ (flx/flx) cells, had a membrane potential during the stimulus almost twice as big compared to the WT cells (Fig. 46G, Kruskal-Wallis test, $H(2) = 39.04$, ### $p < 0.001$, $n_{WT} = 35$, $n_{GFP+ (WT)} = 9$, $n_{GFP+ (flx/flx)} = 22$). A Dunn's multiple comparisons post hoc test showed that the membrane potential after the end of the stimulus (MP1) of the GFP+ (WT) cells was significantly more depolarized compared to WT (Fig. 46G, *** $p < 0.001$) and it did not differ from the GFP+ (flx/flx) cells (Fig. 46G, ns, $p > 0.999$).

In summary, these results suggest that the strong plateau potential observed in the infected cells is mediated, completely or mainly, by side effects related to the viral infection. The expression of Cre and/or GFP was probably exerting toxicity effects on the infected neurons and altering their electrophysiological properties. In fact, the properties of the GFP+ cells recorded in WT were very similar to the GFP+ cells recorded in TRPC5 flx/flx mice. Effects related to the lack of TRPC5 in the GFP positive (flx/flx) cells could have also contribute in part to the strong depolarization they showed as these neurons were in average more depolarized compared to GFP+ (WT). However, these results indicate that the unspecific effects related to the viral infection are the main responsible of the strong depolarization observed in GFP positive cells 4 weeks after infection in both WT and TRPC5 flx/flx animals.

3.5.6 TRPC5 conditional KO cells two weeks after AAV infection

In TRPC5 flx/flx animals, the firing frequency, and the membrane depolarization of the GFP positive cells were shown to be heavily affected by the viral infection. Unexpectedly these effects were observed also in GFP positive cells recorded in wild type animals infected with the same AAV-Cre-GFP virus. This indicated that the strong effects on the membrane potential depolarization were mainly mediated by unwanted side effects of the infection rather than by the TRPC5 conditional KO. As already mentioned before, previous studies reported that the overexpression of both Cre or GFP can led to cytotoxicity.

To further assess if the unexpected and strong membrane depolarization observed in TRPC5 flx/flx and WT mice was related to side effects of the viral infection, in my experiments I tried to use animals 2 weeks after viral infection instead of 4 weeks. By waiting less time after the viral infection, I wanted to see how the infected neurons would respond when the virus had less time to exert its side effects. In these experiments, TRPC5 flx/flx mice were infected with the AAV-Cre-GFP as previously described. Two groups of cells were recorded: GFP positive and GFP negative. The only difference compared to the previous experiments was that this time the mice were used 2 weeks after the viral infection, and not 4. After 2 weeks, GFP was expressed at good levels in the CA1 area making it possible to identify the infected cells with my patch clamp experimental set-up.

3.5.6.1 Persistent firing in GFP positive and negative cells in TRPC5 flx/flx mice

The GFP positive and negative (flx/flx) cells were both recorded in nACSF and then 10 μM carbachol was bath applied. The stimulation protocol was the same previously used (100 pA, 2 seconds) applied from under the firing threshold of the neurons.

In the GFP (flx/flx) positive group, after the application of the cholinergic agonist, none of the cells showed the strong and prolonged depolarization block observed in the GFP+ (flx/flx) cells 4 weeks after infection (Fig. 47A-D). In these neurons recorded 2 weeks after infection, depolarization block was also observed, however it was more similar to the one previously observed in non-infected wild type mice and it was never strong and long lasting like the one observed 4 weeks after infection (Fig. 47D). The firing behaviour of the GFP+ (flx/flx) cells was very similar to the non-infected WT cells. During the application of CCh, 20% of the GFP+ (flx/flx) cells showed long lasting persistent firing, 33% showed short persistent firing, only 13% of them responded with depolarization block and the remaining cells did not show persistent firing (Fig. 48).

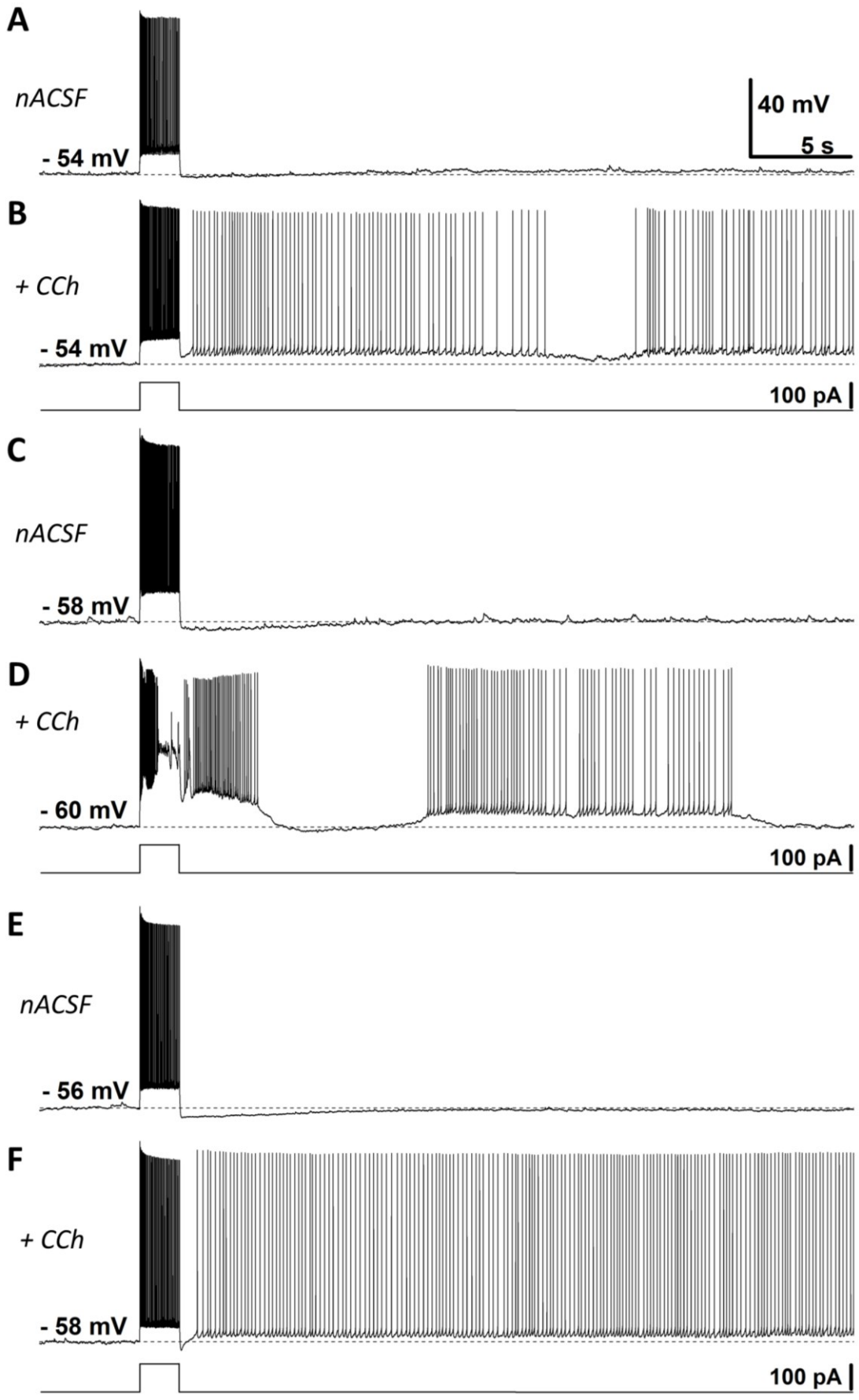

Figure 47 - Persistent firing in TRPC5 flx/flx mice infected with AAV-Cre-GFP, two weeks after infection (caption on next page).

Fig. 47 - Persistent firing in TRPC5 flx/flx mice infected with AAV-Cre-GFP, two weeks after infection (figure on previous page)

(A) The trace shows a GFP positive (flx/flx) cell recorded in control condition (nACSF). (B, top) Example of persistent firing in presence of 10 μM carbachol (CCh) in the same cell recorded in (A). (B, bottom) Current injection used in (A, B) (100 pA, 2 s). (C) The trace shows a GFP positive cell recorded in control condition (nACSF). (D, top) Example of depolarization block in presence of 10 μM carbachol (CCh) in the same cell recorded in (C). (D, bottom) Current injection used in (C, D) (100 pA, 2 s). (E) The trace shows a GFP negative cell recorded in control condition (nACSF). (F, top) Example of long-lasting persistent firing in presence of 10 μM carbachol (CCh) in the same cell recorded in (E). (F, bottom) Current injection used in (E, F) (100 pA, 2 s).

Of the recorded GFP+ (flx/flx) cells, only 2 of them showed the depolarized and bursting persistent firing that was previously observed in the GFP+ cells in TRPC5 flx/flx animals 4 weeks after infection. In general, the GFP positive (flx/flx) cells two weeks after injection showed persistent firing with properties very similar to the one observed in WT animals and in GFP negative cells.

In the GFP negative (flx/flx) cells during the application of carbachol, the firing behaviour during and after the end of the stimulus was comparable to WT cells and the firing behaviour was normal (Fig. 47E-F). Of the recorded cells, 37.5% showed long persistent firing, 25% showed short persistent firing and the remaining cells showed no persistent firing. None of the recorded cells showed the strong depolarization block previously observed in GFP positive cells recorded 4 weeks after infection.

In the TRPC5 flx/flx animals, both GFP+ and GFP- cells seemed to have similar properties when recorded 2 weeks after infection. To have a better overview I will now compare: GFP positive and negative cells recorded from infected TRPC5 flx/flx and, WT cells recorded from non-infected animals. The firing frequency of the WT cells was in average higher compared to the other two groups, however there were no significant differences between the groups (Fig. 48B, one-way ANOVA, $F(2, 55) = 0.88$, ns, $p = 0.422$, $n_{WT} = 35$, $n_{GFP+} = 15$, $n_{GFP-} = 8$). The average membrane potential values of both MP1 and MP2 were also not different among the groups (Fig. 48C, MP1, one-way ANOVA, $F(2, 55) = 0.48$, ns, $p = 0.622$, $n_{WT} = 35$, $n_{GFP+} = 15$, $n_{GFP-} = 8$; Fig. 48D, MP2, one-way ANOVA, $F(2, 55) = 0.081$, ns, $p = 0.922$, $n_{WT} = 35$, $n_{GFP+} = 15$, $n_{GFP-} = 8$). During the application of the stimulus, the GFP+ (flx/flx) cells were in average more depolarized compared to the GFP- (flx/flx) and WT cells and, differences were detected among the groups (Fig. 48E, one-way ANOVA, $F(2, 55) = 4.24$, # $p < 0.05$, $n_{WT} = 35$, $n_{GFP+} = 15$, $n_{GFP-} = 8$). A Tukey's multiple comparisons post hoc test showed that the membrane potential during the stimulus of the GFP+ (flx/flx) cells was significantly higher compared to WT (Fig. 48E, * $p < 0.05$) and it did not differ from the GFP- (flx/flx) cells (Fig. 48E, ns, $p = 0.203$). The GFP- (flx/flx) cells had similar values compared to WT cells (Fig. 48E, ns, $p = 0.937$).

In control condition (nACSF), the GFP positive (flx/flx) cells were in average slightly more depolarized after the application of the stimulus (MP1), however no differences among the groups were detected (Fig. 48F, MP1, one-way ANOVA, F (2, 55) = 0.78, ns, p = 0.465, n_{WT} = 35, n_{GFP+} = 15, n_{GFP-} = 8). In nACSF the membrane potential during the stimulus of the GFP+ (flx/flx) cells was in average higher compared to WT, and differences between the groups were detected (Fig. 48G, one-way ANOVA, F (2, 55) = 5.02, ## p < 0.01, n_{WT} = 35, n_{GFP+} = 15, n_{GFP-} = 8). A Tukey's multiple comparisons post hoc test showed that the membrane potential during the stimulus of the GFP+ (flx/flx) cells was significantly higher compared to WT (Fig. 48G, * p < 0.05) and it did not differ from the GFP- (flx/flx) cells (Fig. 48G, ns, p = 0.867). The GFP- (flx/flx) cells was in average higher compared to WT cells, however the difference was not significant (Fig. 48G, ns, p = 0.189).

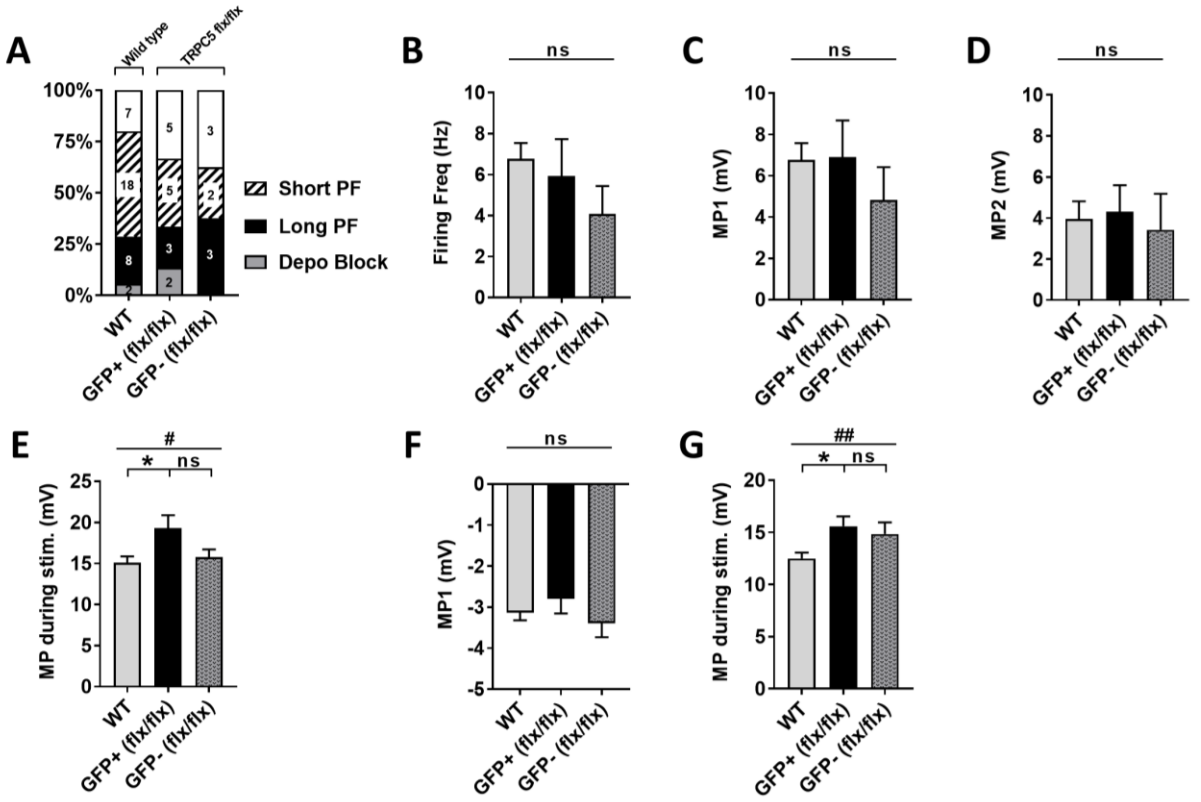

Fig. 48 - Properties of GFP positive and negative cells in TRPC5 flx/flx mice infected with AVV-Cre-GFP, two weeks after infection.

(A) Percentages of cells that showed persistent firing in carbachol (10 μM) in wild type animals (WT) and in GFP positive and negative cells recorded from TRPC5 flx/flx animals infected with AVV-Cre-GFP. The numbers on the graph represent the sample size. (B) Post-stimulus firing frequency in CCh (one-way ANOVA, ns, p = 0.422, n_{WT} = 35, n_{GFP+} = 15, n_{GFP-} = 8). (C) Post-stimulus depolarization in CCh (MP1, one-way ANOVA, ns, p = 0.622, n_{WT} = 35, n_{GFP+} = 15, n_{GFP-} = 8). (D) Post-stimulus depolarization in CCh (MP2, one-way ANOVA, ns, p = 0.992, n_{WT} = 35, n_{GFP+} = 15, n_{GFP-} = 8). (E) Membrane potential depolarization during the stimulus application (one-way ANOVA, # p < 0.05, n_{WT} = 35, n_{GFP+} = 15, n_{GFP-} = 8). Tukey's multiple comparison test: WT vs. GFP+, * p < 0.05; GFP+ vs. GFP-, ns, p = 0.203, WT vs GFP-, ns, p = 0.937. (F) Post-stimulus depolarization in control condition (nACSF) (MP1, one-way ANOVA, ns, p = 0.465, n_{WT} = 35, n_{GFP+} = 15, n_{GFP-} = 8). (G) Membrane potential depolarization during the stimulus application in control condition (nACSF) (one-

way ANOVA, ## $p < 0.05$, $n_{WT} = 35$, $n_{GFP+} = 15$, $n_{GFP-} = 8$). Tukey's multiple comparison test: WT vs. GFP+, * $p < 0.05$; GFP+ vs. GFP-, ns, $p = 0.867$, WT vs GFP-, ns, $p = 0.189$. All the recorded cells, shown in (A), were included in (B-G).

In summary, these data showed that 2 weeks after the viral infection, the GFP+ (flx/flx) cells did not show the strong plateau potential previously observed in GFP+ cells recorded 4 weeks after infection. In fact, these neurons responded similarly to the control groups: GFP- (flx/flx) and WT cells. The firing behaviour and the membrane potential depolarization of the infected cells was in general similar to the one observed in wild type. As expected, the GFP negative were also very similar when compared to wild type cells. However, the GFP+ (flx/flx) neurons showed to be more depolarized during the application of the stimulus in both CCh and nACSF suggesting that unwanted changes related to the infection were already affecting the infected cells. The presence of persistent firing in GFP+ cells could explain in two ways: (1) compensation mechanisms are already compensating the loss of TRPC5 or (2) TRPC5 are still present 2 weeks after infection.

3.5.6.2 Application of 3 µM clemizole hydrochloride on GFP positive cells

To test if TRPC5 were still present in the GFP positive (flx/flx) cells two weeks after infection, I used 3 µM clemizole hydrochloride. This TRPC channels blocker is selective for TRPC5 at this concentration. In these experiments GFP positive cells were recorded in 10 µM carbachol and, if persistent firing was observed, 3 µM clemizole hydrochloride was applied on top (Fig. 49).

In the GFP positive (flx/flx) cells showing persistent firing, after 15 minutes from the application of 3 µM clemizole hydrochloride there was a strong reduction of the firing activity. In 4 out of 8 cells there was a complete block of the firing frequency and in the remaining cells, there was a reduction of the firing frequency. The suppressing effect of CLE on the firing frequency of persistent firing was highly significant (Fig. 49E, Wilcoxon test, ** $p < 0.01$, $n = 8$).

The application of 3 µM clemizole hydrochloride significantly inhibited also the depolarization observed after the end of the stimulus (MP1) during the application of CCh (Fig. 49F, paired t-test, * $p < 0.05$, $n = 8$). The MP2 values were not affected by the application of CLE (Fig. 49G, paired t-test, ns, $p = 0.758$, $n = 8$).

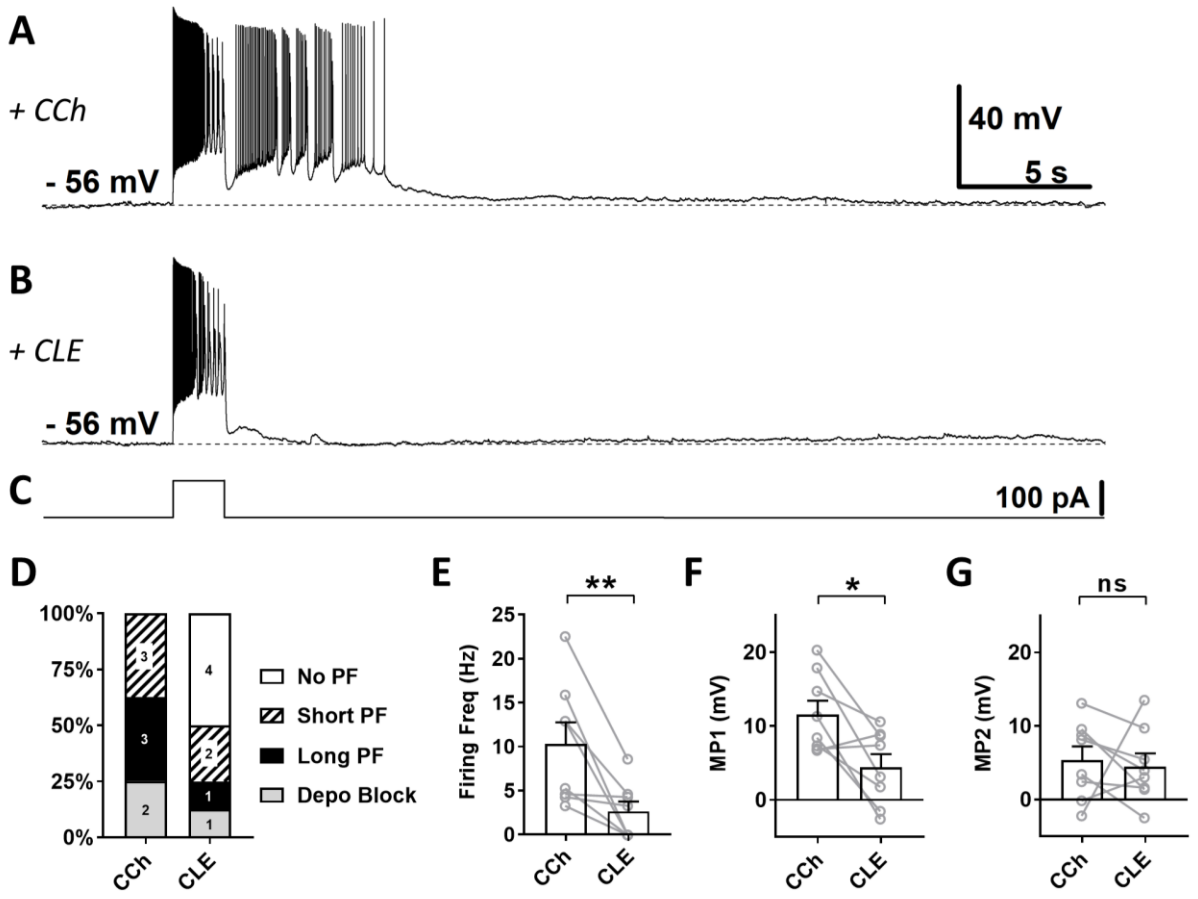

Figure 49 - The effect of clemizole hydrochloride (3 µM) on persistent firing in GFP positive (flx/flx) cells, two weeks after infection

(A) Example of persistent firing in CCh (10 µM). (B) Suppressed persistent firing in clemizole hydrochloride (CLE, 3 µM) in the same cell shown in (A). (C) Current injection used in (A, B) (100 pA, 2 s). (D) Percentages of cells that showed persistent firing in CCh and during the application of CLE. The numbers on the graph represent the sample size. (E) Post-stimulus firing frequency (Wilcoxon test, ** $p < 0.01$, $n = 8$). (F) Post-stimulus depolarization (MP1, paired t-test, * $p < 0.05$, $n = 8$). (G) Post-stimulus depolarization (MP2, paired t-test, ns, $p = 0.758$, $n = 8$).

Co-application of clemizole hydrochloride and ML204

In the cells in which the firing frequency was reduced but not fully block by the application of 3 µM clemizole hydrochloride, 10 µM ML204 was applied on top to see if blocking also TRPC4 channels could totally suppress persistent firing (Fig. 50). In all the tested cells persistent firing was completely suppressed and the average firing frequency was in reduced (Fig. 50E, n = 3). The membrane depolarization values after the end of the stimulus (MP1 and MP2) were reduced in all cells by ML204 application on top of CLE (Fig. 50F-G, n = 3).

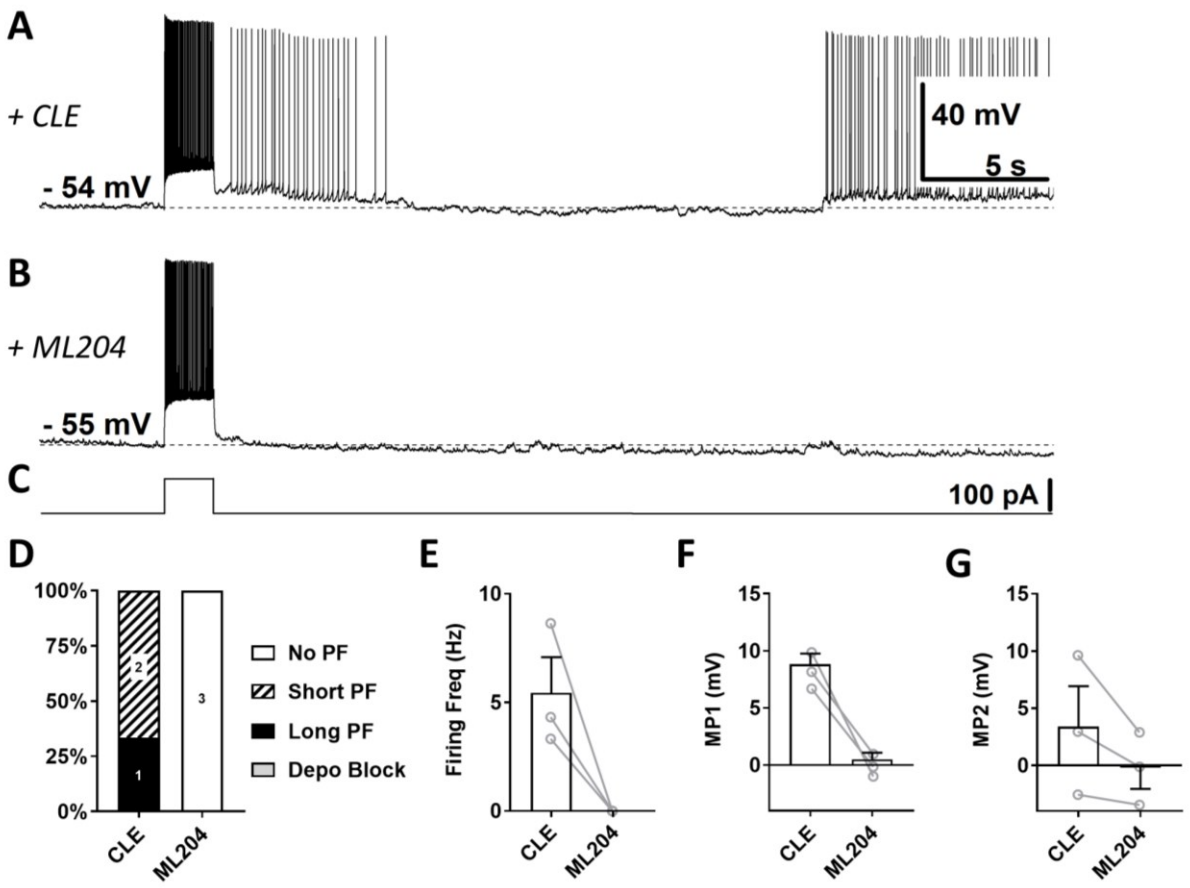

Figure 50 - The effect of clemizole hydrochloride (3 µM) and ML204 (10 µM) co-application on persistent firing in GFP positive (flx/flx) cells, two weeks after infection.

(A) Example of persistent firing in CLE (3 µM). (B) Suppressed persistent firing in ML204 (10 µM) in the same cell shown in (A). (C) Current injection used in (A, B) (100 pA, 2 s). (D) Percentages of cells that showed persistent firing during the application of CLE and ML204. The numbers on the graph represent the sample size. (E) Post-stimulus firing frequency (n = 3). (F) Post-stimulus depolarization (MP1, n = 3). (G) Post-stimulus depolarization (MP2, n = 3).

In summary, in GFP positive (flx/flx) cells the application of 3 µM clemizole hydrochloride showed a strong suppressing effect on persisting firing. Like previously observed in wild type animals, in some cells persistent firing was inhibited but not completely suppressed by the application of CLE and only the co-application of CLE and ML204 completely blocked it.

Taken together these data suggest that, 2 weeks after the infection with AAV-Cre-GFP, TRPC5 channels are still present in GFP positive cells in TRPC5 flx/flx mice.

3.5.7 Wild type animals two weeks after AAV infection

In the previous section I showed that GFP positive (flx/flx) cells, recorded 2 weeks after infection, did not show the strong depolarization observed in the GFP+ cells recorded 4 weeks the viral infection. To test if the same thing would happen also in infected WT cells, I injected WT animals with the same AAV-Cre-GFP previously used. The experimental conditions were the same used before: the cells were kept in nACSF and then 10 μM carbachol was bath applied. As control group for these GFP+ (WT) cells, I used cells recorded from non-infected wild type animals. To have a better overview I compared GFP positive cells from WT and TRPC5 flx/flx, and WT cells from non-infected animals (as control).

During the application of carbachol, none of the GFP+ (WT) cells showed the strong plateau potential, often leading to depolarization block, that was present neurons recorded four weeks after the viral infection (Fig. 51). The average firing frequency of the GFP+ (WT) cells was similar to the control group (WT) and to the GFP+ (flx/flx), no differences were detected between groups (Fig. 51E, one-way ANOVA, $F(2, 58) = 0.15$, ns, $p = 0.858$, $n_{WT} = 35$, $n_{GFP+ (WT)} = 11$, $n_{GFP+ (flx/flx)} = 15$).

The membrane potential depolarization of the GFP+ (WT) cells after and during the stimulus showed similar properties compared to the other groups. The average MP1 value of the GFP+ (WT) cells was slightly higher compared to WT. However there were no differences between the groups (Fig. 51F, MP1, one-way ANOVA, $F(2, 58) = 0.42$, ns, $p = 0.660$, $n_{WT} = 35$, $n_{GFP+ (WT)} = 11$, $n_{GFP+ (flx/flx)} = 15$). The average MP2 value of the GFP+ (WT) cells was also slightly more depolarized but again, no significant differences were detected between the groups (Fig. 51G, MP2, one-way ANOVA, $F(2, 58) = 0.66$, ns, $p = 0.520$, $n_{WT} = 35$, $n_{GFP+ (WT)} = 11$, $n_{GFP+ (flx/flx)} = 15$). The membrane potential of the GFP+ (WT) during the stimulus was in average higher compared to control (Fig. 51H, one-way ANOVA, $F(2, 58) = 4.77$, # $p < 0.05$, $n_{WT} = 35$, $n_{GFP+ (WT)} = 11$, $n_{GFP+ (flx/flx)} = 15$). However, a Tukey's multiple comparisons post hoc test showed that the membrane potential during the stimulus of the GFP+ (WT) cells was not significantly higher compared to WT (Fig. 51H, ns, $p = 0.173$) and it did not differ from the GFP+ (flx/flx) cells (Fig. 51H, ns, $p = 0.867$). The membrane potential during the stimulus of the GFP+ (flx/flx) cells was in average higher compared to WT cells, and the difference was significant (Fig. 51H, * $p < 0.05$).

In control condition (nACSF), the GFP+ (WT) cells showed to be in average more depolarized compared to the control and the GFP+ (flx/flx) groups (Fig. 51I, MP1, one-way ANOVA, $F(2, 58) = 3.29$, # $p < 0.05$, $n_{WT} = 35$, $n_{GFP+ (WT)} = 11$, $n_{GFP+ (flx/flx)} = 15$). A Tukey's

multiple comparisons post hoc test showed that the MP1 of the GFP+ (WT) cells was significantly more depolarized compared to WT (Fig. 51I, * $p < 0.05$) and it did not differ from the GFP+ (flx/flx) cells (Fig. 51I, ns, $p = 0.280$). There were no differences between the GFP+ (flx/flx) and WT groups (Fig. 51I, ns, $p = 0.653$).

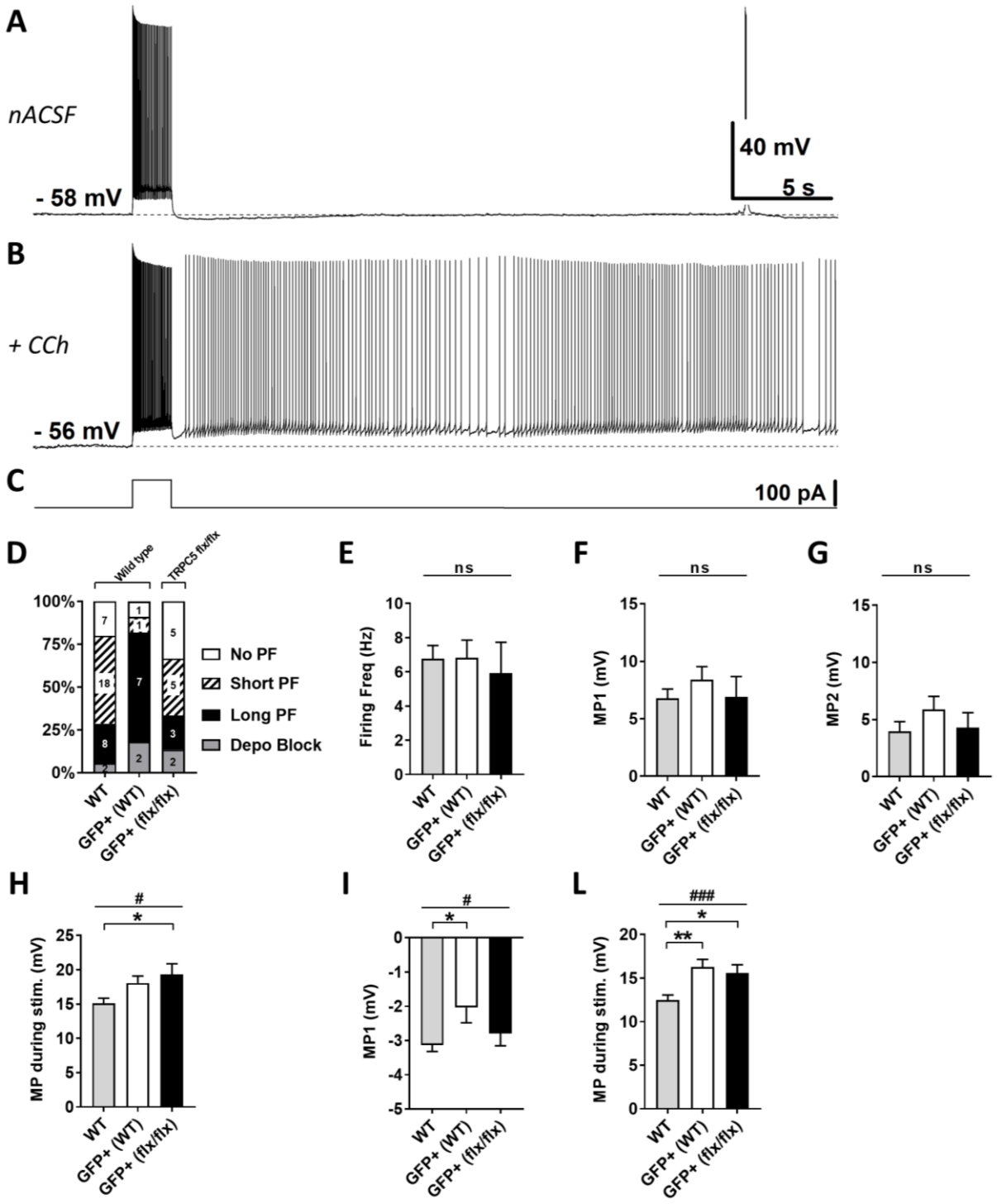

Figure 51 - Persistent firing in wild type mice infected with AAV-Cre-GFP, two weeks after infection.

(A) The trace shows a GFP positive (WT) cell recorded in control condition (nACSF). (B) Example of long-lasting persistent firing in presence of 10 µM carbachol (CCh) in the same cell recorded in (A). (C) Current injection used in (A,B) (100 pA, 2 s). (D) Percentages of cells that showed persistent firing in carbachol (10 µM)

in wild type animals (WT) and in GFP positive cells recorded from wild type and TRPC5 flx/flx mice infected with AVV-Cre-GFP. The numbers on the graph represent the sample size. (E) Post-stimulus firing frequency (one-way ANOVA, ns, $p = 0.858$, $n_{WT} = 35$, $n_{GFP+ (WT)} = 11$, $n_{GFP+ (flx/flx)} = 15$). (F) Post-stimulus depolarization in CCh (MP1, one-way ANOVA, ns, $p = 0.660$, $n_{WT} = 35$, $n_{GFP+ (WT)} = 11$, $n_{GFP+ (flx/flx)} = 15$). (G) Post-stimulus depolarization in CCh (MP2, one-way ANOVA, ns, $p = 0.520$, $n_{WT} = 35$, $n_{GFP+ (WT)} = 11$, $n_{GFP+ (flx/flx)} = 15$). (H) Membrane potential depolarization during the stimulus application (one-way ANOVA, # $p < 0.05$, $n_{WT} = 35$, $n_{GFP+ (WT)} = 11$, $n_{GFP+ (flx/flx)} = 15$). Tukey's multiple comparison test: WT vs GFP+ (WT), ns, $p = 0.173$; GFP+ (WT) vs GFP+ (flx/flx), ns, $p = 0.785$; WT vs GFP+ (flx/flx), * $p < 0.05$. (I) Post-stimulus depolarization in control condition (nACSF) (MP1, one-way ANOVA, # $p < 0.05$, $n_{WT} = 35$, $n_{GFP+ (WT)} = 11$, $n_{GFP+ (flx/flx)} = 15$). Tukey's multiple comparison test: WT vs GFP+ (WT), * $p < 0.05$; GFP+ (WT) vs GFP+ (flx/flx), ns, $p = 0.280$; WT vs GFP+ (flx/flx), ns, $p = 0.653$. (L) Membrane potential depolarization during the stimulus application in control condition (nACSF) (one-way ANOVA, ### $p < 0.001$, $n_{WT} = 35$, $n_{GFP+ (WT)} = 11$, $n_{GFP+ (flx/flx)} = 15$). Tukey's multiple comparison test: WT vs GFP+ (WT), ** $p < 0.01$; GFP+ (WT) vs GFP+ (flx/flx), ns, $p = 0.860$; WT vs GFP+ (flx/flx), * $p < 0.05$. All the recorded cells, shown in (D), were included in (E-L).

In nACSF, the membrane potential depolarization during the stimulus application of the GFP+ cells recorded in WT and TRPC5 flx/flx mice were in average higher compared to WT (Fig. 51L, one-way ANOVA, $F(2, 58) = 7.88$, ### $p < 0.001$, $n_{WT} = 35$, $n_{GFP+ (WT)} = 11$, $n_{GFP+ (flx/flx)} = 15$). A Tukey's multiple comparisons post hoc test showed that the depolarization of the GFP+ (WT) cells was significantly higher compared to WT (Fig. 51L, ** $p < 0.01$) and it did not differ from the GFP+ (flx/flx) cells (Fig. 51L, ns, $p = 0.860$).

In summary, the electrophysiological properties of GFP positive (WT) cells 2 weeks after infection were very similar compared to WT cells recorded in non-infected animals (control). The strong plateau potential observed 4 weeks after the infection was never observed in these experiments performed 2 weeks after the infection. This indicates that 2 weeks after infection the unspecific effects mediated by the virus were still not to be present. However, the average membrane potential of the GFP+ (WT) cells was always slightly more depolarized compared to WT cells and these differences were in fact significant in control condition (nACSF).

Taken together these data indicate that in wild type animals, 2 weeks after infection, GFP positive cells are still not affected by the nonspecific side effects related to the AAV-Cre-GFP. However, as the GFP+ (WT) cells seemed to be in general slightly more depolarized, this may indicate that already after 2 weeks some changes were already happening the infected cells. A tendency to be more depolarized, in carbachol and especially in control condition (nACSF), was also observed in the previously shown experiments testing the virus 2 weeks after infection in TRPC5 flx/flx animals.

4 RESULTS – Persistent firing in the layer II of the medial entorhinal cortex

In some recent publications from Tonegawa's lab it was reported that the entorhinal-hippocampal network is driving and regulating temporal association memory [54,281]. Takashi Kitamura (2017) proposed a model where the trisynaptic pathway originating from ocean cells (calbindin negative) in EC layer II primarily process context and space, whereas the direct pathways from the EC layer III and layer II islands (calbindin positive) are responsible for the temporal properties of episodic memory, with the layer II island having a central role gating the information coming from the EC layer III and directed to CA1 [78]. One of the mechanism proposed to support temporal association is persistent neuronal firing, as it can bridge the delay period in working memory tasks [22,24]. In the entorhinal cortex, TRPC channels are highly expressed and, in light of the aforementioned model, these channels could have a central role in supporting and regulating the activity of island and ocean cells in the MEC layer II, affecting temporal association memory. Previous studies in the entorhinal cortex showed that persistent activity is present in the layer II, III and V [50,66,111,113,158,161,170,176,178]. In some of these previous studies the role of TRPC channels in persistent firing was investigated, but only in the deeper entorhinal cortex in the layer III and layer V.

Given the specific roles of island and ocean cells in MEC layer II proposed by Kitamura and given the lack of information about the role of TRPC channels in supporting persistent firing in the EC layer II, in this second project I focused on this superficial layer. First, I checked the expression pattern of TRPC4, TRPC5 and calbindin in the MEC layer II. Then, I tested with a novel blocker if TRPC channels were supporting persistent firing in this brain area.

4.1 TRPC4 and TRPC5 channels expression in mouse layer II of medial entorhinal cortex

TRPC channels are widely expressed in the brain [204] and it has been shown that, among the seven TRPC channels subtypes, TRPC4 and TRPC5 are the predominant subunits expressed in rodent brain [205]. In addition, previous studies also reported that TRPC1, TRPC4 and TRPC5 channels are expressed in large number in the entorhinal cortex layer [113,209].

In the layer II of the medial entorhinal cortex, calbindin, a calcium binding protein, is expressed in clusters forming the so called "calbindin island" [54,69,70]. It has been suggested that calbindin could be used as a marker to distinguish between two cellular population present in the layer II: pyramidal cells, expressing calbindin, and stellate cells, not expressing calbindin. In this view, the pyramidal calbindin positive cells are called "island cells", and the stellate cells, not expressing calbindin, are called "ocean cells" [64,79,282].

The main goal of the immunohistochemical (IHC) experiments was to check if the expression pattern of TRPC4 and TRPC5 channels correlated or not with the expression pattern of calbindin forming clusters in the layer II of the medial entorhinal cortex.

The IHC protocols and antibodies used for the TRPC4 and TRPC5 were like the one already used in the hippocampus. In these experiments double staining using calbindin and TRPC4 or TRPC5 antibodies were performed. Several primary antibodies were tested for both TRPC4 and TRPC5 and the results were compared to already published data, when possible, or to the expected expression estimated from the mRNA expression levels provided by the Allen brain mouse atlas (http://portal.brain-map.org/). The antibodies were chosen according to their specificity in labelling the EC region and to their effective concentration. The secondary antibodies were chosen accordingly to the used primary antibodies and their specificity was confirmed by low level of background signal in the control experiments.

4.1.1 Calbindin and TRPC4 expression

In these experiments, anti-calbindin D-28K antibodies (monoclonal, Swant) and anti-TRPC4 (extracellular) antibodies from Alomone Labs were used to perform a double IHC staining in mouse brain slices (Fig. 52). As expected, calbindin positive cells formed island clusters in the layer II of medial entorhinal cortex and interestingly cells expressing TRPC4 seemed to be more concentrated in the calbindin positive cells in the islands (Fig. 52A-B). This pattern was present in different animals, slices, and stainings. An analysis of the average intensity differences between the island and the ocean regions of interest, showed that TRPC4 were predominantly expressed in island clusters (Fig. 52F, paired t-test, * $p < 0.05$, $n = 5$). This analysis was performed by Jens Schweihoff under my supervision.

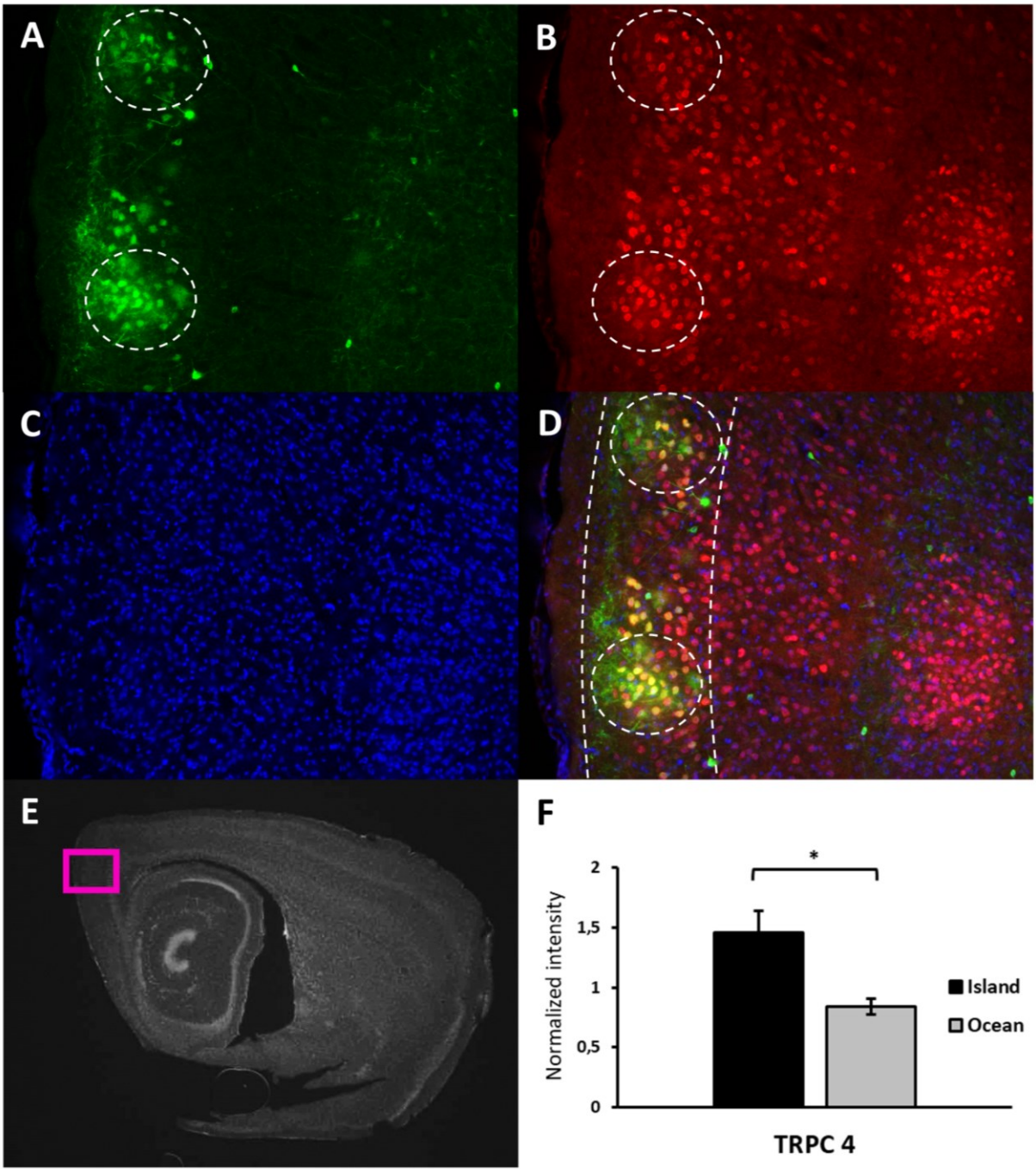

Figure 52 - Calbindin and TRPC4 expression in mouse medial entorhinal cortex.

(A-D) The pictures show the expression of calbindin and TRPC4 observed in a double IHC staining. (B) Calbindin expression in a sagittal slice of MEC. The dashed circle highlights the island area (calbindin cluster). (B) TRPC4 expression in the sagittal slice of MEC showed in (A). The dashed circle highlights the island area showed in (A). (C) DAPI staining of the slice showed in (A, B). (D) Merged image of the pictures showed in (A, B, C). The dashed lines delimit the layer II area. (E) Low magnification image indicating the location of the images in (A, B, C, D). (F) Average intensity of TRPC4 labelling in island and ocean clusters. The regions of interests were manually chosen, and the intensity was normalized with the average intensity of the layer II, (paired t-test, * $p < 0.05$, $n = 5$).

4.1.2 Calbindin and TRPC5 expression

In these experiments anti-calbindin D-28K antibodies (polyclonal, Swant) and anti-TRPC5 antibodies from Neuromab were used to perform a double staining in mouse brain slices (Fig. 53). Calbindin showed its classic island expression pattern in the layer II of MEC (Fig. 53A). Surprisingly, the TRPC5 detection revealed that these channels seemed to be more concentrated out of the island clusters in the so called “ocean cells” (Fig. 53B). This pattern was present in different animals, slices and staining. An analysis of the average intensity differences between the island and the ocean regions of interest, showed that TRPC5 channels were predominantly expressed in the ocean cells (Fig. 53F, paired t-test, * $p < 0.05$, $n = 5$). This analysis was performed by Jens Schweihoff under my supervision.

In summary, taken together these data indicate that in the entorhinal cortex layer II both TRPC4 and TRPC5 are expressed differently in calbindin positive and negative cells. While TRPC4 are predominantly expressed in island cells (calbindin clusters), TRPC5 are predominantly expressed in ocean cells (out of the calbindin clusters).

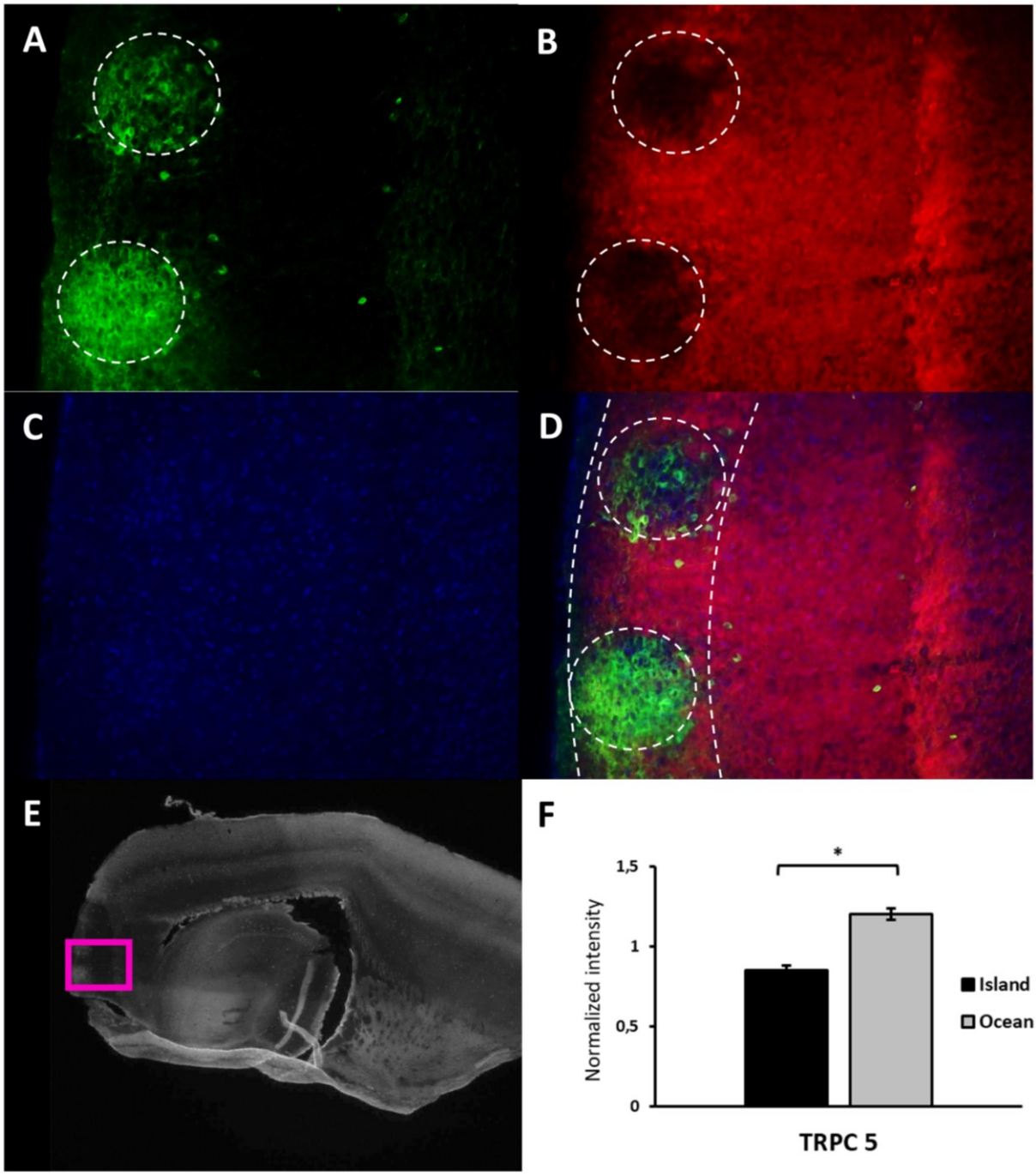

Figure 53 - Calbindin and TRPC5 expression in mouse medial entorhinal cortex.

(A-D) The pictures show the expression of calbindin and TRPC5 observed in a double IHC staining. (B) Calbindin expression in a sagittal slice of MEC. The dashed circle highlights the island area (calbindin cluster). (B) TRPC5 expression in the sagittal slice of MEC showed in (A). The dashed circle highlights the island area showed in (A). (C) DAPI staining of the slice showed in (A, B). (D) Merged image of the pictures showed in (A, B, C). The dashed lines delimit the layer II area. (E) Low magnification image indicating the location of the images in (A, B, C, D). (F) Average intensity of TRPC5 labelling in island and ocean clusters. The regions of interests were manually chosen, and the intensity was normalized with the average intensity of the layer II, (paired t-test, * $p < 0.05$, $n = 5$).

4.2 Cholinergic-dependent persistent firing of layer II neurons in the mouse medial entorhinal cortex

Persistent firing is present in many brain areas [22–26] and, in previous studies in the entorhinal cortex, it has been suggested that TRPC channels are supporting the mechanism generating persistent firing in the layers II, III and V [50,111,113,158,178,184]. In this previous studies, persistent firing was induced using a depolarizing current step during cholinergic or glutamatergic stimulation. In my experiments in the layer II of the medial entorhinal cortex (MEC), persistent firing was also induced by a current pulse during the application of carbachol, the cholinergic agonist that I used also in the previous project focusing on the hippocampal CA1. Carbachol was chosen because, in a previous study in the MEC layer II, it was successfully used to induce persistent firing in rats [184]. In addition, carbachol has been used to induce persistent firing also in other layers of the entorhinal cortex [50,111,113,158,178]. Following the approaches used in these studies, I investigate the presence and the properties of persistent firing in mice layer II MEC neurons.

4.2.1 Cholinergic-dependent persistent firing in medial entorhinal cortex layer II

Persistent firing was induced applying the same protocol previously used in the hippocampus. During the bath application of 10 μM carbachol, the membrane potential of the neuron was depolarized just below its firing threshold and a square current pulse of 100 pA lasting 2 seconds was applied to induce persistent activity. The membrane potential was always depolarized to reach the firing threshold of the cell, so that persistent firing could be studied and compared among the different pharmacological conditions used.

During the control condition (nACSF), none of the tested cells showed persistent firing. After the application of the cholinergic agonist 48% of the cells showed persistent firing (Fig. 54A-B) and the rest did not respond to the stimulation (Fig. 54D-E). The average firing frequency of all the recorded neurons was 3.97 Hz ± 1.21, the average MP1 was 1.18 mV ± 0.51 and the average MP2 was 2.04 mV ± 0.41.

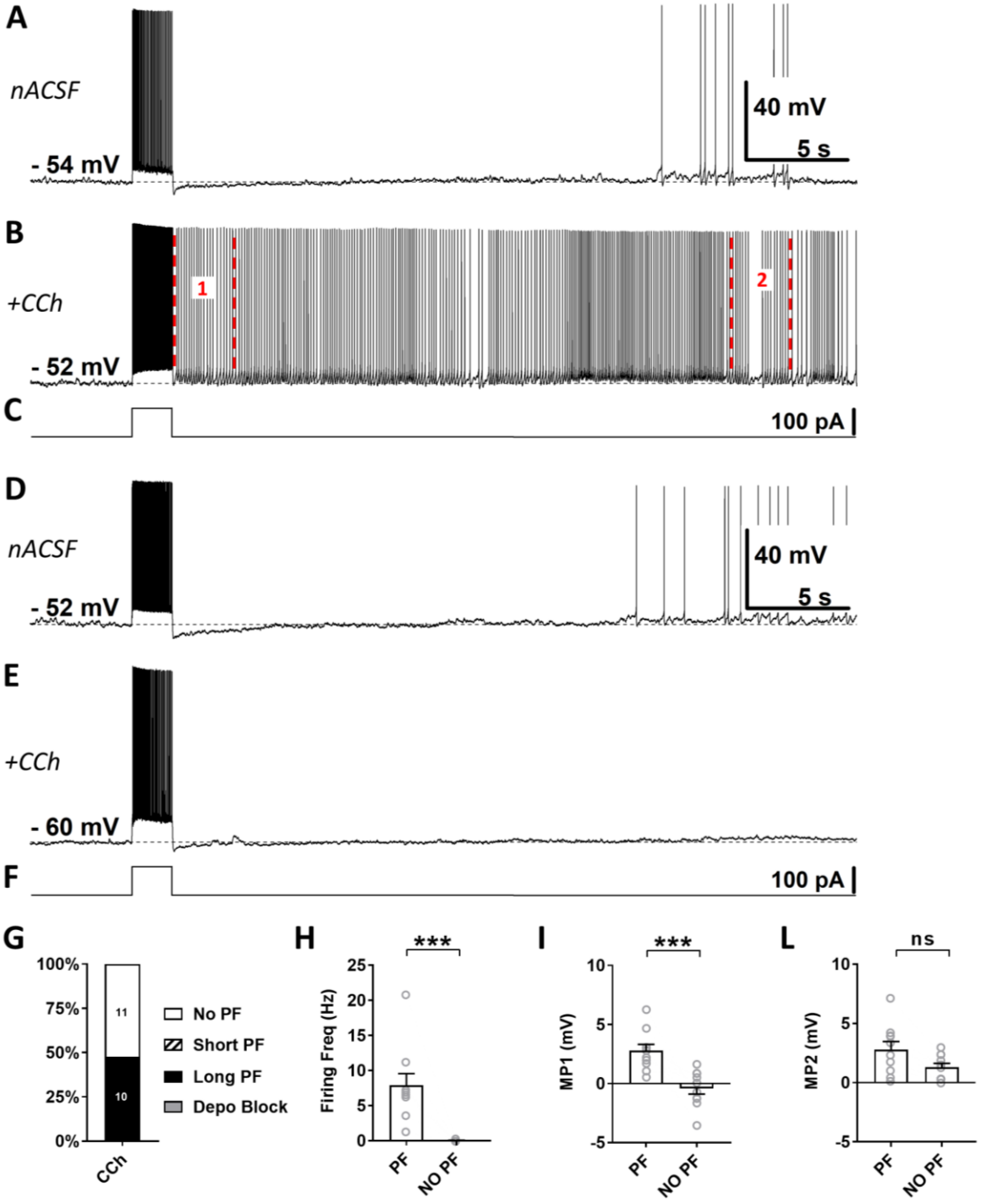

Figure 54 – Persistent firing in MEC layer II neurons.

(A) The trace shows a cell recorded in control condition (nACSF). (B) Example of long lasting persistent in presence of 10 µM carbachol (CCh) in the same cell shown in (A). In this trace the 3 seconds interval used to measure the firing frequency and MP1 is delimited with dashed lines and marked with "1". The 3 seconds interval 27 seconds after the end of the stimulus used to measure MP2 is marked with "2". (C) Current injection used in (A, B, C) (100 pA, 2 s). (D) The trace shows a cell recorded in control condition (nACSF). (E) After the application of CCh (10 µM), the cell showed in (D) did not respond with persistent firing (F) Current injection used in (D, E) (100 pA, 2 s). (G) Percentages of cells that showed persistent firing during the application of carbachol. (H) Post-stimulus firing frequency of cells showing (PF) and not showing persistent firing (NO PF) (Mann-Whitney, *** $p < 0.001$, $n_{PF} = 10$, $n_{NO\ PF} = 11$). (I) Post-stimulus depolarization (MP1) measured in an interval 3 seconds after the end of the stimulus (unpaired t-test, *** $p < 0.001$, $n_{PF} = 10$, $n_{NO\ PF} = 11$). (L) Post-stimulus depolarization (MP2) measured in an interval 27 seconds after the end of the stimulus (unpaired t-test, ns, $p = 0.062$, $n_{PF} = 10$, $n_{NO\ PF} = 11$).

Given this division in half of the population of the recorded neurons, I analysed separately cells showing or not showing persistent firing. In the cells showing persistent activity the firing frequency was in average 7.9 ± 1.67 Hz and all of them showed long lasting persistent firing (Fig. 54G-H). When the firing frequency of cells showing persistent firing was compared to cells showing no persistent firing the difference was strongly significant (Fig. 54H, Mann-Whitney, *** $p < 0.001$, $n_{PF} = 10$, $n_{NO\ PF} = 11$).

In the cells that showed persistent firing, the membrane depolarization after the end of the stimulus (MP1) was also significantly higher compared to the cells not showing PF (Fig. 54I, unpaired t-test, *** $p < 0.001$, $n_{PF} = 10$, $n_{NO\ PF} = 11$). The cells not showing persistent firing did not respond to the stimulation with a depolarization and after the end of the stimulus their membrane potential went back to values observed before stimulation. As already mentioned, the cells showing persistent firing responded in all cases with long lasting persistent firing and this can be seen by the measure of MP2, the membrane potential depolarization measured 27 seconds after the end of the stimulus. The MP2 values of the cells showing persistent firing were in fact very similar to the ones measured for MP1, indicating that the depolarization plateau was long-lasting (paired t-test, ns, $p = 0.962$, $n = 10$). The cells showing persistent firing had in average more depolarized values of MP2 compared to cells not showing PF but the difference observed was not significant (Fig. 54L, unpaired t-test, ns, $p = 0.062$ $n_{PF} = 10$, $n_{NO\ PF} = 11$). This was probably explained by a late depolarizing shift of the membrane potential of the cells not showing PF. In fact, in the cells not showing persistent firing the MP2 values were significantly more depolarized compared to the MP1 values (paired t-test, ** $p < 0.01$, $n = 11$).

Taken together these results indicate that cholinergic-dependent persistent firing is present in the mice layer II and that the population of recorded neurons was divide in half, cells showing and cells not showing persistent firing.

4.2.2 Persistent firing in pyramidal-like and stellate-like cells

In the MEC layer II, the excitatory type of cells are mainly pyramidal and stellate cells, these two population of cells has been extensively described [65,67] and in more recent studies it has been found that there are also at least two other population of cells between stellate and pyramidal cells having intermediate morphologies and electrophysiological properties [64,68]. To see if the ability to support persistent firing was a property related to a specific population of excitatory neurons, I divided the recorded cells in two group: stellate and pyramidal cells. I decided to divide the recorded cells only in two group, without intermediate groups, because my sample size was small compared to those studies categorizing the cells not only in pyramidal and stellate, but also in one or more intermediate groups [64,68].

Following a criteria used in a previous publication of our lab in the MEC layer II [184], I divided my cells in two population according to their sag ratio: when the sag ratio was bigger than 0.3 a neuron was categorized as stellate (Fig. 55A), when it was smaller than 0.3 it was categorized as pyramidal (Fig. 55B). This classification, based on electrophysiological properties, was chosen because in my biocytin staining in several cells, due to low staining quality, it was possible to detect their anatomical position, but it was not possible to clearly identify their morphology. Given the fact that I could not divide them based on their morphology, I will refer to them as stellate-like and pyramidal-like cells.

The sag ratio was calculated by measuring the voltage responses to a negative current pulse lasting 1 s applied from -65mV. The intensity of this negative stimulus was chosen to achieve the sag peak as close as possible to -90 mV. This was made to be sure to have a good visualization of the sag by facilitating the activation of the current supporting it.

In my experiments, both the pyramidal-like and the stellate-like cells showed persistent firing in 50% of the cases (Fig. 55C, $n_{PYR} = 8$, $n_{STE} = 12$). The measure of the sag ratio differed between the two groups of cells and the sag ratio of the stellate cells was significantly higher compared to pyramidal-like cells (Fig. 55D, Mann-Whitney test, *** $p < 0.001$, $n_{PYR} = 8$, $n_{STE} = 12$). Another parameter often used to distinguish between stellate and pyramidal cells is the input resistance, in line with the previous literature in my cells the input resistance of the pyramidal-like cells was significantly higher compared to stellate-like cells (Fig. 55E, unpaired t-test, * $p < 0.05$, $n_{PYR} = 8$, $n_{STE} = 12$). The firing frequency and the membrane potential depolarization (MP1) did not significantly differ between the two groups (Fig. 55F-G; firing frequency, Mann-Whitney test, ns, $p = 0.650$; MP1, unpaired t-test, ns, p =

0.508; for both groups: n_{PYR} = 8, n_{STE} = 12). As final test, I tried to see if there was a correlation between persistent firing frequency and the sag ratio of the all examined cells, however there was no correlation (Fig. 55H, linear reg., ns, p = 0.735, R^2 = 0.006).

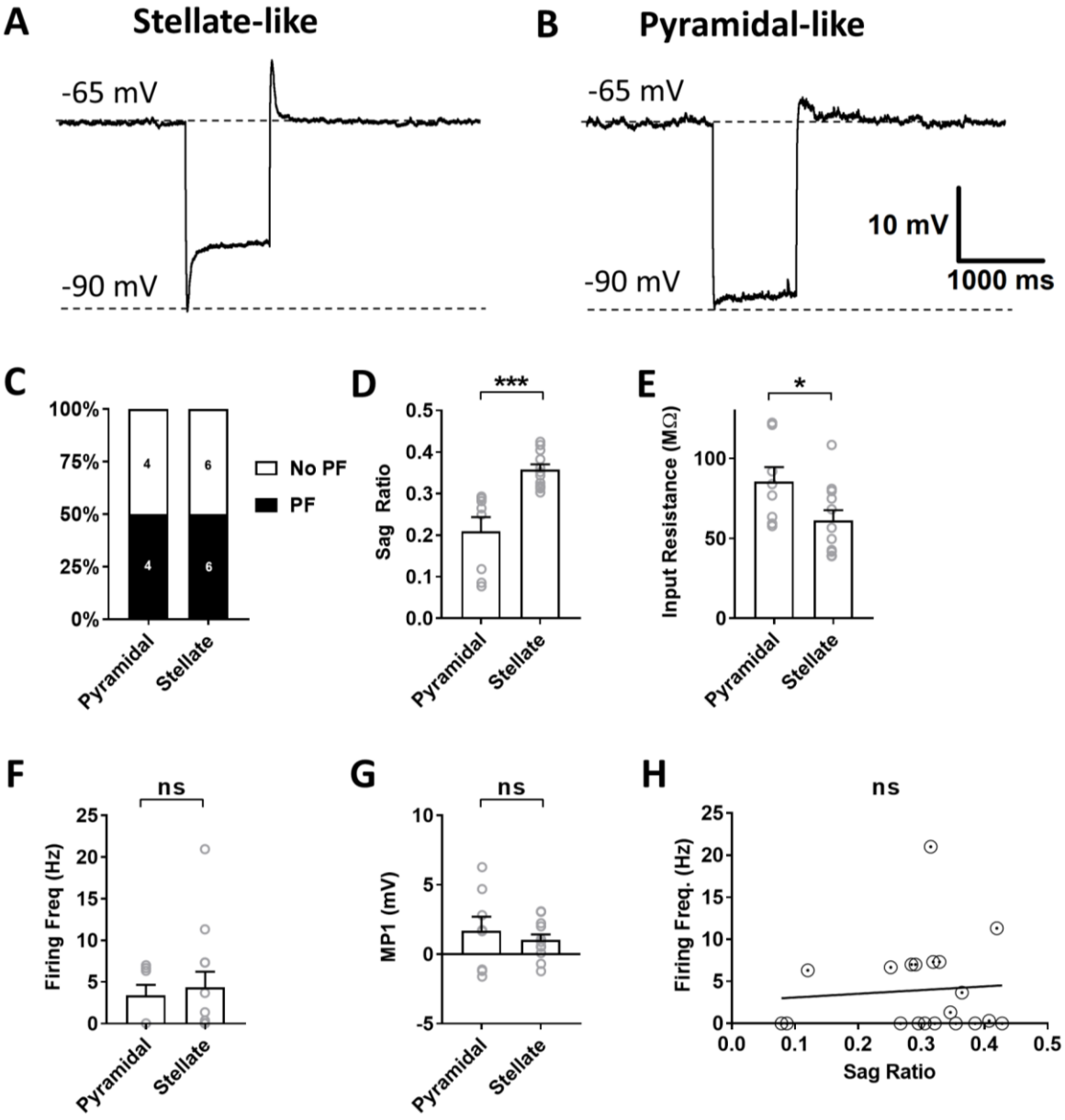

Figure 55 - Properties of pyramidal-like and stellate-like cells divided using the sag ratio.

(A) Example of sag in a stellate-like cell. The stimulation protocol was applied from -65mV and the intensity of the 1 second hyperpolarizing step was chosen to achieve the peak of the sag as close as possible to – 90 mV. (B) Example of sag in a pyramidal cell. (C) Percentage of pyramidal-like and stellate-like cells showing persistent firing. The numbers on the graph represent the sample size. (D) Sag Ratio of pyramidal-like and stellate-like cells (Mann-Whitney test, *** $p < 0.001$, n_{PYR} = 8, n_{STE} = 12). (E) Input resistance of pyramidal-like and stellate-like cells (unpaired t-test, * $p < 0.05$, n_{PYR} = 8, n_{STE} = 12). (F) Firing frequency of PF in pyramidal-like and stellate-like cells (Mann-Whitney test, ns = 0.650, n_{PYR} = 8, n_{STE} = 12). (G) Membrane potential depolarization (MP1, unpaired t-test, ns, p = 0.508, n_{PYR} = 8, n_{STE} = 12. (H) Correlation between persistent firing frequency and the sag ratio of all examined cells (linear reg., ns, p = 0.735, R^2 = 0.006).

In addition to the measure of the sag ratio, I tried to classify my neurons using another parameter, the spike latency. In a previous study from Alonso and Klink it was shown that stellate cells had smaller spike latency (42 ± 17 ms) compared to pyramidal cells (180 ± 66 ms) [65]. In my experiments the cells were kept at -65 mV and positive current pulses lasting 1 second (1s, 50 pA) were consecutively applied increasing at every sweep the current intensity of 50 pA. The spike latency was calculated using the first sweep that could induce an action potential.

Based on the difference observed in the paper from Alonso and Klink (1993), I divided my cells in two groups using 60 ms as threshold: if the spike latency was smaller than 60 ms the cells were categorized as stellate, if bigger as pyramidal (Fig. 56). Using this method, I obtained 16 stellate-like cells, of which 9 showing PF, and 3 pyramidal-like cells, of which 1 was showing PF (Fig. 56C). These results indicated that either I record mainly stellate cells or that this classification method was not effective for my data. I tried to see if there was a correlation between persistent firing frequency and the spike latency, however there was no correlation (Fig. 56E, ns, linear reg., $p = 0.904$, $R^2 = 0.001$).

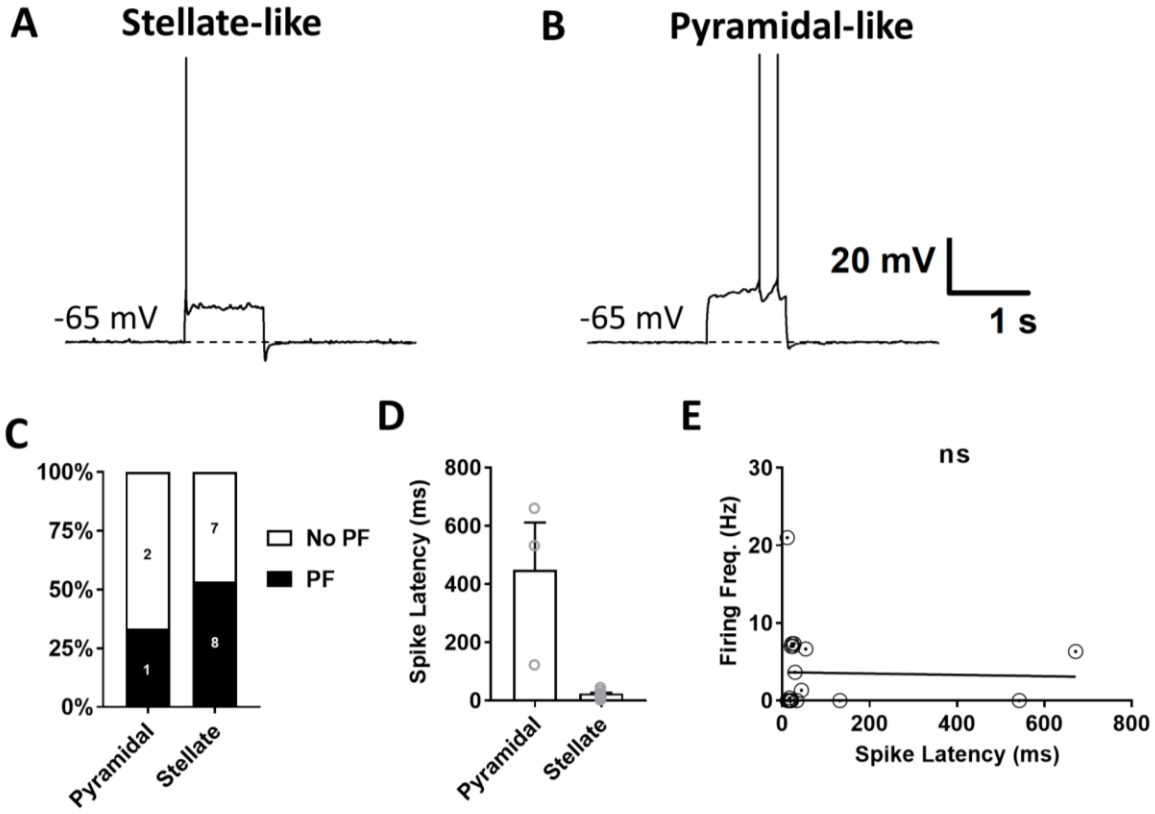

Fig. 56 – Properties of pyramidal-like and stellate-like cells divided using the spike latency.

(A) Example of spike latency in a stellate-like cell. The stimulation protocol was applied from -65mV and the intensity of the 1 second hyperpolarizing step was chosen to achieve at least one spike. (B) Example of spike latency in a pyramidal-like cell. (C) Percentage of pyramidal-like and stellate-like cells showing persistent firing.

The numbers on the graph represent the sample size. (D) Spike latency of pyramidal-like and stellate-like cells, $n_{PYR} = 3$, $n_{STE} = 15$). (E) Correlation between persistent firing frequency and the spike latency of all examined cells (ns, linear reg., $p = 0.904$, $R^2 = 0.001$).

Taken together these results suggest that, in the layer II of MEC in mice, pyramidal-like and stellate-like cells have similar chances to show persistent firing, when dividing them using the sag ratio. Nevertheless, these data are preliminary and need to be deepened by increasing the sample size and by taking in consideration both electrophysiological and morphological properties of the cells.

4.2.3 Effect of DHPG application on cells not showing persistent firing

In the layer II of MEC persistent firing and a plateau potential were induced in the 48% of the neurons, the rest of the cells did not respond to the cholinergic stimulation. In the cells that did not respond to the cholinergic stimulation with carbachol I tested if they would rather respond to the stimulation with DHPG, a potent agonist of group I metabotropic glutamate receptors (mGluRs) that can activate mGluR1 and mGluR5 receptors. This agonist was chosen as previous in studies it was used to induce persistent activity in the entorhinal cortex [50,158].

In my experiments, the cells were first recorded in nACSF and then 10 μM carbachol was bath applied. If persistent firing was not observed during carbachol application, 20 μM DHPG was bath applied on top (Fig. 57). DHPG was applied on top of carbachol in 6 cells that did not show persistent firing during CCh application. During DHPG application, only in 2 cells some spikes were recorded after the end the stimulus, but only 1 of them could be categorized as short PF (Fig. 57D). In my experiments a cell was considered to show persistent firing when the firing frequency was bigger than 1 Hz. The application DHPG did not induce any significant increase of the firing frequency (Fig. 57E, Wilcoxon test, ns, $p = 0.250$, $n = 6$).

The average membrane potential after the end of the stimulus (MP1) got slightly more hyperpolarized after the application of DHPG, however there was no significant difference compared to the previous condition (Fig. 57F, Wilcoxon test, ns, $p = 0.156$, $n = 6$). Also the values of MP2 were more hyperpolarized after the application of DHPG, however the observed difference was not significant (Fig. 57G, paired t-test, ns, $p = 0.079$, $n = 6$).

These results indicate that the cells not showing persistent firing during cholinergic stimulation, did not respond also to glutamatergic stimulation. This suggest that the ionic mechanism responsible for the generation of PF might be absent in these neurons. These results are in line with a previous study from Zhang et al. (2010) in the anterior cingulate cortex. In this study it was shown that persistent firing could be induced by both carbachol and DHPG in the same of cells, indicating that the two agonist activate the same intracellular pathway leading to persistent firing [180].

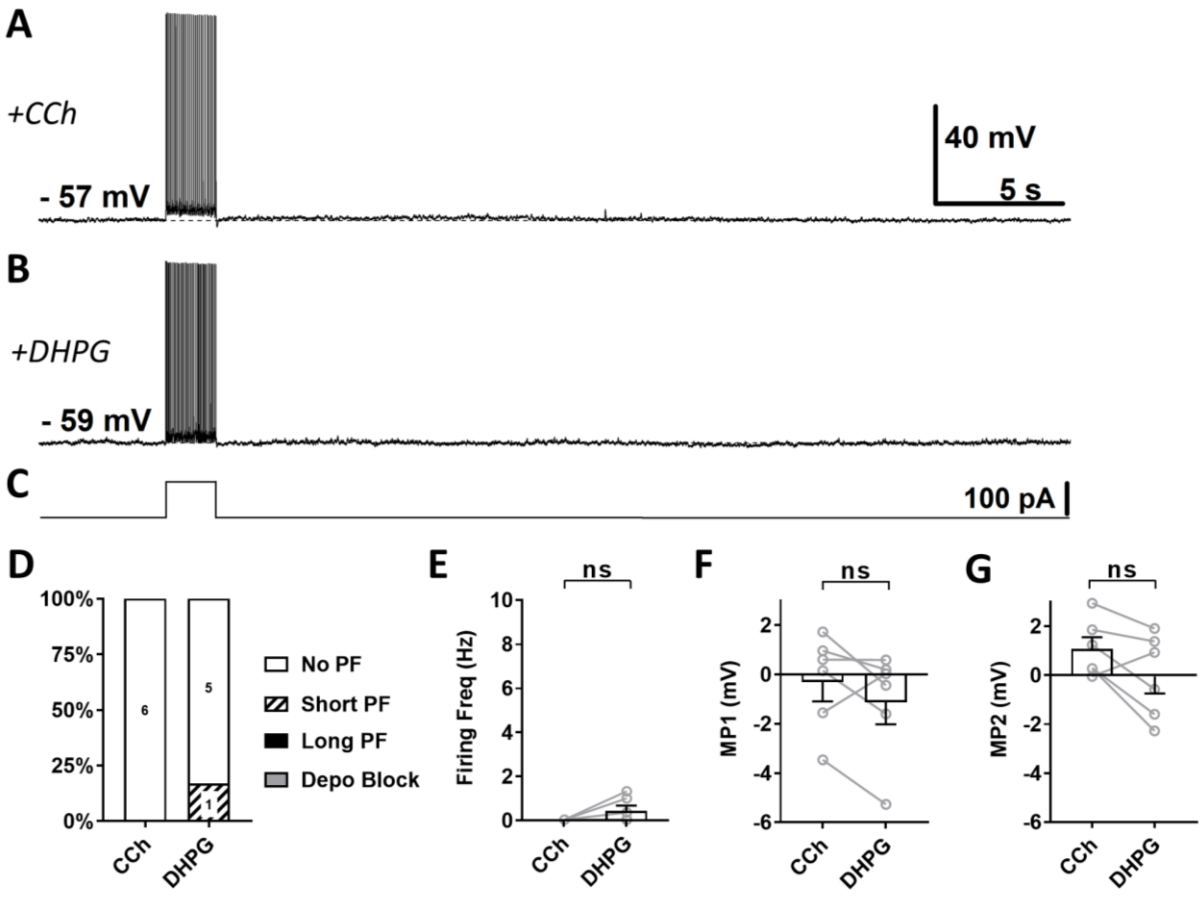

Figure 57 - The effect of DHPG (10 µM) on cell not showing persistent firing during cholinergic stimulation.

(A) Example of cell not showing persistent firing during carbachol (10 µM) application. (B) After the application of DHPG (10 µM) on top of CCh, the cell showed in (A) did not respond with persistent firing. (C) Current injection used in (A, B) (100 pA, 2 s). (D) Percentages of cells that showed persistent firing in CCh and during the application of DHPG. The numbers on the graph represent the sample size. (E) Post-stimulus firing frequency (Wilcoxon test, ns, $p = 0.250$, $n = 6$). (F) Post-stimulus depolarization (MP1, Wilcoxon test, ns, $p = 0.156$, $n = 6$). (G) Post-stimulus depolarization (MP2, paired t-test, ns, $p = 0.079$, $n = 6$).

4.2.4 Effect of 20 µM clemizole hydrochloride on persistent firing

Given the presence of both TRPC4 and TRPC5 channels in the layer II of the medial entorhinal cortex, I tested if these channels were supporting persistent firing in this brain area. In the entorhinal cortex, the TRPC channels has been shown to support persistent firing in the layer V [111]. In this study to show that TRPC were supporting the PF mechanism not only general TRPC blockers (FFA, SKF-96365, 2-APB) were tested, but also the heptapeptide EQVTTRL, that selectively inhibits TRPC4 and TRPC5. Nevertheless, a recent paper using TRPC KO mice reported that these channels are not supporting persistent firing in layer V neurons [113], however in this study, they did not take in account or mentioned a possible compensatory effect affecting the expression of other ion channels.

To assess if TRPC4 and TRPC5 channels were supporting persistent firing in the layer II neurons of MEC, I used clemizole hydrochloride (CLE), the novel and selective TRPC blocker that I also used in the hippocampus. Up to now, clemizole hydrochloride has never been used in the MEC layer II to test its effects on persistent firing. In my experiments 20 µM CLE was bath applied for 15 minutes on cells showing persistent firing during the application of 10 µM carbachol. The experimental approach used was the same described previously: the cells were kept first in nACSF and if persistent firing was observed during CCh application, 20 µM CLE was bath applied on top of the cholinergic agonist (Fig. 58). The stimulation protocol was the same previously used.

On the cells showing persistent firing during CCh application, CLE was applied and completely blocked persistent firing in 7 out of 9 cells. In the remaining 2 cells persistent firing was inhibited (Fig. 58E). The application of CLE significantly inhibited persistent firing (Fig. 58F, Wilcoxon test, ** $p < 0.01$, $n = 9$). In the paper from Richter et al. (2014), a reversible CLE block has been reported [254] and in my experiments it was also possible to wash out the blocker and completely recover persistent firing in 2 cells (Fig. 58C).

The application of clemizole hydrochloride also affected membrane potential after the end of the stimulus. During CCh application, the membrane depolarization after the end of the stimulus (MP1) was significantly suppressed by the application of CLE (Fig. 58G, paired t-test, * $p < 0.05$, $n = 9$). It is very interesting to notice that, in the layer II MEC neurons, 20 µM CLE never induced depolarization block, while in the CA1 hippocampal neuron CLE induced depolarization block in the 71% of the test cells. Also the MP2 was significantly reduced by the application of CLE (Fig. 58H, paired t-test, * $p < 0.05$, $n = 9$).

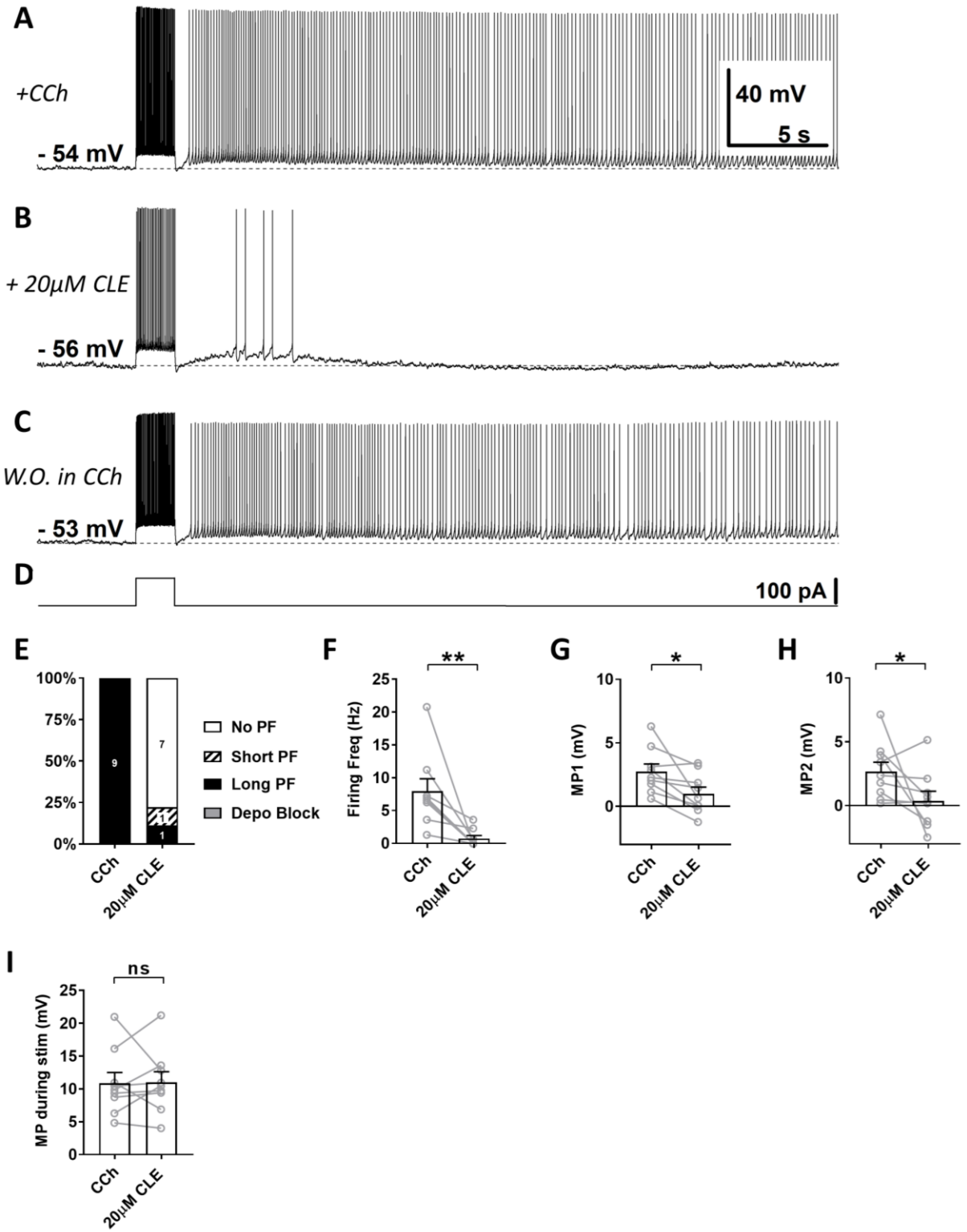

Figure 58 - The effect of clemizole hydrochloride (20 μM) on persistent firing in MEC layer II neurons.

(A) Example of persistent firing in CCh (10 μM). (B) Suppressed persistent firing in clemizole (CLE, 20 μM) in the same cell shown in (A). (C) Persistent firing was recovered after washing out (W.O.) back in CCh. The cell is the same cell shown in (A, B). (D) Current injection used in (A, B, C) (100 pA, 2 s). (E) Percentages of cells that showed persistent firing in CCh and during the application of CLE. The numbers on the graph represent the sample size. (F) Post-stimulus firing frequency (Wilcoxon test, ** $p < 0.01$, $n = 9$). (G) Post-stimulus depolarization (MP1, paired t-test, * $p < 0.05$, $n = 9$). (H) Post-stimulus depolarization (MP2, paired t-test, * $p < 0.05$, $n = 9$). (I) Membrane potential depolarization during the stimulus application (paired t-test, ns, $p = 0.905$, $n = 9$).

The average membrane potential depolarization during the application of the stimulus was not significantly different after the application of 20 μM CLE (Fig. 58I, paired t-test, ns, p = 0.941, n = 9). This is again very interesting to notice because, in hippocampal CA1 pyramidal cell, the application of 20 μM CLE on top of carbachol induced a strong depolarization already during the stimulus that led very often to depolarization block.

In summary, these data indicate that TRPC channels, including TRPC4 and TRPC5, support persistent firing in MEC layer II neurons. It is interesting to notice that in this brain area 20 μM clemizole hydrochloride never induced depolarization block during or after the end of the stimulus. This behaviour was completely different from what it was previously observed in CA1 pyramidal neurons during the application of the same drug at the same concentration. One possible explanation is that in the hippocampus higher concentration of CLE can unspecifically affect ion channels that in the MEC layer II are either not expressed or expressed at lower concentration compared to CA1.

4.2.5 Effect of 3μM clemizole hydrochloride on persistent firing

In the IHC stainings we saw that TRPC4 and TRPC5 are distributed in the layer II of MEC in different ways. While TRPC4 are preferentially distributed in the island cells, TRPC5 are preferentially distributed in the ocean cells. To test if the cells showing persistent firing were mainly expressing TRPC5 I used 3 μM clemizole hydrochloride (Fig. 59). At lower concentration, this TRPC channels blocker is mainly selective for TRPC5.

Persistent firing was observed in 5 cells during CCh application and in all the cells persistent firing was still present after the application of clemizole hydrochloride. The average firing frequency was slightly reduced, however the effect was not significant (Fig. 59F, paired t-test, ns, p = 0.196, n = 5). When 3 μM clemizole hydrochloride was used to suppressed persistent firing CA1 pyramidal neurons, the inhibitory effect was very strong: it reduced the firing frequency of the 74% and completely suppressed persistent firing in 67% of the tested cells. In the MEC layer II, the application of 3 μM CLE reduced the firing frequency of the 18% and it never led to a full block of persistent firing.

The membrane potential depolarization after the end of the stimulus (MP1) was also not affected. The depolarization induced by the stimulus during CCh application was only slightly reduced and not significantly affected by the application of CLE (Fig. 59G, paired t-test, ns, p = 0.347, n = 5).

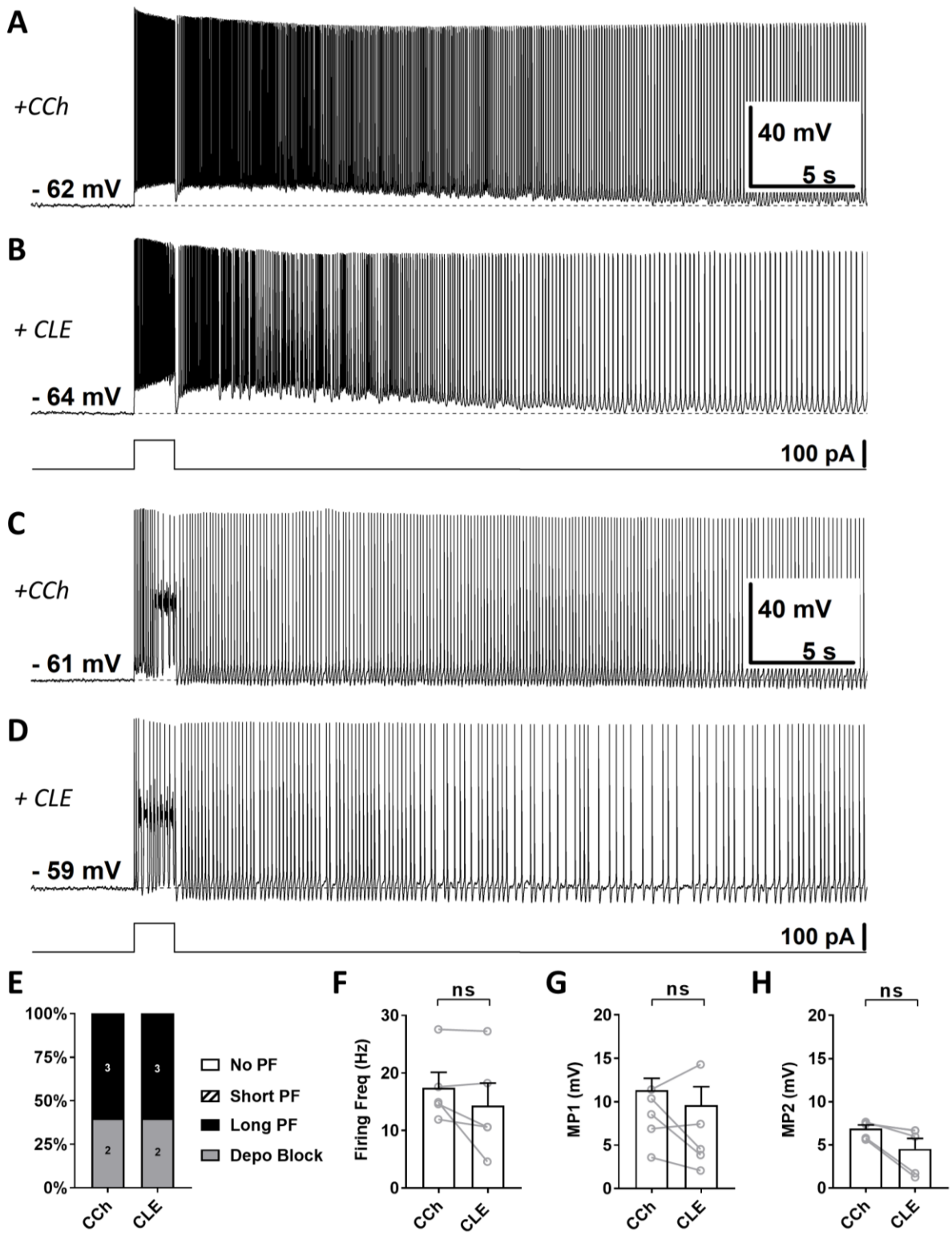

Figure 59 - The effect of clemizole hydrochloride (3 µM) on persistent firing in MEC layer II neurons.

(A) Example of persistent firing in CCh (10 µM). (B, top) Persistent firing was not suppressed by clemizole hydrochloride (CLE, 3 µM) application in the same cell shown in (A). (B, bottom) Current injection used in (A, B) (100 pA, 2 s). (C) Example of depolarization block and persistent firing in CCh (10 µM). (D, top) Persistent firing was not suppressed by clemizole hydrochloride (CLE, 3 µM) application in the same cell shown in (C). (D, bottom) Current injection used in (C, D) (100 pA, 2 s). (E) Percentages of cells that showed persistent firing in CCh and during the application of CLE. The numbers on the graph represent the sample size. (F) Post-stimulus firing frequency (paired t-test, ns, $p = 0.196$, $n = 5$). (G) Post-stimulus depolarization (MP1, paired t-test, ns, $p = 0.347$, $n = 5$). (H) Post-stimulus depolarization (MP2, Wilcoxon test, $p = 0.062$, $n = 5$).

In the CA1 hippocampus, CLE suppressed the depolarization observed during CCh application of the 69%, in the MEC the suppression was only of the 15%. In the experiments in the medial entorhinal cortex, two cells showed depolarization block during CCh application and the same cells showed depolarization block during CLE application, indicating that this effect was not mediated by the TRPC blocker (Fig. 59C-D). The average MP2 value was also less depolarized after the application of CLE, however the difference was not significant (Fig. 59H, Wilcoxon test, ns, $p = 0.062$, $n = 5$).

In these experiments testing 3 μM CLE, the intracellular solution, the recording solution and the cutting solution were slightly different from the one previously used in the other experiments in the MEC and in addition they contained synaptic blockers, kynurenic acid (2 mM) and picrotoxin (0.1 mM). This was made to test and find optimal solutions for the recordings in this brain area (for more information about the solution please refer to the method section). Nevertheless, recent unpublished data from our lab using nACSF without synaptic blockers confirmed these results and indicated that the no-effect of CLE (3 μM) was not mediated by these differences in the recording solution.

In summary, the application of 3 μM clemizole hydrochloride did not affect persistent firing in MEC layer II neurons indicating that TRPC5 channels do not have a central role in the mechanism supporting PF in these neurons and in this brain area.

5 DISCUSSION

In the following I will present and discuss the results supporting the involvement of TRPC4 and TRPC5 channels in persistent firing in the hippocampal CA1 and in the medial entorhinal cortex layer II. TRPC channels are highly expressed in the medial temporal lobe and growing evidence indicates that these channels have a central role in supporting persistent firing. Given the recent controversial reports on the role of TRPC channels in cholinergic persistent firing, in my patch clamp experiments I used different approaches to target these channels, such as novel blockers, selective antibodies, and different KO models. In this way I aimed to test and give a conclusive answer to the involvement of TRPC4 and TRPC5 channels in persistent firing in the hippocampal CA1 and in the MEC layer II. These two areas of the MTL has been reported to be involved in working memory and, persistent firing is one of the mechanisms proposed to support it [22–26].

In the CA1 pyramidal neurons, the results I obtained with novel pharmacological tools and antibodies indicate that TRPC4 and TRPC5 channels support persistent firing. However the results obtained using TRPC5 conditional KO did not give a conclusive answer. In the layer II of the entorhinal cortex, the data collected using clemizole hydrochloride indicated that TRPC channels, excluding TRPC5, are supporting PF. Interestingly in the entorhinal cortex, while TRPC4 were predominantly expressed in calbindin positive cells forming clusters (island cells), the TRPC5 were predominantly expressed in calbindin negative cells (ocean cells). This suggest a possible differential role of these two channels in the MEC.

I will first present the data collected in the hippocampal CA1 pyramidal cells, and then the data collected in the MEC layer II neurons. After discussing the findings of each project, I will draw some final conclusions.

5.1 Involvement of TRPC4 and TRPC5 channels in persistent firing in hippocampal CA1 pyramidal cells

5.1.1 Expression of TRPC4 and TRPC5 in CA1 hippocampus

The immunohistochemical (IHC) stainings targeting TRPC4 and TRPC5 indicated that both are expressed in the CA1 area of the hippocampus. These data were in agreement with previous publications showing that TRPC4 and TRPC5 are highly expressed in CA1 in both rats and mice [204,205,208]. In addition, my data agreed also with the in-situ hybridization data provided by the Allen Brain Atlas, indicating high expression of both TRPC4 and TRPC5 in the hippocampal CA1 (http://portal.brain-map.org/).

5.1.2 Persistent firing in mouse CA1 pyramidal cells

In my experiments, cholinergic-dependent persistent firing was present in mice CA1 pyramidal cells similarly to our previous study in rat CA1 [110]. As previously done in rats, also in mice it was possible to categorize persistent firing in long-lasting, self-terminating and in neurons showing depolarization block. However, while the ratio of cells which responded with persistent firing was only slightly lower in mice (81%) compared to that in rats (100%), the ratio of cells responding with long-lasting persistent firing in mice (24%) was clearly lower than in rats (73%). In my experiments most of the neurons (51%) responded with self-terminating persistent firing, in rats only the 13% of the cells responded in this way. In addition, the average firing frequency of persistent firing and depolarization of the membrane in mice after the end of the stimulus (6.76 Hz and 6.77 mV) were slightly lower than those in rats (10.0 Hz and 11.3 mV). All these data indicate that persistent firing is present in mice CA1 pyramidal cells, however they also indicate that persistent firing might be somewhat weaker in mice than in rats.

5.1.3 Effects of TRPC4 and TRPC5 blockers

The first step to test the involvement of TRPC4 and TRPC5 in persistent firing has been to apply TRPC blockers and see their effect on cholinergic-dependent persistent firing. As mentioned in the introduction, the classic TRPC channels inhibitors, such as such as SKF-93635, 2-APB and flufenamic acid, has been often criticized for their lack of specificity. In fact they can affect several channels other than TRPC such as the L-type and T-type calcium channels [172,194,247], voltage-gated sodium channels [248,249], chloride channels [250], cardial potassium currents [251], and some members of TRPM, TRPV and TRPA channels

[252]. In addition, these general blockers do not show selectivity for specific TRPC channel subfamilies. For all these reasons, in my project I tested more recently identified and more specific antagonists, such as ML204, clemizole hydrochloride, and Pico145.

The first novel TRPC blocker that I tested was ML204. This drug has been reported to be a potent and selective TRPC4 blocker [253]. In my experiments ML204 (10 μM) strongly inhibited both persistent firing and the associated plateau depolarization observed during cholinergic stimulation. ML204 exerts its blocking effect by directly interacting with TRPC4, and in fluorescent intracellular Ca^{2+} assays the IC_{50} of ML204 for TRPC4 is 0.96 μM [253]. At 10 μM, ML204 blocks the current mediated by TRPC4 completely and it can partially block (65%) the current mediated by TRPC5 [253]. However, 10 μM ML204 did not affect TRPV1, TRPV3, TRPA1, TRPM8, KCNQ2, voltage-gated sodium, potassium, and calcium channels in mouse dorsal root ganglion neurons, having a superior selectivity for TRPC channels compared to the classical general blockers mentioned above [253]. Even if ML204 used at 10 μM could have affected TRPC5, I opted to use this concentration because ML204 has been reported to be heat sensitive. This has been observed in previously published studies [177,253] and also in an unpublished pilot study of our laboratory. In our previous pilot experiments in rat CA1 pyramidal cells, when ML204 was used with a bath temperature of 35°C neither 10 μM or 20 μM affected persistent firing. This probably happened because to achieve the temperature of 35°C in the recording chamber, the recording solution had to be pre-heated to 45-50°C by an in-line heater. This suggests that high temperatures may have affected the stability of ML204, also compromising its effectiveness. In my experiments, to perform recordings with a bath temperature of 35°C, a new custom heated chamber was developed. In this way to achieve a bath temperature of 35°C the in-line heater could be set only at 33-35°C. In summary, I overcame the heat sensitivity of ML204 by having a better control of the heating system of my experimental set up, nevertheless I still used a slightly higher concentration of ML204 to compensate in this way a potential loss of the drug potency that could still be mediated by the heat. Therefore, these data using ML204 indicate that TRPC4 channels have a role in supporting persistent firing, however the concentration I used may have partially affected also TRPC5.

Clemizole hydrochloride (CLE) was the second novel TRPC blocker I tested. This drug can block TRPC5 channels directly with an IC_{50} of 1.0–1.3 μM and it can also affect other members of the TRPC family, but only at higher concentration: TRPC4 (IC_{50} = 6.4 μM), TRPC3 (IC_{50} = 9.1 μM), TRPC6 (IC_{50} = 11.3 μM) and TRPC7 (IC_{50} = 26.5 μM) [254]. As we

can see, clemizole hydrochloride is six times more selective for TRPC5 over TRPC4, the closest structural relative of TRPC5 and it is almost 10 times more selective for TRPC5 over TRPC6 and TRPC7. In addition, TRPM3 and TRPM8, and TRPV1, TRPV2, TRPV3, and TRPV4 channels are only weakly suppressed when the concentration of CLE was higher than 20 μM [254]. In my experiments I used clemizole hydrochloride at two concentrations: 3 μM, to inhibit TRPC5 channels, and 20 μM, to inhibit all TRPC channels, including TRPC4 and TRPC5. I will first discuss the results obtained using the lower concentration of CLE and then present the data using the higher concentration. Up to now, this was the first time that clemizole hydrochloride was tested to suppress persistent firing and the first time that it was used in the CA1 hippocampus.

The application of clemizole hydrochloride (3 μM) significantly inhibited cholinergic-dependent persistent firing suggesting that TRPC5 is involved in the mechanism supporting this neural activity. When used at this lower concentration, in some cells persistent firing was inhibited but not completely blocked, for this reason, in these cells CLE (3 μM) was also co-applied with ML204 (10 μM) leading to a full block of persistent firing. A partial inhibition of persistent firing was also observed in the previously discussed experiments using ML204 (10 μM), in some cells persistent firing was not completely blocked by ML204 and only the co-application with CLE (3 μM) completely suppressed persistent firing. Taken together these co-application results indicate that TRPC4 and TRPC5 channels support persistent firing in a synergistic manner.

The application of clemizole hydrochloride at higher concentration (20 μM) significantly inhibited the firing frequency of persistent firing indicating that TRPC channels are supporting it, however it also induced depolarization block in most of the tested cells, suggesting that clemizole hydrochloride was having some unspecific effects when applied at this relatively high concentration. In control experiments, when CLE (20 μM) was applied without carbachol, depolarization block was never observed indicating that this effect was mediated by channels activated by cholinergic modulation. Sometimes drug targeting ion channels or receptors can have special dose-responses effects and depending on their concentration they can inhibit, activate, or even have no effects on their targets. A such complex pharmacological action of clemizole hydrochloride could have explain why depolarization block was observed when this drug was used at higher concentrations, suggesting that the antagonist was activating instead of blocking the targeted channels.

To test if this was the case, and CLE (20 μM) was activating and not blocking TRPC channels, I performed voltage clamp experiments to test how CAN current, mediated by

TRPC channels, was affected by the application of the blocker. The voltage clamp experiments showed that CLE (20 μM) suppressed CAN current evoked during carbachol application, indicating that the antagonist was blocking TRPC channels and confirming that these channels were supporting CAN current. In addition, these results indicated that in hippocampal CA1, when used at high concentration, clemizole hydrochloride was also affecting other channels and not only TRPC.

Pico145 is the most recently discovered TRPC antagonist I tested. So far it is the most selective TRPC antagonist available, affecting the TRPC channels at pico to nano-molar concentrations [255,283]. Up to now, this was the first time that Pico145 was tested to suppress persistent firing and the first time that it was used in the CA1 hippocampus. Pico145, which is referred to as HC-608 by the inventor, has a very similar potency as HC-070, another novel TRPC4 and TRPC4 blocker [283–285]. Pico145 has been reported to block both heteromers, TRPC4-TRPC1 (IC_{50} = 0.033 nM) and TRPC5-TRPC1 (IC_{50} = 0.199 nM), and homomers, TRPC4 (IC_{50} = 0.35 nM) and TRPC5 (IC_{50} = 1.3 nM) [255]. Different groups reported that the IC_{50} values vary slightly among different recording conditions [255,283]. However, the IC_{50} values for TRPC4 and TRPC5 homomers and heteromers are all below 4.7 nM, indicating that Pico145 is a very potent antagonist.

In my experiments I was able to collect only some preliminary data with Pico145 while performing experiments in TRPC5 conditional KO animals. In these experiments in GFP negative cells recorded as control, Pico145 (100nM) reduced in average the firing frequency and the plateau potential of persistent firing. However, even if there was a clear reduction trend, especially looking at the firing frequency, these results were not significant. Nevertheless, in a recently published study from our lab, this preliminary data was deepened and confirmed, showing that Pico145 (100nM) significantly suppress cholinergic-dependent persistent firing in CA1 pyramidal neurons [271]. Pico145 at 100 nM concentration has been shown to have no effect on TRPC3, TRPC6, TRPV1, TRPV4, TRPM2, TRPM8, and TRPA1 [255]. In addition, TRPV3, hERG, Kv1.3, Cav1.2, Nav1.2, Nav1.5 channels are shown to have IC_{50} values that are 11 or more times higher than the concentration we tested [283]. Therefore, my preliminary data correctly suggested an involvement of TRPC1, TRPC4 and TRPC5 channels in persistent firing in CA1 pyramidal cells.

Taken together, the results obtained using all these novel pharmacological blockers provide many pieces of evidence all supporting the hypothesis of an involvement of TRPC4 and TRPC5 channels in persistent firing in CA1 pyramidal cells.

5.1.4 Effects of anti-TRPC4 and anti-TRPC5 antibodies

To further assess the role of TRPC4 and TRPC5 in persistent firing, I applied intracellularly antibodies targeting these channels. When antibodies bind to an ion channel, depending on the targeted epitope they can either activate or inhibit the ion channel. Based on the previous literature, I choose and used antibodies targeting epitopes that led to an inhibition of the activity of the desired channels [189,211,256]. The intracellular application of anti-TRPC4 or anti-TRPC5 antibodies led in both cases to a suppression of persistent firing. These results were in agreement with a previous study from El-Hassar and colleagues (2011) in which anti-TRPC1, anti-TRPC4 and anti-TRPC5 antibodies inhibited the activity of these channels suppressing a sustained depolarization induced by the activation of glutamatergic receptors [189]. The CAN current, supported by TRPC channels, is known to be induced by both cholinergic and glutamatergic activation via G-proteins of the $G_{q/11}$ family [286–288]. Therefore, while glutamatergic activation was used in the study of El-Hassar and colleagues [189], the ionic mechanisms involved in their study might be very similar to the ones involved in the persistent firing I studied in my project. In fact, a study in the anterior cingulate cortex reported that persistent firing could be induced during cholinergic or glutamatergic stimulation in the same population of cells, indicating that the two different receptors activate the same intracellular pathway supporting persistent firing [180].

In my experiments, to demonstrate the specificity of the antibodies, heat-treated antibodies were tested. Heat-treated antibodies were in general less effective in blocking persistent firing, however, while the effect of TRPC5 antibodies was clearly absent after deactivation, heat-treated TRPC4 antibodies still had some effect on the membrane depolarization of persistent firing. While this could potentially indicate that the TRPC4 antibodies were not as specific, it is important to remember that inactivation of antibody by heat treatment is not always possible. Heat treatments lead to irreversible inactivation in most cases, however it has been reported that some domains of antibodies can refold after heat denaturation, making them heat resistant [268]. Interestingly, the previous two studies which used the anti-TRPC4 and anti-TRPC5 antibodies reported only the results of inactivated TRPC5 antibody [189,256].

Taken together, these results using antibodies targeting TRPC4 and TRPC5 confirmed the results obtained in the previous experiments using selective TRPC antagonists and indicated again that TRPC4 and TRPC5 are involved and necessary for the mechanisms supporting persistent firing in CA1 pyramidal cells.

5.1.5 Effects of TRPC channels knockout on persistent firing

In the last part of this project I studied persistent firing in TRPC4 KO and in TRPC5 conditional KO mice. Previous studies have been using TRPC KO mice to assess the role of these channels in supporting plateau potential and persistent firing [113,185,258,259,289]. Despite a number of studies indicating the involvement of TRPC channels in supporting persistent firing, some of the studies using TRPC KO mice are challenging this view [113,258,259,289].

Phelan and colleagues (2012, 2013, 2014) used several KO mice to test the role of TRPC in supporting a glutamatergic-dependent plateau potential that underlies epileptiform bursts in septal and hippocampal neurons [185,258,289]. In septal neurons the plateau potential evoked with glutamatergic stimulation was completely abolished in TRPC1/4 double KO and strongly suppressed in TRPC1 KO [185]. In hippocampal CA1 pyramidal neurons, the plateau potential was suppressed in both TRPC1/4 double KO and TRPC1 KO, however in TRPC5 KO the plateau potential and the spontaneous burst firing, induced by glutamatergic stimulation, were both unaffected [289]. In a following study by the same group using TRPC7 KO mice, it was shown that while in CA3 pyramidal neurons the burst firing was suppressed, the CA1 neurons showed normal burst firing in response to mGluR agonist application [258]. The results reported from Phelan and colleagues in hippocampal pyramidal neurons are in partial contrast with the results of my experiments. In fact, when I selectively targeted TRPC4 but also TRPC5 with novel blockers or antibodies, I observed in all cases a reduction of the firing frequency and of the cholinergic-dependent plateau potential.

Another controversial study using KO animals was published by Dasari and colleagues (2013) [259]. In this study, they reported that in TRPC1, TRPC5, TRPC6 and TRPC5/6 double KO mice the plateau potential was present and apparently not affected by the lack of TRPC channels in the medial prefrontal cortex. These findings are is in contrast with an earlier study, also in the prefrontal cortex, that reported TRPC5 supporting a cholinergic-dependent plateau potential [194].

In the medial entorhinal cortex layer V, Egorov and colleagues (2019) reported that persistent firing was unchanged both in TRPC1/4/5 triple-KO, and in TRPC1-7 hepta-KO mice. These finding contradict earlier studies in the same area using pharmacological tools as well as a selective TRPC4/5 binding peptide, which indicated TRPC4 and TRPC5 having a role in supporting persistent firing [50,111]. Nevertheless, the results from the TRPC hepta-KO mice clearly indicate that persistent firing can be supported without any member of the TRPC family at least in the layer V of the medial entorhinal cortex.

In my experiments I used TRPC4 KO and TRPC5 conditional KO mice. To the best of my knowledge, no study using conditional KO animals and investigating the role of TRPC channels in hippocampal persistent firing has been published so far. I will first discuss about the data collected with TRPC4 KO animals and then I will present the data collected with the TRPC5 conditional KO mice, also discussing the problems I have encountered during these experiments.

In the experiments I performed on TRPC4 KO mice persistent firing was present in CA1 neurons and the electrophysiological properties were similar to the one observed in wild type animals. The application clemizole hydrochloride (20 μM) significantly suppressed persistent firing indicating that the remaining TRPC channels were still supporting it. Taken together these data indicate that, in this model, TRPC4 are not essential to support persistent firing and plateau potential. These results are in contrast with the results I obtained using TRPC4 antagonists and anti-TRPC4 antibodies, showing that TRPC4 channels are essential to support persistent firing in CA1 neurons in wild type animals. In addition the results I obtained in TRPC4 KO mice are in contrast also with a previous study in CA1 pyramidal cells showing that in a double TRPC1/4 KO the plateau potential, evoked by a glutamatergic agonist, was inhibited [289]. Interestingly, in my experiments on the TRPC4 KO mice, I observed that in control condition the membrane potential during the stimulation was significantly more depolarized compared to WT. This may suggest that compensatory mechanisms were buffering the lack of TRPC4. However, this is only a speculation, as this is not a direct proof of changes in the expression levels of other ion channels.

After the experiments using TRPC4 KO mice, I studied persistent firing in TRPC5 conditional KO mice. A conditional KO model was chosen to avoid possible compensatory mechanisms, reported in many studies using KO models [269]. Up to date the only conditional KO model available is for TRPC5. The conditional knock out was obtained using an adenoviral vector (AAV-Cre-GFP): after infection, the GFP positive cells were also expressing Cre recombinase that could excise the sequence encoding for a structural part of TRPC5, located between two lox sites, leading in this way to the TRPC5 conditional KO.

Quantitative PCR was used to test if the TRPC5 conditional KO happened. In addition the whole TRPC family, excluding TRPC2, was tested to assess if compensatory mechanisms were already buffering the lack of TRPC5 channel by changing their expression levels. In the infected area, only the 6% of the TRPC5 mRNA was left in CA1 and the same effect was observed also in CA3, confirming that the conditional KO happened. Surprisingly, even if these qPCRs were performed only 4 weeks after infection, some compensatory mechanisms

were already present changing the expression levels of TRPC3 and TRPC4. In the CA1 area, while the transcription of TRPC4 was significantly reduced, the transcription of TRPC3 was significantly increased. In the CA3 area, the TRPC4 expression was also significantly reduced, but the TRPC3 levels were not affected.

After testing the successful TRPC5 conditional KO, patch clamp experiments were performed to assess how and if persistent firing could have been affected. Four weeks after infection, TRPC5 conditional KO neurons (GFP+ (flx/flx)) still showed persistent firing and responded to the stimulus with a strong plateau potential. During cholinergic stimulation, GFP+ (flx/flx) cells responded to the stimulus with depolarization block in almost 50% of the tested cells and the cells showing persistent firing were also very depolarized showing an unusual burst firing behaviour. The depolarization block observed by the GFP+ (flx/flx) neurons was completely different from the one previously observed in WT cells: it was stronger and lasting longer. In fact, in many neurons the depolarization block was so strong that prevented the firing of any action potential. In the GFP positive (flx/flx) cells, the membrane potential depolarization was larger compared to both control groups (GFP negative (flx/flx) and wild type cells). Interestingly the GFP positive (flx/flx) cells responded to the stimulus with a strong depolarization already in control condition (nACSF) and the cholinergic stimulation with carbachol amplified this depolarization. In fact, when a lower concentration of carbachol (3 μM) was tested, it significantly but only partially reduced the amplitude of this depolarization. The application of ML204 significantly but not completely suppressed this depolarization indicating that TRPC4 channels, homomer or heteromer, were at least in part supporting it. These results seem to indicate that TRPC4 was partially supporting the strong depolarization leading often to depolarization block, however it was still not clear which one was the main actor supporting it.

Besides compensatory mechanisms, another possible explanation for the strong depolarization triggered by the stimulus in infected cells was that the adenoviral vector had unspecific effects, mediated for example by Cre recombinase or by GFP overexpression. To test if the unusual plateau potential was mediated by unspecific effects related to the adenoviral vector, I infected wild type animals with the AAV-Cre-GFP virus previously used in TRPC5 flx/flx mice. As these animals were wild type, both GFP and Cre recombinase were expressed in the infected cells but, as the lox sites were missing, no genetic modifications were supposed to happen. Unexpectedly, four weeks after infection, the GFP+ (WT) cells showed a strong plateau potential, showing a very strong depolarization block like the one previously observed in GFP positive cells recorded in TRPC flx/flx mice. This data indicates

that the AAV-Cre-GFP virus had unwanted and strong side effects not related to the TRPC5 conditional KO.

In many studies it is assumed that the expression of Cre recombinase does not affect the physiology of the host cells, however there are many reports of toxic effects related to Cre [272–276]. Cre activity can induce toxicity or unwanted changes in the cells when it targets sites similar to lox sites (pseudo-lox sites) that are present in the DNA, inducing in this way mis-recombination and DNA damage. In addition, these effects have also been proven to related to the expression level of Cre recombinase. In most of the cases, the mice strains in which Cre recombinase is expressed seems not to be affected by Cre toxicity, however this potential problem when using the Cre-lox system it is often ignored and in many published studies proper controls are missing [290]. In addition, also GFP, one of the most used and popular markers since decades, in some cases has been reported to have cytotoxicity effects and even to induce cellular death. These effects could be provoked by immunogenicity, oxidative stress, aggregation of GFP proteins [277–280,291,292]. All these potential cytotoxicity effects must be taken in consideration when interpreting data, as they can lead to a wrong interpretation of the results both *in vitro* and *in vivo*, especially when proper controls are missing.

To further test how side effects related to the virus, such as over expression of Cre or GFP could underlie the strong depolarization plateau observed in GFP positive cells, I infected mice with the same AAV-Cre-GFP virus previously used but this time I performed the patch clamp experiments two weeks after infection instead of four. I tried in this way to leave less time to Cre and GFP to overexpress and/or mediate their effects. These experiments were performed in both TRPC5 flx/flx and wild type mice. Even if the infection time was shorter, the GFP was expressed at a good level making it possible to identify the GFP positive cells with my patch clamp experimental set up. I will first discuss the results obtained in the TRPC5 flx/flx mice and then present the data obtained in WT mice.

After two week from the infection, GFP positive cells in TRPC5 flx/flx animals did not show any sign of the strong depolarization block observed four weeks after infection. Nevertheless, they showed a trend to be more depolarized when they were compared with GFP negative cells and wild type cells, indicating that some unwanted changes mediated by the virus were already affecting the neurons. In GFP+ (flx/flx) cells persistent firing was present, and the cells showed a normal firing behaviour. This indicated either that TRPC5 were still present and two weeks were not enough to obtain the conditional KO, or that compensatory mechanisms were already present. The application of clemizole hydrochloride

(3 μM) completely suppressed persistent firing suggesting that TRPC5 were still present. This is also suggested by the fact that in non-infected WT cells clemizole hydrochloride had similar suppressing effects on persistent firing. In both WT cells and GFP positive (flx/flx) cells, the firing frequency was reduced of the 74%. The reduction of membrane potential depolarization after the end of the stimulus was also similar, in the WT was of the 69% and in the GFP positive (flx/flx) cells was of the 74%.

Two weeks after infection, also the GFP positive cells recorded in WT animals did not show any sign of the strong depolarization observed 4 weeks after infection, in fact the firing frequency and the membrane potential depolarization during and after the stimulus were very similar to non-infected WT animals. Taken together, this data indicates that, two weeks after infection, the cells were still not affected by the side effects mediated by the AAV-Cre-GFP. However, like observed in the flx\flx animals, two weeks after infection the GFP positive cells showed a trend to be more depolarized, indicating that some changes mediated by the virus were already happening.

5.2 Conclusions on the hippocampal CA1 project

In this project focusing on the role of TRPC channels in supporting persistent firing in the CA1 pyramidal cells, I used several and diverse methods to target TRPC4 and TRPC5 channels, such as novel TRPC antagonists, anti-TRPC antibodies applied intracellularly and KO models. As in the last years controversies raised about the role of these channels in supporting persistent firing and depolarization plateau, this multimodal approach was chosen. In this way, by using different methods to target and inhibit TRPC channels I aimed to have a clear answer on the role of these channels in supporting persistent firing in the CA1 pyramidal neurons.

The results of the experiments performed in the CA1 pyramidal cells indicate that both TRPC4 and TRPC5 are involved in the mechanism supporting persistent firing. The patch clamp experiments using novel and selective blockers, such as ML204 and clemizole hydrochloride, indicated that TRPC4 and TRPC5 are involved in persistent firing, probably in a synergistic way. These results obtained using pharmacological blockers were confirmed using anti-TRPC4 and anti-TRPC5 antibodies, in both cases the intracellular application of the antibodies inhibited persistent firing. Taken together these results using antagonist and antibodies indicate that TRPC4 and TRPC5 are involved in the mechanism supporting persistent firing.

However, as previously mentioned, some recent studies using TRPC KO put in discussion the role of TRPC channels in supporting persistent firing. There are at least three explanations for these contradictory observations.

The first possibility is that, in different brain areas, persistent firing may not rely on TRPC channels. This was suggested by the study of Egorov and colleagues (2019) in the EC layer V, where it was shown that in hepta-TRPC KO mice persistent firing was still present and not affected by the lack of TRPC channels. While this study clearly shows that persistent firing can be observed also in absence of TRPC channels in the EC layer V, it does not mean that that persistent firing was also unaffected by the lack of TRPC channels in other brain areas. In fact, this hypothesis can be in line with other studies using TRPC KO mice, indicating that TRPC channels are supporting the plateau potential in other brain areas. In the septum and in the hippocampus the lack of TRPC1, TRPC4 and TRPC7 has been shown to decrease the plateau potential [185,258,289]. Nevertheless, while the study from Phelan and colleague in the CA1 showed that TRPC1/4 double KO had a reduced plateau potential, the TRPC5 KO showed an unaltered plateau potential [289]. These results are partially in

contradiction with my findings obtained using antagonists and antibodies and indicating that not only TRPC4 but also TRPC5 is supporting persistent firing in CA1 pyramidal neurons. In addition, in my experiments on TRPC4 KO mice I observed cholinergic-dependent persistent firing. These findings disagree with my previous results using antagonist and antibodies, and also with a study from Phelan and colleagues (2013) indicating that in TRPC1/4 double KO the plateau potential was suppressed in CA1 [289].

These contradictions can be explained by a second possibility. While in wild type mice persistent firing is normally supported by TRPC channels, in TRPC KO mice due to compensatory mechanisms, other ion mechanism may be supporting persistent firing [269]. Surprisingly among the studies using TRPC KO mice, this point was considered only in the study from Dasari and colleagues [259] and there was no mention of it in the other studies I mentioned before [113,185,258,289]. This hypothesis is in agreement with several previous studies, as it does not preclude the involvement of TRPC channels in persistent firing and plateau potential, and it is in agreement with my results using novel TRPC antagonist and anti-TRPC antibodies. Despite a growing number of studies, it remains unclear what alternative mechanisms than TRPC could support persistent firing in TRPC KO mice compensating for their lack (e.g., TRPC hepta-KO). However a possible alternative mechanism could rely on channels such as TRPM4 and TRPM5 [293], and hERG [112]. It is also interesting to point out that Egorov and colleagues (2019) observed neurons which did not show persistent firing only in the TRPC hepta-KO group [113]. In these mice due to the deletion of all TRPC family members, compensation of the mechanisms supporting persistent firing might be more challenging compared to TRPC1/4/5 triple-KO mice in which the remaining members of the TRPC family could have compensate for the loss of the missing channels.

In my experiments, to avoid the presence of compensatory mechanisms, I used a TRPC5 conditional KO model. The qPCR results indicated that four weeks after the conditional TRPC5 KO happened, however these data also indicated that some compensatory mechanisms were already happening in CA1 pyramidal neurons, altering the expression of TRPC3 and TRPC4. Unexpectedly, the AAV vector used to induce the conditional KO model had unspecific and unwanted sides effects probably mediated by over expression GFP or Cre recombinase. Four weeks after infection the GFP neurons responded to the stimulus application with a strong plateau potential and often showed depolarization block or a very depolarized burst firing. These effects were not present when GFP positive (flx/flx) cells were recorded two weeks after infection. However, in these neurons persistent firing was still

present and the application of clemizole hydrochloride (3 μM) completely suppressed it indicating that TRPC5 channels were still present and that two weeks were not enough to obtain a conditional KO.

These findings using a conditional KO model did not help to add another piece of evidence supporting the role of TRPC5 in supporting persistent firing. In the GFP positive (flx/flx) cells, persistent firing was still present 4 weeks after infection, this could indicate that TRPC5 are not essential to support PF. However, I cannot draw any clear conclusion because the viral infection had unspecific effects making the neurons responding with a very strong depolarization during and after the stimulus application while applying carbachol.

Nevertheless, these results indicate the vital importance of having always proper controls when using viral vectors and genetically modified models to avoid a potentially wrong interpretation of the data. This is particularly important as in many published studies proper controls are often missing [269]. In addition, these findings indicate that compensatory mechanisms are present also in KO conditional models, even after 4 weeks from the genetic modification.

One third possibility, explaining why persistent firing is still present in previous studies using KO models, is that this neural activity does not rely on TRPC channels in any brain area in both KO and wild type animals and, for this reason, all the studies indicating the involvement of TRPC channels in PF are wrong. This hypothesis would agree with the results I obtained in TRPC4 KO mice and with the TRPC5 conditional KO neurons showing bursting persistent firing four weeks after infection. Although this hypothesis would be in contrast with the majority of the results I obtained using TRPC antagonists and antibodies, it is not possible to exclude it. In fact, binding assays indicated that ML204 (10 μM) could inhibit G protein-coupled receptors (GPCRs) including α1A and α2A adrenergic receptors, histamine H1 receptors, M2 and M3 muscarinic receptors [253,294]. In addition, clemizole has recently been shown to block cardiac hERG channels [295]. Pico145 is more selective and hERG channels are not affected significantly, however, its effects on TRPM4 and TRPM5 channels, for example, have not been reported. However, the results I obtained using pharmacological tools are backed up by the results obtained using antibodies and showing the same inhibitory effects. When TRPC4 were blocked with using ML204 or anti-TRPC4 antibodies, persistent firing was inhibited and the same happened when clemizole hydrochloride (3 μM) or anti-TRPC5 antibodies were used to target TRPC5. The only unexpected results were observed when clemizole hydrochloride (20 μM) inhibited persistent firing but induced depolarization block, indicating that at this concentration in CA1 pyramidal cells it had nonspecific effects.

Interestingly in the layer II MEC neurons, clemizole hydrochloride (20 μM) never induced depolarization block and it suppressed both the firing frequency and the plateau potential. This suggested that in this area the channels affected by CLE are either not present or not highly expressed.

In summary, the results obtained using novel and selective TRPC antagonist, together with the data collected using anti-TRPC antibodies added many pieces of evidence indicating that both TRPC4 and TRPC5 channels contribute to persistent firing in CA1 pyramidal cells. Unexpectedly, the TRPC5 conditional KO model did not work as expected and the virus had unspecific effects. The data collected in WT animals infected with the AAV-Cre-GFP virus suggest that the strong plateau potential, observed in GFP positive cells 4 weeks after infection, was induced by unspecific effects related to the adenoviral infection. In the literature there are many examples of cytotoxicity effects mediated by GFP or by unspecific cuts of the Cre-recombinase on pseudo-lox sites. In recent unpublished data from our lab using a TRPC4-shRNA vector expressing also GFP, we observed that when the virus was used at high titer the tested GFP cells showed depolarization block. This suggests that the over expression of GFP could be mediating this effect. Taken together these data suggest that depolarization block is mediated by an unspecific effect of the viral infection, however I cannot rule out the possibility that also compensatory mechanisms, as suggested by the qPCR data, could play a role in this phenomenon. Even if the experiments using TRPC5 conditional KO mice did not work as expected, I showed that compensatory mechanisms can happen also in conditional KO models, in addition, these results highlight the importance of planning proper controls, especially when using genetically modified animals.

5.3 Involvement of TRPC4 and TRPC5 channels in persistent firing in MEC layer II neurons

5.3.1 Different expression of TRPC4 and TRPC5 in medial entorhinal cortex layer II

The immunohistochemical stainings targeting TRPC4 and TRPC5 showed that both channels are expressed in the layer II of medial entorhinal cortex. These data were in agreement with a previous publication indicating that TRPC4 and TRPC5 are highly expressed in the entorhinal cortex, especially in the layers II and III [205]. In the MEC layer II, the IHC stainings confirmed the presence of island clusters of calbindin positive cells. These results were in agreement with previous studies in mice reporting this expression pattern of calbindin [64,71]. Interestingly the double IHC stainings showed that TRPC4 and TRPC5 had a different distribution pattern and were expressed differently in calbindin positive and negative cells. While TRPC4 were predominantly expressed in island cells, TRPC5 were predominantly expressed in ocean cells. In all the previous studies testing the distribution of TRPC channels, this particular distribution has never been reported [210,296]. In my stainings, this special expression pattern was not shown in the deeper layers of MEC, where TRPC4 and TRPC5 seemed to be uniformly distributed showing no region-specific distribution. It was surprising to see how these two closely related channels have a distinct distribution among island and ocean cells.

5.3.2 Persistent firing in layer II neurons of medial entorhinal cortex

In my experiments, I observed cholinergic-dependent persistent firing in mice MEC layer II neurons, however my results were slightly different compared to a previous study of our lab in the same area, but in rat [184]. While in rats 57% of the cells showed persistent firing, in mice 48% did. In addition, while in the previous study in rat it was possible to observe long-lasting (54%) and self-terminating (13%) persistent firing, in mice all neurons showed long lasting persistent firing (48%). In my experiments in mice the average firing frequency was lower (3.97 Hz) compared to the one measured in rats (5.4 Hz). These data indicate that persistent firing is present in mice layer II neurons, however it seems less frequent than in rats.

In my experiments, given the high number of cells not showing persistent firing, I tried to see if stellate and pyramidal cells, the two main population of neurons in the MEC layer II [64,65,67,68], had the same chances to show persistent firing. I tried to divide the cells in two

population using electrophysiological criteria used in previous studies to distinguish between pyramidal and stellate cells [65,184]. After dividing the recorded cells in pyramidal-like and stellate-like cells using the sag ratio, I saw that both populations had the same chances to show persistent firing. Nevertheless, this preliminary data needs to be deepened by increasing the sample size and also by taking in consideration the morphology of the recorded cells.

In my experiments in the layer II of the medial entorhinal cortex, 52% of the recorded neurons did not show persistent firing during cholinergic stimulation. One possible explanation for this result was that these cells did not have cholinergic receptors but rather glutamatergic receptors. In fact in some studies in the entorhinal cortex, persistent firing has been also observed during glutamatergic stimulation [50,158]. For this reason, in the neurons not showing persistent firing during cholinergic stimulation I applied on top a glutamatergic receptor agonist (DHPG). Strong and long lasting persistent firing was never observed during the co-application of cholinergic and glutamatergic agonists, suggesting that either these neurons did not have cholinergic and glutamatergic receptors, or that in these neurons the activation of these receptors could not activate the intracellular pathways leading to persistent firing. These results agreed with a previous study showing that in the cingulate cortex in the same population of cells, persistent firing could be induced by both carbachol and DHPG, indicating that the activation of these different receptors activate a shared intracellular path leading to persistent firing [180].

5.3.3 Effects of the application of clemizole hydrochloride

In this project in the MEC layer II, to test the involvement of TRPC channels in supporting persistent firing I only used clemizole hydrochloride. Almost the totality of the experiments performed in the medial entorhinal cortex were performed before the heating system of my recording chamber was updated (for more details please refer to the method section). For this technical reason I could not test ML204, this drug is in fact very sensitive to high temperatures [177,253] and with my old heating system, having only an in-line heater, the recording solution needed to be pre-heated to 45-50°C to achieve 35°C in the recording chamber. In unpublished and published observation from our lab, when ML204 was used with this heating system having a recording temperature of 35°C, neither 10 μM or 20 μM had an effect on persistent firing in rat CA1 pyramidal cells [177]. For this reason, in the layer II of the medial entorhinal cortex I was only able to test clemizole hydrochloride.

In my experiments I used two different concentrations of clemizole hydrochloride, a higher concentration (20 μM) to target both TRPC4 and TRPC5, and a lower concentration (3

μM) to target TRPC5. Up to date this is the first time that this novel TRPC antagonist is used in the entorhinal cortex. I will first discuss the results obtained using the higher concentration and then present the data collected using the lower concentration.

The application of clemizole hydrochloride (20 μM) suppressed cholinergic-dependent persistent firing, reducing both the firing frequency depolarization and the plateau potential. This data indicated that TRPC channels were involved in supporting persistent firing in MEC layer II neurons. Surprisingly 20 μM CLE never induced depolarization block like previously observed in the CA1 pyramidal neurons (71% of the neurons), and it significantly reduced the membrane depolarization after the end of the stimulus. This data suggests that the channels that are unspecifically targeted by higher concentration of CLE are either not expressed in this area or are expressed at lower level compared to CA1 pyramidal neurons.

The application of clemizole hydrochloride (3 μM) unexpectedly had no effects on persistent firing in the MEC layer II neurons, there was only a partial and non-significant reduction of both firing frequency and membrane potential depolarization, 18% and 15% respectively. These results were unexpected as in the CA1 pyramidal layer the firing frequency and the membrane depolarization were significantly reduced of the 74% and 69% respectively. As at this concentration CLE targets TRPC5, these data indicated that in the layer II of the medial entorhinal cortex TRPC5 are not required to support persistent firing.

5.4 Conclusions on MEC layer II project

In this project in the layer II of the medial entorhinal cortex, I tested the involvement of TRPC channels in supporting cholinergic-dependent persistent firing. One of the most interesting findings of this project came from the immunohistochemical stainings showing that while TRPC4 were predominantly expressed in calbindin clusters (islands), TRPC5 were predominantly expressed in calbindin negative cells (ocean).

The results collected with the patch clamp experiments showed that cholinergic-dependent persistent firing is present in the MEC layer II neurons of mice. In my experiments, pyramidal-like and stellate-like cells had the same chances to show persistent firing. In total 48% of all tested neuron showed persistent firing during cholinergic stimulation and, in cells showing PF, clemizole hydrochloride (20 μM) suppressed persistent firing indicating that TRPC channels are supporting persistent firing. Surprisingly clemizole hydrochloride never induced depolarization block suggesting that in this brain area the antagonist had apparently no unspecific effects. The application of clemizole hydrochloride (3 μM) unexpectedly had no suppressing effects indicating that TRPC5 channels are not necessary to support persistent firing in layer II MEC neurons. Taken together these data indicate that, in this brain area, while TRPC4 are involved in supporting persistent firing, TRPC5 are not. While this finding is in agreement with a previous study in the EC layer V, indicating that TRPC were involved in persistent firing [111], it is in contrast with a more recent publication using hepta-TRPC KO mice [113]. The explanations for these contradictory observations are the same one I already discussed in the previous project. I will now go through them.

Compensatory mechanisms could lead to over-expression of other channels supporting PF to buffer the lack of the TRPC channels in the hepta KO [269]. As a result, KO animals will show persistent firing, not because the KO channels are not essential in wild type animals, but rather because other ion channels are now supporting it (for more details please go back to the discussion of the CA1 project).

One other possibility is that TRPC channels are not indeed involved in supporting persistent firing, in both KO and wild type animals. However, this hypothesis would be in contrast with my results and with most of the published studies indicating that TRPC channels are supporting the persistent firing mechanism in the entorhinal cortex II, III and V layers. However as already discussed, clemizole hydrochloride has been recently shown to block hERG channels [295], so I cannot exclude this hypothesis. However, in my experiments in the MEC layer II, clemizole hydrochloride (20 μM) never showed depolarization block, suggesting that it had no unspecific effects like previously observed in CA1 pyramidal cells.

Another explanation is that different channels are supporting persistent firing in different brain areas. This is in agreement with the study using hepta TRPC KO [113], showing that in the layer V neurons persistent firing was still present. This hypothesis can also fit with the results of the experiments I performed in the layer II of the medial entorhinal cortex. In addition, this hypothesis can also explain the reason why while in the CA1 pyramidal cells I found that both TRPC4 and TRPC5 are supporting persistent firing, in the MEC layer II only TRPC4 is supporting this neural activity.

All together my results are pointing to a differential role of TRPC4 and TRPC5 channels in the medial entorhinal cortex layer II, as also indicated by the different expression pattern of these two channels. In my IHC stainings I observed that TRPC4 were predominantly expressed in the calbindin islands and in my patch clamp experiments I saw that TRPC5 are not essential to support persistent firing. Taken together these results could indicate that the cells showing persistent firing are mainly expressing TRPC4 and are calbindin positive. Following this reasoning, the cells expressing TRPC5 and not expressing calbindin could represent the cellular population not showing persistent firing. In fact in the literature it has been reported that, in mice and rats, cholinergic innervation preferentially targeted calbindin patches [71]. However, as no double staining for TRPC4 and TRPC5 was performed I cannot rule out the hypothesis that in some neurons both channels are expressed in the same cell and this remain for now a hypothetical assumption.

Nevertheless, even if these preliminary findings needs to be deepened, they indicate that TRPC4 and TRPC5 are promising markers that could be used along with other well-known markers, such as calbindin, to distinguish cell population in the layer II of the medial entorhinal cortex.

5.5 Concluding remarks

This dissertation pursued two different projects having one common goal: study the involvement of TRPC channels in supporting persistent firing in the CA1 pyramidal cells and in the medial entorhinal cortex layer II neurons. In the first project, focused on the hippocampal CA1, I tested some of the most novel and selective TRPC antagonist showing that blocking both TRPC4 and\or TRPC5 suppress persistent firing. To back up these data obtained with novel TRPC antagonist, I successfully used anti-TRPC antibodies targeting TRPC4 and TRPC5 to suppress persistent firing. To give a conclusive answer to the controversies about the role of TRPC raised by some studies using KO mice, I planned to use a conditional KO model. Unexpectedly, even if the TRPC5 conditional KO was successful, the adenoviral vector had unspecific effects probably due to overexpression of Cre recombinase or GFP. In addition, I observed that, in TRPC5 conditional KO animals, compensatory mechanisms were already present 4 weeks after infection, altering the expression of TRPC3 and TRPC4. Nevertheless, even if these results using conditional KO mice did not give a conclusive answer, they highlighted the need and importance to create a new genetically modified model, not affected by compensatory mechanisms and not affected by unspecific effect mediated by the genetic modifications.

In the second project, centred on the medial entorhinal cortex, I showed that while TRPC4 are preferentially distributed in cells expressing calbindin in island clusters, TRPC5 are preferentially distributed out of these clusters. In the MEC layer II neurons, TRPC4 but not TRPC5 have a role in supporting cholinergic persistent firing. Even if these preliminary data suggest that TRPC4-calbindin positive cells are the one predominantly showing persistent firing, this is still a hypothetical assumption and needs to be investigated with more experiments.

Potential contributions of persistent firing in cognitive functions

The results I obtained investigating the role of TRPC channels in supporting persistent firing, will help to have a better understanding of the intracellular mechanisms that are underlying working memory. In fact, persistent neural firing is one possible mechanism contributing to the maintenance of information during working memory tasks and it has been recorded in several brain areas associated with memory functions [22–26]. Another physiological mechanism that could contribute to the maintenance of information is the time cells activity [142–145]. In the hippocampal CA1, subset of neurons has been reported to show temporally organized and sequential firing during the delay periods of various tasks.

While these hypothesis are in contrast with all the *in vivo* studies reporting persistent firing during the maintenance period of working memory tasks, it would explain why some studies did not observed these activity but rather a more sparse firing [140,297]. Nevertheless, even if the sparse firing activity of time cells differs from the one observed during persistent firing, the intracellular mechanism underlying both neuronal activities might be the same. In fact, a recent modelling study from our group suggests that both mechanism might be supported by the same intracellular mechanism [80]. In this modelling study CAN-mediated persistent firing could develop into time cell-like activity when lateral inhibition was added to the network.

Even if multiple mechanisms have been proposed, the cellular and molecular mechanisms supporting persistent firing still remain largely unclear [23,25]. Here, with this dissertation work, I have unveiled some new pieces of evidence, showing that TRPC channels have a role in the intrinsic mechanism supporting persistent firing in CA1 pyramidal and in MEC layer II neurons. The involvement of TRPC channels in supporting persistent firing do not preclude other ion channels to have a role in the mechanism, in fact different brain region have different cell type, affected by different modulators and expressing different receptors and ion channels [23]. Nevertheless, TRPC channels remain promising and intriguing targets for future *in vitro* and *in vivo* studies, for their role in supporting persistent firing, and also because of recent findings indicating that TRPC channels have a role in supporting working memory processes [262,263]. In these recent behavioural studies it was shown that TRPC1/4/5 triple KO mice [262] and TRPC1 KO mice [263] are impaired in working memory tasks, in line with the hypothesis that TRPC dependent persistent firing support working memory.

Future direction

Future research should focus on developing different genetic approaches to target TRPC channels without having compensatory mechanisms or unspecific effects related to the viral infection and\or genetic modification. The use of RNA silencing or the development of a new adenoviral vector, will surely help to get conclusive answers. Nevertheless, given the results I obtained with my conditional KO model, special consideration must be taken when testing these new models to be sure that compensatory mechanisms will not affect the results. Currently our lab is developing and testing the knock down of TRPC4 via shRNA (short hairpin RNA), the results from these experiments will help for sure to bring more clarity on the role of these channels.

As mentioned already, the preliminary data I obtained in layer II of the medial entorhinal cortex must be deepened. A double staining targeting TRPC4 and TRPC5 will help to understand if the two channels are exclusively expressed in one population or if some cells are expressing both. In addition, more patch clamp experiments using TRPC4 antagonist, such as ML204 and Pico145 will help to better understand the role of TRPC channels in the medial entorhinal cortex layer II.

General Conclusion

In this dissertation I aimed to understand the role of TRPC channels in supporting persistent firing in two different areas of the medial temporal lobe. To do that I focused on two areas that have been reported to be important in the temporal association in working memory tasks: the hippocampal CA1 pyramidal cells and the layer II neurons of the medial entorhinal cortex.

In the project focusing on the hippocampal CA1, by using novel and selective TRPC antagonist and antibodies applied intracellularly I showed that TRPC4 and TRPC5 channels are crucial to support persistent firing. However, the data I collected using KO models where either in contrast with my previous findings, like in the case of TRPC4 KO mice, or gave me not conclusive results, like in the case of the TRPC5 conditional KO. Nevertheless, the qPCRs performed on TRPC5 conditional KO mice gave an interesting result, showing that compensatory mechanisms were present already four weeks after the viral infection. In addition, given the side effects mediated by the viral infection, these results strongly evidence the importance of having the right controls when performing experiments with genetically modified animals.

In the second project I focused on the layer II of the medial entorhinal cortex. The most interesting results were obtained with the immunohistochemical stainings showing that TRPC4 channels were predominantly expressed in calbindin clusters (island) and that TRPC5 were predominantly expressed in calbindin negative cells (ocean cells). I showed that TRPC channels, excluding TRPC5, are supporting persistent firing. However, this preliminary results need to be deepened to test if the two cellular population present in the layer II, pyramidal and stellate cells, are differentially expressing TRPC channels. In this way, a better comprehension of the specific roles of these channels in the entorhinal cortex will be reached.

In this dissertation I focused on the role of TRPC channels in memory functions, however, during the last years the interest in TRPC channels raised and these channels has been shown to be involved also in several pathologies affecting not only the nervous system

but also other systems [298,299]. TRPC channels has been reported to be involved in pathologies affecting hearth, kidneys, lungs and they have been reported to have a role in different type of cancer [298]. In the central nervous system the TRPC channels has been linked to several pathologies, such has Alzheimer's disease [300,301], Huntington's disease [302], Parkinson's disease [303,304] and epilepsy [185,258,289,305]. Also mental disorders such as autism, intellectual disabilities, bipolar disorder and depression have all been linked to malfunctions of the TRPC channels [306].

As can be seen, TRPC channels play a role in many pathologies and conditions, inside and outside of the nervous system making them attractive therapeutic targets. A better understanding of the functions of these channels is fundamental for the developing of new treatments and therapeutic approaches.

6 References

1. Chai, W.J.; Abd Hamid, A.I.; Abdullah, J.M. Working memory from the psychological and neurosciences perspectives: A review. *Front. Psychol.* **2018**, *9*, 1–16.
2. Baddeley, A. The episodic buffer: a new component of working memory? *Trends Cogn. Sci.* **2000**, *40*, 6267–6279.
3. Dickerson, B.C.; Eichenbaum, H. The Episodic Memory System : Neurocircuitry and Disorders. *Neuropsychopharmacology* **2009**, *35*, 86–104.
4. Hasselmo, M.E.; Stern, C.E. Mechanisms underlying working memory for novel information. *Trends Cogn. Sci.* **2006**, *10*, 487–493.
5. Squire, L.R.; Stark, C.E.L.; Clark, R.E. The medial temporal lobe. *Annu. Rev. Neurosci.* **2004**, *27*, 279–306.
6. Rempel-clower, N.L.; Zola, S.M.; Squire, L.R.; Amaral, D.G. Three Cases of Enduring Memory Impairment after Bilateral Damage Limited to the Hippocampal Formation. **1996**, *16*, 5233–5255.
7. Zola-morgan, S.; Larry, R.; Amaralt, D.G. Human Amnesia and the Medial Temporal Region : Enduring Memory Impairment Following a Bilateral Lesion Limited to Field CA1 of the Hippocampus. **1986**, 2950–2967.
8. Fernández, G.; Brewer, J.B.; Zhao, Z.; Glover, G.H.; Gabrieli, J.D.E. Level of sustained entorhinal activity at study correlates with subsequent cued-recall performance: A functional magnetic resonance imaging study with high acquisition rate. *Hippocampus* **1999**, *9*, 35–44.
9. Kirchhoff, B.A.; Wagner, A.D.; Maril, A.; Stern, C.E. Prefrontal-temporal circuitry for episodic encoding and subsequent memory. *J. Neurosci.* **2000**, *20*, 6173–6180.
10. Preston, A.R.; Bornstein, A.M.; Hutchinson, J.B.; Gaare, M.E.; Glover, G.H.; Wagner, A.D. High-resolution fMRI of content-sensitive subsequent memory responses in human medial temporal lobe. *J. Cogn. Neurosci.* **2010**, *22*, 156–173.
11. Zola-Morgan, S.; Squire, L.R. Memory Impairment in Monkeys Following Lesions Limited to the Hippocampus. *Behav. Neurosci.* **1986**, *100*, 155–160.
12. Eichenbaum, H. A Cortical–Hippocampal System for Declarative Memory. *Nat. Rev. Neurosci.* **2000**, *1*, 1–10.
13. Milner, B.; Squire, L.R.; Kandel, E.R. Cognitive neuroscience and the study of memory. *Neuron* **1998**, *20*, 445–468.
14. Ranganath, C.; D'Esposito, M. Medial temporal lobe activity associated with active maintenance of novel information. *Neuron* **2001**, *31*, 865–873.
15. Jeneson, A.; Squire, L.R. Working memory, long-term memory, and medial temporal lobe function. *Learn. Mem.* 2012, *19*, 15–25.
16. Nauer, R.K.; Whiteman, A.S.; Dunne, M.F.; Stern, C.E.; Schon, K. Hippocampal subfield and medial temporal cortical persistent activity during working memory reflects ongoing encoding. *Front. Syst. Neurosci.* **2015**, *9*, 30.
17. Graham, K.S.; Barense, M.D.; Lee, A.C.H. Going beyond LTM in the MTL: A synthesis of neuropsychological and neuroimaging findings on the role of the medial temporal lobe in memory and perception. *Neuropsychologia* **2010**, *48*, 831–853.

18. Ranganath, C.; Blumenfeld, R.S. Doubts about double dissociations between short- and long-term memory. *Trends Cogn. Sci.* **2005**, *9*, 374–380.

19. Jensen, O.; Lisman, J.E. An oscillatory short-term memory buffer model can account for data on the Sternberg task. *J. Neurosci.* **1998**, *18*, 10688–10699.

20. Jensen, O.; Lisman, J.E. Hippocampal sequence-encoding driven by a cortical multi-item working memory buffer. *Trends Neurosci.* **2005**, *28*, 67–72.

21. Koene, R.A.; Hasselmo, M.E. First-in-first-out item replacement in a model of short-term memory based on persistent spiking. *Cereb. Cortex* **2007**, *17*, 1766–1781.

22. Lundqvist, M.; Herman, P.; Miller, E.K. Working Memory: Delay Activity, Yes! Persistent Activity? Maybe Not. *J. Neurosci.* **2018**, *38*, 7013–7019.

23. Major, G.; Tank, D. Persistent neural activity: Prevalence and mechanisms. *Curr. Opin. Neurobiol.* **2004**, *14*, 675–684.

24. Constantinidis, C.; Funahashi, S.; Lee, D.; Murray, J.D.; Qi, X.-L.; Wang, M.; Arnsten, A.F.T. Persistent Spiking Activity Underlies Working Memory. *J. Neurosci.* **2018**, *38*, 7020–7028.

25. Zylberberg, J.; Strowbridge, B.W. Mechanisms of Persistent Activity in Cortical Circuits: Possible Neural Substrates for Working Memory. *Annu. Rev. Neurosci.* **2017**, *40*, 603–627.

26. Reboreda, A.; Theissen, F.M.; Valero-Aracama, M.; Arboit, A.; Corbu, M.A.; Yoshida, M. Do TRPC channels support working memory? Comparing modulations of TRPC channels and working memory through G-protein coupled receptors and neuromodulators. *Behav. Brain Res.* **2018**.

27. Hartley, T.; Bird, C.M.; Chan, D.; Cipolotti, L.; Husain, M.; Vargha-khadem, F.; Burgess, N. The Hippocampus Is Required for Short-Term Topographical Memory in Humans. **2007**, *48*, 34–48.

28. Hannula, D.E.; Tranel, D.; Cohen, N.J. The Long and the Short of It : Relational Memory Impairments in Amnesia , Even at Short Lags. **2006**, *26*, 8352–8359.

29. Cashdollar, N.; Malecki, U.; Rugg-gunn, F.J.; Duncan, J.S.; Lavie, N.; Duzel, E. Hippocampus-dependent and -independent theta-networks of active maintenance. *PNAS* **2009**, *106*, 20493–20498.

30. Weiss, C.; Bouwmeester, H.; Power, J.M.; Disterhoft, J.F. Hippocampal lesions prevent trace eyeblink conditioning in the freely moving rat. *Behav. Brain Res.* **1999**, *99*, 123–32.

31. Kesner, R.P.; Hunsaker, M.R.; Gilbert, P.E. The Role of CA1 in the Acquisition of an Object-Trace-Odor Paired Associate The Role of CA1 in the Acquisition of an Object – Trace – Odor Paired Associate Task. *Behav. Neurosci.* **2005**, *119*, 1–7.

32. Ainge, J.A.; Meer, M.A.A. Van Der; Langston, R.F.; Wood, E.R. Exploring the Role of Context-Dependent Hippocampal Activity in Spatial Alternation Behavior. **2007**, *1002*, 988–1002.

33. Bangasser, D.A. Trace Conditioning and the Hippocampus: The Importance of Contiguity. *J. Neurosci.* **2006**, *26*, 8702–8706.

34. McEchron, M.D.; Tseng, W.; Disterhoft, J.F. Neurotoxic lesions of the dorsal hippocampus disrupt auditory-cued trace heart rate (fear) conditioning in rabbits. *Hippocampus* **2000**, *10*, 739–751.

35. McEchron, M.D.; Disterhoft, J.F. Hippocampal encoding of non-spatial trace

conditioning. *Hippocampus* **1999**, *9*, 385–396.

36. Tseng, W.; Guan, R.; Disterhoft, J.F.; Weiss, C. Trace eyeblink conditioning is hippocampally dependent in mice. *Hippocampus* **2004**, *14*, 58–65.
37. Rawlins, J.N.; Feldon, J.; Butt, S. The effects of delaying reward on choice preference in rats with hippocampal or selective septal lesions. *Behav. Brain Res.* **1985**, *15*, 191–203.
38. Solomon, P.R.; Vander Schaaf, E.R.; Thompson, R.F.; Weisz, D.J. Hippocampus and trace conditioning of the rabbit's classically conditioned nictitating membrane response. *Behav. Neurosci.* **1986**, *100*, 729–744.
39. Gilbert, P.E.; Kesner, R.P. Role of the Rodent Hippocampus in Paired-Associate Learning Involving Associations Between a Stimulus and a Spatial Location. *Behav. Neurosci.* **2002**, *116*, 63–71.
40. Campoy, G. The special role of item – context associations in the direct-access region of working memory. *Psychol. Res.* **2016**.
41. Axmacher, N.; Henseler, M.M.; Jensen, O.; Weinreich, I.; Elger, C.E.; Fell, J. Cross-frequency coupling supports multi-item working memory in the human hippocampus. *PNAS* **2010**.
42. Huerta, P.T.; Sun, L.D.; Wilson, M.A.; Tonegawa, S. Formation of Temporal Memory Requires NMDA Receptors within CA1 Pyramidal Neurons. *Neuron* 2000, *25*.
43. Fransén, E. Functional role of entorhinal cortex in working memory processing. *Neural Networks* **2005**, *18*, 1141–1149.
44. Moser, M.-B.; Rowland, D.C.; Moser, E.I. Place cells, grid cells, and memory. *Cold Spring Harb. Perspect. Biol.* **2015**, *7*, a021808.
45. Schon, K.; Newmark, R.E.; Ross, R.S.; Stern, C.E. A Working Memory Buffer in Parahippocampal Regions: Evidence from a Load Effect during the Delay Period. *Cereb. Cortex* **2016**, *26*, 1965–1974.
46. Olsen, R.K.; Nichols, E.A.; Chen, J.; Hunt, J.F.; Glover, G.H.; Gabrieli, J.D.E.; Wagner, A.D. Performance-Related Sustained and Anticipatory Activity in Human Medial Temporal Lobe during Delayed Match-to-Sample. *J. Neurosci.* **2009**, *29*, 11880–90.
47. Newmark, R.E.; Schon, K.; Ross, R.S.; Stern, C.E. Contributions of the hippocampal subfields and entorhinal cortex to disambiguation during working memory. *Hippocampus* **2013**, *23*, 467–475.
48. Suzuki, W.A.; Miller, E.K.; Desimone, R. Object and place memory in the macaque entorhinal cortex. *J Neurophysiol* **1997**, *78*, 1062–1081.
49. Young, B.J.; Otto, T.; Fox, G.D.; Eichenbaum, H. Memory representation within the parahippocampal region. *J. Neurosci.* **1997**, *17*, 5183–5195.
50. Egorov, A. V.; Hamam, B.N.; Fransen, E.; Hasselmo, M.E.; Alonso, A.A. Graded persistent activity in entorhinal cortex neurons. *Nature* **2002**, *420*, 173–178.
51. Ryou, J.; Cho, S.; Kim, H. Lesions of the Entorhinal Cortex Impair Acquisition of Hippocampal-Dependent Trace Conditioning. *Neurobiol. Learn. Mem.* **2001**, *127*, 121–127.
52. Esclassan, F.; Coutureau, E.; Di Scala, G.; Marchand, A.R. A Cholinergic-Dependent Role for the Entorhinal Cortex in Trace Fear Conditioning. *J. Neurosci.* **2009**, *29*, 8087–8093.

53. Suh, J.; Rivest, A.J.; Nakashiba, T.; Tominaga, T.; Tonegawa, S. Entorhinal cortex layer III input to the hippocampus is crucial for temporal association memory. *Science (80-.).* **2011**, *334*, 1415–1420.

54. Kitamura, T.; Pignatelli, M.; Suh, J.; Kohara, K.; Yoshiki, A.; Abe, K.; Tonegawa, S. Island Cells Control Temporal Association Memory. *Science (80-.).* **2014**, *343*, 896–901.

55. Van Strien, N.M.; Cappaert, N.L.M.; Witter, M.P. The anatomy of memory: An interactive overview of the parahippocampal- hippocampal network. *Nat. Rev. Neurosci.* **2009**, *10*, 272–282.

56. Amaral, D.G.; Witter, M.P. The three-dimensional organization of the hippocampal formation: A review of anatomical data. *Neuroscience* **1989**, *31*.

57. Striedter, G.F. Evolution of the hippocampus in reptiles and birds. *J. Comp. Neurol.* **2016**, *524*, 496–517.

58. Strange, B.A.; Witter, M.P.; Lein, E.S.; Moser, E.I. Functional organization of the hippocampal longitudinal axis. *Nat. Rev. Neurosci.* **2014**, *15*, 655–669.

59. Eichenbaum, H.; Dudchenko, P.; Wood, E.; Shapiro, M.; Tanila, H. The hippocampus, memory, and place cells: Is it spatial memory or a memory space? *Neuron* 1999, *23*, 209–226.

60. Cappaert, N.L.M.; Strien, N.M. Van; Witter, M.P. *Hippocampal Formation*; Fourth Edi.; Elsevier Inc., 2014; ISBN 9780123742452.

61. Schultz, C.; Engelhardt, M. Anatomy of the hippocampal formation. *Hippocampus Clin. Neurosci.* **2014**, *34*, 6–17.

62. Witter, M.P. The perforant path: projections from the entorhinal cortex to the dentate gyrus. *Prog. Brain Res.* **2007**, *163*, 43–61.

63. Witter, M.P.; Groenewegen, H.J.; Lopes da Silva, F.H.; Lohman, A.H.M. Functional organization of the extrinsic and intrinsic circuitry of the parahippocampal region. *Prog. Neurobiol.* **1989**, *33*, 161–253.

64. Witter, M.P.; Doan, T.P.; Jacobsen, B.; Nilssen, E.S.; Ohara, S. Architecture of the Entorhinal Cortex A Review of Entorhinal Anatomy in Rodents with Some Comparative Notes. **2017**, *11*, 1–12.

65. Alonso, A.; Klink, R. Differential electroresponsiveness of stellate and pyramidal-like cells of medial entorhinal cortex layer II. *J. Neurophysiol.* **1993**, *70*, 128–143.

66. Klink, R.; Alonso, A. Ionic mechanisms of muscarinic depolarization in entorhinal cortex layer II neurons. *J. Neurophysiol.* **1997**, *77*, 1829–43.

67. Canto, C.B.; Witter, M.P. Cellular properties of principal neurons in the rat entorhinal cortex. II. The medial entorhinal cortex. *Hippocampus* **2012**, *22*, 1277–1299.

68. Fuchs, E.C.; Neitz, A.; Pinna, R.; Melzer, S.; Caputi, A.; Monyer, H. Local and Distant Input Controlling Excitation in Layer II of the Medial Entorhinal Cortex. *Neuron* **2016**, *89*, 194–208.

69. Fujimaru, Y.; Kosaka, T. The distribution of two calcium binding proteins, calbindin D-28K and parvalbumin, in the entorhinal cortex of the adult mouse. *Neurosci. Res.* **1996**, *24*, 329–343.

70. Ray, S.; Naumann, R.; Burgalossi, A.; Tang, Q.; Schmidt, H.; Brecht, M. Grid-layout and theta-modulation of layer 2 pyramidal neurons in medial entorhinal cortex. *Science (80-.).* **2014**, *343*, 891–896.

71. Naumann, R.K.; Ray, S.; Prokop, S.; Las, L.; Heppner, F.L.; Brecht, M. Conserved size and periodicity of pyramidal patches in layer 2 of medial/caudal entorhinal cortex. *J. Comp. Neurol.* **2016**, *524*, 783–806.

72. Canto, C.B.; Wouterlood, F.G.; Witter, M.P. What Does the Anatomical Organization of the Entorhinal Cortex Tell Us ? **2008**, *2008*.

73. Li, X.G.; Somogyi, P.; Ylinen, A.; Buzsaki, G. The hippocampal CA3 network: An in vivo intracellular labeling study. *J. Comp. Neurol.* **1994**, *339*, 181–208.

74. Amaral, D.G. Emerging principles of intrinsic hippocampal organization. *Curr. Opin. Neurobiol.* **1993**, *3*, 123–132.

75. Cenquizca, L.A.; Swanson, L.W. Analysis of direct hippocampal cortical field CA1 axonal projections to diencephalon in the rat. *J. Comp. Neurol.* **2006**.

76. Clark, R.E.; Squire, L.R. Similarity in form and function of the hippocampus in rodents , monkeys , and humans. **2013**, *110*, 10365–10370.

77. Nilssen, E.S.; Doan, T.P.; Nigro, M.J.; Ohara, S.; Witter, M.P. Neurons and networks in the entorhinal cortex : A reappraisal of the lateral and medial entorhinal subdivisions mediating parallel cortical pathways. **2019**, 1238–1254.

78. Kitamura, T. Driving and Regulating Temporal Association Learning Coordinated by Entorhinal-Hippocampal Network. *Neurosci. Res.* **2017**.

79. Kitamura, T.; Pignatelli, M.; Suh, J.; Kohara, K.; Yoshiki, A.; Abe, K.; Tonegawa, S. Island Cells Control Temporal Association Memory. *Science (80-.).* **2014**, *343*, 896–901.

80. Saravanan, V.; Arabali, D.; Jochems, A.; Cui, A.X.; Gootjes-Dreesbach, L.; Cutsuridis, V.; Yoshida, M. Transition between encoding and consolidation/replay dynamics via cholinergic modulation of CAN current: A modeling study. *Hippocampus* **2015**, *25*, 1052–1070.

81. Picciotto, M.R.; Higley, M.J.; Mineur, Y.S. Acetylcholine as a Neuromodulator: Cholinergic Signaling Shapes Nervous System Function and Behavior. *Neuron* **2012**, *76*, 116–129.

82. Gold, P.E. Acetylcholine modulation of neural systems involved in learning and memory. *Neurobiol. Learn. Mem.* **2003**, *80*, 194–210.

83. Dannenberg, H.; Young, K.; Hasselmo, M. Modulation of Hippocampal Circuits by Muscarinic and Nicotinic Receptors. *Front. Neural Circuits* **2017**, *11*, 1–18.

84. Newman, E.L.; Gupta, K.; Climer, J.R.; Monaghan, C.K.; Hasselmo, M.E. Cholinergic modulation of cognitive processing : insights drawn from computational models. *Front. Behav. Neurosci.* **2012**, *6*, 1–19.

85. Bloem, B.; Poorthuis, R.B.; Mansvelder, H.D. Cholinergic modulation of the medial prefrontal cortex: the role of nicotinic receptors in attention and regulation of neuronal activity. *Front. Neural Circuits* **2014**, *8*, 1–16.

86. Sarter, M.; Hasselmo, M.E.; Bruno, J.P.; Givens, B. Unraveling the attentional functions of cortical cholinergic inputs : interactions between signal-driven and cognitive modulation of signal detection. **2005**, *48*, 98–111.

87. Kaneko, T.; Thompson, R.F. Disruption of trace conditioning of the nictitating membrane response in rabbits by central cholinergic blockade. *Psychopharmacology (Berl).* **1997**, *131*, 161–166.

88. Weiss, C.; Preston, A.R.; Oh, M.M.; Schwarz, R.D.; Welty, D.; Disterhoft, J.F. The M1

Muscarinic Agonist CI-1017 Facilitates Trace Eyeblink Conditioning in Aging Rabbits and Increases the Excitability of CA1 Pyramidal Neurons. *J. Neurosci.* **2000**, *20*, 783–790.

89. Buzsaki, G. Theta Oscillations in the Hippocampus. *Neuron* **2002**, *33*, 325–340.
90. Desikan, S.; Koser, D.E.; Neitz, A.; Monyer, H. Target selectivity of septal cholinergic neurons in the medial and lateral entorhinal cortex. **2018**, *115*.
91. Müller, C.; Remy, S. Septo – hippocampal interaction. *Cell Tissue Res.* **2018**, 565–575.
92. Carpenter, F.; Burgess, N.; Barry, C. Modulating medial septal cholinergic activity reduces medial entorhinal theta frequency without affecting speed or grid coding. *Sci. Rep.* **2017**, 1–12.
93. Tang, Y.; Mishkin, M.; Aigner, T.G. Effects of muscarinic blockade in perirhinal cortex during. *Proc Natl Acad Sci USA* **1997**, *94*, 12667–12669.
94. Winters, B.D.; Bussey, T.J. Removal of cholinergic input to perirhinal cortex disrupts object recognition but not spatial working memory in the rat. **2005**, *21*, 2263–2270.
95. Blokland, A.; Honig, W.; Raaijmakers, W.G.M. Effects of intra-hippocampal scopolamine injections in a repeated spatial acquisition task in the rat. *Psychopharmacology (Berl).* **1992**, *109*, 373–376.
96. Elvander, E.; Schött, P.A.; Sandin, J.; Bjelke, B.; Kehr, J.; Yoshitake, T.; Ögren, S.O. Intraseptal muscarinic ligands and galanin: Influence on hippocampal acetylcholine and cognition. *Neuroscience* **2004**, *126*, 541–557.
97. Asaka, Y.; Seager, M.A.; Griffin, A.L.; Berry, S.D. Medial Septal Microinfusion of Scopolamine Disrupts Hippocampal Activity and Trace Jaw Movement Conditioning. **2000**, *114*, 1068–1077.
98. Bartus, R.T.; Johnson, H.R. Short-term memory in the rhesus monkey: disruption from the anti-cholinergic scopolamine. *Pharmacol. Biochem. Behav.* **1976**, *5*, 39–46.
99. Fontán-lozano, Á.; Troncoso, J.; Múnera, A.; Carrión, Á.M.; Delgado-garcía, J.M. Cholinergic septo-hippocampal innervation is required for trace eyeblink classical conditioning. *Learn. Mem.* **2005**, *12*, 557–563.
100. McGaughy, J.; Koene, R.A.; Eichenbaum, H.; Hasselmo, M.E. Cholinergic deafferentation of the entorhinal cortex in rats impairs encoding of novel but not familiar stimuli in a delayed nonmatch-to-sample task. *J. Neurosci.* **2005**, *25*, 10273–10281.
101. Croxson, P.L.; Kyriazis, D.A.; Baxter, M.G. Cholinergic modulation of a specific memory function of prefrontal cortex. *Nat. Neurosci.* **2011**, *14*, 1510–1512.
102. Hasselmo, M.E.; Sarter, M. Modes and models of forebrain cholinergic neuromodulation of cognition. *Neuropsychopharmacology* **2011**, *36*, 52–73.
103. Deiana, S.; Platt, B.; Riedel, G. The cholinergic system and spatial learning. *Behav. Brain Res.* **2011**, *221*, 389–411.
104. Cole, A.E.; Nicoll, R.A. The Pharmacology of Cholinergic Excitatory Responses in Hippocampal Pyramidal Cells. *Brain Res.* **1984**, *305*, 283–290.
105. Madison, D. V.; Nicoll, R.A. Control Of The Repetitive Discharge Of Rat CA1 Pyramidal Neurones In Vitro. *J. Physiol.* **1984**, 319–331.
106. Gil, Z.; Connors, B.W.; Amitai, Y. Differential Regulation of Neocortical Synapses by Neuromodulators and Activity. *Neuron* **1997**, *19*, 679–686.

107. Hasselmo, M.E. Neuromodulation : acetylcholine and memory consolidation. *Trends Cogn. Sci.* **1999**, *3*, 351–359.

108. Heys, J.G.; Schultheiss, N.W.; Shay, C.F.; Tsuno, Y.; Hasselmo, M.E. Effects of acetylcholine on neuronal properties in entorhinal cortex. *Front. Behav. Neurosci.* **2012**, *6*, 32.

109. Yoshida, M.; Hasselmo, M.E. Persistent firing supported by an intrinsic cellular mechanism in a component of the head direction system. *J. Neurosci.* **2009**, *29*, 4945–4952.

110. Knauer, B.; Jochems, A.; Valero-Aracama, M.J.; Yoshida, M. Long-lasting intrinsic persistent firing in rat CA1 pyramidal cells: a possible mechanism for active maintenance of memory. *Hippocampus* **2013**, *23*, 820–831.

111. Zhang, Z.; Reboreda, A.; Alonso, A.; Barker, P.A.; Séguéla, P. TRPC channels underlie cholinergic plateau potentials and persistent activity in entorhinal cortex. *Hippocampus* **2011**, *21*, 386–397.

112. Cui, E.D.; Strowbridge, B.W. Modulation of Ether-à-Go-Go Related Gene (ERG) Current Governs Intrinsic Persistent Activity in Rodent Neocortical Pyramidal Cells. *J. Neurosci.* **2018**, *38*, 423–440.

113. Egorov, A. V.; Schumacher, D.; Medert, R.; Birnbaumer, L.; Freichel, M.; Draguhn, A. TRPC channels are not required for graded persistent activity in entorhinal cortex neurons. *Hippocampus* **2019**, 1–11.

114. Hasselmo, M.E. The role of acetylcholine in learning and memory. *Curr. Opin. Neurobiol.* **2006**, *16*, 710–715.

115. Haam, J.; Yakel, J.L. Cholinergic modulation of the hippocampal region and memory function. *J. Neurochem.* **2017**, *142*, 111–121.

116. Hasselmo, M.E.; Mcgaughy, J. High acetylcholine levels set circuit dynamics for attention and encoding and low acetylcholine levels set dynamics for consolidation. *Prog. Brain Res.* **2004**, *145*.

117. Marrosu, F.; Portas, C.; Mascia, M.S.; Casu, M.A.; Fg, M.; Giagheddu, M.; Imperato, A.; Gessa, G.L. Microdialysis measurement of cortical and hippocampal acetylcholine release during sleep-wake cycle in freely moving cats. *Brain Res.* **1995**, *671*, 329–332.

118. Acquas, E.; Wilson, C.; Fibiger, H.C. Conditioned and Unconditioned Stimuli Cortical and Hippocampal Acetylcholine Novelty , Habituation , and Fear Increase Frontal Release : Effects of. *J. Neurosci.* **1996**, *76*, 3089–3096.

119. Ceccarelli, I.; Casamenti, F.; Massafra, C.; Pepeu, G.; Scali, C.; Aloisi, A.M. Effects of novelty and pain on behavior and hippocampal extracellular ACh levels in male and female rats. *Brain Res.* **1999**, *815*, 169–176.

120. Giovannini, M.G.; Rakovska, A.; Benton, R.S.; Pazzagli, M.; Bianchi, L.; Pepeu, G. Effects Of Novelty And Habituation On Acetylcholine , Gaba , And Glutamate Release From The Frontal Cortex And Hippocampus Of Freely Moving Rats. *Neuroscience* **2001**, *106*, 43–53.

121. Bianchi, L.; Ballini, C.; Colivicchi, M.A.; Corte, L. Della; Giovannini, M.G.; Pepeu, G. Investigation on Acetylcholine , Aspartate , Glutamate and GABA Extracellular Levels from Ventral Hippocampus during Repeated Exploratory Activity in the Rat *. *Neurochem. Res.* **2003**, *28*, 565–573.

122. Goldman-Rakic Cellular Basis of Working Memory Review. *Neuron* **1995**, *14*, 477–485.

123. Fuster, J.M.; Alexander, G.E. Neuron Activity Related to Short-Term Memory. *Science (80-.).* **1971**, *173*, 652–654.

124. Kubota, K.; Niki, H. Prefrontal cortical unit activity and delayed alternation performance in monkeys. *J. Neurophysiol.* **1971**, *34*, 337–347.

125. Funahashi, S.; Bruce, C.J.; Goldman-Rakic, P.S. Mnemonic coding of visual space in the monkey's dorsolateral prefrontal cortex. *J. Neurophysiol.* **1989**, *61*, 331–349.

126. Fuster, J.M.; Jervey, J.P. Inferotemporal neurons distinguish and retain behaviourally relevant features of visual stimuli. *Science (80-.).* **1981**, *212*, 952–955.

127. Miyashita, Y.; Chang, H.S. Neuronal correlate of pictorial short-term memory in the primate temporal cortex. *Nature* **1988**, *331*, 68–70.

128. Hampson, R.E.; Pons, T.P.; Stanford, T.R.; Deadwyler, S.A. Categorization in the monkey hippocampus: A possible mechanism for encoding information into memory. *Proc. Natl. Acad. Sci.* **2004**, *101*, 3184–3189.

129. Colombo, M.; Gross, C.G. Responses of inferior temporal cortex and hippocampal neurons during delayed matching to sample in monkeys (Macaca fascicularis). *Behav. Neurosci.* **1994**, *108*, 443–455.

130. Hampson, R.E.; Deadwyler, S.A. Temporal firing characteristics and the strategic role of subicular neurons in short-term memory. *Hippocampus* **2003**, *13*, 529–541.

131. McEchron, M.D.; Weible, A.P.; Disterhoft, J.F. Aging and Learning-Specific Changes in Single-Neuron Activity in CA1 Hippocampus During Rabbit Trace Eyeblink Conditioning. *J. Neurophysiol.* **2001**, *86*, 1839–1857.

132. Fuster, J.M. Unit Activity in Prefrontal Cortex During Neuronal Correlates Performance : Memory of Transient. **1973**.

133. Zhou, X.; Zhu, D.; Qi, X.L.; Lees, C.J.; Bennett, A.J.; Salinas, E.; Stanford, T.R.; Constantinidis, C. Working memory performance and neural activity in prefrontal cortex of peripubertal monkeys. *J. Neurophysiol.* **2013**, *110*, 2648–2660.

134. Fuster, J.M. Unit activity in prefrontal cortex during delayed-response performance: neuronal correlates of transient memory. *J. Neurophysiol.* **1973**, *36*, 61–78.

135. Kamiński, J.; Sullivan, S.; Chung, J.M.; Ross, I.B.; Mamelak, A.N.; Rutishauser, U. Persistently active neurons in human medial frontal and medial temporal lobe support working memory. *Nat. Neurosci.* **2017**.

136. Stern, C.E.; Sherman, S.J.; Kirchhoff, B.A.; Hasselmo, M.E. Medial temporal and prefrontal contributions to working memory tasks with novel and familiar stimuli. *Hippocampus* **2001**, *11*, 337–346.

137. Schon, K. Persistence of Parahippocampal Representation in the Absence of Stimulus Input Enhances Long-Term Encoding: A Functional Magnetic Resonance Imaging Study of Subsequent Memory after a Delayed Match-to-Sample Task. *J. Neurosci.* **2004**, *24*, 11088–11097.

138. Axmacher, N.; Mormann, F.; Fernández, G.; Cohen, M.X.; Elger, C.E.; Fell, J. Sustained Neural Activity Patterns during Working Memory in the Human Medial Temporal Lobe. *J. Neurosci.* **2007**, *27*, 7807–7816.

139. Kaminski, J.; Sullivan, S.; Jm, C.; Ib, R.; An, M.; Rutishauser, U. Persistently active neurons in human medial frontal and medial temporal lobe support working memory. *Nat. Publ. Gr.* **2017**, 7–9.

140. McEchron, M.D.; Tseng, W.; Disterhoft, J.F. Single neurons in CA1 hippocampus

encode trace interval duration during trace heart rate (fear) conditioning in rabbit. *J. Neurosci.* **2003**, *23*, 1535–1547.

141. Gilmartin, M.R.; McEchron, M.D. Single neurons in the medial prefrontal cortex of the rat exhibit tonic and phasic coding during trace fear conditioning. *Behav. Neurosci.* **2005**, *119*, 1496–1510.
142. Macdonald, C.J.; Lepage, K.Q.; Eden, U.T.; Eichenbaum, H. Hippocampal ‘“ Time Cells ”’ Bridge the Gap in Memory for Discontiguous Events. *Neuron* **2011**, *71*, 737–749.
143. Kitamura, T.; Macdonald, C.J.; Tonegawa, S. Entorhinal – hippocampal neuronal circuits bridge temporally discontiguous events. *Learn. Mem.* **2015**, *22*, 438–443.
144. Gill, P.R.; Mizumori, S.J.Y.; Smith, D.M. Hippocampal episode fields develop with learning. *Hippocampus* **2011**, *21*, 1240–9.
145. Pastalkova, E.; Itskov, V.; Amarasingham, A.; Buzsaki, G. Internally Generated Cell Assembly Sequences in the Rat Hippocampus. *Science (80-.).* **2008**, *321*, 1322–1327.
146. Wang, X.J. Synaptic reverberation underlying mnemonic persistent activity. *Trends Neurosci.* **2001**, *24*, 455–463.
147. Jochems, A.; Yoshida, M. A robust in vivo-like persistent firing supported by a hybrid of intracellular and synaptic mechanisms. *PLoS One* **2015**, *10*, 1–22.
148. Hasselmo, M.E.; Schnell, E.; Barkai, E. Dynamics of learning and recall at excitatory recurrent synapses and cholinergic modulation in rat hippocampal region CA3. *J. Neurosci.* **1995**, *15*, 5249–62.
149. McNaughton, B.L.; Morris, R.G.M. Hippocampal synaptic enhancement and information storage within a distributed memory system. *Trends Neurosci.* **1987**, *10*, 408–415.
150. Treves, A.; Rolls, E.T. Computational analysis of the role of the hippocampus in memory. *Hippocampus* **1994**, *4*, 374–391.
151. Wiebe, S.P.; Stäubli, U. V.; Ambros-Ingerson, J. Short-term reverberant memory model of hippocampal field CA3. *Hippocampus* **1997**, *7*, 656–665.
152. Willshaw, D.J.; Buckingham, J.T. An assessment of Marr’s theory of the hippocampus as a temporary memory store. *Philos. Trans. R. Soc. Lond. B. Biol. Sci.* **1990**, *329*, 205–15.
153. Sanchez-Vives, M. V; McCormick, D.A. Cellular and network mechanisms of rhythmic recurrent activity in neocortex. *Nat. Neurosci.* **2000**, *3*, 1027–1034.
154. Castro-Alamancos, M. a; Favero, M. NMDA receptors are the basis for persistent network activity in neocortex slices. *J. Neurophysiol.* **2015**, *113*, 3816–26.
155. Fujisawa, S.; Matsuki, N.; Ikegaya, Y. Single neurons can induce phase transitions of cortical recurrent networks with multiple internal states. *Cereb. Cortex* **2006**, *16*, 639–654.
156. Larimer, P.; Strowbridge, B.W. Representing information in cell assemblies: persistent activity mediated by semilunar granule cells. *Nat. Neurosci.* **2010**, *13*, 213–222.
157. Wang, M.; Yang, Y.; Wang, C.J.; Gamo, N.J.; Jin, L.E.; Mazer, J.A.; Morrison, J.H.; Wang, X.J.; Arnsten, A.F.T. NMDA Receptors Subserve Persistent Neuronal Firing during Working Memory in Dorsolateral Prefrontal Cortex. *Neuron* **2013**, *77*, 736–749.
158. Yoshida, M.; Fransén, E.; Hasselmo, M.E. mGluR-dependent persistent firing in entorhinal cortex layer III neurons. *Eur. J. Neurosci.* **2008**, *28*, 1116–1126.

159. Yamada-Hanff, J.; Bean, B.P. Persistent sodium current drives conditional pacemaking in CA1 pyramidal neurons under muscarinic stimulation. *J. Neurosci.* **2013**, *33*, 15011–21.

160. Jochems, A.; Yoshida, M. Persistent firing supported by an intrinsic cellular mechanism in hippocampal CA3 pyramidal cells. *Eur. J. Neurosci.* **2013**, *38*, 2250–2259.

161. Fransén, E.; Tahvildari, B.; Egorov, A. V.; Hasselmo, M.E.; Alonso, A.A. Mechanism of Graded Persistent Cellular Activity of Entorhinal Cortex Layer V Neurons. *Neuron* **2006**, *49*, 735–746.

162. Navaroli, V.L.; Zhao, Y.; Boguszewski, P.; Brown, T.H. Muscarinic receptor activation enables persistent firing in pyramidal neurons from superficial layers of dorsal perirhinal cortex. *Hippocampus* **2012**, *22*, 1392–1404.

163. Hsiao, C.-F.; Del Negro, C. a; Trueblood, P.R.; Chandler, S.H. Ionic basis for serotonin-induced bistable membrane properties in guinea pig trigeminal motoneurons. *J. Neurophysiol.* **1998**, *79*, 2847–2856.

164. D'Ascenzo, M.; Podda, M.V.; Fellin, T.; Azzena, G.B.; Haydon, P.; Grassi, C. Activation of mGluR5 induces spike afterdepolarization and enhanced excitability in medium spiny neurons of the nucleus accumbens by modulating persistent Na+ currents. *J. Physiol.* **2009**, *587*, 3233–50.

165. Winograd, M.; Destexhe, A.; Sanchez-Vives, M. V Hyperpolarization-activated graded persistent activity in the prefrontal cortex. *Proc. Natl. Acad. Sci. U. S. A.* **2008**, *105*, 7298–7303.

166. Elgueta, C.; Kohler, J.; Bartos, M. Persistent Discharges in Dentate Gyrus Perisoma-Inhibiting Interneurons Require Hyperpolarization-Activated Cyclic Nucleotide-Gated Channel Activation. *J. Neurosci.* **2015**, *35*, 4131–4139.

167. Sheffield, M.E.J.; Best, T.K.; Mensh, B.D.; Kath, W.L.; Spruston, N. Slow integration leads to persistent action potential firing in distal axons of coupled interneurons. *Nat. Neurosci.* **2011**, *14*, 200–207.

168. Krook-Magnuson, E.; Luu, L.; Lee, S.-H.; Varga, C.; Soltesz, I. Ivy and neurogliaform interneurons are a major target of μ-opioid receptor modulation. *J. Neurosci.* **2011**, *31*, 14861–70.

169. Thuault, S.J.; Malleret, G.; Constantinople, C.M.; Nicholls, R.; Chen, I.; Zhu, J.; Panteleyev, A.; Vronskaya, S.; Nolan, M.F.; Bruno, R.; et al. Prefrontal Cortex HCN1 Channels Enable Intrinsic Persistent Neural Firing and Executive Memory Function. *J Neurosci. Aug* **2013**, *21*, 13583–13599.

170. Tahvildari, B.; Alonso, A.A.; Bourque, C.W. Ionic Basis of ON and OFF Persistent Activity in Layer III Lateral Entorhinal Cortical Principal Neurons. *J. Neurophysiol.* **2008**, *99*, 2006–2011.

171. Fraser, D.D.; MacVicar, B.A. Cholinergic-dependent plateau potential in hippocampal CA1 pyramidal neurons. *J. Neurosci.* **1996**, *16*, 4113–4128.

172. Singh, A.; Garcia, E. The transient receptor potential channel antagonist SKF96365 is a potent blocker of low-voltage-activated T-type calcium channels Abbreviations : **2010**, 1464–1475.

173. Tai, C.; Hines, D.J.; Choi, H.B.; MacVicar, B.A. Plasma membrane insertion of TRPC5 channels contributes to the cholinergic plateau potential in hippocampal CA1 pyramidal neurons. *Hippocampus* **2011**, *21*, 958–967.

174. Reboreda, A.; Jiménez-Díaz, L.; Navarro-López, J.D. TRP Channels and Neural Persistent Activity. *Transient Recept. Potential Channels, Adv. Exp. Med. Biol.* **2011**, *704*, 323–339.

175. Egorov, A. V.; Unsicker, K.; Von Bohlen Und Halbach, O. Muscarinic control of graded persistent activity in lateral amygdala neurons. *Eur. J. Neurosci.* **2006**, *24*, 3183–3194.

176. Tahvildari, B.; Fransén, E.; Alonso, A.A.; Hasselmo, M.E. Switching Between '"On"' and '"Off"' States of Persistent Activity in Lateral Entorhinal Layer III Neurons. *Hippocampus* **2007**, *17*, 801–812.

177. Knauer, B.; Yoshida, M. Switching between persistent firing and depolarization block in individual rat CA1 pyramidal neurons. **2019**, 1–19.

178. Jochems, A.; Reboreda, A.; Hasselmo, M.E.; Yoshida, M. Cholinergic receptor activation supports persistent firing in layer III neurons in the medial entorhinal cortex. *Behav. Brain Res.* **2013**, *254*, 108–115.

179. Haj-dahmane, S.; Andrade, R. Ionic Mechanism of the Slow Afterdepolarization Induced by Muscarinic Receptor Activation in Rat Prefrontal Cortex. *J. Neurophysiol.* **1998**, *80*, 1197–210.

180. Zhang, Z.; Séguéla, P. Metabotropic induction of persistent activity in layers II/III of anterior cingulate cortex. *Cereb. Cortex* **2010**, *20*, 2948–2957.

181. Haj-Dahmane, S.; Andrade, R. Ionic mechanism of the slow afterdepolarization induced by muscarinic receptor activation in rat prefrontal cortex. *J. Neurophysiol.* **1998**, *80*, 1197–210.

182. Reboreda, A.; Raouf, R.; Alonso, A.; Se, P. Development of Cholinergic Modulation and Graded Persistent Activity in Layer V of Medial Entorhinal Cortex. **2007**, 3937–3947.

183. Yoshida, M.; Knauer, B.; Jochems, A. Cholinergic modulation of the CAN current may adjust neural dynamics for active memory maintenance, spatial navigation and time-compressed replay. *Front. Neural Circuits* **2012**, *6*, 10.

184. Yoshida, M.; Jochems, A.; Hasselmo, M.E. Comparison of Properties of Medial Entorhinal Cortex Layer II Neurons in Two Anatomical Dimensions with and without Cholinergic Activation. *PLoS One* **2013**, *8*.

185. Phelan, K.D.; Mock, M.M.; Kretz, O.; Shwe, U.T.; Kozhemyakin, M.; Greenfield, L.J.; Dietrich, A.; Birnbaumer, L.; Freichel, M.; Flockerzi, V.; et al. Heteromeric Canonical Transient Receptor Potential 1 and 4 Channels Play a Critical Role in Epileptiform Burst Firing and Seizure-Induced Neurodegeneration. *Mol. Pharmacol.* **2012**, *81*, 384–392.

186. Shu, Y.; Duque, A.; Yu, G.; Haider, B.; McCormick, D.A. Properties of action-potential initiation in neocortical pyramidal cells: Evidence from whole cell axon recordings. *J. Neurophysiol.* **2007**, *97*, 746–760.

187. Apostolides, P.F.; Milstein, A.D.; Grienberger, C.; Bittner, K.C.; Magee, J.C. Axonal Filtering Allows Reliable Output during Dendritic Plateau-Driven Complex Spiking in CA1 Neurons. *Neuron* **2016**, *89*, 770–783.

188. Alexander, S.P.; Davenport, A.P.; Kelly, E.; Marrion, N.; Peters, J.A.; Benson, H.E.; Faccenda, E.; Pawson, A.J.; Sharman, J.L.; Southan, C.; et al. The Concise Guide to PHARMACOLOGY 2015/16: G protein-coupled receptors. *Br. J. Pharmacol.* **2015**, *172*, 5744–5869.

189. El-Hassar, L.; Hagenston, A.M.; D'Angelo, L.B.; Yeckel, M.F. Metabotropic glutamate receptors regulate hippocampal CA1 pyramidal neuron excitability via Ca(2)(+) wave-dependent activation of SK and TRPC channels. *J. Physiol.* **2011**, *589*, 3211–3229.

190. Park, J.-Y.; Spruston, N. Synergistic Actions of Metabotropic Acetylcholine and Glutamate Receptors on the Excitability of Hippocampal CA1 Pyramidal Neurons. *J. Neurosci.* **2012**, *32*, 6081–6091.

191. Benardo, L.S.; Prince, D.A. Cholinergic excitation of mammalian hippocampal pyramidal cells. *Brain Res.* **1982**, *249*, 315–331.

192. Cole, A.E.; Nicoll, R.A. Characterization of a slow cholinergic post-synaptic potential recorded in vitro from rat hippocampal pyramidal cells. *J. Physiol.* **1984**, *352*, 173–188.

193. Kawasaki, H.; Palmieri, C.; Avoli, M. Muscarinic receptor activation induces depolarizing plateau potentials in bursting neurons of the rat subiculum. *J. Neurophysiol.* **1999**, *82*, 2590–601.

194. Yan, H.-D.; Villalobos, C.; Andrade, R. TRPC Channels Mediate a Muscarinic Receptor-Induced Afterdepolarization in Cerebral Cortex. *J. Neurosci.* **2009**, *29*, 10038–46.

195. Venkatachalam, K.; Montell, C. TRP Channels. *Annu. Rev. Biochem.* **2007**, *76*, 1–5.

196. Pedersen, S.F.; Owsianik, G.; Nilius, B. TRP channels: An overview. *Cell Calcium* **2005**, *38*, 233–252.

197. Vazquez, G.; Wedel, B.J.; Aziz, O.; Trebak, M.; Putney, J.W. The mammalian TRPC cation channels. *Biochim. Biophys. Acta - Mol. Cell Res.* **2004**, *1742*, 21–36.

198. Strübing, C.; Krapivinsky, G.; Krapivinsky, L.; Clapham, D.E. TRPC1 and TRPC5 form a novel cation channel in mammalian brain. *Neuron* **2001**, *29*, 645–655.

199. Strübing, C.; Krapivinsky, G.; Krapivinsky, L.; Clapham, D.E. Formation of novel TRPC channels by complex subunit interactions in embryonic brain. *J. Biol. Chem.* **2003**, *278*, 39014–39019.

200. Hofmann, T.; Schaefer, M.; Schultz, G.; Gudermann, T. Subunit composition of mammalian transient receptor potential channels in living cells. *Proc. Natl. Acad. Sci. U. S. A.* **2002**, *99*, 7461–6.

201. Goel, M.; Sinkins, W.G.; Schilling, W.P. Selective association of TRPC channel subunits in rat brain synaptosomes. *J. Biol. Chem.* **2002**, *277*, 48303–48310.

202. Wes, P.D.; Chevesich, J.; Jeromin, A.; Rosenbergt, C.; Stettent, G.; Montell, C.; Lane, M.D. TRPC1, a human homolog of a Drosophila store-operated channel Communicated by. *Cell Biol.* **1995**, *92*, 9652–9656.

203. Montell, C. The TRP Superfamily of Cation Channels. *Sci. Signal.* **2005**, *2005*, re3–re3.

204. Vennekens, R.; Menigoz, A.; Nilius, B. TRPs in the Brain. **2012**, *49*.

205. Fowler, M.A.; Sidiropoulou, K.; Ozkan, E.D.; Phillips, C.W.; Cooper, D.C. Corticolimbic expression of TRPC4 and TRPC5 channels in the rodent brain. *PLoS One* **2007**, *2*.

206. Chung, Y.H.; Sun Ahn, H.; Kim, D.; Hoon Shin, D.; Su Kim, S.; Yong Kim, K.; Bok Lee, W.; Ik Cha, C. Immunohistochemical study on the distribution of TRPC channels in the rat hippocampus. *Brain Res.* **2006**, *1085*, 132–137.

207. Nagy, G.A.; Botond, G.; Borhegyi, Z.; Plummer, N.W.; Freund, T.F.; Hájos, N. DAG-sensitive and Ca $^{2+}$ permeable TRPC6 channels are expressed in dentate granule cells and interneurons in the hippocampal formation. *Hippocampus* **2013**, *23*, 221–232.

208. Zechel, S.; Werner, S.; von Bohlen Und Halbach, O. Distribution of TRPC4 in developing and adult murine brain. *Cell Tissue Res.* **2007**, *328*, 651–6.

209. Von Bohlen Und Halbach, O.; Hinz, U.; Unsicker, K.; Egorov, A. V. Distribution of TRPC1 and TRPC5 in medial temporal lobe structures of mice. *Cell Tissue Res.* **2005**, *322*, 201–206.

210. Freichel, M.; Vennekens, R.; Olausson, J.; Stolz, S.; Philipp, S.E.; Weißgerber, P.; Flockerzi, V. Functional role of TRPC proteins in native systems : implications from knockout and knock-down studies. **2005**, *1*, 59–66.

211. Amaral, M.D.; Pozzo-Miller, L. TRPC3 channels are necessary for brain-derived neurotrophic factor to activate a nonselective cationic current and to induce dendritic spine formation. *J. Neurosci.* **2007**, *27*, 5179–89.

212. Tai, C.; Hines, D.J.; Choi, H.B.; MacVicar, B.A. Plasma membrane insertion of TRPC5 channels contributes to the cholinergic plateau potential in hippocampal CA1 pyramidal neurons. *Hippocampus* **2010**, *967*, 958–967.

213. Tian, J.; Thakur, D.P.; Lu, Y.; Zhu, Y.; Freichel, M.; Flockerzi, V.; Zhu, M.X. Dual depolarization responses generated within the same lateral septal neurons by TRPC4-containing channels. *Pflugers Arch. Eur. J. Physiol.* **2014**, *466*, 1301–1316.

214. Essen, L.; Perisic, O.; Katan, M.; Wu, Y.; Roberts, M.F.; Williams, R.L. Structural Mapping of the Catalytic Mechanism for a Mammalian Phosphoinositide-Specific Phospholipase C. *Biochemistry* **1997**, *2960*, 1704–1718.

215. Kim, H.; Kim, J.; Jeon, J.; Myeong, J.; Wie, J.; Kim, H.J.; Jeon, J.; So, I.; Kim, H.; Kim, J.; et al. The roles of G proteins in the activation of TRPC4 and TRPC5 transient receptor potential channels. **2012**, *6950*.

216. Chen, X.; Li, W.; Riley, A.; Soliman, M.; Chakraborty, S.; Stamatkin, C.; Obukhov, A. Molecular Determinants of the Sensitivity to Gq/11-Phospholipase C-dependent Gating, Gd3+ Potentiation, and Ca2+ Permeability in the Transient Receptor Potential Canonical Type 5 (TRPC5) Channel. *J. Biol. Chem.* **2017**, *292*, 898–911.

217. Schaefer, M.; Plant, T.D.; Obukhov, A.G.; Hofmann, T.; Gudermann, T.; Schultz, G. Receptor-mediated Regulation of the Nonselective Cation Channels TRPC4 and TRPC5. *J. Biol. Chem.* **2000**, *275*, 17517–17526.

218. Kim, J.; Kwak, M.; Jeon, J.-P.; Myeong, J.; Wie, J.; Hong, C.; Kim, S.-Y.; Jeon, J.-H.; Kim, H.J.; So, I. Isoform- and receptor-specific channel property of canonical transient receptor potential (TRPC)1/4 channels. *Pflügers Arch. - Eur. J. Physiol.* **2014**, *466*, 491–504.

219. Otsuguro, K. -i.; Tang, J.; Tang, Y.; Xiao, R.; Freichel, M.; Tsvilovskyy, V.; Ito, S.; Flockerzi, V.; Zhu, M.X.; Zholos, A. V. Isoform-specific Inhibition of TRPC4 Channel by Phosphatidylinositol 4,5-Bisphosphate. *J. Biol. Chem.* **2008**, *283*, 10026–10036.

220. Trebak, M.; Lemonnier, L.; DeHaven, W.I.; Wedel, B.J.; Bird, G.S.; Putney, J.W. Complex functions of phosphatidylinositol 4,5-bisphosphate in regulation of TRPC5 cation channels. *Pflügers Arch. - Eur. J. Physiol.* **2009**, *457*, 757–769.

221. Tang, J.; Lin, Y.; Zhang, Z.; Tikunova, S.; Birnbaumer, L.; Zhu, M.X. Identification of common binding sites for calmodulin and inositol 1,4,5-trisphosphate receptors on the carboxyl termini of trp channels. *J. Biol. Chem.* **2001**, *276*, 21303–10.

222. Yuan, J.P.; Kiselyov, K.; Shin, D.M.; Chen, J.; Shcheynikov, N.; Kang, S.H.; Dehoff, M.H.; Schwarz, M.K.; Seeburg, P.H.; Muallem, S.; et al. Homer Binds TRPC Family Channels and Is Required for Gating of TRPC1 by IP3 Receptors. *Cell* **2003**, *114*, 777–789.

223. Zhang, Z.; Tang, J.; Tikunova, S.; Johnson, J.D.; Chen, Z.; Qin, N.; Dietrich, A.; Stefani, E.; Birnbaumer, L.; Zhu, M.X. Activation of Trp3 by inositol 1,4,5-trisphosphate receptors through displacement of inhibitory calmodulin from a common binding domain. *Proc. Natl. Acad. Sci.* **2001**, *98*, 3168–3173.

224. Kiselyov, K.; Mignery, G.A.; Zhu, M.X.; Muallem, S. The N-terminal domain of the IP3 receptor gates store-operated hTrp3 channels. *Mol. Cell* **1999**, *4*, 423–9.

225. Boulay, G.; Brown, D.M.; Qin, N.; Jiang, M.; Dietrich, A.; Zhu, M.X.; Chen, Z.; Birnbaumer, M.; Mikoshiba, K.; Birnbaumer, L. Modulation of Ca(2+) entry by polypeptides of the inositol 1,4, 5-trisphosphate receptor (IP3R) that bind transient receptor potential (TRP): evidence for roles of TRP and IP3R in store depletion-activated Ca(2+) entry. *Proc. Natl. Acad. Sci. U. S. A.* **1999**, *96*, 14955–60.

226. Zhu, M.X.; Tang, J. TRPC channel interactions with calmodulin and IP3 receptors. *Novartis Found. Symp.* **2004**, *258*, 44–58; discussion 58-62, 98–102, 263–6.

227. Yuan, J.P.; Lee, K.P.; Hong, J.H.; Muallem, S. The closing and opening of TRPC channels by Homer1 and STIM1. *Acta Physiol.* **2012**, *204*, 238–247.

228. Venkatachalam, K.; Zheng, F.; Gill, D.L. Regulation of Canonical Transient Receptor Potential (TRPC) Channel Function by Diacylglycerol and Protein Kinase C. *J. Biol. Chem.* **2003**, *278*, 29031–29040.

229. Ordaz, B.; Tang, J.; Xiao, R.; Salgado, A.; Sampieri, A.; Zhu, M.X.; Vaca, L. Calmodulin And Calcium Interplay In The Modulation Of Trpc5 Channel Activity: Identification Of A Novel C-Terminal Domain For Calcium/Calmodulin-Mediated Facilitation. *J. Biol. Chem.* **2005**, *280*, 30788–30796.

230. Singh, B.B.; Liu, X.; Tang, J.; Zhu, M.X.; Ambudkar, I.S. Calmodulin regulates Ca(2+)-dependent feedback inhibition of store-operated Ca(2+) influx by interaction with a site in the C terminus of TrpC1. *Mol. Cell* **2002**, *9*, 739–50.

231. Hofmann, T.; Obukhov, A.G.; Schaefer, M.; Harteneck, C.; Gudermann, T.; Schultz, G. Direct activation of human TRPC6 and TRPC3 channels by diacylglycerol. *Nature* **1999**, *397*, 259–263.

232. Lucas, P.; Ukhanov, K.; Leinders-Zufall, T.; Zufall, F. A diacylglycerol-gated cation channel in vomeronasal neuron dendrites is impaired in TRPC2 mutant mice: mechanism of pheromone transduction. *Neuron* **2003**, *40*, 551–61.

233. Zhu, M.H.; Chae, M.; Kim, H.J.; Lee, Y.M.; Kim, M.J.; Jin, N.G.; Yang, D.K.; So, I.; Kim, K.W. Desensitization of canonical transient receptor potential channel 5 by protein kinase C. *AJP Cell Physiol.* **2005**, *289*, C591–C600.

234. Storch, U.; Forst, A.; Pardatscher, F.; Erdogmus, S.; Philipp, M. Dynamic NHERF interaction with TRPC4 / 5 proteins is required for channel gating by diacylglycerol. **2016**.

235. Jeon, J.-P.; Lee, K.P.; Park, E.J.; Sung, T.S.; Kim, B.J.; Jeon, J.-H.; So, I. The specific activation of TRPC4 by Gi protein subtype. *Biochem. Biophys. Res. Commun.* **2008**, *377*, 538–543.

236. Sung, T.S.; Jeon, J.P.; Kim, B.J.; Hong, C.; Kim, S.Y.; Kim, J.; Jeon, J.H.; Kim, H.J.; Suh, C.K.; Kim, S.J.; et al. Molecular determinants of PKA-dependent inhibition of

TRPC5 channel. *AJP Cell Physiol.* **2011**, *301*, C823–C832.

237. Hong, C.; Kim, J.; Jeon, J.-P.; Wie, J.; Kwak, M.; Ha, K.; Kim, H.; Myeong, J.; Kim, S.Y.; Jeon, J.-H.; et al. Gs cascade regulates canonical transient receptor potential 5 (TRPC5) through cAMP mediated intracellular Ca2+ release and ion channel trafficking. *Biochem. Biophys. Res. Commun.* **2012**, *421*, 105–111.

238. Schon, K. Scopolamine Reduces Persistent Activity Related to Long-Term Encoding in the Parahippocampal Gyrus during Delayed Matching in Humans. *J. Neurosci.* **2005**, *25*, 9112–9123.

239. Zhou, X.; Qi, X.L.; Douglas, K.; Palaninathan, K.; Kang, H.S.; Buccafusco, J.J.; Blake, D.T.; Constantinidis, C. Cholinergic modulation of working memory activity in primate prefrontal cortex. *J. Neurophysiol.* **2011**, *106*, 2180–2188.

240. Gahwiler, B.H.; Dreifuss, J.J. Multiple actions of acetylcholine on hippocampal pyramidal cells in organotypic explant cultures. *Neuroscience* **1982**, *7*, 1243–1256.

241. Andrade, R. Cell excitation enhances muscarinic cholinergic responses in rat association cortex. *Brain Res.* **1991**, *548*, 81–93.

242. Cole, A.E.; Nicoll, R.A. Acetylcholine mediates a slow synaptic potential in hippocampal pyramidal cells. *Science* **1983**, *221*, 1299–1301.

243. Halliwell, J. V; Adams, P.R. Voltage-clamp analysis of muscarinic excitation in hippocampal neurons. *Brain Res.* **1982**, *250*, 71–92.

244. Madison, D. V; Lancaster, B.; Nicoll, R.A. Voltage Clamp Analysis of Cholinergic Action in the Hippocampus. *J. Neurosci.* **1987**, *7*, 733–741.

245. Caeser, M.; Brown, D.A.; Gahwiler, B.H.; Knopfel, T. Characterization of a calcium-dependent current generating a slow afterdepolarization of CA3 pyramidal cells in rat hippocampal slice cultures. *Eur. J. Neurosci.* **1993**, *5*, 560–569.

246. Haj-Dahmane, S.; Andrade, R. Muscarinic receptors regulate two different calcium-dependent non-selective cation currents in rat prefrontal cortex. *Eur. J. Neurosci.* **1999**, *11*, 1973–1980.

247. Franzius, D.; Hoth, M.; Penner, R. Non-specific effects of calcium entry antagonists in mast cells. *Pflügers Arch. Eur. J. Physiol.* **1994**, *428*, 433–438.

248. Chen, K.H.; Liu, H.; Yang, L.; Jin, M.W.; Li, G.R. SKF-96365 strongly inhibits voltage-gated sodium current in rat ventricular myocytes. *Pflugers Arch. Eur. J. Physiol.* **2015**, *467*, 1227–1236.

249. Yau, H.-J.; Baranauskas, G.; Martina, M. Flufenamic acid decreases neuronal excitability through modulation of voltage-gated sodium channel gating. *J. Physiol.* **2010**, *588*, 3869–3882.

250. Rae, M.G.; Hilton, J.; Sharkey, J. are non-competitive antagonists at recombinant human a 1 b 2 c 2 GABA A receptors. *Neurochem. Int.* **2012**, *60*, 543–554.

251. Liu, H.; Yang, L.; Chen, K.H.; Sun, H.Y.; Jin, M.W.; Xiao, G.S.; Wang, Y.; Li, G.R. SKF-96365 blocks human ether-à-go-go-related gene potassium channels stably expressed in HEK 293 cells. *Pharmacol. Res.* **2016**, *104*, 61–69.

252. Guinamard, R.; Simard, C.; Del Negro, C. Flufenamic acid as an ion channel modulator. *Pharmacol. Ther.* **2013**, *138*, 272–284.

253. Miller, M.; Shi, J.; Zhu, Y.; Kustov, M.; Tian, J. Bin; Stevens, A.; Wu, M.; Xu, J.; Long, S.; Yang, P.; et al. Identification of ML204, a novel potent antagonist that selectively modulates native TRPC4/C5 ion channels. *J. Biol. Chem.* **2011**, *286*,

33436–33446.

254. Richter, J.M.; Schaefer, M.; Hill, K. Clemizole hydrochloride is a novel and potent inhibitor of transient receptor potential channel TRPC5. *Mol. Pharmacol.* **2014**, *86*, 514–521.

255. Rubaiy, H.N.; Ludlow, M.J.; Henrot, M.; Gaunt, H.J.; Miteva, K.; Cheung, S.Y.; Tanahashi, Y.; Hamzah, N.; Musialowski, K.E.; Blythe, N.M.; et al. Picomolar, selective, and subtype-specific small-molecule inhibition of TRPC1/4/5 channels. *J. Biol. Chem.* **2017**, *292*, 8158–8173.

256. Faber, E.S.L.L.; Sedlak, P.; Vidovic, M.; Sah, P. Synaptic activation of transient receptor potential channels by metabotropic glutamate receptors in the lateral amygdala. *Neuroscience* **2006**, *137*, 781–794.

257. Kim, S.J.; Kim, Y.S.; Yuan, J.P.; Petralia, R.S.; Worley, P.F.; Linden, D.J. Activation of the TRPC1 cation channel by metabotropic glutamate receptor mGluR1. *Nature* **2003**, *426*, 285–291.

258. Phelan, K.D.; Shwe, U.T.; Abramowitz, J.; Birnbaumer, L.; Zheng, F. Critical role of canonical transient receptor potential channel 7 in initiation of seizures. *PNAS* **2014**, *111*, 11533–8.

259. Dasari, S.; Abramowitz, J.; Birnbaumer, L.; Gulledge, A.T. Do canonical transient receptor potential channels mediate cholinergic excitation of cortical pyramidal neurons? *Neuroreport* **2013**, *24*, 550–4.

260. Obukhov, A.G.; Nowycky, M.C. TRPC5 activation kinetics are modulated by the scaffolding protein ezrin/radixin/moesin-binding phosphoprotein-50 (EBP50). *J. Cell. Physiol.* **2004**, *201*, 227–235.

261. Tang, Y.; Tang, J.; Chen, Z.; Trost, C.; Flockerzi, V.; Li, M.; Ramesh, V.; Zhu, M.X. Association of Mammalian Trp4 and Phospholipase C Isozymes with a PDZ Domain-containing Protein, NHERF. *J. Biol. Chem.* **2000**, *275*, 37559–37564.

262. Bröker-Lai, J.; Kollewe, A.; Schindeldecker, B.; Pohle, J.; Nguyen Chi, V.; Mathar, I.; Guzman, R.; Schwarz, Y.; Lai, A.; Weißgerber, P.; et al. Heteromeric channels formed by TRPC1, TRPC4 and TRPC5 define hippocampal synaptic transmission and working memory. *EMBO J.* **2017**, *36*, 2770–2789.

263. Lepannetier, S.; Gualdani, R.; Tempesta, S.; Schakman, O.; Seghers, F.; Kreis, A.; Yerna, X.; Slimi, A.; de Clippele, M.; Tajeddine, N.; et al. Activation of TRPC1 Channel by Metabotropic Glutamate Receptor mGluR5 Modulates Synaptic Plasticity and Spatial Working Memory. *Front. Cell. Neurosci.* **2018**, *12*.

264. Freichel, M.; Suh, S.H.; Pfeifer, A.; Schweig, U.; Trost, C.; Weißgerber, P.; Biel, M.; Philipp, S.; Freise, D.; Droogmans, G.; et al. Lack of an endothelial store-operated Ca2+ current impairs agonist-dependent vasorelaxation in TRP4-/- mice. *Nat. Cell Biol.* **2001**, *3*, 121–127.

265. Rubaiy, H.N.; Ludlow, M.J.; Bon, R.S.; Beech, D.J. Pico145 - powerful new tool for TRPC1 / 4 / 5 channels. *Channels* **2017**, *11*, 362–364.

266. Miller, A.M.; Shi, J.; Wu, M.; Engers, J.; Hopkins, C.; Lindsley, C. Novel Chemical Inhibitor of TRPC4 Channels. *Mol. Libaries, Probe Rep.* **2010**, *50*, 1–35.

267. Magistretti, J. Spike Patterning by Ca2+-Dependent Regulation of a Muscarinic Cation Current in Entorhinal Cortex Layer II Neurons. *J. Neurophysiol.* **2004**, *92*, 1644–1657.

268. Akazawa-ogawa, Y.; Nagai, H.; Hagihara, Y. Heat denaturation of the antibody , a multi-domain protein. *Biophys. Rev.* **2018**, 255–258.

269. El-Brolosy, M.A.; Stainier, D.Y.R.R.; Kontarakis, Z.; Rossi, A.; Kuenne, C.; Günther, S.; Fukuda, N.; Kikhi, K.; Boezio, G.L.M.; Takacs, C.M.; et al. Genetic compensation: A phenomenon in search of mechanisms. *PLoS Genet.* **2017**, *13*, 1–17.

270. Birnbaumer, L.; Yidirim, E.; Abramowitz, J. A comparison of the genes coding for canonical TRP channels and their M, V and P relatives. *Cell Calcium* **2003**, *33*, 419–432.

271. Arboit, A.; Reboreda, A.; Yoshida, M. Involvement of TRPC4 and 5 Channels in Persistent Firing in Hippocampal CA1 Pyramidal Cells. *Cells* **2020**, *9*, 1–20.

272. Schmidt-Supprian, M.; Rajewsky, K. Vagaries of conditional gene targeting. **2007**, *8*, 665–668.

273. Loonstra, A.; Vooijs, M.; Beverloo, H.B.; Allak, B. Al; Drunen, E. Van; Kanaar, R.; Berns, A.; Jonkers, J. Growth inhibition and DNA damage induced by Cre recombinase in mammalian cells. **2001**, *98*, 9209–9214.

274. Schmidt, E.E.; Taylor, D.S.; Prigge, J.R.; Barnett, S.; Capecchi, M.R. Illegitimate Cre-dependent chromosome rearrangements in transgenic mouse spermatids. *PNAS* **2000**, *97*.

275. Thyagarajan, B.; Guimara, M.J.; Groth, A.C.; Calos, M.P. Mammalian genomes contain active recombinase recognition sites. **2000**, *244*, 1–8.

276. Silver, D.P.; Livingston, D.M. Self-Excising Retroviral Vectors Encoding the Cre Recombinase Overcome Cre-Mediated Cellular Toxicity. *Mol. Cell* **2001**, *8*, 233–243.

277. Ansari, A.M.; Ahmed, A.K.; Matsangos, A.E.; Lay, F.; Born, L.J.; Marti, G.; Harmon, J.W.; Sun, Z. Cellular GFP Toxicity and Immunogenicity : Potential Confounders in in Vivo Cell Tracking Experiments. *Stem Cell Rev. Reports* **2016**, 553–559.

278. Liu, H.; Jan, M.; Chou, C.; Chen, P.; Ke, N. Is Green Fluorescent Protein Toxic to the Living Cells ? *Biochem. Biophys. Res. Commun. 260,* **1999**, *717*, 712–717.

279. Ganini, D.; Leinisch, F.; Kumar, A.; Jiang, J.; Tokar, E.J.; Malone, C.C.; Petrovich, R.M.; Mason, R.P. Redox Biology Fluorescent proteins such as eGFP lead to catalytic oxidative stress in cells ☆. *Redox Biol.* **2017**, *12*, 462–468.

280. Link, C.D.; Fonte, V.; Hiester, B.; Yerg, J.; Ferguson, J.; Csontos, S.; Silverman, M.A.; Stein, G.H. Conversion of Green Fluorescent Protein into a Toxic , Aggregation-prone Protein by C-terminal Addition of a. *J. Biol. Chem.* **2006**, *281*, 1808–1816.

281. Kitamura, T.; Sun, C.; Martin, J.; Kitch, L.J.; Schnitzer, M.J.; Tonegawa, S. Entorhinal Cortical Ocean Cells Encode Specific Contexts and Drive Context-Specific Fear Memory. *Neuron* **2015**, *87*, 1317–1331.

282. Saikat Ray, Robert Naumann, Andrea Burgalossi, Qiusong Tang, Helene Schmidt, M.B. Grid-Layout and Theta-Modulation of Layer 2 Pyramidal Neurons in Medial Entorhinal Cortex. **2014**, *447*, 443–447.

283. Just, S.; Chenard, B.L.; Ceci, A.; Strassmaier, T.; Chong, J.A.; Blair, N.T.; Gallaschun, R.J.; Del Camino, D.; Cantin, S.; D'Amours, M.; et al. Treatment with HC-070, a potent inhibitor of TRPC4 and TRPC5, leads to anxiolytic and antidepressant effects in mice. *PLoS One* **2018**, *13*, e0191225.

284. Chenard, B.; Gallaschun, R. Substituted Xanthines and Methods of Use Thereof. Patent No. WO2014/143799, 18 September 2014.

285. Chenard, B.; Gallaschun, R. Substituted Xanthines and Methods of Use Thereof. U.S. Patent No. 9,359,359, 7 June 2016.

286. Araneda, R.; Andrade, R. 5-Hydroxytryptamine2 and 5-hydroxytryptamine1A receptors mediate opposing responses on membrane excitability in rat association cortex. *Neuroscience* **1991**, *40*, 399–412.

287. Greene, C.C.; Schwindt, P.C.; Crill, W.E. Properties and ionic mechanisms of a metabotropic glutamate receptor-mediated slow afterdepolarization in neocortical neurons. *J. Neurophysiol.* **1994**, *72*, 693–704.

288. Sidiropoulou, K.; Lu, F.-M.; Fowler, M.A.; Xiao, R.; Phillips, C.; Ozkan, E.D.; Zhu, M.X.; White, F.J.; Cooper, D.C. Dopamine modulates an mGluR5-mediated depolarization underlying prefrontal persistent activity. *Nat. Neurosci.* **2009**, *12*, 190–199.

289. Phelan, K.D.; Shwe, U.T.; Abramowitz, J.; Wu, H.; Rhee, S.W.; Howell, M.D.; Gottschall, P.E.; Freichel, M.; Flockerzi, V.; Birnbaumer, L.; et al. Canonical transient receptor channel 5 (TRPC5) and TRPC1/4 contribute to seizure and excitotoxicity by distinct cellular mechanisms. *Mol. Pharmacol.* **2013**, *83*, 429–38.

290. Lee, J.; Ristow, M.; Lin, X.; White, M.F.; Magnuson, M.A.; Hennighausen, L. RIP-Cre Revisited , Evidence for Impairments of Pancreatic. *J. biolo* **2006**, *281*, 2649–2653.

291. Jensen, E.C. Use of Fluorescent Probes : Their Effect on Cell Biology and Limitations. *Anat. Rec.* **2012**, *2036*, 2031–2036.

292. Costantini, L.M.; Fossati, M.; Francolini, M.; Snapp, E.L. Assessing the Tendency of Fluorescent Proteins to Oligomerize Under Physiologic Conditions. *Traffic* **2012**, *13*, 643–649.

293. Lei, Y.-T.; Thuault, S.J.; Launay, P.; Margolskee, R.F.; Kandel, E.R.; Siegelbaum, S.A. Differential contribution of TRPM4 and TRPM5 nonselective cation channels to the slow afterdepolarization in mouse prefrontal cortex neurons. *Front Cell Neurosci.* **2014**, *8*, 267.

294. Alom, F.; Miyakawa, M.; Matsuyama, H.; Nagano, H.; Tanahashi, Y.; Unno, T. Possible antagonistic effects of the TRPC4 channel blocker ML204 on M2 and M3 muscarinic receptors in mouse ileal and detrusor smooth muscles and atrial myocardium. *J. Vet. Med. Sci.* **2018**, *80*, 1407–1415.

295. Jie, L.-J.; Wu, W.-Y.; Li, G.; Xiao, G.-S.; Zhang, S.; Li, G.-R.; Wang, Y. Clemizole hydrochloride blocks cardiac potassium currents stably expressed in HEK 293 cells. *Br. J. Pharmacol.* **2017**, *174*, 254–266.

296. von Bohlen und Halbach, O.; Hinz, U.; Unsicker, K.; Egorov, A. V. Distribution of TRPC1 and TRPC5 in medial temporal lobe structures of mice. *Cell Tissue Res.* **2005**, *322*, 201–6.

297. Gilmartin, M.R.; Mcechron, M.D. Single Neurons in the Dentate Gyrus and CA1 of the Hippocampus Exhibit Inverse Patterns of Encoding During Trace Fear Conditioning. *Behav. Neurosci.* **2005**, *119*, 164–179.

298. Wang, Y. *Transient Receptor Potential Canonical Channels and Brain Diseases*; Wang, Y., Ed.; Advances in Experimental Medicine and Biology; Springer Netherlands: Dordrecht, 2017; Vol. 976; ISBN 978-94-024-1086-0.

299. Nilius, B. TRP channels in disease. **2007**, *1772*, 805–812.

300. Poduslo, S.E.; Huang, R.; Huang, J. The frequency of the TRPC4AP haplotype in Alzheimer's patients. *Neurosci. Lett.* **2009**, *450*, 344–6.

301. Lu, R.; He, Q.; Wang, J. TRPC Channels and Alzheimer's Disease. **2017**.

302. Hong, C.; Seo, H.; Kwak, M.; Jeon, J.; Jang, J.; Jeong, E.M.; Myeong, J.; Hwang, Y.J.; Ha, K.; Kang, M.J.; et al. Increased TRPC5 glutathionylation contributes to striatal neuron loss in Huntington's disease. *Brain* **2015**, *138*, 3030–3047.

303. Sun, Y.; Zhang, H.; Selvaraj, S.; Sukumaran, P.; Lei, S.; Birnbaumer, L.; Singh, B.B. Inhibition of L-Type Ca $^{2+}$ Channels by TRPC1-STIM1 Complex Is Essential for the Protection of Dopaminergic Neurons. *J. Neurosci.* **2017**, *37*, 3364–3377.

304. Sukumaran, P.; Sun, Y.; Schaar, A. TRPC Channels and Parkinson's Disease. **2017**.

305. Fang, Z. TRPC Channels and Epilepsy. **2017**, 123–135.

306. Griesi-Oliveira, K.; Suzuki, A.M.; Muotri, A.R. TRPC Channels and Mental Disorders. *Transient Recept. Potential Canonical Channels Brain Dis. B.* **2017**, 85–94.

7 Abbreviations

2-APB	2-aminoethoxydiphenyl borate
AAV	adeno-associated virus
AB	antibodies
ABC	avidin–biotinylated horseradish peroxidase complex
ACh	acetylcholine
AMPA	α-amino-3-hydroxy-5-methyl-4-isoxazolepropionic acid
AP	anterior-posterior
BL	baseline
BOLD	blood oxygenation level dependent
BSA	bovine serum albumin
CA	cornu ammonis
CAM	calmodulin
cAMP	cyclic adenosine monophosphate
CAN	cationic non-selective
CCh	carbachol
cDNA	complementary DNA
CLE	clemizole hydrochloride
CT	cycle threshold
DAB	diaminobenzidine
DAG	diacylglycerol
DB	depolarization block
dCT	difference of cycle times
DG	dentate gyrus
DHPG	(s)-3,5-dihydroxyphenylglycine
DMDC	dimethyldicarbonate
DMS	delayed matching-to-sample
DMSO	dimethyl sulfoxide
DNMS	delayed non match to sample
dNTPs	deoxynucleotide triphosphates
DV	dorso-ventral
DZNE	deutsches zentrum für neurodegenerative erkrankungen e.v.
EC	entorhinal cortex
EEG	electroencephalography
ERG	ether-a-go-go related gene
FFA	flufenamic acid
flx/flx	floxed/floxed
fMRI	functional magnetic resonance imaging
GABA	gamma-aminobutyric acid
GFP	green fluorescent protein
GFP-	GFP positive
GFP+	GFP negative
GTP	guanosine-5'-triphosphate
hERG	human ether-à-go-go-related gene

HF	hippocampal formation
Hz	hertz
ICF	intracellular fluid
IHC	immunohistochemical .. check old
IP_3	inositol trisphosphate
IR	input resistance
KO	knock out
LEC	later entorhinal cortex
M1-5	muscarinic acetylcholine receptor types 1 - 5
MEC	median entorhinal cortex
mGluR1	metabotropic glutamate receptor
ML	medio-lateral
MP	membrane potential
MPEP	2-methyl-6-(phenylethynyl)pyridine hydrochloride
mRNA	messenger RNA
MTL	medial temporal lobe
mV	millivolt
nACSF	normal artificial cerebrospinal fluid
NMDA	n-methyl-d-aspartate
pA	picoampere
PaS	parasubiculum
PBS	phosphate buffered solution
PBST	phosphate buffered solution + triton-x
PDZ	psd-95/discs-large/zo-1
PER	perirhinal cortex
PF	persistent firing
PFA	paraformaldehyde
PFC	prefrontal cortex
PH	parahippocampal area
Pico	pico145
PIP2	phosphatidylinositol 4,5-bisphosphate
PKA	protein kinase a
PKC	protein kinase k
PLC	phospholipase c
POR	postrhinal cortex
PrS	presubiculum
PYR	Pyramidal-like
qPCR	quantitative polymerase chain reaction
R	receptor
ROI	region of interest
RQ%	relative quantification
RT	room temperature
shRNA	short harpin RNA
SL	stratum lacunosum
SM	stratum moleculare
STE	Stellate-like
SUB	subiculum

TBST	tris buffered solution
TRP	transient receptor potential
TRPC	canonical transient receptor potential
TRPA	ankyrin transient receptor potential
TRPM	melastatin transient receptor potential
TRPP	polycistin transient receptor potential
TRPV	vanilloid transient receptor potential
TTX	tetrodotoxin
W.O.	wash out
Wfs1	Wolframin 1

8 Supplementary material

8.1 - Protocol used for the horseradish peroxidase biocytin staining:

Whole slice staining protocol

(Traditional version based on but modified from Nathalie - August 2002)

Labeling and Fixing the cell:

Number of slices

Label cells with 1% Biocytin in the intra-cellular solution.
Place slices in 4% Paraformaldehyde in 0.1 M NaPB (sodium phosphate buffer) at 4ºC for 1 to 20 days.

Staining Protocol for DAB:

Use 1 to 1,5 ml per slice.

Calculate with exact amount of slices because safety amount is within the amount for 1 slice already.

Day 1

1. Check if there is enough ABC and DAB kit.

2. Prepare 0.1 M NaPB solution. 35 ml for 1 slice.
   - 0.013 M/L NaH_2PO_4 (FW=137.99) = 1.794g/l = 0.179g/100ml
   - 0.087 M/L Na_2HPO_4 (FW=177,99) = 15,48g/l = 1.54g/100ml

___ ml for ___ slices

NaH_2PO_4: _____ g

Na_2HPO_4: _____ g

3. Rinse slices for 5 min, 3 times in 0.1 M NaPB on a rotating table

4. While waiting, prepare NaPB + Gelatin (0.2%) + Triton (0.25%).
   20 ml for 1 slice. (Triton is like sope → don't shake)
   - Warm up 100 ml NaPB, dissolve 0.2g Gelatin, filter, cool down to room temp, add 250µl of Triton X-100 and mix well.

___ ml for ___ slices

_____ ml NaPB

_____ g Gelatine

_____ ml Triton

5. Suppress endogenous peroxidase with 2% H_2O_2 in NaPB for 30 min.
   1.5 ml for 1 slice.
   - For 10 ml, 0.67 ml of 30% H_2O_2 + 9.33 ml of NaPB. Fill the wells up.

___ ml for ___ slices

_____ ml 30% H_2O_2

_____ ml NaPB

6. Rinse slices for 5 min, 3 times in 0.1 M NaPB on a rotating table (keep rest of NaPB because needed on day 3)

7. This step makes holes in the cell membrane and blocks antibody with NaPB + Triton (0.25%) + Gelatin (0.2%) for 30 min.

8. While waiting, prepare AB Complex on rotating table and wait for 30 min before use.
   1.5 ml for 1 slice.
   - For 10 ml NaPB, mix 2 drops of A and 2 drops of B
   - 30 µl Triton X-100

___ ml for ___ slices

_____ ml NaPB

_____ drops of A and B

9. Transfer to AB Complex overnight.

Day 2

Long wash with NaPB / gelatine / Triton.

1 Rinse slices for 5 min, 4 times.

2 6 more washes. 1 hour, 6 times.

3 Final wash overnight.

Day 3

1. Rinse in 0.1 M Tris Buffered Saline (TBS) for 10 min, 3 times.
   4,5 ml for 1 slice.
   For in 100 ml of water add
   Trizma Base (FW= 121.1) 1.2g + NaCl (FW = 58.44) 1g.
   Then adjust pH to 7.6 using HCl.

___ ml for ___ slices

_____ ml dH_2O

_____ g Trizma Base

_____ g NaCl

2. While waiting, prepare a new well, syringe, filter, needle, etc. for DAB.

3. Wear gloves and mask, and prepare DAB solution (light sensitive) on rotating table

___ ml for ___ slices

_____ drops Buffer

_____ drops DAB

_____ drops H_2O_2

_____ drops Nickel

   For 10 slices, in 10ml distilled water, add:
   4 drops of Buffer Stock Solution and mix well (stirring platform)
   8 drops of DAB Stock Solution
   4 drops of Hydrogen Peroxide solution
   4 drops of Nickel Solution

4. Filter (0.2 μm) and place DAB solution in a **new well dish**.
   Transfer slices using a brush.
   Cover the well dish to be dark and
   wait until slices get purplish.

_____ ml NaPB

CHECK IF ENOUGH LEFT!

5. Stop the reaction by rinsing in NaPB (10 min, 3 times) 1.5 ml for 1 slice.
6. Prepare slides (write slice names), coverslips, unfreeze mowiol.
7. Put slices on glass slide and check for a cell under the microscope. Turn the slice with the cell facing up. Let the slice dry for about 2 min. Put 3 drops of Mowiol per slice. Put coverslips on from above for not distorting the shape of the slice.
8. Soak all containers that touch DAB solution in bleach.

8.2 - Example of an IHC double-staining protocol:

IHC Protocol Double-Stainining Calbindin & TRPC5

Day 1:

1) Rinse 3x10min in PBS (0.1M, pH 7.4)
2) Quench 30min, incubate with 30%-H_2O_2 (0.2% in PBS) in dark at RT
3) Rinse 3x5min in PBS
4) Incubate 30 min in PBS + 0.3% Triton X + 3% BSA
5) primary AB - Rabbit Anti-Calbindin in PBS + 3% BSA + 0.3% Triton X

Overnight, under hood, on rotating table, ***sealed with parafilm****, at room temperature.*

Day 2:

6) Rinse 3x10min PBS
7) 60min secondary AB Goat Anti-Rabbit in PBS + 3% BSA + 0,3% Triton X
8) Rinse 3x10min in PBS
9) Cy3 for 7 min (120ul Cy3 in 6ml diluent) – *cover with aluminium foil*
10) Rinse 3x10min TBST
11) Quench 30min, incubate with 30%-H_2O_2 (0.2% in PBS) in dark at RT
12) Incubate 30min in PBS + mouse anti mouse blocking agent (Vector Lab.)
13) Rinse 3x10min TBST
14) primary AB - Mouse Anti-TRPC5 in PBS + 3% BSA + 0.3% Triton X

Overnight, under hood, on rotating table, ***sealed with parafilm****, at room temperature*

Day 3:

15) Rinse 3x10min in PBS
16) 60min secondary AB Sheep Anti-Mouse in PBS + 3% BSA + 0.3% Triton X
17) Rinse 3x10min in PBS
18) Cy5 for 7min (120 ul Cy5 in 6ml diluent) – *cover with aluminium foil*
19) Rinse 3x10 in TBST
20) 20min DAPI in TBST (1ul in 100ml TBST)
21) Rinse 3x10min in TBST

Mount with Glycerol, seal with nail polish. Store at +4°C.

8.3 – Solutions for IHC stainings:

1M PBS (1L, aka 10x PBS)
90.0g NaCl
31.18 g NaH_2PO_4 H_2O (monobasic)
185.918 g Na_2HPO_4 7 H_2O (dibasic)
H_2O dest. up to 1L
Dilute 1:10 to obtain 0.1 M PBS, pH 7.4

Tris Base Solution (50 ml)
0.608 g Trizma Base
0.292 g NaCl
5 ml $MgCl_2$ Stock-solution (1M)
H_2O dest. up to 50 ml

TBST (trisma buffered solution + Tween 20)
15 ml 5 M NaCl
250 µl Tween 20
50 ml Tris Base Solution
H_2O dest. up to 500 ml

H_2O_2 solution
15 ml PBS
100 µl H_2O_2 (30%) – Stock

Dapi in TBST
1 µl stock solution (usually 1:10000)
in 100 ml TBST

Block-Solution
3% BSA
0,3% Triton X
In PBS 0,1 M pH 7,4

Declaration of Honour

I hereby declare that I prepared this thesis without impermissible help of third parties and that none other than the indicated tools have been used; all sources of information are clearly marked, including my own publications.

In particular I have not consciously:

- Fabricated data or rejected undesired results
- Misused statistical methods with the aim of drawing other conclusions than those warranted by the available data
- Plagiarized external data or publications
- Presented the results of other researchers in a distorted way

I am aware that violations of copyright may lead to injunction and damage claims of the author and also to prosecution by the law enforcement authorities.

I hereby agree that the thesis may be reviewed for plagiarism by mean of electronic data

processing.

This work has not yet been submitted as a doctoral thesis in the same or a similar form in Germany or in any other country. It has not yet been published as a whole.

Magdeburg 11.09.2020,